THE DUAL RECIPROCITY BOUNDARY ELEMENT METHOD SOLUTION OF FLUID
FLOW PROBLEMS

A THESIS SUBMITTED TO
THE GRADUATE SCHOOL OF APPLIED MATHEMATICS
OF
MIDDLE EAST TECHNICAL UNIVERSITY

BY

SEVİN GÜMGÜM

IN PARTIAL FULFILLMENT OF THE REQUIREMENTS
FOR
THE DEGREE OF DOCTOR OF PHILOSOPHY
IN
SCIENTIFIC COMPUTING

FEBRUARY 2010

Approval of the thesis:

THE DUAL RECIPROCITY BOUNDARY ELEMENT METHOD SOLUTION OF FLUID FLOW PROBLEMS

submitted by **SEVİN GÜMGÜM** in partial fulfillment of the requirements for the degree of **Doctor of Philosophy in Department of Scientific Computing, Middle East Technical University** by,

Prof. Dr. Ersan Akyıldız
Director, Graduate School of **Applied Mathematics**   _____

Prof. Dr. Bülent Karasözen
Head of Department, **Scientific Computing**   _____

Prof. Dr. Münevver Tezer
Supervisor, **Department of Mathematics, METU**   _____

Examining Committee Members:

Prof. Dr. Bülent Karasözen
Department of Scientific Computing, METU   _____

Prof. Dr. Münevver Tezer
Department of Mathematics, METU   _____

Prof. Dr. Haluk Aksel
Department of Mechanical Engineering, METU   _____

Prof.Dr. Tanıl Ergenç
Department of Mathematics, Atılım University   _____

Prof.Dr. Nevzat Güneri Gençer
Department of Electrical and Electronics Engineering, METU   _____

Date: _____

I hereby declare that all information in this document has been obtained and presented in accordance with academic rules and ethical conduct. I also declare that, as required by these rules and conduct, I have fully cited and referenced all material and results that are not original to this work.

Name, Last Name: SEVİN GÜMGÜM

Signature   :

ABSTRACT

THE DUAL RECIPROCITY BOUNDARY ELEMENT METHOD SOLUTION OF FLUID
FLOW PROBLEMS

Gümgüm, Sevin

Ph.D., Department of Scientific Computing

Supervisor   : Prof. Dr. Münevver Tezer

February 2010, 185 pages

In this thesis, the two-dimensional, transient, laminar flow of viscous and incompressible fluids is solved by using the dual reciprocity boundary element method (DRBEM). Natural convection and mixed convection flows are also solved with the addition of energy equation. Solutions of natural convection flow of nanofluids and micropolar fluids in enclosures are obtained for highly large values of Rayleigh number. The fundamental solution of Laplace equation is used for obtaining boundary element method (BEM) matrices whereas all the other terms in the differential equations governing the flows are considered as nonhomogeneity. This is the main advantage of DRBEM to tackle the nonlinearities in the equations with considerably small computational cost. All the convective terms are evaluated by using the DRBEM coordinate matrix which is already computed in the formulation of nonlinear terms. The resulting systems of initial value problems with respect to time are solved with forward and central differences using relaxation parameters, and the fourth-order Runge-Kutta method. The numerical stability analysis is developed for the flow problems considered with respect to the choice of the time step, relaxation parameters and problem constants. The stability analysis is made through an eigenvalue decomposition of the final coefficient matrix in

the DRBEM discretized system. It is found that the implicit central difference time integration scheme with relaxation parameter value close to one, and quite large time steps gives numerically stable solutions for all flow problems solved in the thesis. One-and-two-sided lid-driven cavity flow, natural and mixed convection flows in cavities, natural convection flow of nanofluids and micropolar fluids in enclosures are solved with several geometric configurations. The solutions are visualized in terms of streamlines, vorticity, microrotation, pressure contours, isotherms and flow vectors to simulate the flow behaviour.

Keywords: DRBEM, Navier-Stokes equations, Natural convection, Nanofluids, Micropolar fluids

ÖZ

KARŞILIKLI SINIR ELEMANLARI YÖNTEMİ İLE AKIŞKANLAR MEKANİĞİ
PROBLEMLERİNİN ÇÖZÜMÜ

Gümgüm, Sevin

Doktora, Bilimsel Hesaplama Bölümü

Tez Yöneticisi   : Prof. Dr. Münevver Tezer

Şubat 2010, 185 sayfa

Bu tezde, viskoz ve sıkıştırılamayan akışkanların iki boyutlu, zamana bağlı, katmanlı akımları karşılıklı sınır elemanları yöntemi ile çözülmüştür. Enerji denkleminin eklenmesiyle doğal ve karışık konveksiyon akımları da çözülmüştür. Nano ve mikropolar akışkanların kapalı bölgelerdeki doğal konveksiyon akımlarının çözümü oldukça yüksek Rayleigh sayıları için elde edilmiştir. Sınır elemanları yöntemindeki matrisler Laplace denkleminin temel çözümü kullanılarak elde edilirken, akımı temsil eden diferensiyel denklemlerdeki diğer bütün terimler sağ taraf fonksiyonu olarak değerlendirilmiştir. Karşılıklı sınır elemanları yönteminin en temel avantajı doğrusal olmayan terimler içeren diferensiyel denklemleri oldukça küçük hesaplama maliyetiyle çözmesidir. Konveksiyon terimleri, karşılıklı sınır elemanları yönteminin içerdiği ve daha önce doğrusal olmayan terimlerin formülasyonunda kullanılmış olan koordinat matrisi ile hesaplanmıştır. Oluşan zamana bağlı başlangıç değer problemleri, yumuşatma katsayıları ile birlikte ileri ve merkezi farklar yöntemleri, ve dördüncü derece Runge-Kutta yöntemi ile çözülmüştür. Akışkanlar mekaniği problemleri için zaman aralığı, yumuşatma katsayıları ve problem sabitlerinin seçimine göre sayısal kararlılık analizi geliştirilmiştir. Sayısal kararlılık analizi, karşılıklı sınır elemanları yöntemi ile ayrıklaştırılan sistemin en son elde

edilen katsayı matrisinin özdeğer ayrışımı doğrultusunda yapılmıştır. Kapalı merkezi fark-lar yönteminin, yumuşatma katsayılarının bire yakın değerleri ve oldukça yüksek zaman aralıkları ile birlikte tezde çözülen akışkanlar mekaniği problemleri için sayısal olarak kararlı çözümler verdiği tespit edilmiştir. Tek ve çift taraflı kapak hareketli kanal akımları, kanallar-daki doğal ve karışık konveksiyon akımları, nano ve mikropolar akışkanların kapalı bölgelerdeki doğal konveksiyon akımları değişik geometriler için çözülmüştür. Akım davranışlarını görebilmek için çözümler, akış çizgileri, vorticity ve basınç eğrileri, eşısı eğrileri ve akış vektörleri ile gösterilmiştir.

Anahtar Kelimeler: Karşılıklı sınır elemanları yöntemi, doğal konveksiyon, nano akışkanlar, mikropolar akışkanlar

To my parents, Beyhan and Bahattin,
and my sister, Sinem

ACKNOWLEDGMENTS

TABLE OF CONTENTS

LIST OF TABLES

TABLES

LIST OF FIGURES

FIGURES

CHAPTER 1

INTRODUCTION

Computational fluid dynamics is an important area for numerical analysis because the behaviour of fluids can be observed in almost all areas of life. Generally, interactions between different fluid particles, forces between moving fluids and solids at rest, and a moving solid in a fluid at rest are investigated. In this thesis, we will consider the laminar flow of incompressible, viscous fluid. Laminar flow is a smooth, constant fluid motion which occurs when viscous forces are dominant. It is the opposite of turbulent flow. Turbulent flow occurs when inertial forces are dominant and produces vortices and random eddies. Incompressible fluid is a fluid with a constant density. Actually, it is an idealization used to simplify calculations. By making this assumption, the governing equations of the fluid flow can be simplified significantly.

In this chapter, we first give the basic equations of the mass and momentum conservations (Navier-Stokes equations) in terms of primitive variables for an incompressible, viscous fluid. This formulation contains the velocity and the pressure of the fluid which are the original unknowns. The difficulties arise due to the satisfaction of the continuity equation and missing pressure equation. Thus, in most of the numerical procedures these equations are transformed to stream function-vorticity and velocity-vorticity formulations. In the next section, Poisson equations for the velocity components as well as the pressure are derived and then the stream function-vorticity formulation is explained. Natural and mixed convection flows are discussed by the adding energy equation to the Navier-Stokes equations. The physical details of the nanofluids are given in Section 1.3. Finally, the microrotation equation is added to the Navier-Stokes and energy equations. We end up this chapter with the literature survey for the flows considered in the thesis, and the plan of the thesis.

1.1 The Navier-Stokes Equations

The Navier-Stokes equations are nonlinear partial differential equations which describe the motion of fluids, i.e. liquids and gases. These equations state that changes in momentum in infinitesimal volumes of fluid are the sum of dissipative forces, changes in pressure, gravity and other forces acting inside the fluid [17]. They are applications of the Newton's second law. The nonlinearity in these equations is due to convective acceleration and makes the most problems difficult or impossible to solve. The equations can be simplified to linear equations only in some cases, like one-dimensional flow and Stokes flow. The solution of the Navier-Stokes equations describes the velocity of the fluid at a given point in space and time, and is called a velocity field. The pressure is also the original unknown appearing in the numerical equations. Other quantities of interest can be found easily after obtaining the velocity field, [36].

The Navier-Stokes equations are one of the most useful sets of equations because they can be used to describe many different engineering problems. They may be used to model weather, ocean currents, water flow in a pipe, flow around an airfoil, and motion of stars inside a galaxy, the design of aircraft and cars, the study of blood flow, the design of power stations, the analysis of the effects of pollution, etc. Coupled with Maxwell's equations they can be used to model and study magnetohydrodynamics, [17].

1.1.1 Primitive Variable Formulation

The two-dimensional, transient, laminar flow of incompressible Navier-Stokes equations in primitive variables form is governed by the following equations [36];

Momentum equations

$$\rho\left(\frac{\partial u'}{\partial t'} + u'\frac{\partial u'}{\partial x'} + v'\frac{\partial u'}{\partial y'}\right) = -\frac{\partial p'}{\partial x'} + \mu\left(\frac{\partial^2 u'}{\partial x'^2} + \frac{\partial^2 u'}{\partial y'^2}\right)$$

$$(1.1)$$

$$\rho\left(\frac{\partial v'}{\partial t'} + u'\frac{\partial v'}{\partial x'} + v'\frac{\partial v'}{\partial y'}\right) = -\frac{\partial p'}{\partial y'} + \mu\left(\frac{\partial^2 v'}{\partial x'^2} + \frac{\partial^2 v'}{\partial y'^2}\right),$$

continuity equation

$$\frac{\partial u'}{\partial x'} + \frac{\partial v'}{\partial y'} = 0 \tag{1.2}$$

where u' and v' are the velocity components, p' is the pressure of the fluid, μ is the dynamic viscosity and ρ is the density.

In order to obtain the non-dimensional forms of equations (1.1) and (1.2), we introduce a characteristic length L', a characteristic velocity U' and define the dimensionless quantities as

$$u = \frac{u'}{U'} \quad , \quad v = \frac{v'}{U'} \quad , \quad x = \frac{x'}{L'} \quad , \quad y = \frac{y'}{L'} \quad , \quad t = \frac{t'}{L'} \quad , \quad p = \frac{p'}{\rho\, U'^2}.$$

Thus, the Navier-Stokes equations can be written in non-dimensional form as

Momentum equations

$$\frac{\partial u}{\partial t} + u\frac{\partial u}{\partial x} + v\frac{\partial u}{\partial y} = -\frac{\partial p}{\partial x} + \frac{1}{Re}\nabla^2 u$$

(1.3)

$$\frac{\partial v}{\partial t} + u\frac{\partial v}{\partial x} + v\frac{\partial v}{\partial y} = -\frac{\partial p}{\partial y} + \frac{1}{Re}\nabla^2 v,$$

continuity equation

$$\frac{\partial u}{\partial x} + \frac{\partial v}{\partial y} = 0.$$

(1.4)

where $\nabla^2 = \dfrac{\partial^2}{\partial x^2} + \dfrac{\partial^2}{\partial y^2}$ is the Laplace operator.

Here, Re is the dimensionless *Reynolds number* which is the ratio of inertial forces to viscous forces. It quantifies the relative importance of these two types of forces. Thus, it identifies whether the flow regime is laminar or turbulent. When Reynolds number is below the critical value (≈ 2100) for that fluid the flow is laminar, when it exceeds the critical number the flow is turbulent.

Reynolds number is defined as follows

$$Re = \frac{\rho U' L'}{\mu}.$$

The Navier-Stokes equations are usually supplied with essential boundary conditions for the velocity components as

$$u(x_s, y_s) = f_{u_s} \quad , \quad v(x_s, y_s) = f_{v_s}$$

where the subscript 's' restricts (x, y) to the boundary of the region under consideration, and f_{u_s}, f_{v_s} are given functions. If $f_{u_s} = f_{v_s} = 0$, then no fluid penetrates the boundary and the

3

fluid is at rest there. This condition is known as the no-slip condition. There is no boundary condition for the pressure physically. It may be derived during the computations if the primitive variables form is used.

1.1.2 Derivation of the Poisson Equations for Velocities and Pressure

In this section, we will derive the Poisson equations for velocities u and v, and pressure p. The equations for the velocity components can be derived by using the continuity equation

$$\frac{\partial u}{\partial x} + \frac{\partial v}{\partial y} = 0 \tag{1.5}$$

and the definition of vorticity

$$\omega = \frac{\partial v}{\partial x} - \frac{\partial u}{\partial y} \ . \tag{1.6}$$

Vorticity is a vector quantity whose direction is along the axis of fluid's rotation. It is the curl of the velocity that gives the amount of circulation in a fluid flow. Vorticity is a powerful concept especially for the flows when the Reynolds number is high, which means that the viscosity is low.

Thus, equation (1.6) is the z-component (axis of the flow) of the vorticity vector for a two-dimensional flow.

Differentiating equation (1.5) with respect to x and (1.6) with respect to y gives

$$\frac{\partial^2 u}{\partial x^2} + \frac{\partial^2 v}{\partial x \partial y} = 0 \tag{1.7}$$

and

$$\frac{\partial^2 v}{\partial y \partial x} - \frac{\partial^2 u}{\partial y^2} = \frac{\partial \omega}{\partial y} \ . \tag{1.8}$$

The second term of equation (1.7) and the first term of equation (1.8) are equal (interchangeability of the order of derivatives). Thus, substitution of $\dfrac{\partial^2 v}{\partial x \partial y}$ from equation (1.7) in the equation (1.8) gives the Poisson equation for u

$$-\frac{\partial^2 u}{\partial x^2} - \frac{\partial^2 u}{\partial y^2} = \frac{\partial \omega}{\partial y} \tag{1.9}$$

which can be expressed using the Laplace operator as

$$\nabla^2 u = -\frac{\partial \omega}{\partial y} \ . \tag{1.10}$$

4

Cross differentiating equations (1.5) and (1.6) with respect to y and x gives

$$\frac{\partial^2 u}{\partial y \partial x} + \frac{\partial^2 v}{\partial y^2} = 0 \tag{1.11}$$

and

$$\frac{\partial^2 v}{\partial x^2} - \frac{\partial^2 u}{\partial x \partial y} = \frac{\partial \omega}{\partial x}. \tag{1.12}$$

Combining equations (1.11) and (1.12) in a similar way gives the Poisson equation for v

$$\nabla^2 v = \frac{\partial \omega}{\partial x}. \tag{1.13}$$

In order to derive the Poisson equation for pressure we will use the momentum equations

$$\frac{\partial u}{\partial t} + u\frac{\partial u}{\partial x} + v\frac{\partial u}{\partial y} = -\frac{\partial p}{\partial x} + \nabla^2 u \tag{1.14}$$

$$\frac{\partial v}{\partial t} + u\frac{\partial v}{\partial x} + v\frac{\partial v}{\partial y} = -\frac{\partial p}{\partial y} + \nabla^2 v. \tag{1.15}$$

Differentiating equation (1.14) with respect to x and (1.15) with respect to y, and adding them together, we get

$$\frac{\partial}{\partial t}\underbrace{\left(\frac{\partial u}{\partial x} + \frac{\partial v}{\partial y}\right)}_{=\,0} + \left(\frac{\partial u}{\partial x}\right)^2 + \left(\frac{\partial v}{\partial y}\right)^2 + u\frac{\partial}{\partial x}\underbrace{\left(\frac{\partial u}{\partial x} + \frac{\partial v}{\partial y}\right)}_{=\,0} - 2\frac{\partial v}{\partial x}\frac{\partial u}{\partial y} + v\frac{\partial}{\partial y}\underbrace{\left(\frac{\partial u}{\partial x} + \frac{\partial v}{\partial y}\right)}_{=\,0}$$

$$= -\left(\frac{\partial^2 p}{\partial x^2} + \frac{\partial^2 p}{\partial y^2}\right) + \frac{\partial^2}{\partial x^2}\underbrace{\left(\frac{\partial u}{\partial x} + \frac{\partial v}{\partial y}\right)}_{=\,0} + \frac{\partial^2}{\partial y^2}\underbrace{\left(\frac{\partial u}{\partial x} + \frac{\partial v}{\partial y}\right)}_{=\,0}. \tag{1.16}$$

Thus, the Poisson equation for pressure is

$$\nabla^2 p = -\left(\frac{\partial u}{\partial x}\right)^2 - \left(\frac{\partial v}{\partial y}\right)^2 - 2\frac{\partial v}{\partial x}\frac{\partial u}{\partial y}. \tag{1.17}$$

So, the Navier-Stokes equations can be expressed for the variables u, v and p in terms of

vorticity and velocity as

$$\nabla^2 u \;=\; -\frac{\partial\, \omega}{\partial\, y}$$

$$\nabla^2 v \;=\; \frac{\partial\, \omega}{\partial\, x} \tag{1.18}$$

$$\nabla^2 p \;=\; -\Big(\frac{\partial\, u}{\partial\, x}\Big)^2 - \Big(\frac{\partial\, v}{\partial\, y}\Big)^2 - 2\frac{\partial\, v}{\partial\, x}\frac{\partial\, u}{\partial\, y}\,.$$

These Poisson equations for velocity components and pressure can be solved iteratively when an initial estimate for vorticity is provided.

The boundary conditions of pressure can be computed from the momentum equations [36, 78]

$$\frac{\partial\, p}{\partial\, x} \;=\; \frac{1}{Re}\frac{\partial^2\, u}{\partial\, x^2} \quad \text{along the vertical boundaries}$$

$$\frac{\partial\, p}{\partial\, y} \;=\; \frac{1}{Re}\frac{\partial^2\, v}{\partial\, y^2} \quad \text{along the horizontal boundaries}$$

and again essential boundary conditions are usually given for velocity components u and v.

1.1.3 Stream Function-Vorticity Formulation

In this section, we express the Navier-Stokes equations in terms of stream function and vorticity.

The stream function is defined for two-dimensional flows. It can be used to plot streamlines, which are the contour lines of constant values of stream function.

The partial derivatives of stream function are linked with the velocity components through the relation [36, 81]

$$\frac{\partial\, \psi(x,y)}{\partial\, x} = -v \quad , \quad \frac{\partial\, \psi(x,y)}{\partial\, y} = u \tag{1.19}$$

for satisfying the continuity equation automatically.

In order to show that the continuity equation is satisfied, we substitute the defining equations of stream function (1.19) in the continuity equation (1.4), and from the integrability condition we get

$$\frac{\partial}{\partial\, x}\Big(\frac{\partial\, \psi}{\partial\, y}\Big) + \frac{\partial}{\partial\, y}\Big(\frac{-\partial\, \psi}{\partial\, x}\Big) = \frac{\partial^2\, \psi}{\partial\, x\partial\, y} - \frac{\partial^2\, \psi}{\partial\, y\partial\, x} = 0.$$

6

In two-dimensions, the Navier-Stokes equations are generally expressed in terms of stream function ψ and vorticity ω instead of the primitive variables u, v, and p. Because, in this formulation the pressure is eliminated and equations include only two variables.

First, we derive the vorticity transport equation using the momentum equations given in equation (1.3)

$$\frac{\partial u}{\partial t} + u\frac{\partial u}{\partial x} + v\frac{\partial u}{\partial y} = -\frac{\partial p}{\partial x} + \frac{1}{Re}\nabla^2 u$$

$$\frac{\partial v}{\partial t} + u\frac{\partial v}{\partial x} + v\frac{\partial v}{\partial y} = -\frac{\partial p}{\partial y} + \frac{1}{Re}\nabla^2 v.$$

(1.20)

The first equation is differentiated with respect to y and the second equation is differentiated with respect to x. Then, the first equation is subtracted from the second one, so that the pressure is eliminated. Substituting the definition of vorticity $\omega = \frac{\partial v}{\partial x} - \frac{\partial u}{\partial y}$ yields

$$\frac{\partial}{\partial t}\Big(\underbrace{\frac{\partial v}{\partial x} - \frac{\partial u}{\partial y}}_{=\,\omega}\Big) + \frac{\partial u}{\partial x}\Big(\underbrace{\frac{\partial v}{\partial x} - \frac{\partial u}{\partial y}}_{=\,\omega}\Big) + \frac{\partial v}{\partial y}\Big(\underbrace{\frac{\partial v}{\partial x} - \frac{\partial u}{\partial y}}_{=\,\omega}\Big) + u\frac{\partial}{\partial x}\Big(\underbrace{\frac{\partial v}{\partial x} - \frac{\partial u}{\partial y}}_{=\,\omega}\Big) + v\frac{\partial}{\partial y}\Big(\underbrace{\frac{\partial v}{\partial x} - \frac{\partial u}{\partial y}}_{=\,\omega}\Big)$$

$$= \Big(\underbrace{-\frac{\partial^2 p}{\partial x\partial y} + \frac{\partial^2 p}{\partial y\partial x}}_{=\,0}\Big) + \frac{1}{Re}\Big[\frac{\partial^2}{\partial x^2}\Big(\underbrace{\frac{\partial v}{\partial x} - \frac{\partial u}{\partial y}}_{=\,\omega}\Big) + \frac{\partial^2}{\partial y^2}\Big(\underbrace{\frac{\partial v}{\partial x} - \frac{\partial u}{\partial y}}_{=\,\omega}\Big)\Big].$$

(1.21)

The second and the third terms in the left-hand side of the equation (1.21) are eliminated since they satisfy the continuity equation.

Thus, the vorticity transport equation can be expressed as [36]

$$\frac{1}{Re}\nabla^2\omega = \frac{\partial \omega}{\partial t} + u\frac{\partial \omega}{\partial x} + v\frac{\partial \omega}{\partial y}.$$

(1.22)

To obtain the Poisson equation for stream function, we substitute the defining equations of stream function into that of vorticity

$$\omega = \frac{\partial v}{\partial x} - \frac{\partial u}{\partial y} = \frac{\partial}{\partial x}\Big(-\frac{\partial \psi}{\partial x}\Big) - \frac{\partial}{\partial y}\Big(\frac{\partial \psi}{\partial y}\Big) = -\frac{\partial^2 \psi}{\partial x^2} - \frac{\partial^2 \psi}{\partial y^2}.$$

Hence, we have

$$\nabla^2\psi = -\omega.$$

(1.23)

7

This formulation has many advantages. It reduces the number of equations through the elimination of pressure. Partial derivatives of stream function are related to the velocity components and it satisfies the continuity equation through this relation. These reasons make this formulation attractive for the solution of high Reynolds number Navier-Stokes equations. Especially, vorticity plays an important role when studying vortex dominated flows.

The boundary conditions for stream function are usually of Dirichlet type since a boundary is normally considered as a streamline which has constant value of stream function. Vorticity boundary conditions may be derived through the relation $\nabla^2 \psi = -\omega$. Thus,

$$\psi(x_s, y_s) = f_{\psi_s} \quad , \quad \omega(x_s, y_s) = f_{\omega_s}$$

where f_{ψ_s}, f_{ω_s} are given functions. Stream function is usually specified on the boundary and the vorticity boundary condition is derived from the stream function equation or from its definition, which becomes again of Dirichlet type.

1.2   Natural Convection Flow

Analyzing heat transfer within the fluid flow is important since it has many applications in industries such as energy conservation process, energy storage, meteorology and climatology. Numerical simulation plays an important role in these areas because experiments are often costly.

In the previous sections, we give the Navier-Stokes equations of two-dimensional, transient, laminar flow of viscous incompressible fluid. Now, we extend the model by adding the energy equation. This equation results from the conservation of energy which states that the total energy of a system and its surroundings remains constant [16].

The main effect of temperature on the fluid is the change of fluids density due to the changes in temperature. These changes cause buoyancy forces. Because of these effects the modeling equations are difficult to treat. Thus, Boussinesq approximation is used for necessary simplifications, [36].

• Density is constant except in the buoyancy terms.

• All other fluid properties are assumed constant.

• Viscous dissipation is negligibly small.

With the first assumption, we consider the incompressible form of the continuity equation in which density varies only in the body force term. Other assumptions enable us to investigate the effect of buoyancy forces by simplifying the equations.

Convection is an important phenomena in heat transfer. It occurs due to the random movement of molecules within the fluids and advection. In general, convection can be explained as the sum of advective and diffusive transfer [43]. It combines the energy equation with the continuity and momentum equations.

Convective heat transfer can be analyzed in two categories, namely the natural and forced convection. Combination of the natural and forced convection is called as the mixed convection.

In this section, we will focus on the natural convection in which the fluid motion depends only on the local buoyancy differences. Natural convection is an important heat transfer mechanism and has many application areas such as boilers, fire control, nuclear reactor systems and energy storage.

The two-dimensional, unsteady, laminar flow of an incompressible, viscous fluid are given in terms of non-dimensional stream function, vorticity and temperature as [51]

$$\nabla^2 \psi = -\omega$$

$$Pr\nabla^2 \omega = \frac{\partial \omega}{\partial t} + u\frac{\partial \omega}{\partial x} + v\frac{\partial \omega}{\partial y} - RaPr\frac{\partial T}{\partial x} \qquad (1.24)$$

$$\nabla^2 T = \frac{\partial T}{\partial t} + u\frac{\partial T}{\partial x} + v\frac{\partial T}{\partial y}$$

where T is the temperature, Ra is the Rayleigh number and Pr is the Prandtl number.

The above non-dimensional equations are obtained by using the following non-dimensional variables [70]

$$u = \frac{u'L'}{\alpha} \quad , \quad v = \frac{v'L'}{\alpha} \quad , \quad x = \frac{x'}{L'} \quad , \quad y = \frac{y'}{L'} \quad , \quad t = \frac{t'}{L'} \quad , \quad p = \frac{p'L'^2}{\rho\,\alpha^2} \quad , \quad T = \frac{\theta' - \theta'_c}{\theta'_h - \theta'_c}.$$

In natural convection, *Rayleigh number* expresses important properties of the fluid. This

dimensionless number is given by

$$Ra = \frac{g\beta(T_s - T_\infty)L'^3}{\alpha \nu}$$

where g is the local gravitational acceleration, L' is the characteristic length, α is the thermal diffusivity, β is the coefficient of thermal expansion, T_s is the temperature of the wall, T_∞ is the fluid temperature far from the surface of the object, and $\nu = \mu/\rho$ is the kinematic viscosity.

Rayleigh number controls the form of heat transfer, whether its laminar or turbulent. When it is below the critical value of the fluid then conduction occurs, when it is greater then the critical value then convection occurs ($10^3 \leq Ra \leq 10^6$).

Prandtl number, Pr, is used to control the relative thickness of the momentum and thermal boundary layers. It is defined as [85]

$$Pr = \frac{\nu}{\alpha} = \frac{\text{viscous diffusion rate}}{\text{thermal diffusion rate}} = \frac{U'L'}{\alpha Re}.$$

Prandtl number is taken as 0.7 for air and many other gases, around 7 for water, around 7×10^{21} for Earth's mantle, between 100 and 40000 for engine oil, between 4 and 5 for $R - 12$ refrigerant and around 0.015 for mercury.

Another important parameter for natural convection is the *Nusselt number* which is the ratio of convective and conductive heat transfer across the boundary. The dimensionless number is defined by [36]

$$Nu = \frac{Q_{\text{convection}}}{Q_{\text{heat diffusion}}}.$$

Thus, the Nusselt number is given as

$$Nu = \frac{\int_0^{L_y} \left(-\frac{\partial T}{\partial x} \right)_{x=0} dy}{L_y \, (T_l - T_r)/L_x}$$

where L_y is the height and L_x is the length of the fluid container under consideration, and T_l and T_r are the temperatures at the left and right walls.

Selection of the characteristic lengths, L_x and L_y, should be in the direction of growth (or thickness) of the boundary layer. Some examples of characteristic lengths are: the outer diameter of a cylinder in (external) cross flow (perpendicular to the cylinder axis), the length of a vertical plate undergoing natural convection, or the diameter of a sphere. When Nusselt

number is close to unity then natural convection and conduction are of similar magnitude. This is also a characteristic of laminar flow. A larger Nusselt number corresponds to more active convection. If the flow is turbulent, then the Nusselt number is between $100 - 1000$, [96].

Temperature boundary conditions can be defined either Dirichlet or Neumann type as

$$T\Big|_{\partial\Omega} = T_1 \quad , \quad \frac{\partial T}{\partial n}\Big|_{\partial\Omega} = -\frac{q}{k}$$

where 'q' is the heat flux across the wall.

Boundary conditions can be generally expressed as Dirichlet type for stream function (no-slip condition for velocities), and Dirichlet type for vorticity since it is obtained from vorticity definition, or through relationship of vorticity with stream function. Thus, we can express the boundary conditions generally as

$$\psi(x_s, y_s) = f_{\psi_s} \quad , \quad \omega(x_s, y_s) = f_{w_s}$$

$$T(x_s, y_s) = f_{t_s} \quad , \quad \frac{\partial T}{\partial n}(x_s, y_s) = f_{t_n}.$$

If $T = T_h$ then the corresponding boundary is heated, if $T = T_c$ then the boundary is cooled. If $T = \frac{\partial T}{\partial n} = 0$ then the boundary is adiabatic, which means that no heat is transferred through the boundary.

1.2.1 Mixed Convection Flow

Mixed convection is an important heat transfer mechanism and has many applications such as electronic cooling, drying, heat exchangers and insulation of buildings. It is the combination of forced and natural convection. When the effects of natural and forced convection are comparable neither of the process can be neglected. Thus, understanding the physics of this process is very important.

Two-dimensional mixed convection flows can be characterized by the buoyancy parameter Gr/Re^2, where Re is the Reynolds number and Gr is the Grashof number. This parameter measures the effect of the natural and forced convection on the fluid flow. Generally, mixed convection occurs on the range of $(Gr/Re^2)_{min} \leq Gr/Re^2 \leq (Gr/Re^2)_{max}$, where

$(Gr/Re^2)_{min}$ and $(Gr/Re^2)_{max}$ are the lower and the upper bounds of the regime. Outside this region, either the forced convection or the natural convection plays the role as a dominating mechanism. For a mixed convection flow, analyzing the effect of buoyancy forces is important since they may aid or oppose the flow and cause a decrease or increase in the heat transfer rates [8].

The two-dimensional equations of momentum (in stream function-vorticity formulation) and energy for a transient, laminar and incompressible mixed convection flow can be expressed as [62]

$$\nabla^2 \psi = -\omega$$

$$\frac{1}{Re}\nabla^2 \omega = \frac{\partial \omega}{\partial t} + u\frac{\partial \omega}{\partial x} + v\frac{\partial \omega}{\partial y} - \frac{Gr}{Re^2}\frac{\partial T}{\partial x} \qquad (1.25)$$

$$\frac{1}{RePr}\nabla^2 T = \frac{\partial T}{\partial t} + u\frac{\partial T}{\partial x} + v\frac{\partial T}{\partial y}$$

where the following dimensionless variables are defined

$$u = \frac{u'}{U'} \quad , \quad v = \frac{v'}{U'} \quad , \quad x = \frac{x'}{L'} \quad , \quad y = \frac{y'}{L'} \quad , \quad t = \frac{t'}{L'} \quad , \quad p = \frac{p'}{\rho\, U'^2} \quad , \quad T = \frac{\theta' - \theta'_c}{\theta'_h - \theta'_c}$$

in non-dimensionalizing.

Here, Gr is the *Grashof number* which approximates the ratio of the buoyancy and viscous forces, and defined by, [36]

$$Gr = \frac{g\beta(T_s - T_\infty)L'^3}{\nu^2} = \frac{Ra}{Pr}$$

where g is the acceleration due to Earth's gravity, β is the volumetric thermal expansion coefficient, T_s is the source temperature, T_∞ is the quiescent temperature, L' is the characteristic length, ν is the kinematic viscosity.

General expression of the boundary conditions can be given as

$$\psi(x_s, y_s) = f_{\psi_s} \quad , \quad \omega(x_s, y_s) = f_{w_s}$$

$$T(x_s, y_s) = f_{t_s} \quad , \quad \frac{\partial T}{\partial n}(x_s, y_s) = f_{t_n}.$$

12

Generally mixed convection occurs when $\dfrac{Gr}{Re^2} \approx 1$. Forced and natural convection are dominant when $\dfrac{Gr}{Re^2} \ll 1$ and $\dfrac{Gr}{Re^2} \gg 1$, respectively [43].

1.3   Nanofluids and Basic Equations

Nanofluids are made of nanoparticles suspended in a base fluid. They are studied because of their enhanced heat transfer capabilities. Typical nanoparticles are metal or metal oxide nanoparticles such as Al_2O_3, CuO, Cu, TiO. Generally water and ethylene glycol is used as the base fluid, [47].

Fluid heating and cooling are important in many industries such as power, manufacturing, transportation, and electronics. Especially, effective cooling techniques are greatly needed for cooling any sort of high-energy device. But, common heat transfer fluids, e.g. water, ethylene glycol, engine oil, have low heat transfer properties. Thus, their heat transfer capabilities are limited. On the other hand, thermal conductivities of metals are up to three times higher than these fluids. So, these substances are combined and a new heat transfer medium, which behaves like a fluid but has the thermal conductivity of the metal, is produced.

In general, nanofluids contain up to a %5 volume fraction of nanoparticles. Even at low concentrations, they significantly increase heat transfer rates. Thermal conductivity enhancements are in the range of %15 − 40 over the base fluid. Increase in heat transfer rate can not just be explained from the thermal conductivity of the added nanoparticles [47]. The main reasons may be listed as follows [91].

• The suspended nanoparticles increase the surface area and the heat capacity of the fluid.

• The suspended nanoparticles increase the effective thermal conductivity of the fluid.

• The interaction and collision among particles, fluid and the flow passage surface are intensified.

• The mixing fluctuation and turbulence of the fluid are intensified.

• The dispersion of nanoparticles flattens the transverse temperature gradient of the fluid.

The non-dimensional, unsteady equations of motion and energy for nanofluids can be written

in terms of stream function (ψ), vorticity (ω) and temperature (T) as follows [3]

$$\nabla^2 \psi = -\omega$$

$$\frac{\mu_{nf}}{\rho_{nf}\alpha_f}\nabla^2\omega = \frac{\partial\omega}{\partial t} + u\frac{\partial\omega}{\partial x} + v\frac{\partial\omega}{\partial y} - RaPr\frac{(\rho\beta)_{nf}}{\rho_{nf}\beta_f}\frac{\partial T}{\partial x} \qquad (1.26)$$

$$\frac{\alpha_{nf}}{\alpha_f}\nabla^2 T = \frac{\partial T}{\partial t} + u\frac{\partial T}{\partial x} + v\frac{\partial T}{\partial y}$$

where $(x, y) \in \Omega \subset R^2$, $t > 0$. *Ra* and *Pr* are the Rayleigh number and Prandtl number. The subscripts 'nf', and 'f' refer to nanofluid and pure fluid, respectively.

Non-dimensional forms of the equations are obtained by introducing the following dimensionless parameters [3]

$$u = \frac{u'L'}{\alpha_f} \quad , \quad v = \frac{v'L'}{\alpha_f} \quad , \quad x = \frac{x'}{L'} \quad , \quad y = \frac{y'}{L'} \quad , \quad t = \frac{t'}{L'} \quad , \quad p = \frac{p'L'^2}{\rho_{nf}\alpha_f{}^2} \quad , \quad T = \frac{\theta' - \theta'_c}{\Delta T}$$

$$Ra = \frac{g\beta_f\Delta T\, L'^3}{\alpha_f\, \nu_f} \quad , \quad Pr = \frac{\nu_f}{\alpha_f} \quad , \quad \Delta t = \frac{q''\, L'}{k_f}$$

where q'' is the heat generation per area, and k_f is the thermal conductivity of the fluid.

The effective dynamic viscosity [24] and the effective density [61] of the nanofluid are given by

$$\mu_{nf} = \frac{\mu_f}{(1-\varphi)^{2.5}} \quad , \quad \rho_{nf} = (1-\varphi)\rho_f + \varphi\rho_s$$

where φ is the volume fraction of nanoparticles, μ_f is the dynamic viscosity of the fluid, ρ_f and ρ_s are the density of the fluid and nanoparticle, respectively.

Thermal diffusivity of the nanofluid is defined by, [63]

$$\alpha_{nf} = \frac{k_{nf}}{(\rho C_p)_{nf}}.$$

Here k_{nf} is the thermal conductivity of the nanofluid given by, [54]

$$k_{nf} = k_f\frac{k_s + 2k_f - 2\varphi(k_f - k_s)}{k_s + 2k_f + \varphi(k_f - k_s)}$$

where the subscript 's' refer to nanoparticle.

It is important to note that the effective thermal conductivity of nanofluids depends on the thermal conductivity of solid particles and base fluid, particle volume fraction, shape of particles and the thickness of the thermal conductivity of nanolayer [47].

The heat capacitance of the nanofluid and part of the Boussinesq term are defined as [61]

$$(\rho C_p)_{nf} = (1 - \varphi)(\rho C_p)_f + \varphi(\rho C_p)_s$$

$$(\rho \beta)_{nf} = (1 - \varphi)\rho_f \beta_f + \varphi \rho_s \beta_s.$$

The local and average Nusselt numbers for the wall with constant heat flux are given as in [40]

$$Nu = -\frac{k_{nf}}{k_f} \frac{\partial T}{\partial x}\Big|_{heated\ vertical\ wall} \quad , \quad Nu_{av} = \int_0^1 Nu\, dy\,.$$

The equations in (1.26) are supplied with the initial conditions

$$\omega(x, y, 0) = \omega_0(x, y) \quad , \quad T(x, y, 0) = T_0(x, y)$$

where $\omega_0(x, y)$ and $T_0(x, y)$ are given functions of space and time.

Corresponding boundary conditions are given by

$$\psi(x_s, y_s) = f_{\psi_s} \quad , \quad \omega(x_s, y_s) = f_{\omega_s}$$

$$T(x_s, y_s) = f_{t_s} \quad \text{or} \quad \frac{\partial T}{\partial n}(x_s, y_s) = f_{t_n}.$$

The velocity components are given in terms of stream function as $u = \dfrac{\partial \psi}{\partial y}, \quad v = -\dfrac{\partial \psi}{\partial x}, \quad$ and the vorticity is defined by $\omega = \dfrac{\partial v}{\partial x} - \dfrac{\partial u}{\partial y}.$

1.4   Micropolar Fluids and Basic Equations

In the previous sections, we use the Navier-Stokes equations to model two-dimensional, laminar, transient flow of an incompressible fluid. But this model is inadequate for fluids with microstructure such as polymeric suspensions, blood and liquid crystals. In order to describe the behaviour of such fluids, we need a model that takes into account geometry and movement of these microstructures [52].

15

Eringen [31] generalized the Navier-Stokes equations and introduced a model for micropolar fluids. In this model, only one equation is added to the Navier-Stokes equations. This equation represents the conservation of angular momentum and describes the rotation of microparticles. When the viscosity of the microrotation is zero, then the fluid becomes independent from the presence of the microstructure. Thus, the microrotation viscosity measures the deviation of the micropolar fluid model from the Navier-Stokes model, [52].

The non-dimensional, unsteady equations of motion, energy and microrotation can be written in terms of stream function, vorticity, temperature and microrotation as follows [9, 10]

$$\nabla^2 \psi = -\omega$$

$$(1+K)\nabla^2\omega = \frac{\partial \omega}{\partial t} + u\frac{\partial \omega}{\partial x} + v\frac{\partial \omega}{\partial y} + K\nabla^2\bar{N} - \frac{Ra}{Pr}\frac{\partial T}{\partial x}$$

$$\frac{1}{Pr}\nabla^2 T = \frac{\partial T}{\partial t} + u\frac{\partial T}{\partial x} + v\frac{\partial T}{\partial y}$$ (1.27)

$$\left(1+\frac{K}{2}\right)\nabla^2\bar{N} = \frac{\partial \bar{N}}{\partial t} + u\frac{\partial \bar{N}}{\partial x} + v\frac{\partial \bar{N}}{\partial y} + 2K\bar{N} - K\omega$$

where K is the material parameter and $\bar{N}$ is the component of the microrotation vector normal to the xy-plane. It is noticed that the microrotation equation is also convection diffusion type in nature for the microrotation $\bar{N}$. Microrotation $\bar{N}$ represents the angular velocity of rotation of particles of the fluid.

Non-dimensional forms of the equations are obtained by introducing the following dimensionless parameters [9]

$$u = \frac{u'L'}{\nu} \quad , \quad v = \frac{v'L'}{\nu} \quad , \quad x = \frac{x'}{L'} \quad , \quad y = \frac{y'}{L'} \quad , \quad t = \frac{t'\nu}{L'^2} \quad , \quad T = \frac{\theta' - \theta_0'}{\theta_h' - \theta_c'}$$

$$\bar{N} = \frac{N'L'^2}{\nu} \quad , \quad \omega = \frac{\omega'L'^2}{\nu} \quad , \quad \gamma = \left(\mu + \frac{k'}{2}\right)j = \mu\left(1 + \frac{K}{2}\right)$$

where γ is the spin gradient viscosity, j is the microinertia density, and $\theta_0' = \dfrac{\theta_h' + \theta_c'}{2}$ is the characteristic temperature.

Equations (1.27) are supplied with the initial conditions

$$\omega(x,y,0) = \omega_0(x,y) \quad , \quad T(x,y,0) = T_0(x,y) \quad \text{or} \quad \bar{N}(x,y,0) = \bar{N}_0(x,y)$$

16

and Dirichlet or Neumann type boundary conditions

$$\psi(x_s, y_s) = f_{\psi_s} \quad , \quad \omega(x_s, y_s) = f_{w_s}$$

$$T(x_s, y_s) = f_{t_s} \quad , \quad \frac{\partial T}{\partial n}(x_s, y_s) = f_{t_n}$$

$$\bar{N}(x_s, y_s) = \bar{n}\frac{\partial v}{\partial x} \quad \text{or} \quad \bar{N}(x_s, y_s) = -\bar{n}\frac{\partial u}{\partial y}.$$

where $\bar{n}$ is a constant ($0 \leq \bar{n} \leq 1$). The case $\bar{n} = 0$ indicates $\bar{N} = 0$ on the boundary, which means that the microelements close to wall surface are unable to rotate. The case $\bar{n} = 1/2$ indicates the vanishing of anti-symmetric part of the stress tensor and denotes weak concentration. The case $\bar{n} = 1$ is used for modeling of turbulent boundary layer flows [9].

Here, $\omega_0(x, y)$, $\bar{N}_0(x, y)$ are known functions and $T_h(T_c)$ is known value of the temperature (hot or cold). The vorticity boundary conditions are either derived from the definition of vorticity, $\omega = \frac{\partial v}{\partial x} - \frac{\partial u}{\partial y}$ or from the Taylor series expansion of stream function through the relation $\nabla^2\psi = -\omega$.

For $K = 0$, stream function, vorticity transport and energy equations are reduced to the classical problem of natural convection of a Newtonian fluid in a differentially heated rectangular enclosures [9, 29].

1.5   Literature Survey

The lid-driven cavity flow of a Newtonian fluid has attracted much interest for a long time and several methods have been developed. Majority of the papers dealing with the numerical solution to the lid-driven cavity problem have been concerned with the two-dimensional problem.

In the early study of Bercovier and Engelman [18], a finite element of the penalization type for the solution of incompressible viscous Navier-Stokes equations using an isoparametric parabolic element is presented. The cavity problem is solved for $Re = 1000$ with a step size of $h = 1/12$ and a total of 625 nodal points. A novel implicit cell-vertex finite volume method is described for the solution of the Navier-Stokes equations at high Reynolds numbers by Şahin and Owens [71]. The method is applied to both steady and unsteady flows at

Reynolds numbers up to 10000. They used (257×257) mesh in order to simulate the flow for high Reynolds numbers. Two-dimensional near-incompressible steady lid-driven cavity flows ($Re = 100 - 7500$) are simulated using multi-relaxation-time (MRT) model in the parallel lattice Boltzmann Bhatnager-Gross-Krook (LBGK) method by Wu and Shao [89]. A consistent splitting scheme is used to solve unsteady Navier-Stokes problem by Wong and Chen [88]. Time derivative is discretized by a fully implicit second-order backward differentiation formula. To verify the convergence rate they select the grid range from (65×65) to (513×513). They observed that when the grid size is not fine enough, a reduction of the time step parameter does not enhance the accuracy. For high Reynolds number time step is selected as 0.0005. A new meshless numerical method for the incompressible flows using the radial basis functions is studied in [94]. They introduced several radial basis functions depending on the parameters α and β which should be chosen carefully. The collocation matrix might tend to be singular if α is too large and would be limited if α is too small. At the same time, the parameter β had better not be an integer. Chen *et.al.* [27] studied numerical solution of vorticity-stream function formulation of the Navier-Stokes equations using a lattice Boltzmann model. They solved the one-sided lid-driven cavity problem for ($50 \leq Re \leq 2000$) with the grid resolution (100×100). For higher Re, they used a finer grid. Time step is taken as 0.001 and iteration numbers are 2200, 4500 and 6100, respectively for $Re = 50, 400$ and 1000. In another study [32] the widely studied benchmark problem, two-dimensional-driven cavity flow problem is discussed in detail in terms of physical and mathematical and also numerical aspects. A very brief literature survey on studies on the driven cavity flow is given.

Onishi *et.al.* [60] studied the boundary element method (BEM) solution of two-dimensional Navier-Stokes equations using stream function-vorticity formulation. They showed that larger time increment can be used in BEM. In another study Sarler and Kuhn [72] used the dual reciprocity BEM to solve transient incompressible two-dimensional Navier-Stokes equations in primitive variables. They solved the driven cavity problem for $Re = 100$ only, using constant elements. The time derivative is discretized by forward difference method and Δt is taken as 0.001. In a recent study, Choi and Balaras [28] applied DRBEM to solve the unsteady Navier-Stokes equations, where a fractional step algorithm is utilized for the time advancement. A fully implicit second order Adams-Bashforth scheme is used for the nonlinear convective terms. They could able to solve the lid-driven cavity flow up to $Re = 400$. For $Re = 100$, time step is set to 0.001 for 40 and 80 boundary elements, and $\Delta t = 0.0005$ for 160 boundary

elements. For $Re = 400$, time step is set to 0.0001 for 40 and 80 boundary elements and $\Delta t = 0.00005$ for 160 boundary elements.

The vorticity-stream function formulation of the two-dimensional, incompressible Navier-Stokes equations is used to study the effectiveness of the coupled strongly implicit multigrid (CSI-MG) method in the determination of high-Re, fine-mesh flow solutions by Ghia *et.al.* [35]. The driven flow in a square cavity is used as the model problem. Solutions are obtained for configurations with Reynolds number as high as 10000 and meshes consisting of as many as (257×257) points. For $Re = 1000$, the (129×129) grid solution required. An automatic adaptive refinement technique has been coupled to the multigrid approach to produce an efficient and stable solution strategy for solving the steady-state incompressible Navier-Stokes equations by Thompson and Ferziger [82]. Solutions have been obtained for the driven cavity and flow over a backward-facing step, for Reynolds numbers up to 5000 and 800, respectively. The refinement criterion is based on the local truncation error. Mansour and Hamed [53] presents an implicit procedure for the solution of the incompressible Navier-Stokes equations in primitive variables. The time dependent momentum equations are solved implicitly for the velocity field using the approximate factorization technique. A consistent finite-difference scheme which satisfies the compatibility condition using a non-staggered grid is used in the finite difference approximation of the static pressure Poisson equation. Numerical results obtained for the steady state static pressure in the driven cavity are presented at $Re = 1000$ using a non-staggered grid.

Natural convection heat transfer in enclosures has been of considerable research interest in recent years due to the coupling of fluid flow and energy transport. Most of the previous studies on natural convection in enclosures have been related to Newtonian fluids. An excellent review article is given by De Vahl Davis and Jones [30]. Their study summarizes and discusses the main features of the contributions and provides a quantitative comparison between them. They used central difference for the spatial derivatives and forward difference for the time derivative. Natural convection of air in a square cavity is studied by De Vahl Davis [29]. Again the combination of the central and forward difference methods is used for the solution of the problem. In order to obtain a better accuracy an extrapolation scheme is used by fixing the mesh size and taking different time increments. $\Delta t = 0.025$, 0.016 and 0.0125 are used for (21×21) matrices. Smaller time increments are used for finer meshes.

Shu and Xue [79] studied the natural convection in a square cavity using the vorticity-stream function formulation of the Navier-Stokes and energy transport equations as the governing equations. They introduce two approaches to implement the boundary conditions of stream function in generalized DQ (GDQ) simulation. In their study, the optimum time step size was found through a trial-and-error process. They observed that the optimum time step size for the two-layer approach is almost twice as large as that for the one-layer approach. They used time increment between $1.0 \times 10^{-3} - 2.8 \times 10^{-4}$ for $Ra = 10^3 - 10^6$. As the Rayleigh number increases they used finer meshes and small time increments. In another work Shu and Wee [80] studied the Navier-Stokes equations in primitive variable form by using the GDQ method with SIMPLE strategy. They propose a new approach to enforce the continuity condition on the boundary and implement boundary condition for pressure correction equation. They compared the method with the FD method in terms of run times and mesh sizes and observed that SIMPLE-GDQ method needs smaller mesh sizes and shortens run times. The study of Lo *et.al.* [51] represented a numerical algorithm which has been implemented to analyze natural convection in a differentially heated cavity. In their study, differential quadrature method has been used to obtain accurate numerical results while solving the velocity-vorticity form of the Navier-Stokes equations. The time derivative is discretized using a second order finite difference scheme. They obtained the results for the range of Rayleigh number $10^3 - 10^7$. They used (21×21), (25×25) and (31×31) mesh sizes for $Ra = 10^3 - 10^6$, and the time increment varies between 0.01 and 0.00002.

A penalty finite element analysis with bi-quadratic rectangular elements is performed to investigate the influence of uniform and non-uniform heating of wall(s) on natural convection flows in a square cavity by Roy and Basak [70]. They considered steady case of primitive variable formulation. Numerical solutions are obtained for $Ra = 10^3 - 10^5$. Sathiyamoorthy *et.al.* [75] studied the natural convection flow in a closed square cavity when the bottom wall is uniformly heated and vertical wall(s) are linearly heated whereas the top is well insulated. The non-linear coupled PDEs governing the flow have been solved by penalty finite element method with bi-quadratic rectangular elements. Basak *et.al.* [13] studied natural convection flow in a triangular enclosure using finite element method. The problem is solved for Rayleigh number $10^3 - 10^5$ with a mesh size (41×41). They investigate the effects of increasing Rayleigh and Prandtl number on the heat transfer rates and observe that Rayleigh number has stronger effect on heat transfer rate. Natural convection in a two-dimensional, rectangu-

lar enclosure with sinusoidal temperature profile on the upper wall and adiabatic conditions on the bottom and sidewalls is numerically investigated by Sarris *et.al.* [73]. The governing equations are solved using the finite volume method. The mesh size is taken as (61×61). They observed that the values of the maximum and minimum local Nusselt number at the upper wall are increased with increasing Rayleigh number. Barletta *et.al.* [12] presented a numerical study of natural convection in a 2-D enclosure. The governing equations are solved by means of two different software packages based on Galerkin finite element methods. The steady problem is solved for the Rayleigh number between $10^3 - 10^5$. The results show that elliptic boundaries enhance the mean Nusselt number and the dimensionless mean kinetic energy of the fluid.

Natural convection from two-dimensional discrete heat sources in a rectangular enclosure is investigated by Chadwich *et.al.* [26]. The governing equations are solved using a control volume based finite difference technique. The results show that for the single heat source configuration heater locations closer to the bottom of the enclosure yield the highest heat transfer. A finite difference approximation of the Navier-Stokes equations under the Boussinesq-fluid assumption is used to simulate the flow and heat transfer in a two-layer system of an immiscible incompressible fluid by Moshkin [55]. For the parameters used in the numerical and physical experiments a strict correlation between downward and upward flows is observed for the upper and lower layers. The results indicate only qualitative agreement with the experimental data. There are differences in the obtained numerical and physical simulations. Volgin *et.al.* [84] simulate ion transfer under conditions of natural convection by the finite difference method. In order to estimate the efficiency of the method, experiments are performed. They observed that an increase in the region's width leads to an increase in the critical Rayleigh number.

Steady natural convection of air in a two-dimensional enclosure isothermally heated from one side and cooled from the ceiling is analyzed numerically using a stream function-vorticity formulation by Aydın *et.al.* [6]. The vorticity transport and energy equations are solved using the alternating direction implicit method, and the stream function equation is solved by successive over relaxation method. They used a uniform grid of (41×41) points in the computations. For each aspect ratio it is found that a clockwise rotating single cell exists for $Ra \leq 10^6$. They also studied buoyancy-driven laminar flow in an inclined square enclosure heated from one side and cooled from the adjacent side using the same methods, [7]. They

determined the critical values of the inclination angle at which the rate of heat transfer within the enclosure is either maximum or minimum. The time step used in the calculations is varied between 0.004 and 0.00001, depending on Rayleigh number with a nonuniform mesh size (31×31). The Allen discretization scheme is employed to solve steady natural convection in an enclosure heated from below and symmetrically cooled from the sides by Ganzarolli and Milanez [33]. (61×61) and (91×91) grid points are used in the calculations. For the range of parameters studied, a single cell is observed to represent the flow pattern, except for a small secondary cell due to viscous drag observed in some cases for uniform temperature at the cavity floor. A double-population lattice Boltzmann method with non-uniform mesh is used for the simulation of natural convection in a square cavity is studied by Kuznik *et.al.* [50]. The problem is solved for the range of $Ra = 10^3 - 10^8$ with mesh sizes (64×64) - (256×256). The transition from the motionless conduction dominated regime to the convection dominated regime takes place after $Ra = 10^3$.

Aiding and opposing mechanisms of mixed convection in a shear-and buoyancy-driven cavity is studied by Aydın [8]. The focus was on the interaction of the forced convection induced by the moving wall with the natural convection induced by the buoyancy. The ADI is used to solve the vorticity and energy equations, and SOR is used to solve stream function equation. A non-uniform grid system of (31×31) points is adopted. Three different heat transport regimes were defined with the increasing value of Gr/Re^2, namely; the forced convection, the mixed convection and the natural convection. Öztop and Dağtekin [62] studied mixed convection in two-sided lid-driven differentially heated square cavity. The discretization procedure is based on finite control volume using the non-staggered grid arrangement with the SIMPLEM algorithm. (61×61) grid points are used. An under-relaxation parameter of 0.5 is used in order to obtain a stable convergence for the solution of momentum and energy equations. About 2000 iterations were required to obtain the convergence.

Heat transfer enhancement in a two-dimensional enclosure utilizing nanofluids is investigated for various pertinent parameters by Khanafer *et.al.* [48] using finite-volume approach along with the alternating direction implicit method. They analyze the effect of suspended ultrafine metallic nanoparticles on the fluid flow and heat transfer processes within the enclosure. They used an equally spaced mesh of (61×61).

Stream function-vorticity formulation of the transport equations are solved using finite differ-

ence method in [46]. A uniform grid of (61×61) points is used for the calculations. Numerical predictions show the enhancement is critical for nanofluids than pure fluids. They observe that increasing the buoyancy parameter and volume fraction of nanofluids causes an increase in the average heat transfer coefficient. Moreover, for large Rayleigh number values, the effect of free convection is dominated by the buoyancy parameter due to accelerating the flow within the boundary-layer near the wall from the buoyancy force generated in rectangular enclosures.

Tiwari and Das [83] investigated the behaviour of nanofluids inside a two-sided lid-driven differentially heated square cavity using finite volume method. A grid number of (61 × 61) is chosen for computations. They conclude that the nanoparticles immersed in a fluid are capable of increasing the heat transfer capacity of the base fluid. As volume fraction increases, the effect is more pronounced. The variation of average Nusselt number is nonlinear with solid volume fraction. Effect of copper-water nanofluid as a cooling medium has been studied to simulate the behavior of heat transfer due to laminar natural convection in a differentially heated square cavity in [74] using finite volume approach. The computational domain has been divided into (81 × 81) non-uniform grids. Finer grids have been taken at the boundaries. They observed that the heat transfer decreases with increase in volume fraction for a particular Rayleigh number. Numerical simulation of natural convection of nanofluids in a square enclosure is studied by Ho *et.al.* [40] using finite volume method. To ensure the grid convergence of the numerical solutions, different meshes varying from (61 × 61) to (161 × 161) have been employed. Results demonstrate that the uncertainties associated with different formulas adopted for the effective thermal conductivity, and dynamic viscosity of the nanofluid have a strong bearing on the natural convection heat transfer characteristics in the enclosure. Öztop and Abu-Nada [63] studied heat transfer and fluid flow due to buoyancy forces in a partially heated enclosure using different types of nanoparticles. Finite volume method is used to solve the transport equations. It was found that the heater location effects the flow and temperature fields when using nanofluids. The resulted algebraic equations are solved using successive under/over relaxation method. The problem is solved for the range of Rayleigh number $10^3 - 10^5$ with a grid size of (51 × 51). They also studied effects of inclination angle on natural convection in enclosures filled with copper water nanofluid [1]. In another study, Aminossadati and Ghasemi [3] studied natural convection cooling of a localized heat source at the bottom of a nanofluid-filled enclosure using finite volume method. They used (60 × 60) grid points. The results indicate that adding nanoparticles into pure water improves its cooling performance

especially at low Rayleigh numbers. The type of nanoparticles and the length and location of the heat source proved to significantly affect the heat source maximum temperature.

In a recent study, natural convection heat transfer of water-based nanofluids in an inclined enclosure with a heat source is investigated by Öğüt [61]. The governing equations are solved using polynomial differential quadrature method. (31×31) and (51×51) grid points are used for increasing values of the heater length. The computational results were obtained by the successive over-relaxation iteration method. It is observed that the average heat transfer decreases with an increase in the length of the heater.

Hsu and Chen [41] numerically investigated the natural convection of a micropolar fluid in an enclosure heated from below using the cubic spline collocation method. They studied the effects of microstructure on the convective heat transfer and found that heat transfer rate of micropolar fluids was smaller than that of the Newtonian fluid. The grid fineness (21×21) was selected to provide accurate results for the problems which are solved for $Ra = 10^4$ and 10^5. In another work, Hsu *et.al.* [42] studied natural convection of micropolar fluids in an enclosure with isolated heat sources. The coupled equations are solved by the cubic spline alternating direction implicit procedure. An arrangement of (21×21) nonuniform mesh size is used. However, a finer mesh size is needed for large Raleigh number. They observed that the heat transfer rate is sensitive to the microrotation boundary conditions and the average Nusselt number is lower for a micropolar fluid, as compared to a Newtonian fluid. Aydın and Pop [9], numerically investigated the steady natural convective heat transfer of micropolar fluids in a square cavity with differentially heated vertical walls and adiabatic horizontal walls using the finite difference method. The vorticity, energy and microrotation equations are solved using the alternating direction implicit method, and the stream function equation is solved by the successive over relaxation method. The time step varied between 0.00001 and 0.004 with a (31×31) non-uniform and non-staggered grid structure. They also studied the steady laminar natural convective flow and heat transfer of micropolar fluids in enclosures with a centrally located discrete heater in one of its sidewalls by applying the same methods [10]. They found that the average Nusselt number increases with increasing Rayleigh number, and an increase in the material parameter reduces the heat transfer.

The effect of microstructure on the thermal convection in a rectangular box of fluid heated from below has been investigated by Jena and Bhattacharyya [45]. The problem is solved

using Galerkin method. They observed that as the distance between the lateral walls increases the effect of one of the material parameters, characterizing the spin-gradient viscosity, at the onset of stability diminishes. The steady flow of a micropolar fluid between two infinite discs, when one is held at rest and the other rotating with constant angular velocity is studied by Anwar and Guram [4]. The equations of motion are reduced to a system of ordinary differential equations, which in turn is solved numerically using the Gauss-Seidel iterative procedure and Simpson's rule. Time step is taken as 0.025 and 0.0125 in the computations. Kumari and Nath [49] solved unsteady incompressible boundary layer flow of a micropolar fluid at a stagnation point using a quasilinear finite-difference scheme. They observed that the skin friction, microrotation gradient and heat transfer parameters are strongly dependent on the coupling parameter, mass transfer and time, whereas the effect of the microrotation parameter on the skin friction and heat transfer is rather weak, but microrotation gradient is strongly affected by it. Stagnation flow of micropolar fluids with strong and weak interactions is studied by Guram and Smith [37]. The equations of motion are reduced to dimensionless forms which include three dimensionless parameters, and integrated numerically by a Runge-Kutta method.

In a recent study, Zadravec *et.al.* [95] studied numerical simulation of natural convection in micropolar fluids, describing flow of suspensions with rigid and underformable particles with own rotation. They have used boundary element method on the velocity-vorticity form of the Navier-Stokes equations. They found that microrotation of particles in suspension in general decreases overall heat transfer from the heated wall and should not therefore be neglected when computing heat and fluid flow of micropolar fluids.

Ramesh and Lean [69] studied stability of the multiple reciprocity method for transient heat conduction. They consider the numerical stability of the approach through an eigenvalue decomposition of the system matrix. They demonstrate that the multiple reciprocity method for transient heat conduction is stable only for appropriately chosen time steps. Stability analysis for boundary element methods for the diffusion equation is studied by Sharp [77]. It is observed that decreasing progressively the time step in boundary element solutions of the diffusion equation deteriorates the quality of the approximation and indicates a state of instability. In another study, Peratta and Popov [68] studied numerical stability of the BEM for advection-diffusion problems. They present two different one-dimensional BEM formulations for solution of the advection-diffusion problems. Then, they extended their analysis to three-

dimensional problems.

1.6 Plan of The Thesis

In this thesis, we have solved first the two-dimensional, unsteady, laminar flow of viscous and incompressible fluid governed by the Navier-Stokes equations in terms of stream function and vorticity. The DRBEM has been used for transforming the differential equations to boundary integrals by using the fundamental solution of Laplace equation which is rather simple compared to the whole equations. The nonlinearities are considered as inhomogeneity in the equations. Only the boundary of the region is discretized by using constant and linear elements, and some selected interior points are taken in DRBEM for obtaining solution behaviour. Thus, the computational cost is much smaller than the domain discretization methods. Then, the energy equation which is of the same type of vorticity equation has been added for solving natural and mixed convection flows in cavities.

Natural convection flows of nanofluids and micropolar fluids have been also solved easily by using DRBEM since all the other terms in the equations can be taken as inhomogeneous terms. The derivatives in the convective terms are calculated with the help of the coordinate matrix.

Three different time integration methods are used for discretization of the time derivatives in DRBEM discretized vorticity, energy and microrotation equations. The forward and central finite difference schemes are used with relaxation parameters to accelerate the convergence to steady-state. The fourth-order Runge-Kutta method is modified for bringing 'm+1' and 'm' iteration levels to both the unknown and its normal derivative in the final discretized equations. This is required in the DRBEM resulted equations which contain both the problem variable and its normal derivative as unknowns.

In the computations we have used $80 - 120$ boundary elements and quite large time increments as $0.1 - 0.8$ for solving Navier-Stokes equations for considerably large values of Reynolds number. The one-sided and two-sided lid-driven cavity flow problems are solved with very good accuracy and small computational cost compared to the results in the literature.

The natural and mixed convection flows in cavities for different configurations of heated and

cooled walls have been solved by using $60 - 100$ boundary elements and the smallest time increment used was 0.0005. As *Re* or *Ra* increases we need to take large number of boundary elements and smaller time increments. The central difference time integration scheme has been used with relaxation parameter around 0.9. Numerical solutions of natural convection flows of nanofluids and micropolar fluids in enclosures have been obtained for *Ra* values between 10^3 and 10^6, and for several values of problem constants, again by using at most 100 linear boundary elements and at least $\Delta t = 0.001$ for increasing values of *Ra*.

Most of the numerical solution procedures for natural convection flows of nanofluids and micropolar fluids are based on finite difference and finite volume methods. These are domain discretization techniques and result with huge number of system of equations to be solved. The boundary element solution given by Zadravec *et.al.* [95] also is a direct BEM which includes domain integrals due to the source terms in the equations. The DRBEM enables one to obtain boundary integrals for the differential equations used and discretizes the boundary of the domain only. Thus, the size of the resulting system of equations is considerably small compared to all the domain discretization methods. The DRBEM solutions of natural convection flows of nanofluids and micropolar fluids are given in this thesis which are not available in the literature.

We also investigate the numerical stability of the DRBEM solution of flow problems in the thesis following the references [44, 69]. Since the BEM solutions contain both the problem variable and its normal derivative, stability analysis is modified to take into care of this case. The stability analysis developed depends on the choice of the relaxation parameters and the time increment. Once they are chosen properly, the DRBEM is capable of solving all the flow problems considered in this thesis and the solutions are stable.

Chapter 1 gives the governing equations for unsteady, laminar flow of incompressible, viscous fluid together with the energy transport phenomena. The related boundary conditions for lid-driven cavity flow, and natural and mixed convection flows in enclosures are also described. Heat transfer enhancement in enclosures utilizing nanofluids is described and related equations are given with the physical explanations of coefficient parameters. Finally, equations for natural convection flow of micropolar fluids are provided for several configurations of heated walls in enclosures.

In Chapter 2, we explain the dual reciprocity boundary element method on the general Poisson

equation. Boundary discretization is made using both constant and linear elements. Application of DRBEM gives rise to a system of first order differential equations in time. The time derivative is discretized using three different time integration methods, namely, the forward and central difference methods with relaxation parameters, and fourth order Runge-Kutta method.

Chapter 3 presents the DRBEM solutions of fluid flow problems. The governing equations of laminar, transient and viscous flow of incompressible fluid (Navier-Stokes equations) are formulated in non-dimensional form. Then, the application of the method is given on three test problems considering different geometries and physical configurations. The solutions are given in terms of streamlines, vorticity contours as well as the velocity profiles. In the next sections, application of the DRBEM is extended to solve the natural and mixed convection flows and natural convection flow of nanofluids by adding the energy equation to the Navier-Stokes equations. Several test problems are solved on each type of fluid flow. Finally, the method is applied to the solution of the natural convection flow of micropolar fluids in which an additional equation, namely the microrotation equation is used together with the Navier-Stokes and energy equations. Two test problems considering different configurations in each enclosure are considered.

In Chapter 4, we introduce the numerical stability analysis of each type of fluid flow considered in the previous chapter. For all the problems, we showed that the DRBEM solution with FDM time discretization of these flows are stable with the chosen values of time step and relaxation parameters, and the constants of the problems. These are shown with the tables consisting of maximum eigenvalues for vorticity, energy and microrotation equations.

Chapter 5 gives the overall conclusion for the methods and numerical results obtained in the thesis.

CHAPTER 2

THE BOUNDARY ELEMENT METHOD AND THE DUAL RECIPROCITY BOUNDARY ELEMENT METHOD

The boundary element method (BEM) is a numerical technique, which becomes popular over the last two decades, and is an alternative method for the solution of partial differential equations. The main advantage of the BEM is providing a complete solution in terms of boundary values only and savings in the computing effort. Especially for homogeneous PDEs only boundary discretization is necessary. In this method, a boundary integral equation equivalent to the original partial differential equation is derived, and the integral equation is solved discretizing the boundary. This approach reduces the dimension of the problem and permits accurate solutions which are obtained efficiently. This can be thought as the other advantage of the method [21].

When BEM is applied to an inhomogeneous PDE the integral equation involves a domain integral, and the dimension of the problem is not reduced. Therefore, the advantage of the method is lost. There are several methods to deal with this problem but the most successful is the Dual Reciprocity Method (DRM) [65, 66]. In this method, the solution is divided into two parts. The first part is a known particular solution of the inhomogeneous partial differential equation (usually elliptic type) and the second part is a complementary solution of its homogeneous counterpart. Approximate particular solutions can be easily determined when the inhomogeneity is expressed by a series expansion in terms of simpler approximating or interpolating functions which are in turn related to the Laplace equation. Thus, DRBEM applies to the Laplace operator on both sides of the equation. DRBEM can also be applied to time-dependent diffusion problems [86, 87], non-linear problems, and convection-diffusion problems by treating all these terms as inhomogeneity.

29

The BEM, like the Finite Element Method (FEM) and many other numerical methods, can be obtained as a special case of the general weighted residual statement. There are several books on the BEM which are introductory books concentrating on potential and elasticity problems [14, 38, 64]. Recent books have also concentrated on the computational aspects of the BEM [15, 34]. The textbooks of [2, 11, 22], represent the comprehensive work on the BEM and its applications in the various fields of engineering science.

The BEM can be applied to many engineering problems such as creep and fracture problems on solid mechanics, fluid mechanics, inelastic problems, the potential theory, potential fluid flow, acoustics, torsion of shafts, electric and magnetic field theory, elastostatics, elastodynamics, plates and shells, transient heat conduction, visco-elasticity, fracture, plasticity, water waves, viscous fluid flow, ground water flow, Navier-Stokes flow, wave propagation, thermo-elasticity and other time dependent problems [20].

In this chapter, the basic theory of BEM and DRBEM are given. BEM and DRBEM for Poisson equation are explained in Sections 2.1 and 2.2 following the references [21, 65], respectively. Then, in Sections 2.3, 2.4 and 2.5 the method is extended to a more general form where right-hand side includes a function of position, time, the time and space derivatives of the unknown function and a function containing unknown itself. Thus, the right-hand side function may include a non-linear term. In the solution procedure, the spatial derivatives are discretized by using DRBEM in which the fundamental solution of Laplace equation is used. The resulting DRBEM matrices are in terms of integrals of logarithmic function and its normal derivative, which can be computed easily and accurately, either theoretically (constant element case) or numerically (higher order elements). The right-hand side function is approximated by using linear radial basis functions. Application of DRBEM to transient problems gives rise to a first order time-dependent system of ordinary differential equations (ODE). These system of ODEs are then solved with two different time integration methods, namely finite difference method (FDM) and Runge-Kutta method (RKM), which are explained in Section 2.6. These methods are used to discretize the time derivative in order to see the advantages and disadvantages of the methods and make a comparison among them.

We will apply DRBEM in Chapter 3 to solve unsteady laminar viscous flow of incompressible fluids (Navier-Stokes equations), natural convection flow, mixed convection flow, natural convection flow of nano and micropolar fluids. The governing equations of these problems in-

clude inhomogeneous terms. It is difficult and not practical to handle the inhomogeneity with the other numerical methods since the domain discretization is required. But, in DRBEM these terms are approximated using radial basis functions and kept on the right hand side. Convective terms can also be handled easily with this approach by approximating them using radial basis functions.

2.1 BEM solution of Poisson's Equation $\nabla^2 u = b(x, y)$

In this section, boundary integral equation required by the method is going to be derived for the Poisson equation as in [21, 65] using weighted residuals. The Poisson equation in a two-dimensional domain is

$$\nabla^2 u(x, y) = b(x, y) \quad , \quad (x, y) \in \Omega \tag{2.1}$$

supplied with the Dirichlet and Neumann boundary conditions (Fig. (2.1))

$$u(x, y) = \bar{u}(x, y) \quad , \quad (x, y) \in \Gamma_1$$

$$\tag{2.2}$$

$$q(x, y) = \bar{q}(x, y) \quad , \quad (x, y) \in \Gamma_2$$

where $\bar{u}(x, y)$ and $\bar{q}(x, y)$ are given functions. The domain $\Omega \in R^2$ is bounded by a piecewise smooth boundary $\Gamma = \Gamma_1 + \Gamma_2$. $q = \dfrac{\partial u}{\partial n}$, n is the unit outward normal and $\nabla^2 = \dfrac{\partial^2}{\partial x^2} + \dfrac{\partial^2}{\partial y^2}$ is the Laplace operator.

When equation (2.1) is multiplied by the weight function $u^\star$ and integrated over the domain Ω, one gets

$$\int_\Omega (\nabla^2 u - b) u^\star \, d\Omega = 0. \tag{2.3}$$

In the above equation, $u^\star$ is the fundamental solution of Laplace equation and satisfies the Poisson equation $\nabla^2 u^\star + \Delta_i = 0$, [65]. Here, Δ_i represents a Dirac delta function which goes to infinity at the point $i = (x_i, y_i)$ and is equal to zero elsewhere. The integral of Δ_i over the domain is equal to one. Integral property of Dirac delta function gives

$$\int_\Omega u \nabla^2 u^\star d\Omega = \int_\Omega u(-\Delta_i) d\Omega = -c_i u_i$$

31

where $u_i = u(x_i, y_i)$ and $c_i = \begin{cases} \frac{1}{2} & (x_i, y_i) \in \Gamma \\ 1 & (x_i, y_i) \in \Omega \end{cases}$ for a smooth boundary Γ.

Integrating by parts (applying Green's theorem) twice and inserting boundary conditions to equation (2.3) yields

$$c_i \, u_i + \int_{\Gamma_2} u \, q^\star \, d\Gamma + \int_{\Gamma_1} \bar{u} \, q^\star \, d\Gamma + \int_{\Omega} b \, u^\star \, d\Omega = \int_{\Gamma_2} \bar{q} \, u^\star \, d\Gamma + \int_{\Gamma_1} q \, u^\star \, d\Gamma. \qquad (2.4)$$

Since the equation (2.4) applies to a concentrated source at the point $i = (x_i, y_i)$, the values of $u^\star$ and $q^\star = \dfrac{\partial u^\star}{\partial n}$ are those corresponding to that particular point. For each different point a new integral equation is obtained.

For an isotropic two-dimensional medium the fundamental solution of Laplace equation is

$$u^\star = \frac{1}{2\pi} \ln\left(\frac{1}{r}\right) = \frac{1}{2\pi} \ln |\vec{r} - \vec{r_i}| \qquad (2.5)$$

and the normal derivative of the fundamental solution is

$$q^\star = \frac{\partial u^\star}{\partial n} = \frac{1}{2\pi} \frac{(\vec{r} - \vec{r_i}).\vec{n}}{|\vec{r} - \vec{r_i}|^2} \qquad (2.6)$$

where $\vec{r} = (x, y)$ and $\vec{r_i} = (x_i, y_i)$ are the free and fixed (source) points.

In order to make some simplification on the equation (2.4) we introduce the following notations,

$$\widetilde{u} = \begin{cases} u & \text{on} \quad \Gamma_2 \\ \bar{u} & \text{on} \quad \Gamma_1 \end{cases}$$

and

$$\widetilde{q} = \begin{cases} q & \text{on} \quad \Gamma_1 \\ \bar{q} & \text{on} \quad \Gamma_2 \end{cases}$$

where $\bar{u}$ is the known value of u and $\bar{q}$ is the known value of q.

Γ_2

$q = \overline{q}$

Ω
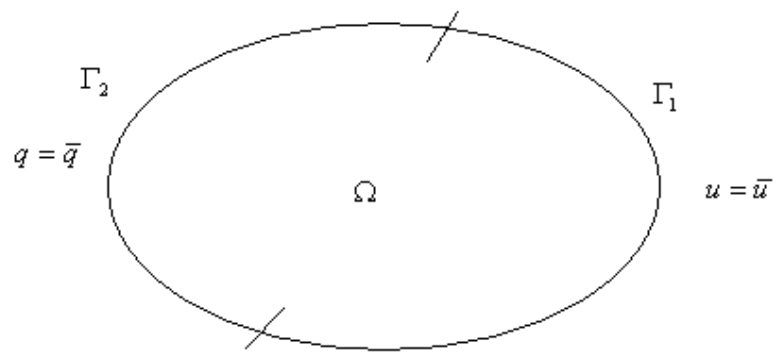
Γ_1

$u = \overline{u}$

Figure 2.1: Domain and the boundary conditions of the problem

Therefore final form of the equation (2.4) becomes

$$c_i \, \tilde{u}_i + \int_\Gamma \tilde{u} \, q^\star \, d\Gamma + \int_\Omega b \, u^\star \, d\Omega = \int_\Gamma \tilde{q} \, u^\star \, d\Gamma. \tag{2.7}$$

Here the function b is known. Thus, the integral in Ω do not introduce any new unknowns but one still needs to carry out a domain integral as well as the boundary integrals. The domain integral is going to be transformed to a boundary integral with the help of DRBEM.

2.2   DRBEM solution of Poisson's Equation $\nabla^2 u = b(x, y)$

The dual reciprocity boundary element method transforms the domain integral resulting in BEM to a boundary integral, and it can be used to solve non-linear and time-dependent problems.

The DRBEM is explained in this section with reference to the equation (2.1) [65]

$$\nabla^2 u(x, y) = b(x, y) \quad , \quad (x, y) \in \Omega \tag{2.8}$$

with the boundary conditions

$$u(x, y) = \bar{u}(x, y) \quad , \quad (x, y) \in \Gamma_1$$

$$\tag{2.9}$$

$$q(x, y) = \bar{q}(x, y) \quad , \quad (x, y) \in \Gamma_2 \, .$$

The solution to equation (2.8) can be expressed as the sum of the solution of the Laplace equation and a particular solution $\hat{u}$ such that

$$\nabla^2 \hat{u} = b. \tag{2.10}$$

Finding a solution $\hat{u}$ that satisfies the equation (2.10) is generally difficult, especially for non-linear or time-dependent problems. The dual reciprocity method proposes a series of particular solutions $\hat{u}_j$ instead of a single function $\hat{u}$. Therefore the expression for b is

$$b \approx \sum_{j=1}^{N+L} f_j \alpha_j \tag{2.11}$$

34

where f_j are related to particular solution $\hat{u}_j$ as

$$\nabla^2 \hat{u}_j = f_j \tag{2.12}$$

and 'N' and 'L' are the number of boundary and internal nodes, respectively. The α_j are unknown coefficients and the f_j are approximating functions.

Substituting equation (2.12) into (2.11) we express the right hand side function b with Laplacian of particular solutions

$$b = \sum_{j=1}^{N+L} \alpha_j (\nabla^2 \hat{u}_j). \tag{2.13}$$

When equation (2.13) is substituted into the original equation (2.8) we have

$$\nabla^2 u = \sum_{j=1}^{N+L} \alpha_j (\nabla^2 \hat{u}_j). \tag{2.14}$$

In equation (2.14), the Laplace operator applies on both sides to the unknown function u and the particular solutions $\hat{u}_j$. So, the procedure for developing the BEM for the Laplace operator will be applied to both sides which is called DRBEM.

Multiplying equation (2.14) by the fundamental solution $u^\star$ of Laplace equation and integrating over the domain, yields

$$\int_\Omega (\nabla^2 u) u^\star d\Omega = \sum_{j=1}^{N+L} \alpha_j \int_\Omega (\nabla^2 \hat{u}_j) u^\star d\Omega. \tag{2.15}$$

When we apply Green's theorem to the above equation, we get the integral equation for each source node i,

$$c_i \tilde{u}_i + \int_\Gamma (\tilde{u} q^\star - \tilde{q} u^\star) d\Gamma = \sum_{j=1}^{N+L} \alpha_j \left(c_i \hat{u}_{ij} + \int_\Gamma (\hat{u}_j q^\star - \hat{q}_j u^\star) d\Gamma \right) \tag{2.16}$$

where $\hat{u}_{ij} = \hat{u}_j(x_i, y_i)$ and the term $\hat{q}_j$ is defined as

$$\hat{q}_j = \frac{\partial \hat{u}_j}{\partial n} = \frac{\partial \hat{u}_j}{\partial x} \frac{\partial x}{\partial n} + \frac{\partial \hat{u}_j}{\partial y} \frac{\partial y}{\partial n}. \tag{2.17}$$

In the rest of the formulation we drop ' $\sim$ ' in u and q for the simplicity of the notation.

35

2.2.1 Discretization with Constant Elements

In this section, we will consider the constant element discretization of the boundary in which nodes are taken at the mid-points of elements (Fig. (2.2)). Thus, for E constant elements we have exactly $E = N$ nodes on the boundary.

The approximations for u and q for a constant element are taken as $u = N_m u_m$, $q = N_m q_m$, and we can write discretized form of equation (2.16)

$$c_i u_i + \sum_{e=1}^{N} \int_{\Gamma_e} u_m N_m q^\star d\Gamma_e - \sum_{e=1}^{N} \int_{\Gamma_e} q_m N_m u^\star d\Gamma_e$$

$$= \sum_{j=1}^{N+L} \alpha_j [c_i \hat{u}_{ij} + \sum_{e=1}^{N} \int_{\Gamma_e} \hat{u}_{jm} N_m q^\star d\Gamma_e - \sum_{e=1}^{N} \int_{\Gamma_e} \hat{q}_{jm} N_m u^\star d\Gamma_e] \tag{2.18}$$

where u_m and q_m are the values of the function and its normal derivative at node m respectively, N_m is the constant trial (shape) function for element e which takes the value 1 at the node m and zero everywhere else.

For constant elements the boundary is always smooth at the nodes. Thus, $c_i = 1/2$. So, the equation (2.18) becomes for N nodes on the boundary

$$\frac{1}{2} u_i + \sum_{k=1}^{N} \bar{H}_{ik} u_k - \sum_{k=1}^{N} G_{ik} q_k = \sum_{j=1}^{N+L} \alpha_j \left(\frac{1}{2} \hat{u}_{ij} + \sum_{k=1}^{N} \bar{H}_{ik} \hat{u}_{kj} - \sum_{k=1}^{N} G_{ik} \hat{q}_{kj} \right) \quad ; \quad i = 1, ..., N \tag{2.19}$$

where the index k is used for the boundary nodes and

$$\bar{H}_{ij} = \int_{\Gamma_j} q^\star \, d\Gamma_j = \frac{1}{2\pi} \int_{\Gamma_j} \frac{(\vec{r} - \vec{r}_i).\vec{n}}{|\vec{r} - \vec{r}_i|^2} d\Gamma_j \quad ; \quad i, j = 1, ..., N \tag{2.20}$$

$$G_{ij} = \int_{\Gamma_j} u^\star \, d\Gamma_j = \frac{1}{2\pi} \int_{\Gamma_j} \ln |\vec{r} - \vec{r}_i| d\Gamma_j \quad ; \quad i, j = 1, ..., N \tag{2.21}$$

and $\vec{r}_i = (x_i, y_i)$, $\vec{r} = (x, y)$ are both varying on the boundary nodes, $\vec{r}(x, y)$ being on the j-th element.
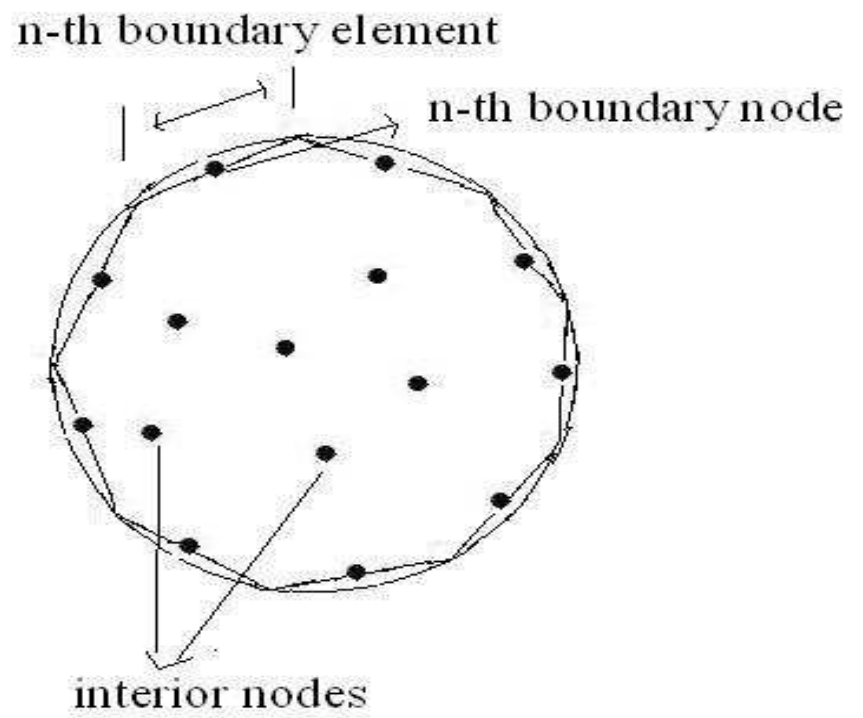
Figure 2.2: Discretization with constant elements

Gauss quadrature formula can be used to calculate the entries of the matrices G_{ij} and $\bar{H}_{ij}$ for $i \neq j$. For $i = j$, a more accurate integration scheme is needed because of the singularity of the fundamental solution. For these integrals higher-order integration rules or a special formula such as logarithmic integration is generally used. For constant element case G_{ij} and $\bar{H}_{ij}$ can be calculated analytically. $\bar{H}_{ii} = 0$ since $\vec{n}.\vec{r} = 0$. The G_{ii} integrals are [21]

$$G_{ii} = \frac{l}{2\pi}\left\{\ln\left(\frac{2}{l}\right) + 1\right\} \tag{2.22}$$

where l is the length of the element.

When $i = j$ we define H_{ij} as

$$H_{ij} = \bar{H}_{ij} + \frac{1}{2}\delta_{ij} \tag{2.23}$$

where δ is the Kronecker delta.

Then, the equation (2.19) can be written as

$$\sum_{k=1}^{N} H_{ik}u_k - \sum_{k=1}^{N} G_{ik}q_k = \sum_{j=1}^{N+L} \alpha_j\left(\sum_{k=1}^{N} H_{ik}\hat{u}_{kj} - \sum_{k=1}^{N} G_{ik}\hat{q}_{kj}\right). \tag{2.24}$$

The matrix-vector form of the above equation is

$$\mathbf{Hu} - \mathbf{Gq} = \sum_{j=1}^{N+L} \alpha_{\mathbf{j}}(\mathbf{H\hat{u}_j} - \mathbf{G\hat{q}_j}) \tag{2.25}$$

where $\mathbf{H}$ and $\mathbf{G}$ are two $N \times N$ matrices, and $\mathbf{u}$ and $\mathbf{q}$ are vectors of length N containing all the nodal values on the boundary.

In equation (2.24) each vector, $\mathbf{\hat{u}_j}$ and $\mathbf{\hat{q}_j}$, is considered to be one column of the matrices $\mathbf{\hat{U}}$ and $\mathbf{\hat{Q}}$, respectively. Thus, equation (2.25) takes the matrix-vector form

$$\mathbf{Hu} - \mathbf{Gq} = (\mathbf{H\hat{U}} - \mathbf{G\hat{Q}})\alpha \tag{2.26}$$

where α is the $(N + L) \times 1$ vector containing the unknown coefficients α_j and the matrices $\mathbf{\hat{U}}$ and $\mathbf{\hat{Q}}$ have the sizes $N \times (N + L)$. The α vector is computed from the system (2.11).

38

2.2.2 Discretization with Linear Elements

Now, we consider linear variation of u and q over an element for which the nodes are located at the ends of the element (Fig. (2.3)).

After discretizing the boundary into series of E linear elements, equation (2.16) can be written as [21, 65]

$$
c_i u_i + \sum_{e=1}^{E} \int_{\Gamma_j} (\sum_{j=1}^{2} u_j N_j) q^\star d\Gamma_j - \sum_{e=1}^{E} \int_{\Gamma_j} (\sum_{j=1}^{2} q_j N_j) u^\star d\Gamma_j
$$

$$(2.27)$$

$$
= \sum_{m=1}^{N+L} \alpha_m [c_i \hat{u}_{im} + \sum_{e=1}^{E} \int_{\Gamma_j} (\sum_{j=1}^{2} \hat{u}_{mj} N_j) q^\star d\Gamma_j - \sum_{e=1}^{E} \int_{\Gamma_j} (\sum_{j=1}^{2} \hat{q}_{mj} N_j) u^\star d\Gamma_j]
$$

where $E = N$ (number of nodes on the boundary) also for linear element case.

Since u and q vary linearly over each element it is not possible to take them out of integrals and the integrals in the above equation are evaluated using numerical integration.

The values of u and q at any point on the element can be defined in terms of their nodal values and two linear interpolation functions N_1 and N_2, which are given in terms of the homogeneous coordinate $\xi \in [-1, 1]$, as

$$
u(\xi) = N_1 u_1 + N_2 u_2 = \begin{bmatrix} N_1 & N_2 \end{bmatrix} \begin{bmatrix} u_1 \\ u_2 \end{bmatrix}
$$

$$(2.28)$$

$$
q(\xi) = N_1 q_1 + N_2 q_2 = \begin{bmatrix} N_1 & N_2 \end{bmatrix} \begin{bmatrix} q_1 \\ q_2 \end{bmatrix}.
$$

The two interpolating functions are defined as

$$
N_1(\xi) = \tfrac{1}{2}(1 - \xi)
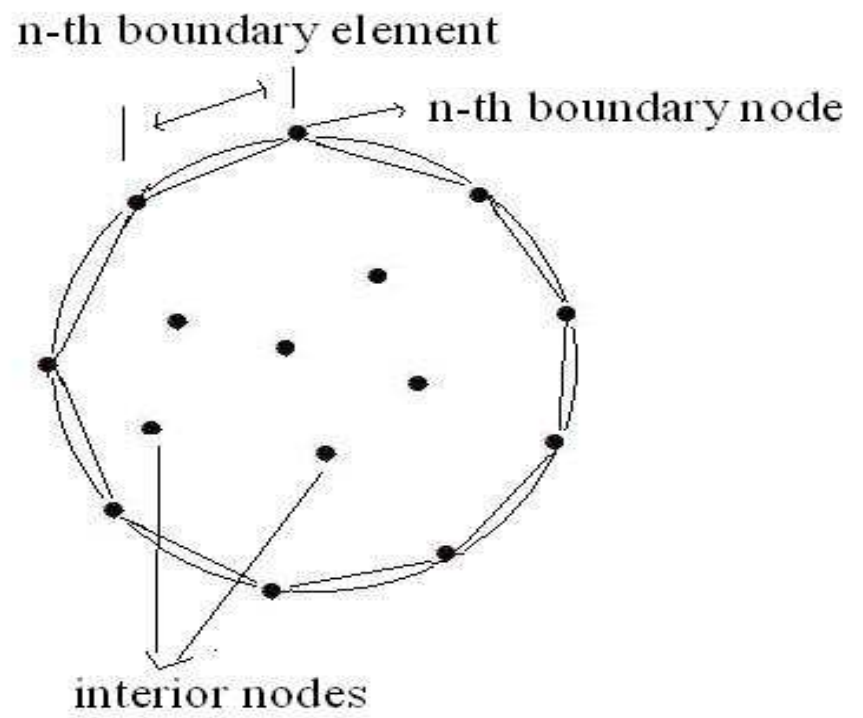$$

$$(2.29)$$

$$
N_2(\xi) = \tfrac{1}{2}(1 + \xi).
$$

Figure 2.3: Discretization with linear elements

The first integral on the left-hand side of (2.27) can be written as,

$$\int_{\Gamma_j} u q^\star d\Gamma = \int_{\Gamma_j} \begin{bmatrix} N_1 & N_2 \end{bmatrix} q^\star d\Gamma \begin{bmatrix} u_1 \\ u_2 \end{bmatrix} = \begin{bmatrix} h_{ij}^1 & h_{ij}^2 \end{bmatrix} \begin{bmatrix} u_1 \\ u_2 \end{bmatrix} \qquad (2.30)$$

where, for each element j, we have the two terms

$$h_{ij}^1 = \int_{\Gamma_j} N_1 q^\star d\Gamma \qquad (2.31)$$

and

$$h_{ij}^2 = \int_{\Gamma_j} N_2 q^\star d\Gamma. \qquad (2.32)$$

Similarly , the second integral on the left-hand side of (2.27) gives

$$\int_{\Gamma_j} q u^\star d\Gamma = \int_{\Gamma_j} \begin{bmatrix} N_1 & N_2 \end{bmatrix} u^\star d\Gamma \begin{bmatrix} q_1 \\ q_2 \end{bmatrix} = \begin{bmatrix} g_{ij}^1 & g_{ij}^2 \end{bmatrix} \begin{bmatrix} q_1 \\ q_2 \end{bmatrix} \qquad (2.33)$$

where

$$g_{ij}^1 = \int_{\Gamma_j} N_1 u^\star d\Gamma \qquad (2.34)$$

and

$$g_{ij}^2 = \int_{\Gamma_j} N_2 u^\star d\Gamma. \qquad (2.35)$$

Integrals h_{ij}^1, h_{ij}^2, g_{ij}^1 and g_{ij}^2 are evaluated numerically by using Gaussian quadrature. In the discretization with linear elements, node 2 of element j is the same point as node 1 of element $j + 1$. So, the entries $\bar{H}_{ij}$ are equal to the h_{ij}^1 term of element j plus the $h_{i,j-1}^2$ term of element $j - 1$.

$$\frac{1}{2} u_i + \sum_{j=1}^{N} \bar{H}_{ij} u_j - \sum_{j=1}^{N} G_{ij} q_j = \sum_{k=1}^{N+L} \alpha_k \left(\frac{1}{2} \hat{u}_{ik} + \sum_{j=1}^{N} \bar{H}_{ij} \hat{u}_{jk} - \sum_{j=1}^{N} G_{ij} \hat{q}_{jk} \right) \qquad (2.36)$$

which becomes

$$\sum_{j=1}^{N} H_{ij} u_j - \sum_{j=1}^{N} G_{ij} q_j = \sum_{k=1}^{N+L} \alpha_k \left(\sum_{j=1}^{N} H_{ij} \hat{u}_{jk} - \sum_{j=1}^{N} G_{ij} \hat{q}_{jk} \right) \qquad (2.37)$$

when the terms c_i have been incorporated onto the principal part of H_{ij}.

Then, the whole set in matrix-vector form becomes

$$\mathbf{Hu} - \mathbf{Gq} = (\mathbf{H\hat{U}} - \mathbf{G\hat{Q}})\alpha \tag{2.38}$$

where the matrices $\mathbf{H}$, $\mathbf{G}$, $\mathbf{\hat{U}}$, $\mathbf{\hat{Q}}$ have sizes $N \times N$, $N \times N$, $N \times (N+L)$, $N \times (N+L)$ respectively, and the vectors $\mathbf{u}$, $\mathbf{q}$, α have lengths N, N and $N+L$ respectively. Each coefficient of the matrices $\mathbf{\hat{U}}$ and $\mathbf{\hat{Q}}$ is a function of the distance between two nodes.

Equation (2.38) (using linear elements) or equation (2.26) (using constant elements) involves discretization of the boundary only. One may define the internal nodes at the locations where it is desirable to know the interior solution. Only the coordinates are needed as input data. Hence, these nodes may be defined in any order.

Since the sizes of the matrices in the equations (2.38) and (2.26) are different, we enlarge the matrices as, [65]

$$\begin{bmatrix} \mathbf{H_b} & \mathbf{0} \\ \mathbf{H_i} & \mathbf{I} \end{bmatrix} \begin{Bmatrix} \tilde{\mathbf{u}}_\mathbf{b} \\ \tilde{\mathbf{u}}_\mathbf{i} \end{Bmatrix} - \begin{bmatrix} \mathbf{G_b} & \mathbf{0} \\ \mathbf{G_i} & \mathbf{0} \end{bmatrix} \begin{Bmatrix} \tilde{\mathbf{q}}_\mathbf{b} \\ \mathbf{0} \end{Bmatrix}$$

$$= \left(\begin{bmatrix} \mathbf{H_b} & \mathbf{0} \\ \mathbf{H_i} & \mathbf{I} \end{bmatrix} \begin{bmatrix} \mathbf{\hat{U}_b} \\ \mathbf{\hat{U}_i} \end{bmatrix} - \begin{bmatrix} \mathbf{G_b} & \mathbf{0} \\ \mathbf{G_i} & \mathbf{0} \end{bmatrix} \begin{bmatrix} \mathbf{\hat{Q}_b} \\ \mathbf{0} \end{bmatrix} \right) \begin{Bmatrix} \alpha \end{Bmatrix} \tag{2.39}$$

where b refers to the boundary nodes and i to the internal nodes. $\mathbf{0}$ and $\mathbf{I}$ are the zero and identity matrices respectively.

Now, all the matrices are of size $(N+L) \times (N+L)$ and the vectors have length $(N+L)$ since there are N boundary and L interior nodes.

The coefficient vector α in (2.38) or (2.26) is computed from equation (2.11)

$$b \approx \sum_{j=1}^{N+L} f_j \alpha_j \tag{2.40}$$

42

by taking the value of b at $(N + L)$ different points, and expressing in matrix form as

$$\mathbf{b} = \mathbf{F}\boldsymbol{\alpha} \tag{2.41}$$

where $\mathbf{F}$ is the $(N + L) \times (N + L)$ position matrix consisting of vectors f_j as columns which contain the values of the function f_j at the $N + L$ points.

Therefore, $\boldsymbol{\alpha}$ vector may be obtained as inverting the equation (2.41)

$$\boldsymbol{\alpha} = \mathbf{F}^{-1}\mathbf{b}. \tag{2.42}$$

When equation (2.42) is substituted back into equation (2.38) or (2.26) we get the system

$$\mathbf{Hu} - \mathbf{Gq} = (\mathbf{H\hat{U}} - \mathbf{G\hat{Q}})\mathbf{F}^{-1}\mathbf{b} \tag{2.43}$$

where right-hand side of equation (2.43) is a known vector now.

In order to define the functions f_j, $\hat{u}_j$ and $\hat{q}_j$ it is customary to propose an expansion for f_j and then compute $\hat{u}_j$ and $\hat{q}_j$. Usually, f_j functions are taken as polynomials in terms of radial distance r. Thus, f's are taken as $f = 1 + r + r^2 + r^3 + ... + r^m$ in which r is the distance between fixed and source points. The resulting $\mathbf{F}$ matrix should be non-singular and the degree m should be properly taken [57].

If $f_j = r$, then the corresponding $\hat{u}_j$ function can be obtained, in the two dimensional case, from the integration of the equation

$$\nabla^2 \hat{u}_j = r \tag{2.44}$$

which is equal to in polar coordinates

$$\frac{1}{r}\frac{\partial}{\partial r}\left(r\frac{\partial \hat{u}}{\partial r}\right) = r. \tag{2.45}$$

Thus, integration gives

$$\hat{u}_j = \frac{r^3}{9} \tag{2.46}$$

in which $r^2 = r_x^2 + r_y^2$. r_x and r_y are the components of r in the direction of the x and y axes.

The function $\hat{q}_j$ will be obtained from (since $\dfrac{\partial r}{\partial x} = \dfrac{r_x}{r}, \dfrac{\partial r}{\partial y} = \dfrac{r_y}{r}$)

$$\hat{q}_j = \frac{\partial \hat{u}_j}{\partial r}\frac{\partial r}{\partial n}$$

43

and substituting the value of $\hat{u}_j$ (2.46) to get

$$\hat{q}_j = \frac{r}{3}[r_x cos(n, x) + r_y cos(n, y)] \qquad (2.47)$$

where direction cosines refer to the outward normal at the boundary with respect to the x and y axes.

In this case the matrix $\mathbf{F}$ will contain zeros on the leading diagonal, but the matrix is non-singular if no double nodes are used.

We may chose f_j as

$$f_j = 1 + r + r^2 + r^3 + \ldots + r^m \qquad (2.48)$$

and since

$$\nabla^2 \hat{u}_j = f_j \quad , \quad \hat{q}_j = \frac{\partial \hat{u}_j}{\partial n}$$

we can compute $\hat{u}_j$ and $\hat{q}_j$ as

$$\hat{u}_j = \frac{r^2}{4} + \frac{r^3}{9} + \ldots + \frac{r^{m+2}}{(m+2)^2} \qquad (2.49)$$

$$\hat{q}_j = (r_x \frac{\partial x}{\partial n} + r_y \frac{\partial y}{\partial n})(\frac{1}{2} + \frac{r}{3} + \ldots + \frac{r^m}{m+2}). \qquad (2.50)$$

Linear radial basis functions $f = 1 + r$ **:**

The presence of the constant guarantees the "completeness" of the expansion, and also implies that the leading diagonal of $\mathbf{F}$ is no longer zero. Each of its entries F_{lj} is a function of the distance between points l and j both of which take all the values from 1 to $N + L$. $\mathbf{F}$ is thus a symmetric matrix and non-singular. So, in equation (2.42) the inverse of $\mathbf{F}$ is well defined [65].

Note that in this case

$$\hat{u} = \frac{r^2}{4} + \frac{r^3}{9} \qquad (2.51)$$

and

$$\hat{q} = \left(\frac{1}{2} + \frac{r}{3}\right)\left(r_x \frac{\partial x}{\partial n} + r_y \frac{\partial y}{\partial n}\right). \qquad (2.52)$$

Quadratic radial basis functions $f = 1 + r + r^2$:

In this case

$$\hat{u} = \frac{r^2}{4} + \frac{r^3}{9} + \frac{r^4}{16} \tag{2.53}$$

and

$$\hat{q} = \left(\frac{1}{2} + \frac{r}{3} + \frac{r^2}{4}\right)\left(r_x \frac{\partial x}{\partial n} + r_y \frac{\partial y}{\partial n}\right). \tag{2.54}$$

Similar to the linear case the matrix $\mathbf{F}$ is non-singular and therefore invertible.

2.3   DRBEM Solution of Time-Dependent Problems $\nabla^2 u = b(x, y, t, \dot{u})$

Now, we will consider the time dependent Poisson's type equation

$$\nabla^2 u = b(x, y, t, \dot{u}) \tag{2.55}$$

where

$$b(x, y, t, \dot{u}) = \frac{\partial u}{\partial t} \tag{2.56}$$

for the time-dependent diffusion equation.

Application of DRBEM to equation (2.55) gives the discretized equations in the matrix vector form

$$\mathbf{Hu} - \mathbf{Gq} = (\mathbf{H\hat{U}} - \mathbf{G\hat{Q}})\mathbf{F}^{-1}\mathbf{b} \tag{2.57}$$

and when equation (2.56) is substituted back into equation (2.57) we get the system

$$\mathbf{Hu} - \mathbf{Gq} = (\mathbf{H\hat{U}} - \mathbf{G\hat{Q}})\mathbf{F}^{-1}\dot{u} \tag{2.58}$$

where $\dot{u}$ is of the length $N + L$ which contains the time derivative values of the vector $\mathbf{u}$.

Writing equation (2.58) as

$$\mathbf{Hu} - \mathbf{Gq} = \mathbf{S}\dot{u} \tag{2.59}$$

where $\mathbf{S} = (\mathbf{H\hat{U}} - \mathbf{G\hat{Q}})\mathbf{F}^{-1}$ we can obtain finally

$$-\mathbf{S}\dot{u} + \mathbf{H}\mathbf{u} - \mathbf{G}\mathbf{q} = \mathbf{0} \tag{2.60}$$

in which $\mathbf{0}$ denotes the zero vector.

Time integration schemes, which are necessary for solving this system to obtain the solution $\mathbf{u}$ at $N + L$ points, will be explained in Section 2.6.

2.4 DRBEM Solution of Convection-Diffusion Problems $\nabla^2 u = b(x, y, t, \dot{u}, u_x, u_y)$

In this section, the range of application of the DRBEM will be extended to problems governed by the equations of the type

$$\nabla^2 u = b(x, y, t, \dot{u}, u_x, u_y) \tag{2.61}$$

where the non-homogeneous term may also be a combination of time and space derivatives of u

$$b(x, y, t, \dot{u}, u_x, u_y) = \frac{\partial u}{\partial t} + \frac{\partial u}{\partial x} + \frac{\partial u}{\partial y} \tag{2.62}$$

which leads to the system

$$\mathbf{b} = \mathbf{F}\alpha. \tag{2.63}$$

Same expression can also be used for the problem variable when dealing with derivatives

$$\mathbf{u} = \mathbf{F}\beta \tag{2.64}$$

where $\beta \neq \alpha$.

Differentiating (2.64) with respect to x and y, gives, respectively

$$\frac{\partial \mathbf{u}}{\partial x} = \frac{\partial \mathbf{F}}{\partial x}\beta \tag{2.65}$$

and

$$\frac{\partial \mathbf{u}}{\partial y} = \frac{\partial \mathbf{F}}{\partial y}\beta. \tag{2.66}$$

The vector β can be obtained by inverting the equation (2.64)

$$\beta = \mathbf{F}^{-1}\mathbf{u}. \tag{2.67}$$

Substituting equations (2.65) and (2.66) back into (2.67), we get

$$\frac{\partial \mathbf{u}}{\partial x} = \frac{\partial \mathbf{F}}{\partial x}\mathbf{F}^{-1}\mathbf{u}$$

$$\frac{\partial \mathbf{u}}{\partial y} = \frac{\partial \mathbf{F}}{\partial y}\mathbf{F}^{-1}\mathbf{u}.$$

(2.68)

Thus, the non-homogeneous term in equation (2.61) can be expressed as

$$\mathbf{b} = \frac{\partial \mathbf{u}}{\partial t} + \left(\frac{\partial \mathbf{F}}{\partial x}\mathbf{F}^{-1} + \frac{\partial \mathbf{F}}{\partial y}\mathbf{F}^{-1}\right)\mathbf{u}.$$

(2.69)

Substituting equation (2.69) into equation (2.43) or (2.57) yields

$$\mathbf{Hu} - \mathbf{Gq} = (\mathbf{H\hat{U}} - \mathbf{G\hat{Q}})\mathbf{F}^{-1}\left(\dot{u} + \left(\frac{\partial \mathbf{F}}{\partial x}\mathbf{F}^{-1} + \frac{\partial \mathbf{F}}{\partial y}\mathbf{F}^{-1}\right)\mathbf{u}\right).$$

(2.70)

Equation (2.70) can be simply written as

$$\mathbf{Hu} - \mathbf{Gq} = \mathbf{S}\dot{u} + \mathbf{D}$$

(2.71)

where

$$\mathbf{S} = (\mathbf{H\hat{U}} - \mathbf{G\hat{Q}})\mathbf{F}^{-1}$$

$$\mathbf{D} = \mathbf{S}\left(\frac{\partial \mathbf{F}}{\partial x}\mathbf{F}^{-1} + \frac{\partial \mathbf{F}}{\partial y}\mathbf{F}^{-1}\right)\mathbf{u}.$$

(2.72)

Finally, one can obtain

$$-\mathbf{S}\dot{u} + (\mathbf{H} - \mathbf{D})\mathbf{u} - \mathbf{Gq} = \mathbf{0}$$

(2.73)

which is similar to equation (2.60).

Now, the system (2.73) will be solved by using some time integration schemes.

2.5   DRBEM Solution of Non-linear Problems $\nabla^2 u = b(x, y, t, \dot{u}, u, u_x, u_y)$

Finally, we give the application of DRBEM to non-linear problems

$$\nabla^2 u = b(x, y, t, \dot{u}, u, u_x, u_y)$$

(2.74)

47

where the non-linear term b is

$$b = \frac{\partial u}{\partial t} + u\left(\frac{\partial u}{\partial x} + \frac{\partial u}{\partial y}\right) \tag{2.75}$$

In Section 2.4, we discuss how to treat the convective terms (equation (2.68)). The non-linear right-hand side term can be expressed as in equation (2.69)

$$\mathbf{b} = \frac{\partial \mathbf{u}}{\partial t} + \mathbf{U}\left(\frac{\partial \mathbf{F}}{\partial x}\mathbf{F}^{-1} + \frac{\partial \mathbf{F}}{\partial y}\mathbf{F}^{-1}\right)\mathbf{u}. \tag{2.76}$$

where $\mathbf{U}$ is diagonal and contains the values of u at each node, i.e.

$$\mathbf{U} = \begin{bmatrix} u_1 & 0 & 0 & \dots & 0 \\ 0 & u_2 & 0 & \dots & 0 \\ \vdots & \vdots & \vdots & \ddots & \vdots \\ 0 & 0 & 0 & \dots & u_{N+L} \end{bmatrix}. \tag{2.77}$$

Substituting equation (2.76) into equation (2.43) or (2.57) yields

$$\mathbf{Hu} - \mathbf{Gq} = (\mathbf{H\hat{U}} - \mathbf{G\hat{Q}})\mathbf{F}^{-1}\left(\dot{u} + \mathbf{U}\left(\frac{\partial \mathbf{F}}{\partial x}\mathbf{F}^{-1} + \frac{\partial \mathbf{F}}{\partial y}\mathbf{F}^{-1}\right)\mathbf{u}\right). \tag{2.78}$$

Equation (2.78) can be simply written as

$$\mathbf{Hu} - \mathbf{Gq} = \mathbf{S}\dot{u} + \mathbf{D1} \tag{2.79}$$

where

$$\mathbf{S} = (\mathbf{H\hat{U}} - \mathbf{G\hat{Q}})\mathbf{F^{-1}}$$

$$\tag{2.80}$$

$$\mathbf{D1} = \mathbf{S}\,\mathbf{U}\left(\frac{\partial \mathbf{F}}{\partial x}\mathbf{F}^{-1} + \frac{\partial \mathbf{F}}{\partial y}\mathbf{F}^{-1}\right)\mathbf{u}.$$

Finally one can obtain the system

$$-\mathbf{S}\dot{u} + (\mathbf{H} - \mathbf{D1})\mathbf{u} - \mathbf{Gq} = \mathbf{0}. \tag{2.81}$$

Now, the system of ordinary differential equations in time, namely equations (2.60), (2.73) and (2.81) are going to be solved for transient time levels.

48

2.6   Time Integration Methods

In this section, two basic numerical methods are employed in solving ODEs that result from the application of DRBEM to time dependent problems. We will consider the application of the Finite Difference and Runge-Kutta methods to the discretized system of ordinary differential equations in time (equation (2.60)). Similar application can be given for equations (2.73) and (2.81).

2.6.1   Finite Difference Method

In most applications of the DRBEM to engineering problems, which are governed by time-dependent partial differential equations, time derivatives are discretized by low order finite difference schemes. For the time-dependent diffusion problems, DRBEM procedures equation (2.60)

$$-\mathbf{S}\dot{u} + \mathbf{H}u - \mathbf{G}q = 0 \tag{2.82}$$

which is the system of ordinary differential equations with respect to time. Number of equations in the system is equal to the number of nodes on the boundary and inside the region.

Finite difference method is a simple and powerful method for solving various heat transfer and flow problems. In this section, the time derivative in the equation (2.82) will be discretized using low order finite difference schemes. We will employ a two-level time integration scheme (Euler scheme), and a three-level integration scheme (Central Difference scheme) .

2.6.1.1   Forward Difference Scheme (Euler Method)

From the Taylor series expansion of $u(x, y, t)$ about $t = t_m$ and evaluated at $t = t_{m+1}$ we have

$$u(x, y, t_{m+1}) = u(x, y, t_m) + \Delta t \, \dot{u}(x, y, t_m) + \frac{\Delta t^2}{2}\ddot{u}(x, y, t_m) + \ldots . \tag{2.83}$$

Equation (2.83) can be truncated after a finite number of terms. For example, if terms of

49

magnitude $(\Delta t)^2$ and higher are neglected, equation (2.83) reduces to

$$u(x, y, t_{m+1}) = u(x, y, t_m) + \Delta t \, \dot{u}(x, y, t_m) \qquad (2.84)$$

which is first order accurate.

If the equation (2.84) is solved for $\dot{u}(x, y, t_m)$, we obtain [44]

$$\dot{u}(x, y, t_m) = \frac{u(x, y, t_{m+1}) - u(x, y, t_m)}{\Delta t} + O(\Delta t) \qquad (2.85)$$

which is called forward difference scheme of first order in Δt, and Δt is the time step, $t_m = m\Delta t$. 'm' indicates the time level.

When the equation (2.85) is substituted in equation (2.60), we get

$$-\mathbf{S} \frac{\mathbf{u}^{m+1} - \mathbf{u}^m}{\Delta t} + \mathbf{H}\mathbf{u}^m - \mathbf{G}\mathbf{q}^m = \mathbf{0} \qquad (2.86)$$

where $\mathbf{u}^m$ and $\mathbf{q}^m$ are vectors at the m-th iteration level.

This is the simplest finite difference discretization of the time derivative equation. Since it is an explicit scheme stability problems are usually encountered. A suitable value of Δt is required by trial and error in the computations. With appropriate values of Δt the stability of numerical results is maintained and confirmed with the stability analysis given in Chapter 4.

A relaxation procedure is used to accelerate the convergence to steady-state and to overcome stability problems for both variables $\mathbf{u}$ and $\mathbf{q}$ in the following form

$$\mathbf{u} = (1 - \beta_u)\mathbf{u}^m + \beta_u \mathbf{u}^{m+1}$$

$$\qquad (2.87)$$

$$\mathbf{q} = (1 - \beta_q)\mathbf{q}^m + \beta_q \mathbf{q}^{m+1}$$

where β_u and β_q are parameters which position the values of $\mathbf{u}$ and $\mathbf{q}$, respectively, between time levels 'm' and 'm+1'. Substituting these approximations into (2.86) yields,

$$\left(-\frac{1}{\Delta t}\mathbf{S} + \beta_u \mathbf{H}\right)\mathbf{u}^{m+1} - \beta_q \mathbf{G}\mathbf{q}^{m+1} = \left[-\frac{1}{\Delta t}\mathbf{S} - (1 - \beta_u)\mathbf{H}\right]\mathbf{u}^m + (1 - \beta_q)\mathbf{G}\mathbf{q}^m. \qquad (2.88)$$

Thus, the normal derivative $\mathbf{q}$ is brought to the 'm+1' level as unknown which is the case for the type of boundary conditions in BEM applications.

The right hand side of equation (2.88) is known at time $m\Delta t$, since it involves values which have been specified as initial condition or calculated previously.

Since the elements of matrices $\mathbf{H}$, $\mathbf{G}$ and $\mathbf{S}$ depend only on geometrical data they can be computed once and stored. The system matrix can be reduced only once as well when Δt is kept constant.

2.6.1.2 Central Difference Scheme

We also employ central difference scheme for the time derivative. From the Taylor series expansion of $u(x, y, t)$ about $t = t_m$ and evaluated at $t = t_{m+1}$ and $t = t_{m-1}$ we have

$$u(x, y, t_{m+1}) = u(x, y, t_m) + \Delta t\, \dot{u}(x, y, t_m) + \frac{\Delta t^2}{2}\ddot{u}(x, y, t_m) + \frac{\Delta t^3}{6}\dddot{u}(x, y, t_m)..... \qquad (2.89)$$

$$u(x, y, t_{m-1}) = u(x, y, t_m) - \Delta t\, \dot{u}(x, y, t_m) + \frac{\Delta t^2}{2}\ddot{u}(x, y, t_m) - \frac{\Delta t^3}{6}\dddot{u}(x, y, t_m)..... \qquad (2.90)$$

Subtracting equation (2.90) from (2.89) one can get the approximation for the first derivative

$$\dot{u}(x, y, t_m) = \frac{u(x, y, t_{m+1}) - u(x, y, t_{m-1})}{2\Delta t} + O(\Delta t)^2 . \qquad (2.91)$$

which is of second order in the time step Δt, [44].

When the time derivative is discretized by using the central difference scheme with the relaxation parameters, one can write the equation (2.60) as

$$-\mathbf{S}\,\frac{\mathbf{u}^{m+1} - \mathbf{u}^{m-1}}{2\Delta t} + \mathbf{H}((1 - \beta_u)\mathbf{u}^{m-1} + \beta_u\mathbf{u}^{m+1}) - \mathbf{G}((1 - \beta_q)\mathbf{q}^{m-1} + \beta_q\mathbf{q}^{m+1}) = \mathbf{0} . \qquad (2.92)$$

Here, also the solution $\mathbf{u}$ and its normal derivative $\mathbf{q}$ are written as linear combinations of the values from 'm-1' and 'm+1' levels for obtaining them in 'm+1' level as unknowns.

51

Equation (2.92) can be arranged such that the right hand side is at time $(m-1)\Delta t$ and known, since they involve values which have been specified as initial condition or calculated previously. And left hand side is at time $(m+1)\Delta t$

$$\Big(-\frac{1}{2\Delta t}\mathbf{S} + \beta_u\mathbf{H}\Big)\mathbf{u}^{m+1} - \beta_q\mathbf{G}\mathbf{q}^{m+1} = \Big[-\frac{1}{2\Delta t}\mathbf{S} - (1-\beta_u)\mathbf{H}\Big]\mathbf{u}^{m-1} + (1-\beta_q)\mathbf{G}\mathbf{q}^{m-1}\ . \quad (2.93)$$

All the matrices in equation (2.93) are computed once and the system is solved recursively for transient time levels for equation (2.60) resulting from the DRBEM application of diffusion equation (2.55). When the convection terms are included as in equations (2.73) and (2.81), the coefficient matrices on the right hand side of equation (2.93) are going to be evaluated at the m-th time level. Although the time step Δt and relaxation parameters β_u and β_q are found by trial and error, with the appropriate values the stability of DRBEM solution is maintained (Chapter 4).

Before we solve systems (2.88) and (2.93), we apply the given boundary conditions to the equations (2.88) and (2.93). The boundary Γ is of two parts in which $\mathbf{u}$ is known on one part and $\mathbf{q}$ is known on the other part. Therefore, in the equations (2.88) and (2.93) there are only $N + L$ unknowns. Once all unknowns are passed to the left-hand side one can write the equations (2.88) and (2.93) as

$$\mathbf{A}\mathbf{x} = \mathbf{y} \qquad\qquad (2.94)$$

where $\mathbf{x}$ is the vector of unknown boundary values of $\mathbf{u}$ and $\mathbf{q}$. The vector $\mathbf{y}$ now contains all the known information from the boundary or from the previous iteration.

2.6.2 Runge-Kutta Method

In this section, we will explain the Runge-Kutta method (RKM) for an ordinary differential equation of the form

$$\dot{u} = f(t, u)$$

$$(2.95)$$

$$u(t_0) = u_0$$

and then modify for our system of equation. Here $f(t, u)$ denotes the given function, and u_0 is the initial condition.

Like FDM, derivation of the RKM is also based on the Taylor series expansion of $f(t, u)$ but without using the partial derivatives of the function.

RKM can be generally expressed as, [25]

$$u(x, y, t_{m+1}) = u(x, y, t_m) + \Delta t \left(\gamma_1 f + \gamma_2 f(t + \alpha \Delta t, u + \alpha \Delta t \, f) \right) \tag{2.96}$$

where γ_1, γ_2 and α are constant to be determined. f refers to $f(t, u)$, and Δt is the time increment, $t_m = m\Delta t$.

The second term in the right hand side of the equation (2.96) can be expanded using the Taylor series expansion of a function in two variables as, [44]

$$f(t+\alpha\Delta t, u+\alpha\Delta t f) = f + \Delta t(\alpha f_t + \alpha f f_u) + (\Delta t)^2 \left(\frac{1}{2}\alpha^2 f_{tt} + \alpha^2 f f_{tu} + \frac{1}{2}\alpha^2 f^2 f_{uu} \right) + O((\Delta t)^3). \tag{2.97}$$

When we substitute equation (2.97) into equation (2.96), we get

$$u(x, y, t_{m+1}) = u(x, y, t_m) + \Delta t \, \gamma_1 f + \Delta t \, \gamma_2 f + (\Delta t)^2 (\gamma_2 \, \alpha \, f_t + \gamma_2 \, \alpha \, f \, f_u)$$

$$\tag{2.98}$$

$$+ (\Delta t)^3 \left(\frac{1}{2}\gamma_2 \, \alpha^2 f_{tt} + \gamma_2 \, \alpha^2 f \, f_{tu} + \frac{1}{2}\gamma_2 \, \alpha^2 f^2 \, f_{uu} \right) + O((\Delta t)^4).$$

The truncation error for equation (2.98) is

$$T(x, y, t_{m+1}) = u(x, y, t_{m+1}) - u(x, y, t_m) - \Delta t \, \gamma_1 f - \Delta t \, \gamma_2 f - (\Delta t)^2 (\gamma_2 \, \alpha \, f_t + \gamma_2 \, \alpha \, f \, f_u)$$

$$- (\Delta t)^3 \left(\frac{1}{2}\gamma_2 \, \alpha^2 f_{tt} + \gamma_2 \, \alpha^2 f \, f_{tu} + \frac{1}{2}\gamma_2 \, \alpha^2 f^2 \, f_{uu} \right) - O((\Delta t)^4).$$
$$\tag{2.99}$$

From the Taylor series expansion of $u(x, y, t)$ about $t = t_m$ and evaluated at $t = t_{m+1}$ we have

$$u(x, y, t_{m+1}) = u(x, y, t_m) + \Delta t \, \dot{u}(x, y, t_m) + \frac{(\Delta t)^2}{2} \ddot{u}(x, y, t_m) + \frac{(\Delta t)^3}{6} u^{(3)}(x, y, t_m) + O((\Delta t)^4) \tag{2.100}$$

where

$$\dot{u} = f(t, u(x, y, t))$$

$$\ddot{u} = f_t + f_u f \tag{2.101}$$

$$u^{(3)} = f_{tt} + 2f_{tu}f + f_{uu}f^2 + f_u f_t + f_u^2 f.$$

53

Substituting equation (2.101) into equation (2.100) yields

$$u(x, y, t_{m+1}) - u(x, y, t_m) = \Delta t\, f + \frac{(\Delta t)^2}{2}(f_t + f_u f)$$

$$+ \frac{(\Delta t)^3}{6}(f_{tt} + 2 f_{tu} f + f_{uu} f^2 + f_u f_t + f_u^2 f) + O((\Delta t)^4).$$

(2.102)

Thus, we can express the truncation error in equation (2.99) by using equation (2.102) as

$$T(x, y, t_{m+1}) = \Delta t\, f + \frac{(\Delta t)^2}{2}(f_t + f_u f) + \frac{(\Delta t)^3}{6}(f_{tt} + 2 f_{tu} f + f_{uu} f^2 + f_u f_t + f_u^2 f) + O((\Delta t)^4)$$

$$- \Delta t(\gamma_1 + \gamma_2) f - (\Delta t)^2(\gamma_2\, \alpha\, f_t + \gamma_2\, \alpha\, f\, f_u)$$

$$- (\Delta t)^3 \left(\tfrac{1}{2}\gamma_2\, \alpha^2 f_{tt} + \gamma_2\, \alpha^2 f\, f_{tu} + \tfrac{1}{2}\gamma_2\, \alpha^2 f^2\, f_{uu} \right) - O((\Delta t)^4)$$

(2.103)

which can be expressed as

$$T(x, y, t_{m+1}) = \Delta t(1 - \gamma_1 - \gamma_2) f + (\Delta t)^2 \left[\left(\frac{1}{2} - \gamma_2\alpha \right) f_t + \left(\frac{1}{2} - \gamma_2\alpha \right) f_u f \right]$$

$$+ (\Delta t)^3 \left[\left(\frac{1}{6} - \frac{1}{2}\gamma_2\alpha^2 \right) f_{tt} + \left(\frac{1}{3} - \gamma_2\alpha^2 \right) f_{tu} f + \left(\frac{1}{6} - \frac{1}{2}\gamma_2\alpha^2 \right) f^2 f_{uu} \right. \quad (2.104)$$

$$\left. + \frac{1}{6} f_u f_t + \frac{1}{6} f_u^2 f \right] + O(\Delta t)^4$$

where all partial derivatives are evaluated at the m-th time level.

In order for the truncation error (equation (2.104)) converge to zero the coefficients of Δt and $(\Delta t)^2$ must be zero. This is because the function f varies arbitrarily so the coefficient of $(\Delta t)^3$ can not be zero. This leads to

$$1 - \gamma_1 - \gamma_2 = 0$$

(2.105)

$$\frac{1}{2} - \gamma_2\alpha = 0$$

from which we obtain $\gamma_2 = \dfrac{1}{2\alpha}$ and $\gamma_1 = 1 - \dfrac{1}{2\alpha}$. There are infinitely many solutions for these parameters.

If we choose $\alpha = 1/2$ we get the modified Euler's method, [44]

$$u^{m+1} = u^m + \Delta t\, f\left(t_m + \frac{\Delta t}{2}, u_m + \frac{\Delta t}{2} f(t_m, u_m) \right), \quad m \geq 0.$$

(2.106)

Here u^{m+1} stands for $u(x, y, t_{m+1})$. Second order Runge-Kutta Method is obtained for the choice of $\alpha = 2/3$, [56, 44]

$$u^{m+1} = u^m + \frac{\Delta t}{4}\left[f(t_m, u_m) + 3f\left(t_m + \frac{2}{3}\Delta t, u_m + \frac{2}{3}\Delta t\, f(t_m, u_m)\right)\right] \quad, \quad m \geq 0 . \qquad (2.107)$$

We can obtain higher order formulas by expressing the general formulation of RKM as, [25]

$$u^{m+1} = u^m + \Delta t \sum_{j=1}^{n} \gamma_i K_j \qquad (2.108)$$

where

$$K_1 = f(t_m, u_m)$$

$$K_j = f(t_m + \alpha_j \Delta t, u_m + \Delta t \sum_{i=1}^{j-1} \beta_{ji} K_i)$$

with $\alpha_j = \sum_{i=1}^{j-1} \beta_{ji}$ and $0 \leq \alpha_j \leq 1$.

We can choose these coefficients to make the leading terms in the truncation error equal to zero and obtain higher order formulas.

For $n = 4$, four stage, fourth order RKM is obtained, [56, 44]

$$u^{m+1} = u^m + \frac{\Delta t}{6}[K_1 + 2K_2 + 2K_3 + K_4] \qquad (2.109)$$

where

$$K_1 = f(t_m, u_m)$$

$$K_2 = f(t_m + \frac{1}{2}\Delta t, u_m + \frac{1}{2}\Delta t K_1)$$

$$K_3 = f(t_m + \frac{1}{2}\Delta t, u_m + \frac{1}{2}\Delta t K_2) \qquad (2.110)$$

$$K_4 = f(t_m + \Delta t, u_m + \Delta t K_3) .$$

Now, we will modify this method to solve our problem. For the time-dependent problem considered in Section 2.3, the DRBEM results in equation (2.60)

$$-\mathbf{S}\dot{u} + \mathbf{H}\mathbf{u} - \mathbf{G}\mathbf{q}=\mathbf{0}. \qquad (2.111)$$

55

In order to use the method we express the equation (2.111) in the form

$$\dot{u} = \mathbf{S}^{-1}\mathbf{Hu} - \mathbf{S}^{-1}\mathbf{Gq}. \tag{2.112}$$

For the simplicity of notations let $\tilde{H} = \mathbf{S}^{-1}\mathbf{H}$ and $\tilde{G} = \mathbf{S}^{-1}\mathbf{G}$. Hence,

$$\dot{u} = \tilde{H}\mathbf{u} - \tilde{G}\mathbf{q}. \tag{2.113}$$

Now, equation (2.113) can be solved by taking $\tilde{H}\mathbf{u} - \tilde{G}\mathbf{q}$ as the vector function $f(t, u)$ (equation 2.95) in the sample problem $\dot{u} = f(t, u)$. Notice that the right hand side of the equation (2.113) includes both $\mathbf{u}$ and $\mathbf{q}$ as unknowns. In equation (2.110), we evaluate $\mathbf{K_1}$ at time t_m, $\mathbf{K_2}$ and $\mathbf{K_3}$ at the average of t_{m+1} and t_m and $\mathbf{K_4}$ at t_{m+1}.

When the time derivative in equation (2.113) is discretized by fourth order RKM, we have

$$\mathbf{u}^{m+1} = \mathbf{u}^m + \frac{\Delta t}{6}[\mathbf{K_1} + 2\mathbf{K_2} + 2\mathbf{K_3} + \mathbf{K_4}] \tag{2.114}$$

where

$$\mathbf{K_1} = \tilde{H}\mathbf{u}^m - \tilde{G}\mathbf{q}^m$$

$$\mathbf{K_2} = \tilde{H}\Big(\frac{\mathbf{u}^{m+1} + \mathbf{u}^m}{2} + \frac{\Delta t}{2}\mathbf{K_1}\Big) - \tilde{G}\Big(\frac{\mathbf{q}^{m+1} + \mathbf{q}^m}{2} + \frac{\Delta t}{2}\mathbf{K_1}\Big)$$

$$\mathbf{K_3} = \tilde{H}\Big(\frac{\mathbf{u}^{m+1} + \mathbf{u}^m}{2} + \frac{\Delta t}{2}\mathbf{K_2}\Big) - \tilde{G}\Big(\frac{\mathbf{q}^{m+1} + \mathbf{q}^m}{2} + \frac{\Delta t}{2}\mathbf{K_2}\Big) \tag{2.115}$$

$$\mathbf{K_4} = \tilde{H}\Big(\mathbf{u}^{m+1} + \Delta t\mathbf{K_3}\Big) - \tilde{G}\Big(\mathbf{q}^{m+1} + \Delta t\mathbf{K_3}\Big)$$

where in $\mathbf{K_2}$ and $\mathbf{K_3}$ average of $\mathbf{u}^m$, $\mathbf{u}^{m+1}$ and $\mathbf{q}^m$, $\mathbf{q}^{m+1}$ are taken as approximations to the values at the point $t_m + \dfrac{\Delta t}{2}$. This is needed to bring both $\mathbf{u}^{m+1}$ and $\mathbf{q}^{m+1}$ as unknowns to the left hand side of the equation (2.114). These values are going to be required for the next iteration.

After substituting equation (2.115) into equation (2.114), we can arrange equation (2.114) such that the right hand side is at time $m\Delta t$ and known and left hand side is at time $(m + 1)\Delta t$. After inserting boundary conditions to the equation (2.114) we get

$$\mathbf{Ax} = \mathbf{y} \tag{2.116}$$

where **x** is the vector of unknown boundary values of both **u** and **q**. The vector **y** contains the known information.

Equations (2.88), (2.93) or (2.114) resulting from the applications of Euler, central difference and Runge-Kutta methods will be solved iteratively until some convergence criteria is met. A possible convergence criteria to terminate the procedure is to determine the difference between the values of **u** at two successive iterates until these are close to one another in some norm. The measure of closeness most frequently used for the successive approximations is the L_∞ norm $max|\mathbf{u}^{m+1} - \mathbf{u}^m| \leq \varepsilon$ where maxima is taken over all the nodes and ε is a pre-assigned tolerance.

In the next chapter, DRBEM with FDM and RKM time integration methods are going to be applied to solve unsteady Navier-Stokes equations defined in terms of stream function and vorticity. Velocity Poisson's equations are also obtained relating the velocity components to vorticity. Thus, flow vector information is also easily obtained from the DRBEM solutions of these Poisson's equations. Then, the energy equation will be added to the Navier-Stokes equations, and natural and mixed convection flows will be discussed. The application will be extended to natural convection flow of nanofluids in which nanoparticles are included in the base fluid, and then to micropolar fluids. In micropolar fluid flow one more equation, namely the microrotation equation which represents the rotation of microstructures will be added to Navier-Stokes and energy equation. The solutions will be given in terms of streamlines, isotherms, vorticity and microrotation contours, velocity profiles as well as tables discussing heat transfer rate of those flows.

CHAPTER 3

APPLICATION OF DRBEM TO FLUID FLOW PROBLEMS

In Chapter 2, DRBEM is applied to Poisson equation with different types of right hand side functions. The application of the method gives rise to a system of first order ODEs which are solved using three time integration methods.

In this chapter, we will apply the method to simulate the transient, laminar flow of incompressible, viscous fluids described by the Navier-Stokes equations. Stream function-vorticity formulation of the equations are considered. The time derivative in the vorticity transport equation will be discretized using forward and central difference methods, and Runge-Kutta method for comparison purposes. Then, the application will be simulated on three test problems. The efficiency of time integration methods will be discussed on the second problem which is the one-sided lid-driven cavity flow.

We will also solve natural and mixed convection flows, and natural convection flow of nanofluids by adding energy equation to Navier-Stokes equations. Test problems will be solved for each type of flow. Natural convection flow in a square cavity with uniformly and non-uniformly heated walls, and in a triangular enclosure are solved.

Finally, the system of equations resulting from natural convection flow will be extended by adding the DRBEM application to the microrotation equation. Two test problems are provided for different physical configurations.

The results for these problems are given in terms of streamlines, vorticity, isotherm and microrotation contours and velocity profiles at the mid-plane of the cavity.

3.1 Navier-Stokes Equations

Two-dimensional, transient and laminar flow of incompressible, viscous fluid is governed by the well known Navier-Stokes equations [36]. They are transformed into the stream function-vorticity form in Chapter 1 (equations (1.22) and (1.23)).

Stream function is related to vorticity with the Poisson equation

$$\nabla^2 \psi = -\omega . \tag{3.1}$$

Vorticity is defined in terms of velocity components as $\omega = \dfrac{\partial v}{\partial x} - \dfrac{\partial u}{\partial y}$, and the vorticity transport equation is given as

$$\frac{1}{Re}\nabla^2 \omega = \frac{\partial \omega}{\partial t} + u\frac{\partial \omega}{\partial x} + v\frac{\partial \omega}{\partial y} \tag{3.2}$$

where $u = \dfrac{\partial \psi}{\partial y}, v = -\dfrac{\partial \psi}{\partial x}$. Re is the Reynolds number of the flow.

We will now propose to solve equations (3.1) and (3.2) with the general boundary conditions

$$\psi(x_s, y_s) = f_{\psi_s} \quad , \quad \omega(x_s, y_s) = f_{\omega_s} \tag{3.3}$$

where the subscript 's' restricts (x, y) to the boundary of the region under consideration and f_{ψ_s}, f_{ω_s} are given functions. Stream function is usually specified on the boundary and the vorticity boundary condition is derived from the stream function equation (3.1) or from its definition, which becomes again Dirichlet type.

Also, the initial conditions for ψ and ω as given with known functions ψ_0 and ω_0

$$\psi(x, y, 0) = \psi_0(x, y) \quad , \quad \omega(x, y, 0) = \omega_0(x, y) . \tag{3.4}$$

Equation (3.2) contains the convective terms $u = \dfrac{\partial \psi}{\partial y}$ and $v = -\dfrac{\partial \psi}{\partial x}$, and the viscous diffusion term $\dfrac{1}{Re}\nabla^2 \omega$. Observe that the equations (3.1) and (3.2) are coupled. The vorticity ω appears in equation (3.1) and the derivatives of ψ appear in equation (3.2) as coefficients. In addition to this, the equation (3.2) is nonlinear.

DRBEM application to the general Poisson equation of the type $\nabla^2 u = b$ results in the matrix equations of the form (equation (2.57))

$$\mathbf{Hu} - \mathbf{Gq} = (\mathbf{H\hat{U}} - \mathbf{G\hat{Q}})\mathbf{F}^{-1}\mathbf{b} \tag{3.5}$$

where the right hand side for the stream function equation (3.1) and vorticity transport equation (3.2) are

$$b = -\omega \tag{3.6}$$

and

$$b = \frac{\partial \omega}{\partial t} + u\frac{\partial \omega}{\partial x} + v\frac{\partial \omega}{\partial y} \tag{3.7}$$

respectively.

Thus, the DRBEM application of stream function and vorticity transport equations will result in the systems

$$\mathbf{H}\psi - \mathbf{G}\psi_q = (\mathbf{H}\hat{\mathbf{U}} - \mathbf{G}\hat{\mathbf{Q}})\mathbf{F}^{-1}(-\omega) \tag{3.8}$$

and

$$\frac{1}{Re}(\mathbf{H}\omega - \mathbf{G}\omega_q) = (\mathbf{H}\hat{\mathbf{U}} - \mathbf{G}\hat{\mathbf{Q}})\mathbf{F}^{-1}\Big(\frac{\partial \omega}{\partial t} + \mathbf{u}\frac{\partial \omega}{\partial x} + \mathbf{v}\frac{\partial \omega}{\partial y}\Big) \tag{3.9}$$

where ψ, ψ_q, ω, ω_q, $\mathbf{u}$ and $\mathbf{v}$ are the vectors. The matrices $\mathbf{H}$, $\mathbf{G}$, $\hat{\mathbf{U}}$, $\hat{\mathbf{Q}}$ and $\mathbf{F}$ are derived in Chapter 2.

The convective terms in the right hand side of the vorticity equation (3.9) are approximated using DRBEM idea (equations in (2.68))

$$\frac{1}{Re}(\mathbf{H}\omega - \mathbf{G}\omega_q) = (\mathbf{H}\hat{\mathbf{U}} - \mathbf{G}\hat{\mathbf{Q}})\mathbf{F}^{-1}\Big[\frac{\partial \omega}{\partial t} + \mathbf{u}\frac{\partial \mathbf{F}}{\partial x}\mathbf{F}^{-1}\omega + \mathbf{v}\frac{\partial \mathbf{F}}{\partial y}\mathbf{F}^{-1}\omega\Big] \tag{3.10}$$

where diagonal matrices are formed with the vectors $\mathbf{u}$ and $\mathbf{v}$ for the purpose of matrix multiplications.

For the simplicity of notations we rewrite the equations (3.8) and (3.10) as

$$\mathbf{H}\psi - \mathbf{G}\psi_q = \tilde{b} \tag{3.11}$$

and

$$\frac{1}{Re}(\mathbf{H}\omega - \mathbf{G}\omega_q) = \mathbf{S}\frac{\partial \omega}{\partial t} + \mathbf{D}\omega \tag{3.12}$$

where the vector $\tilde{b}$ and the matrices $\mathbf{S}$, $\mathbf{D}$ are defined as

$$\tilde{b} = (\mathbf{H}\hat{\mathbf{U}} - \mathbf{G}\hat{\mathbf{Q}})\mathbf{F}^{-1}(-\omega) \quad , \quad \mathbf{S} = (\mathbf{H}\hat{\mathbf{U}} - \mathbf{G}\hat{\mathbf{Q}})\mathbf{F}^{-1} \quad , \quad \mathbf{D} = \mathbf{S}\Big(\mathbf{u}\frac{\partial \mathbf{F}}{\partial x}\mathbf{F}^{-1} + \mathbf{v}\frac{\partial \mathbf{F}}{\partial y}\mathbf{F}^{-1}\Big).$$

Further simplifications can be made to the equation (3.12)

$$-\mathbf{S}\frac{\partial \omega}{\partial t} + \mathbf{H1}\,\omega - \mathbf{G1}\,\omega_q = 0 \qquad (3.13)$$

where $\mathbf{H1} = \dfrac{1}{Re}\mathbf{H} - \mathbf{D}$ and $\mathbf{G1} = \dfrac{1}{Re}\mathbf{G}$.

The right hand side of equation (3.11) is a known vector since vorticity vector ω is given initially. Thus, the equation can be solved iteratively. Equation (3.13) involves the derivative of ω with respect to time, so we need a time integration scheme. We use three different integration methods, namely forward and central difference methods, and Runge-Kutta method. For forward and central difference methods relaxation parameters are used for ω and ω_q as in equation (2.87) to avoid stability problems, and to accelerate the rate of convergence in the iteration.

When the time derivative is discretized with forward difference, and ω and ω_q are positioned using the relaxation parameters, we obtain

$$-\mathbf{S}\frac{\omega^{m+1} - \omega^{m}}{\Delta t} + \mathbf{H1}((1 - \beta_\omega)\omega^{m} + \beta_\omega \omega^{m+1}) - \mathbf{G1}((1 - \beta_{\omega_q})\omega_q{}^{m} + \beta_{\omega_q}\omega_q{}^{m+1}) = \mathbf{0}. \quad (3.14)$$

Equation (3.14) can be arranged such that the left and right hand sides are at time $(m + 1)\Delta t$ and $m\Delta t$, respectively. Thus,

$$\left(\frac{-\mathbf{S}}{\Delta t} + \beta_\omega \mathbf{H1}\right)\omega^{m+1} - \beta_{\omega_q}\mathbf{G1}\omega_q{}^{m+1} = \left[\frac{-\mathbf{S}}{\Delta t} - (1 - \beta_\omega)\mathbf{H1}\right]\omega^{m} + (1 - \beta_{\omega_q})\mathbf{G1}\omega_q{}^{m}. \quad (3.15)$$

If central difference method with relaxation parameters is applied to equation (3.13) then we have

$$-\mathbf{S}\frac{\omega^{m+1} - \omega^{m-1}}{2\Delta t} + \mathbf{H1}((1 - \beta_\omega)\omega^{m-1} + \beta_\omega \omega^{m+1}) - \mathbf{G1}((1 - \beta_{\omega_q})\omega_q{}^{m-1} + \beta_{\omega_q}\omega_q{}^{m+1}) = \mathbf{0}. \quad (3.16)$$

Similarly equation (3.16) can be rewritten as

$$\left(\frac{-\mathbf{S}}{2\Delta t} + \beta_\omega \mathbf{H1}\right)\omega^{m+1} - \beta_{\omega_q}\mathbf{G1}\omega_q{}^{m+1} = \left[\frac{-\mathbf{S}}{2\Delta t} - (1 - \beta_\omega)\mathbf{H1}\right]\omega^{m-1} + (1 - \beta_{\omega_q})\mathbf{G1}\omega_q{}^{m-1} \quad (3.17)$$

where $m = 1, 2, 3, ...$

In the central difference method we use two previous iterations. The iteration process starts with two initial conditions both of which are selected as zero or the first starting values

$(\omega^1, \omega_q{}^1)$ can be taken from the results of equation (3.15). In this iterative procedure the system is solved by using 'm-1' level known values to obtain 'm+1' level unknowns. But, in each iteration the stream function equation (3.11) is solved with the vorticity values from the m-th level, and therefore the matrices $\mathbf{D}$ and $\mathbf{H1}$ are recalculated with this new value. Thus, the iterative procedure makes use of all the previous known values from the m-th and $(m-1)$-th time levels.

Finally, we employed fourth-order Runge-Kutta method to discretize the time derivative in equation (3.13). In order to use the method we express the equation (3.13) in the form

$$\frac{\partial \omega}{\partial t} = \mathbf{S}^{-1}\mathbf{H1}\,\omega - \mathbf{S}^{-1}\mathbf{G1}\,\omega_q \,. \tag{3.18}$$

For the simplicity of the notations let $\tilde{H} = \mathbf{S}^{-1}\mathbf{H1}$ and $\tilde{G} = \mathbf{S}^{-1}\mathbf{G1}$. Thus,

$$\frac{\partial \omega}{\partial t} = \tilde{H}\omega - \tilde{G}\omega_q \,. \tag{3.19}$$

Now, the method can be applied by taking $\tilde{H}\omega - \tilde{G}\omega_q$ as the vector function $f(t, u)$ in the sample problem $\dot{u} = f(t, u)$ explained in Section 2.6.2. Since the resulting equation (3.19) include both ω and ω_q as unknowns we evaluate $\mathbf{K_1}$ at time t_m, $\mathbf{K_2}$ and $\mathbf{K_3}$ at the average of t_{m+1} and t_m, and $\mathbf{K_4}$ at t_{m+1}. This enables us to compute ω_q also at the 'm+1' level.

Thus, we have

$$\omega^{m+1} = \omega^m + \frac{\Delta t}{6}[\mathbf{K_1} + 2\mathbf{K_2} + 2\mathbf{K_3} + \mathbf{K_4}] \tag{3.20}$$

where

$$\mathbf{K_1} = \tilde{H}\omega^m - \tilde{G}\omega_q{}^m$$

$$\mathbf{K_2} = \tilde{H}\Big(\frac{\omega^{m+1} + \omega^m}{2} + \frac{\Delta t}{2}\mathbf{K_1}\Big) - \tilde{G}\Big(\frac{\omega_q{}^{m+1} + \omega_q{}^m}{2} + \frac{\Delta t}{2}\mathbf{K_1}\Big)$$

$$\tag{3.21}$$

$$\mathbf{K_3} = \tilde{H}\Big(\frac{\omega^{m+1} + \omega^m}{2} + \frac{\Delta t}{2}\mathbf{K_2}\Big) - \tilde{G}\Big(\frac{\omega_q{}^{m+1} + \omega_q{}^m}{2} + \frac{\Delta t}{2}\mathbf{K_2}\Big)$$

$$\mathbf{K_4} = \tilde{H}(\omega^{m+1} + \Delta t\mathbf{K_3}) - \tilde{G}\big(\omega_q{}^{m+1} + \Delta t\mathbf{K_3}\big)\,.$$

Equation (3.20) can also be arranged by substituting the equations in (3.21) back into equation (3.20) so that the right hand side is at time $m\Delta t$ and the left hand side is at time $(m+1)\Delta t$.

On the system of equations (3.15), (3.17) or (3.20) there are only $N + L$ unknowns. The right hand sides of these equations are known since they involve values which have been specified as initial condition or calculated previously. In addition to that the elements of matrices $\mathbf{H}$, $\mathbf{G}$, $\mathbf{G1}$, $\tilde{G}$ and $\mathbf{S}$ depend only on geometrical data. Thus, they can all be computed once and stored. But, the matrix $\tilde{H}$ is recalculated in each iteration due to the new values coming from $\mathbf{H1}$ and $\mathbf{D}$. If the value of Δt is kept constant, the system matrix can be reduced only once as well, and the time advance procedure will consist of a simple recursive scheme with only algebraic operations involved.

Once the boundary conditions are inserted to the equations (3.15), (3.17) or (3.20) the known and unknown values of ω and ω_q are passed from one side to another. Thus, we get

$$\mathbf{Ax} = \mathbf{y} \qquad (3.22)$$

where $\mathbf{x}$ is the vector of unknown boundary values of ω and ω_q. The vector $\mathbf{y}$ contains known information.

We start the iteration by solving the stream function equation (3.11) using the initial condition of vorticity. Then the velocity components, $\mathbf{u}$ and $\mathbf{v}$ are calculated using the idea given in equations (2.68). Finally, the vorticity equation (3.13) is solved by using one of the time integration schemes given as forward, central and fourth order Runge-Kutta methods. We set up these new values as initial conditions for the next time step.

63

3.1.1 Test Problem 1

In this problem, the Navier-Stokes equations are solved when an external force is present to see the accuracy and efficiency of present numerical method since the exact solution is available,

$$\nabla^2 \psi \;=\; -\omega$$

$$\frac{1}{Re}\nabla^2 \omega \;=\; \frac{\partial \omega}{\partial t} + v\frac{\partial \omega}{\partial x} + u\frac{\partial \omega}{\partial y} - g$$

(3.23)

where the problem is defined in the region $0 \le x, y \le 1$.

The Dirichlet boundary conditions are given by, [94]

$$\psi = 0 \quad , \quad \omega = -\pi^2 \sin t(\cos 2\pi x + \cos 2\pi y - 2\cos 2\pi x \cos 2\pi y)$$

with the initial condition $\omega_0 = 0$. The analytical solution in terms of ψ, u, v and ω is, [94]

$$\psi = -\sin t \sin^2 \pi x \sin^2 \pi y$$

$$u = \pi \sin t \sin^2 \pi x \sin 2\pi y$$

$$v = -\pi \sin t \sin^2 \pi y \sin 2\pi x$$

$$\omega = -\pi^2 \sin t(\cos 2\pi x + \cos 2\pi y - 2\cos 2\pi x \cos 2\pi y) \,.$$

The source function g is

$$g = -\pi^2 \cos t(\cos 2\pi x + \cos 2\pi y - 2\cos 2\pi x \cos 2\pi y) + \pi^4 \sin^2 t \sin 2\pi x \sin 2\pi y(\cos 2\pi x - \cos 2\pi y)$$

$$-\frac{4}{Re}\pi^4 \sin t(\cos 2\pi x + \cos 2\pi y - 4\cos 2\pi x \cos 2\pi y) \,.$$

The problem is solved by discretizing the time derivative using forward (Euler) difference scheme. Numerical stability problems are overcomed by using relaxation parameters for vorticity and its normal derivative values. The best results are obtained for the relaxation parameters $\beta_\omega = \beta_{\omega_q} = 0.9$ by taking $\Delta t = 0.001$ in forward difference scheme. In this problem, radial basis functions are taken as $f = 1 + r$. Linear boundary elements are used for the boundary discretization. In figures (3.1), (3.2) and (3.3) we compare the effect of number of boundary

nodes on the solution for $Re = 100$. Even $N = 40$ is suitable for small and moderate Re. But for increasing values of Re, $N = 72$ is needed to obtain better accuracy in comparison with the exact solution. Figures (3.4), (3.5) and (3.6) show the streamlines and vorticity contours of the exact and numerical solution for $Re = 500, 1000$ and 3000, respectively. Solutions are presented at the time level $t = 0.03$.

A good agreement is obtained when compared to exact solution [94]. This viscous flow problem has the particularity of having a flow pattern which is independent of the Reynolds number.
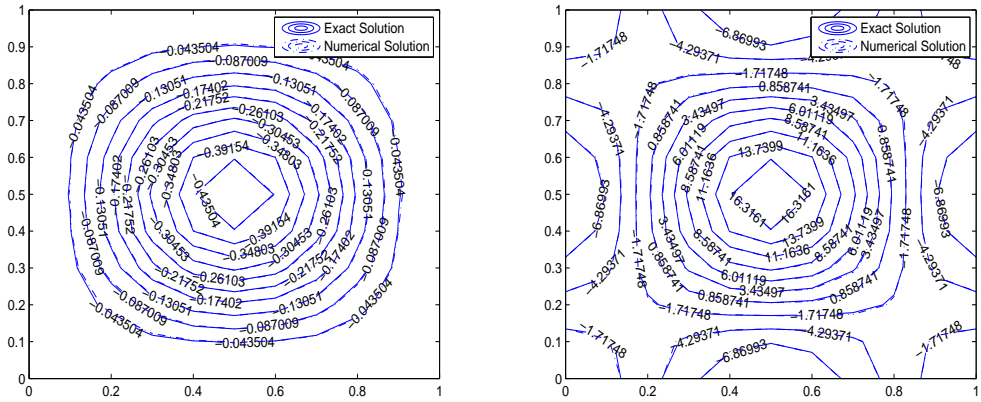
Figure 3.1: Streamlines and vorticity contours for $Re = 100$ at $t = 0.03$ with $N = 40$
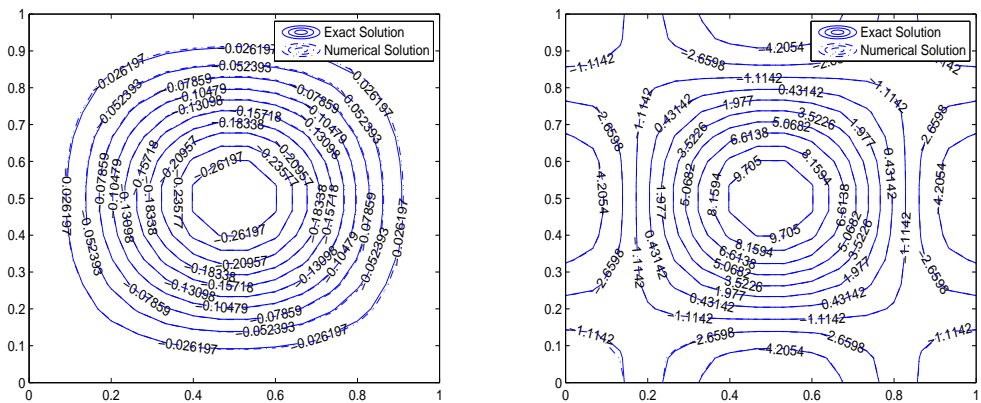
Figure 3.2: Streamlines and vorticity contours for $Re = 100$ at $t = 0.03$ with $N = 60$
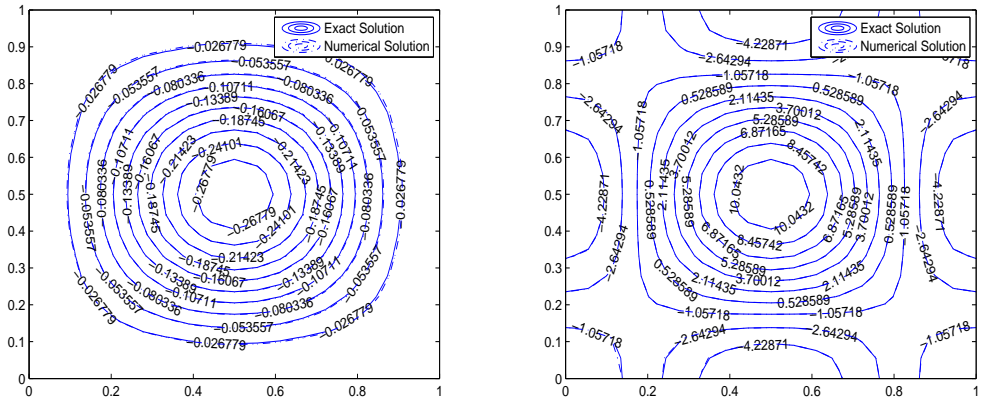
Figure 3.3: Streamlines and vorticity contours for $Re = 100$ at $t = 0.03$ with $N = 72$
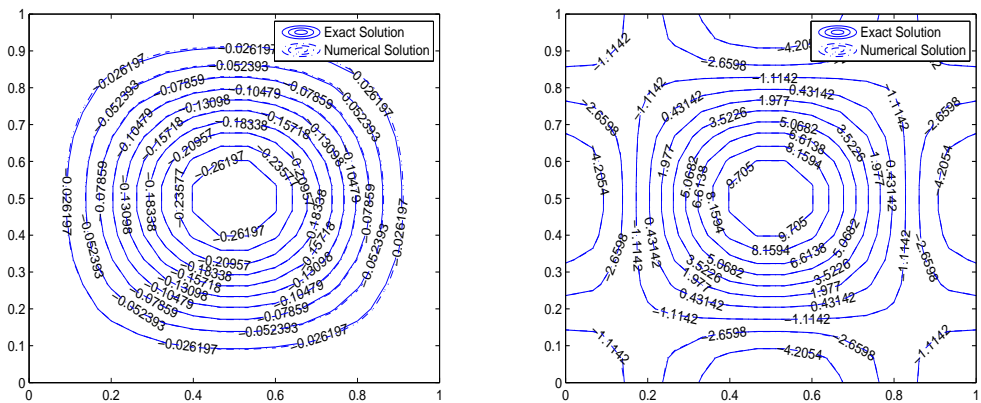
Figure 3.4: Streamlines and vorticity contours for $Re = 500$ at $t = 0.03$ with $N = 72$
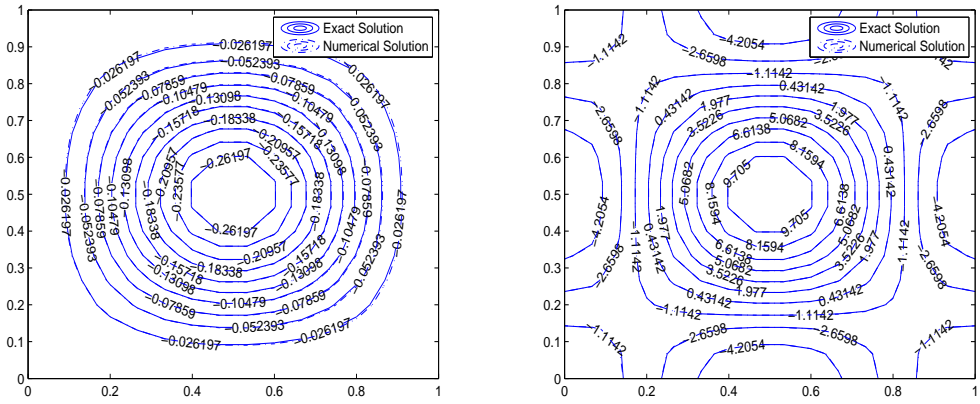
Figure 3.5: Streamlines and vorticity contours for $Re = 1000$ at $t = 0.03$ with $N = 72$
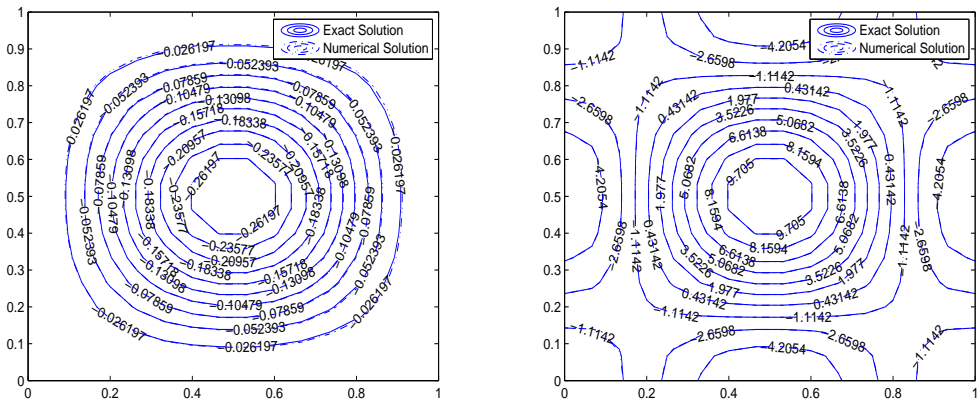
Figure 3.6: Streamlines and vorticity contours for $Re = 3000$ at $t = 0.03$ with $N = 72$

3.1.2 Lid-Driven Cavity Flow

We simulate lid-driven cavity flow in a square cavity $\Omega = [0, 1] \times [0, 1]$ as the second problem, [71]. The lid of the cavity moves at a given, constant velocity, thereby setting the fluid in motion (Figure (3.7)).

The non-dimensional equations in stream function-vorticity formulation are given as

$$\nabla^2 \psi = -\omega$$

$$\frac{1}{Re} \nabla^2 \omega = \frac{\partial \omega}{\partial t} + u \frac{\partial \omega}{\partial x} + v \frac{\partial \omega}{\partial y} .$$

(3.24)

The no-slip conditions are imposed on all segments of the boundary with the exception of the upper boundary, along which the velocity in x-direction is set to 1 to simulate the moving lid. Thus, stream function boundary conditions are zero. The vorticity boundary conditions are derived from $\omega = \dfrac{\partial v}{\partial x} - \dfrac{\partial u}{\partial y}$, which is approximated by using the coordinate matrix **F** (equation (2.68)).

For this problem the time derivative is discretized using forward and central difference methods, and Runge-Kutta method for comparison purposes. Stability analysis is performed for the three methods and explained in Chapter 4. From the numerical stability analysis we observe that the maximum eigenvalues of the coefficient matrix for increasing values of Re when central difference scheme is used are smaller than the eigenvalues of the coefficient matrix when the forward difference scheme is used. When we compare the central difference and Runge-Kutta methods we see that using fourth-order Runge-Kutta method does not effect much the solution in terms of the size of time increment and the number of iterations. This is because of the usage of relaxation parameters in the central difference method. So, we continue to the rest of the computations with the central difference scheme with relaxation parameters $\beta_\omega = \beta_{\omega_q} = 0.9$.

Figures (3.8)-(3.13) represent the forward and central difference methods solution of stream function and vorticity at $Re = 100$, 500 and 1000, respectively. Figure (3.14) shows the horizontal and vertical velocity profiles at the mid-plane of the cavity. One can observe that increasing Reynolds number results an increase in the magnitude of the velocity components, and turning points get closer to the wall [71]. The Runge-Kutta method solution of stream function-vorticity and the velocity components at the mid-plane of the cavity are presented

for $Re = 500$ in Figures (3.15) and (3.16). From the comparison of Figures (3.10), (3.11) with (3.15) and (3.14) with (3.16) we conclude that Runge-Kutta method does not improve the results much. Also, smaller time increments and large number of iterations are required. The solutions are given at steady state in which the stopping criteria is taken as $\varepsilon = 10^{-6}$. The problem is solved using linear boundary elements and the radial basis function is taken as $f = 1 + r + r^2$. For this problem, 80, 96 and 120 boundary nodes with $\Delta t = 0.8$, 0.5 and 0.1 are used for Reynolds numbers 100, 500 and 1000, respectively when forward and central differences are used for the time derivative. 96 boundary elements with $\Delta t = 0.05$ are used for $Re = 500$ in the Runge-Kutta method. As Reynolds number increases it becomes essential to use large number of boundary nodes, [32] and smaller time increment in all time integration methods mentioned here. This is because at high Reynolds numbers thin boundary layers are developed near the walls.

Figures (3.8) and (3.9) present streamlines and vorticity contours at $Re = 100$. From the streamlines, we observe that the primary vortex moves towards the right upper corner and a secondary eddy occurs at the right bottom corner. With the increase in the Reynolds number from 100 to 500, the primary vortex starts to move towards the center of the cavity and it keeps moving to the center at $Re = 1000$. This behaviour can be seen from Figures (3.10)-(3.13). For $Re = 500$, the eddy in the right bottom corner grows and another secondary eddy occurs at the left bottom corner. For $Re = 1000$, another secondary eddy occurs at the left upper corner as expected. The solutions are in good agreement with the ones in [71].

For small Reynolds number the vorticity contours are at the center of the cavity. With an increase in the Reynolds number they move away from the center towards the walls. This behaviour indicates that the vorticity gradients are very strong at the walls. For increasing Reynolds number the center of the cavity is almost stagnant.

We continue to the rest of the computations in the thesis with the central difference scheme together with relaxation parameters. Central difference scheme is practical, easy to use and takes less computational time than the fourth-order Runge-Kutta method.
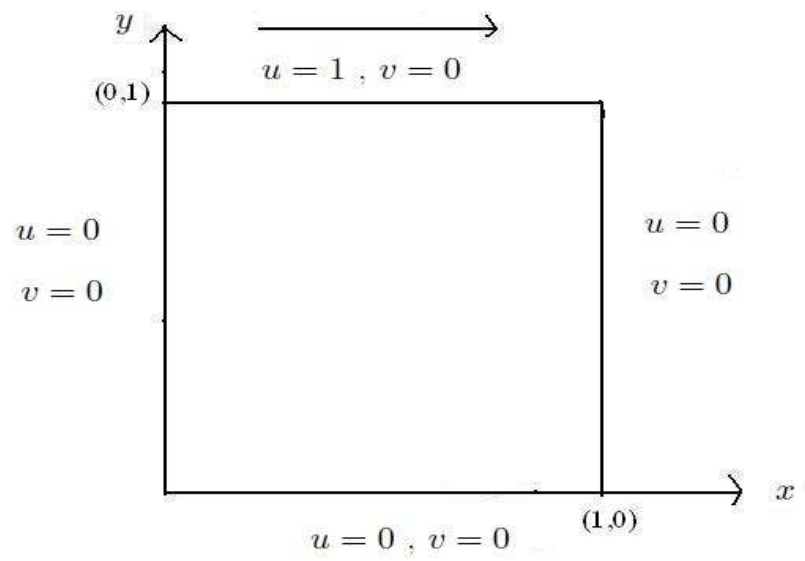
Figure 3.7: Boundary conditions for the lid-driven cavity flow
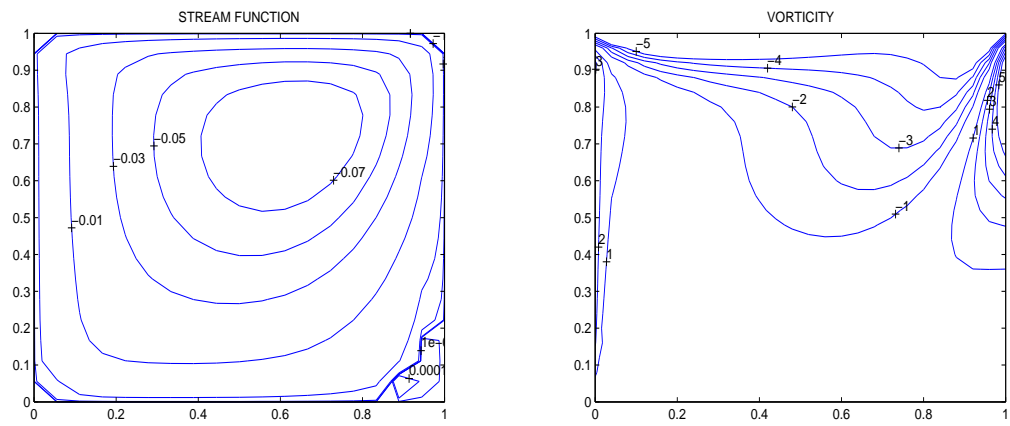
Figure 3.8: Forward difference scheme solution for $Re = 100$, $N = 80$, $\Delta t = 0.8$
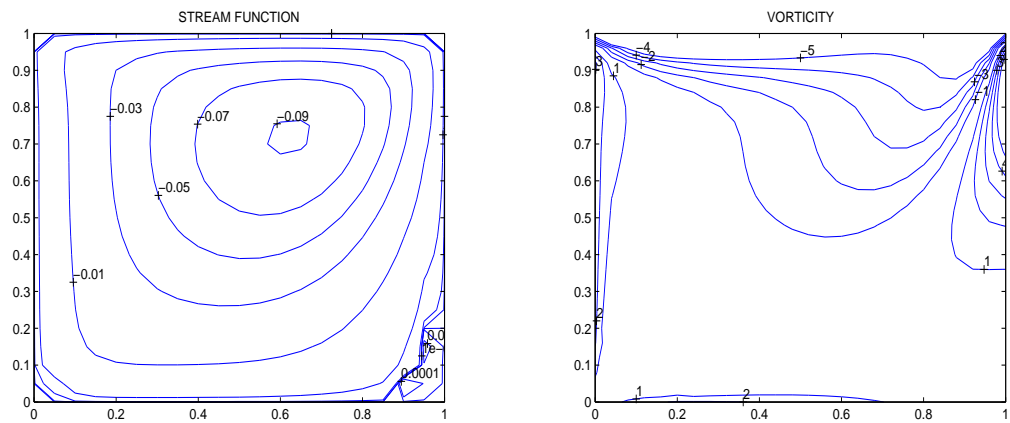
Figure 3.9: Central difference scheme solution for $Re = 100$, $N = 80$, $\Delta t = 0.8$
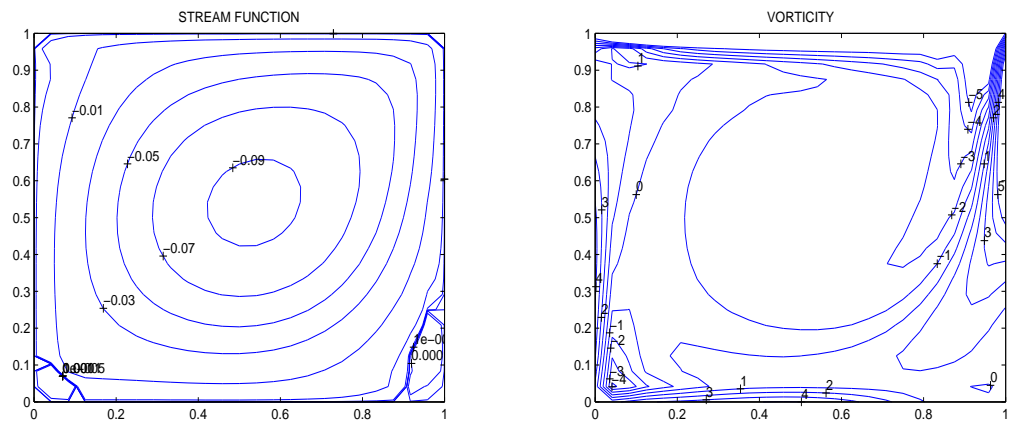
Figure 3.10: Forward difference scheme solution for $Re = 500$, $N = 96$, $\Delta t = 0.5$
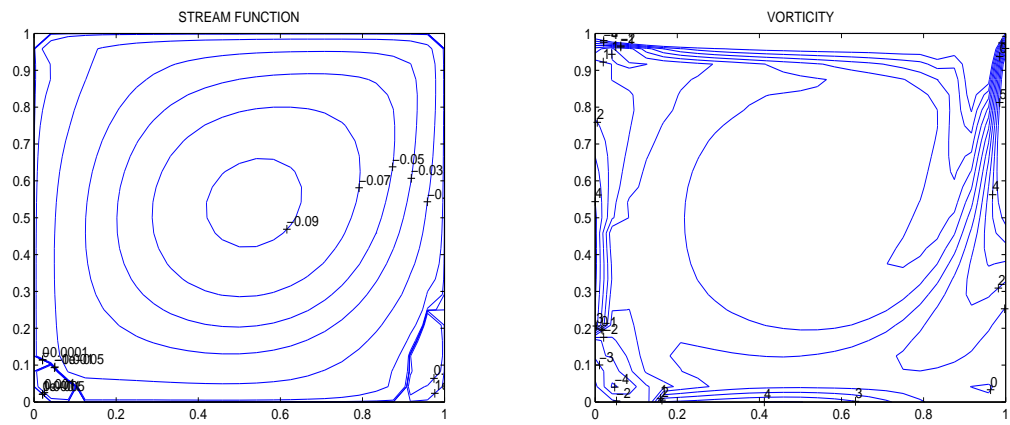
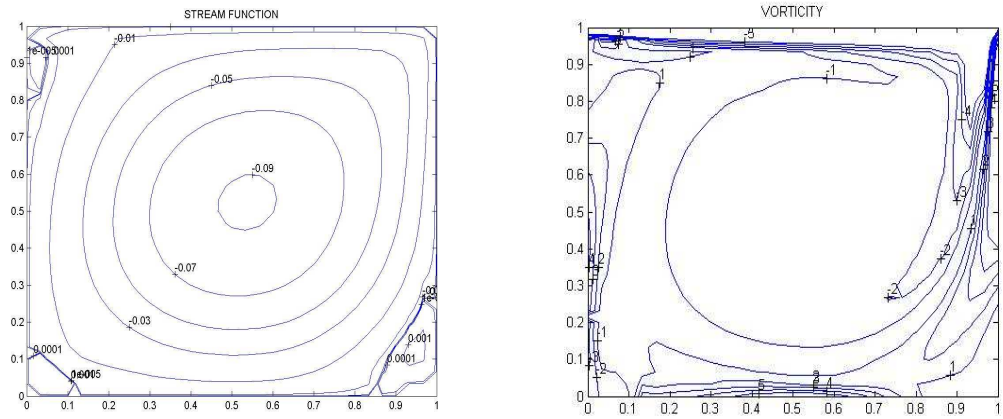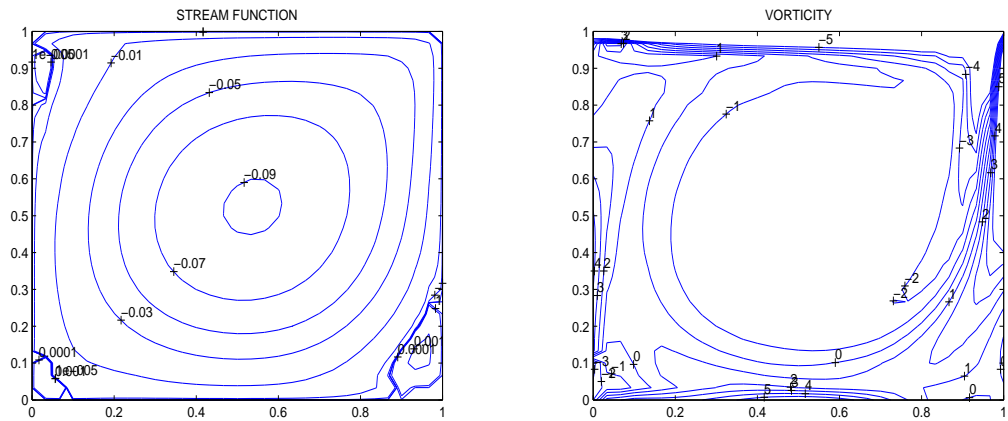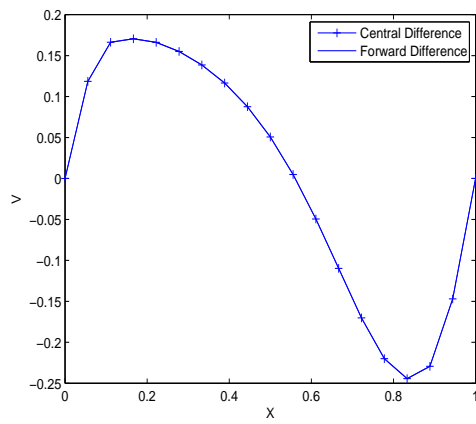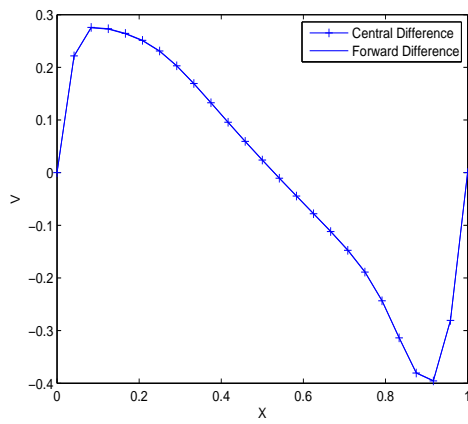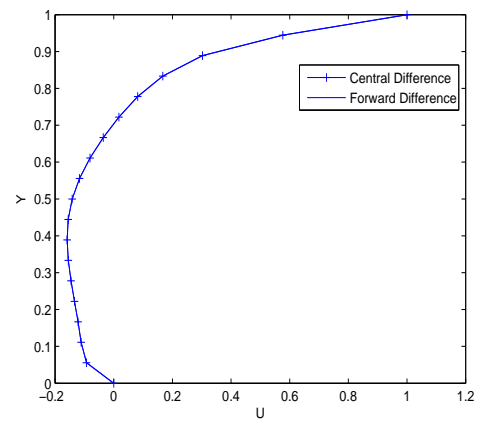Figure 3.11: Central difference scheme solution for $Re = 500$, $N = 96$, $\Delta t = 0.5$

Figure 3.12: Forward difference scheme solution for $Re = 1000$, $N = 120$, $\Delta t = 0.1$

Figure 3.13: Central difference scheme solution for $Re = 1000$, $N = 120$, $\Delta t = 0.1$
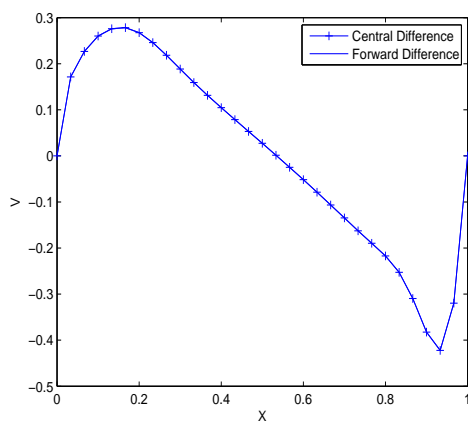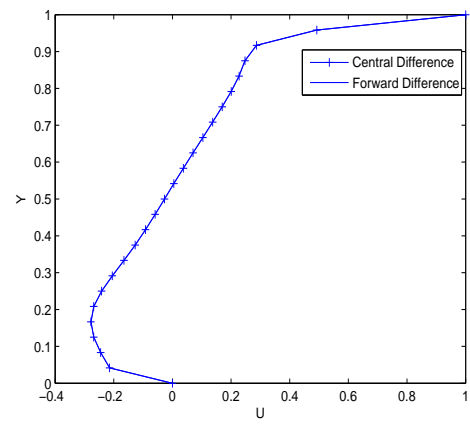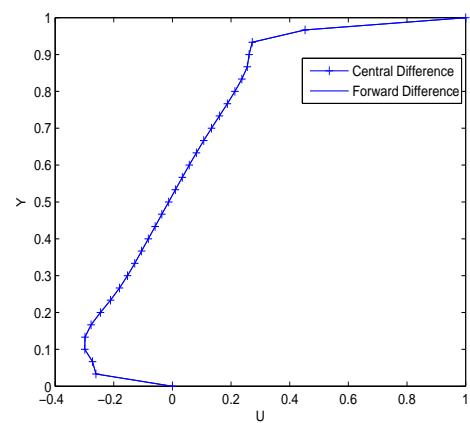
Figure 3.14: Horizontal and vertical velocity profiles along the centerline for $Re = 100, 500$ and 1000
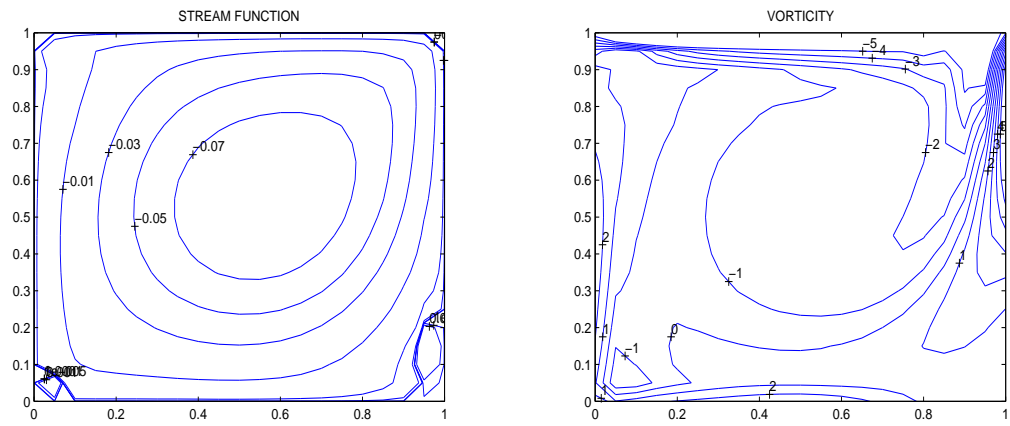
Figure 3.15: Runge-Kutta method solution for $Re = 500$, $N = 96$, $\Delta t = 0.05$
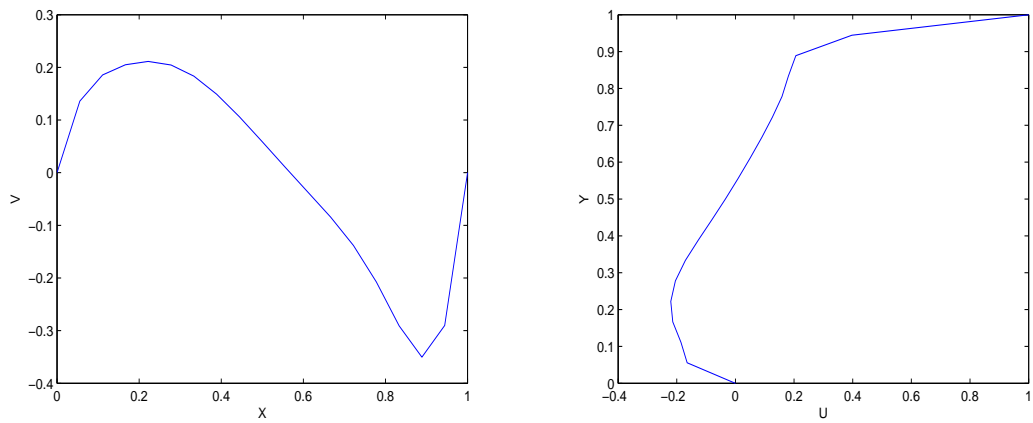
Figure 3.16: Horizontal and vertical velocity profiles with Runge-Kutta method along the centerline for $Re = 500$

3.1.3 Two-Sided Lid-Driven Cavity Flow

In the previous problem we investigate one-sided lid-driven cavity flow in which the upper wall is moving to the right with a constant velocity while the other walls are stationary. In this problem, we investigate two-sided lid-driven cavity flow in which the top wall is moving to the right, the bottom wall is either moving to the right or left with a constant velocity while the horizontal walls are stationary (Figure (3.17) and (3.18)). Two-sided lid-driven cavity flow has been employed to study drying process, polymer processing and thin film coating, [27]. The non-dimensional equations in stream function-vorticity formulation are given as

$$\nabla^2 \psi = -\omega$$

$$\frac{1}{Re}\nabla^2 \omega = \frac{\partial \omega}{\partial t} + u\frac{\partial \omega}{\partial x} + v\frac{\partial \omega}{\partial y} .$$

(3.25)

where $0 \leq x \leq L$ and $0 \leq y \leq H$. The vorticity boundary conditions are obtained from its definition. Linear boundary elements are used with quadratic radial basis functions. The time derivative is discretized by central difference scheme with relaxation parameters ($\beta_\omega = \beta_{\omega_q} = 0.9$). The problem is solved for $Re = 400$ with $\Delta t = 0.5$ for different values of aspect ratio, H/L. The solutions are given at steady state and the convergence criteria is taken as $\varepsilon = 10^{-5}$.

Figure (3.19) shows streamlines and vorticity contours for $Re = 400$ in the case of top and bottom walls are moving in the same and opposite directions when aspect ratio $H/L = 1$ (square cavity). In Figure (3.20), we see the vertical velocity profile at the mid-plane of the cavity for the same cases. One can notice that the movement of the walls in the same direction causes seperation of streamlines and vorticity contours at the center of the cavity whereas the opposite direction movement leaves stagnant regions at the center for both stream function and vorticity. Figures (3.21), (3.23) and (3.22), (3.24) show streamlines, vorticity contours and mid-plane vertical velocity profiles for different aspect ratios as $H/L = 2$ and $H/L = 1/2$, respectively. When aspect ratio is large, the seperation at the center is more dominant in the parallel motion. These three test problems, especially the one sided lid-driven cavity flow problem results show that the Navier-Stokes equations in terms of stream function and vorticity can be easly solved by using DRBEM. The simplicity lies in the treatment of diffusion terms by the fundamental solution of Laplace equation, and all the other terms as nonhomogeneity. The results are obtained for fairly high Reynolds number giving the well known behaviour of lid-driven square cavity flow.
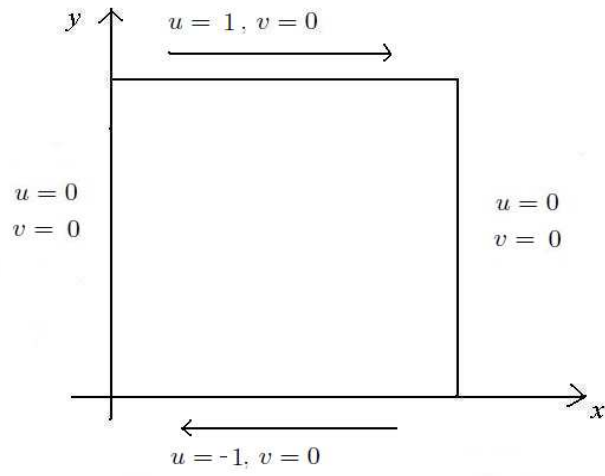
Figure 3.17: Boundary conditions for the two-sided (antiparallel motion) lid-driven cavity flow
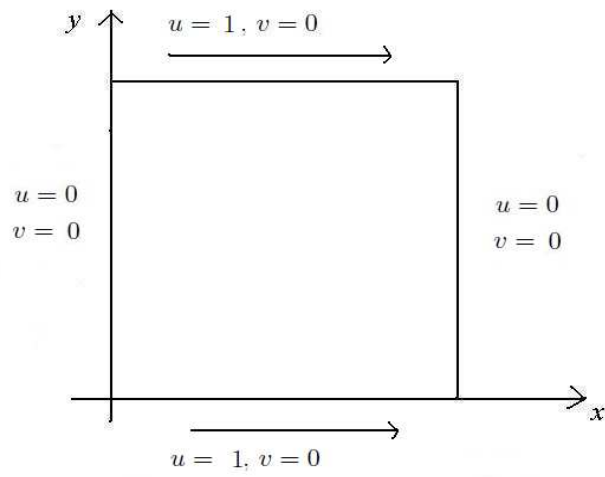

Figure 3.18: Boundary conditions for the two-sided (parallel motion) lid-driven cavity flow
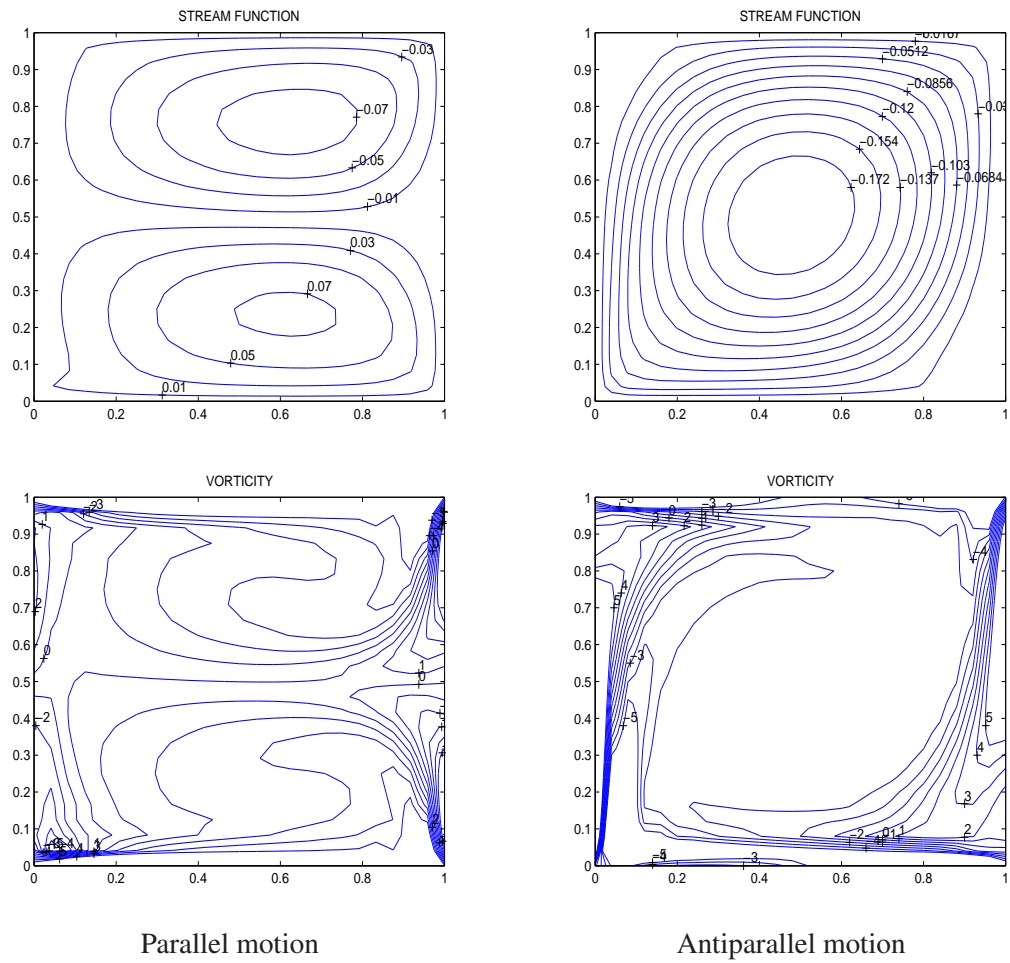
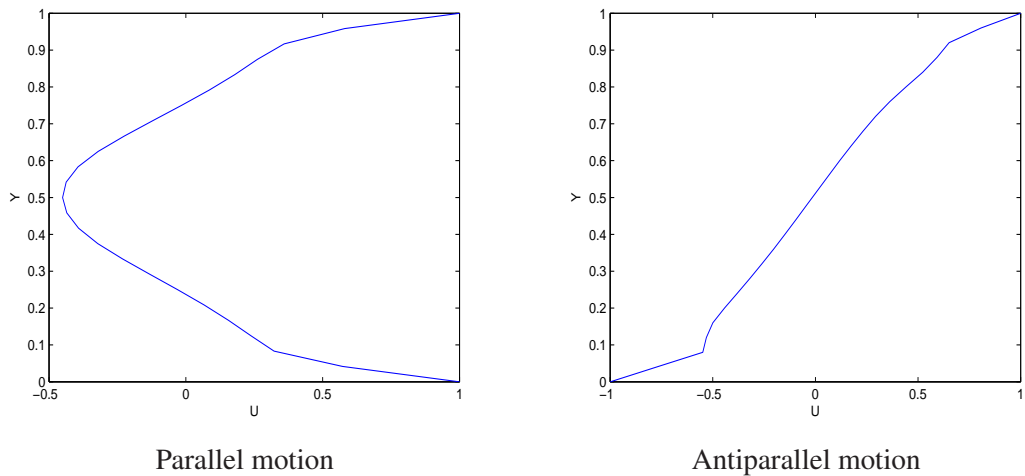Figure 3.19: Streamlines and vorticity contours for $Re = 400$, $H/L = 1$

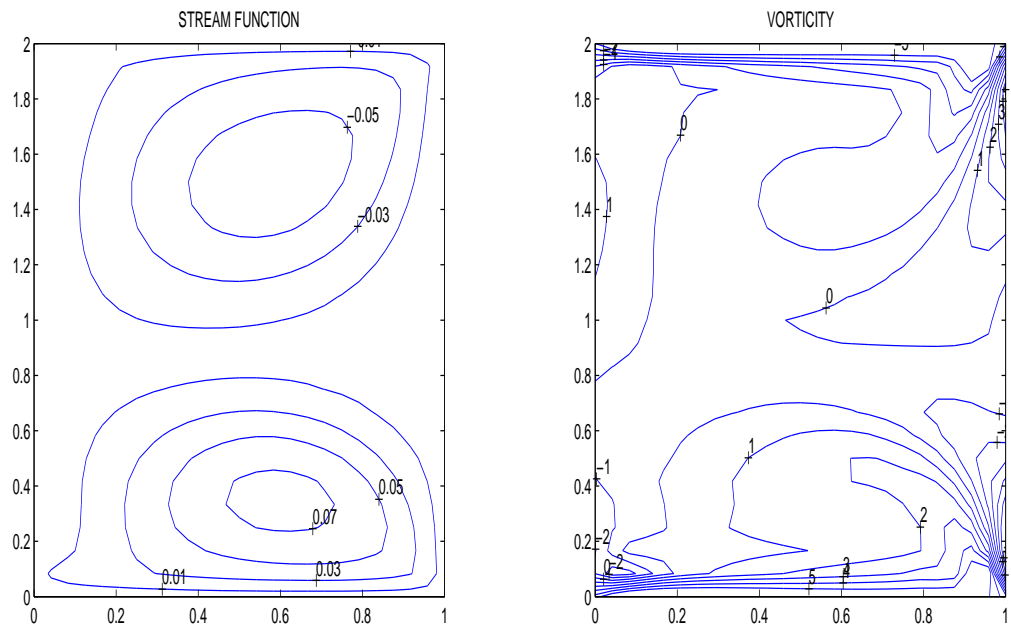Figure 3.20: Vertical velocity profile at the mid-plane of the cavity $Re = 400$, $H/L = 1$

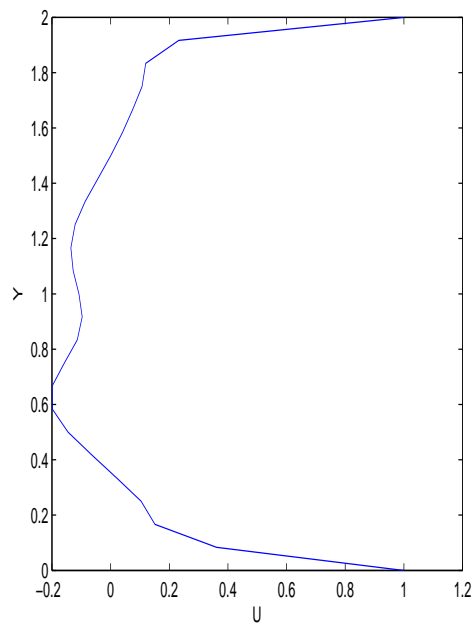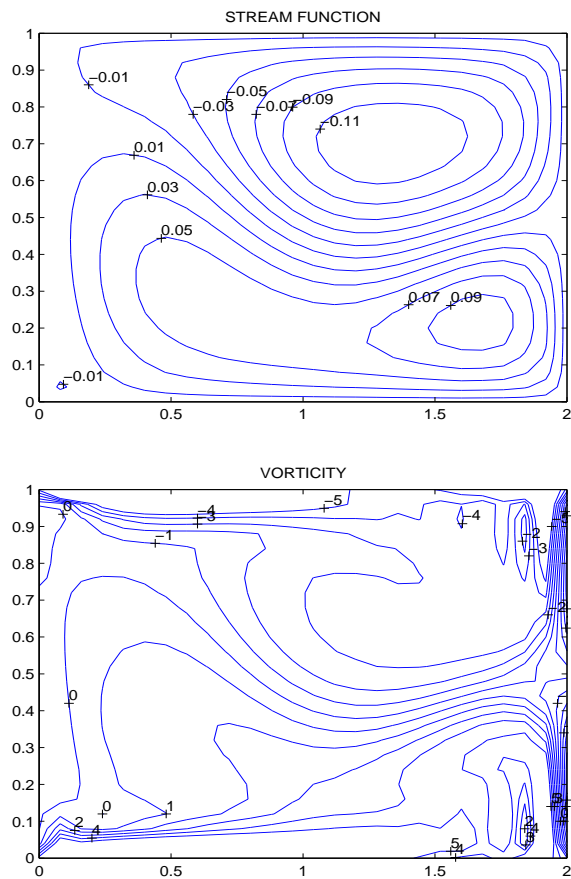Figure 3.21: Streamlines and vorticity contours for parallel motion, $H/L = 2$

Figure 3.22: Vertical velocity profile at the mid-plane of the cavity for parallel motion, $H/L = 2$

Figure 3.23: Streamlines and vorticity contours for parallel motion, $H/L = 1/2$
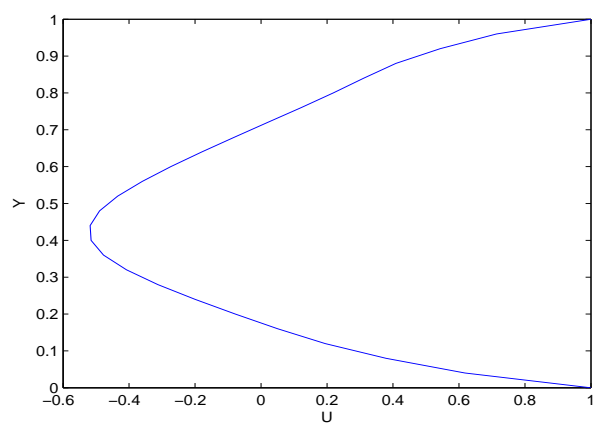

Figure 3.24: Vertical velocity profile at the mid-plane of the cavity for parallel motion, $H/L = 1/2$

3.2   Natural Convection Flow

In this section, we will extend the application of the method to natural convection flow by adding energy equation to the Navier-Stokes equations. This corresponds to the physical situation that heat flux occurs (temperature not constant).

Governing momentum and energy equations in terms of stream function and vorticity are

$$\nabla^2 \psi \;\; = \;\; -\omega$$

$$Pr\nabla^2 \omega \;\; = \;\; \frac{\partial \omega}{\partial t} + u\frac{\partial \omega}{\partial x} + v\frac{\partial \omega}{\partial y} - RaPr\frac{\partial T}{\partial x} \tag{3.26}$$

$$\nabla^2 T \;\; = \;\; \frac{\partial T}{\partial t} + u\frac{\partial T}{\partial x} + v\frac{\partial T}{\partial y}$$

where Ra, Pr and T are the Rayleigh number, Prandtl number and temperature, respectively. Again $u = \dfrac{\partial \psi}{\partial y}$, $v = -\dfrac{\partial \psi}{\partial x}$ and vorticity is defined as $\omega = \dfrac{\partial v}{\partial x} - \dfrac{\partial u}{\partial y}$. The vorticity transport equation is coupled to the energy equation through the buoyancy force $RaPr\dfrac{\partial T}{\partial x}$, and the energy equation is in the same form (velocity components multiply convection terms) of the vorticity transport equation for the Navier-Stokes equations. The velocity and pressure information can also be obtained by using the equations (1.18).

Boundary conditions can be generally expressed as Dirichlet type for stream function (no-slip condition for velocities), and again Dirichlet type for vorticity since it is obtained from vorticity definition. The temperature boundary conditions may be Dirichlet and/or Neumann type according to the heat configuration of the walls. Thus,

$$\psi(x_s, y_s) = f_{\psi_s} \quad , \quad \omega(x_s, y_s) = f_{w_s}$$

$$T(x_s, y_s) = f_{t_s} \quad , \quad \frac{\partial T}{\partial n}(x_s, y_s) = f_{t_n} \tag{3.27}$$

are specified on the boundary where subscript 's' denotes the boundary of the region.

The equations (3.26) are subjected to initial conditions

$$\psi(x, y, 0) = \psi_0(x, y) \quad , \quad \omega(x, y, 0) = \omega_0(x, y) \quad , \quad T(x, y, 0) = T_0(x, y)$$

where ψ_0, ω_0 and T_0 are known functions of space.

82

Application of DRBEM to stream function and vorticity equations are explained in details in Section 3.1. In this section, we will only add the term $RaPr\dfrac{\partial T}{\partial x}$ to vorticity transport equation and give the solution procedure for the energy equation. DRBEM application to the vorticity equation (3.10) of the Navier-Stokes equations results in the final matrix form

$$\frac{1}{Re}(\mathbf{H}\omega - \mathbf{G}\omega_q) = (\mathbf{H}\hat{\mathbf{U}} - \mathbf{G}\hat{\mathbf{Q}})\mathbf{F}^{-1}\left[\frac{\partial\,\omega}{\partial\,t} + \left(\mathbf{u}\,\frac{\partial\mathbf{F}}{\partial x}\mathbf{F}^{-1} + \mathbf{v}\,\frac{\partial\mathbf{F}}{\partial y}\mathbf{F}^{-1}\right)\omega\right]. \qquad (3.28)$$

Thus, we can express the application of the method to the vorticity equation in (3.26) as in equation (3.28)

$$Pr(\mathbf{H}\omega - \mathbf{G}\omega_q) = (\mathbf{H}\hat{\mathbf{U}} - \mathbf{G}\hat{\mathbf{Q}})\mathbf{F}^{-1}\left[\frac{\partial\,\omega}{\partial\,t} + \left(\mathbf{u}\,\frac{\partial\mathbf{F}}{\partial x}\mathbf{F}^{-1} + \mathbf{v}\,\frac{\partial\,\mathbf{F}}{\partial\,y}\mathbf{F}^{-1}\right)\omega - RaPr\frac{\partial\mathbf{T}}{\partial x}\right] \qquad (3.29)$$

where ω and ω_q are vectors containing vorticity and its normal derivative values at the nodes.

The derivative of temperature with respect to x in the equation (3.29) can be approximated as $\dfrac{\partial\,\mathbf{T}}{\partial\,x} = \dfrac{\partial\,\mathbf{F}}{\partial\,x}\mathbf{F}^{-1}\mathbf{T}$. So, the simplified form of equation (3.29) is

$$Pr(\mathbf{H}\omega - \mathbf{G}\omega_q) = \mathbf{S}\frac{\partial\,\omega}{\partial\,t} + \mathbf{D}\,\omega + \tilde{c} \qquad (3.30)$$

where $\mathbf{S}$ and $\mathbf{D}$ are the matrices and $\tilde{c}$ is the vector given by

$$\mathbf{S} = (\mathbf{H}\hat{\mathbf{U}} - \mathbf{G}\hat{\mathbf{Q}})\mathbf{F}^{-1} \quad , \quad \mathbf{D} = \mathbf{S}\left(\mathbf{u}\,\frac{\partial\,\mathbf{F}}{\partial\,x}\mathbf{F}^{-1} + \mathbf{v}\,\frac{\partial\,\mathbf{F}}{\partial\,y}\mathbf{F}^{-1}\right) \quad , \quad \tilde{c} = -\mathbf{S}RaPr\frac{\partial\,\mathbf{F}}{\partial\,x}\mathbf{F}^{-1}\,\mathbf{T} .$$

A similar matrix formulation can be written for the energy equation in (3.26)

$$\mathbf{H}\mathbf{T} - \mathbf{G}\mathbf{T_q} = (\mathbf{H}\hat{\mathbf{U}} - \mathbf{G}\hat{\mathbf{Q}})\mathbf{F}^{-1}\left(\frac{\partial\,\mathbf{T}}{\partial\,t} + \mathbf{u}\,\frac{\partial\,\mathbf{F}}{\partial\,x}\mathbf{F}^{-1}\mathbf{T} + \mathbf{v}\,\frac{\partial\,\mathbf{F}}{\partial\,y}\mathbf{F}^{-1}\mathbf{T}\right) \qquad (3.31)$$

where T and T_q are the temperature and its normal derivative values at the nodes. Equation (3.31) can be expressed as

$$\mathbf{H}\mathbf{T} - \mathbf{G}\mathbf{T_q} = \mathbf{S}\frac{\partial\,\mathbf{T}}{\partial\,t} + \mathbf{D}\mathbf{T} . \qquad (3.32)$$

Finally, stream function, vorticity and energy equations are obtained as

$$\mathbf{H}\psi - \mathbf{G}\psi_q = \tilde{b}$$

$$-\mathbf{S}\frac{\partial\,\omega}{\partial\,t} + \mathbf{H}_\omega\,\omega - \mathbf{G}_\omega\,\omega_q = \tilde{c} \qquad (3.33)$$

$$-\mathbf{S}\frac{\partial\,\mathbf{T}}{\partial\,t} + \mathbf{H}_t\,T - \mathbf{G}_t\,T_q = 0$$

where $H_\omega = Pr\mathbf{H} - \mathbf{D}$, $G_\omega = Pr\mathbf{G}$, $H_t = \mathbf{H} - \mathbf{D}$, $G_t = \mathbf{G}$.

For velocity and pressure Poisson's equations (1.18), the corresponding DRBEM matrix equations are given as

$$\mathbf{Hu} - \mathbf{Gu_q} = (\mathbf{H\hat{U}} - \mathbf{G\hat{Q}})\mathbf{F}^{-1}\left(-\frac{\partial\omega}{\partial y}\right)$$

$$\mathbf{Hv} - \mathbf{Gv_q} = (\mathbf{H\hat{U}} - \mathbf{G\hat{Q}})\mathbf{F}^{-1}\left(\frac{\partial\omega}{\partial x}\right)$$

$$\mathbf{Hp} - \mathbf{Gp_q} = (\mathbf{H\hat{U}} - \mathbf{G\hat{Q}})\mathbf{F}^{-1}\left[\frac{Ra}{Pr}\frac{\partial\mathbf{T}}{\partial y} - \left(\frac{\partial\mathbf{u}}{\partial x}\right)^2 - \left(\frac{\partial\mathbf{v}}{\partial y}\right)^2 - 2\frac{\partial\mathbf{v}}{\partial x}\frac{\partial\mathbf{u}}{\partial y}\right]$$

(3.34)

which as a result become

$$\mathbf{Hu} - \mathbf{Gu_q} = \tilde{m}$$

$$\mathbf{Hv} - \mathbf{Gv_q} = \tilde{n}$$

(3.35)

$$\mathbf{Hp} - \mathbf{Gp_q} = \mathbf{a}$$

the vectors $\mathbf{a}$, $\tilde{m}$ and $\tilde{n}$ are given as

$$\tilde{m} = -\mathbf{S}\frac{\partial\omega}{\partial y} \quad , \quad \tilde{n} = \mathbf{S}\frac{\partial\omega}{\partial x} \quad , \quad \mathbf{a} = \mathbf{S}\left[\frac{Ra}{Pr}\frac{\partial\mathbf{T}}{\partial y} - \left(\frac{\partial\mathbf{u}}{\partial x}\right)^2 - \left(\frac{\partial\mathbf{v}}{\partial y}\right)^2 - 2\frac{\partial\mathbf{v}}{\partial x}\frac{\partial\mathbf{u}}{\partial y}\right].$$

For evaluating vectors $\mathbf{a}$, $\tilde{m}$ and $\tilde{n}$ the derivatives are computed with the help of coordinate matrix $\mathbf{F}$ and multiplications of vectors are handled by forming diagonal matrices from the vector entries.

The time derivative in the vorticity and energy equations in (3.33) are discretized using central difference scheme with relaxation parameters

$$-\mathbf{S}\frac{\omega^{m+1} - \omega^{m-1}}{2\Delta t} + H_\omega((1 - \beta_\omega)\omega^{m-1} + \beta_\omega\omega^{m+1}) - G_\omega((1 - \beta_{\omega_q})\omega_q{}^{m-1} + \beta_{\omega_q}\omega_q{}^{m+1}) = \mathbf{0}$$

$$-\mathbf{S}\frac{T^{m+1} - T^{m-1}}{2\Delta t} + H_t((1 - \beta_t)T^{m-1} + \beta_t T^{m+1}) - G_t((1 - \beta_{t_q})T_q{}^{m-1} + \beta_{t_q}T_q{}^{m+1}) = \mathbf{0}.$$

(3.36)

Equation (3.36) can be written as

84

$$\left(\frac{-\mathbf{S}}{2\Delta t} + \beta_\omega \mathbf{H}_\omega\right)\omega^{m+1} - \beta_{\omega_q}\mathbf{G}_\omega\omega_q{}^{m+1} = \left[\frac{-\mathbf{S}}{2\Delta t} - (1 - \beta_\omega)\mathbf{H}_\omega\right]\omega^{m-1} + (1 - \beta_{\omega_q})\mathbf{G}_\omega\omega_q{}^{m-1}$$

$$\left(\frac{-\mathbf{S}}{2\Delta t} + \beta_t \mathbf{H}_t\right)T^{m+1} - \beta_{t_q}\mathbf{G}_t T_q{}^{m+1} = \left[\frac{-\mathbf{S}}{2\Delta t} - (1 - \beta_t)\mathbf{H}_t\right]T^{m-1} + (1 - \beta_{t_q})\mathbf{G}_t T_q{}^{m-1} .$$

(3.37)

In order to start the iteration process we need the initial conditions for ω, ω_q and T, T_q at time levels 'm-1' and 'm'. All initial conditions are taken as zero in the computations.

Once all unknowns are passed to the left-hand side one can write the equation (3.37) as

$$\mathbf{A}\mathbf{x}_1 = \mathbf{y}_1$$

(3.38)

$$\mathbf{A}\mathbf{x}_2 = \mathbf{y}_2$$

where $\mathbf{x}_1$ and $\mathbf{x}_2$ are the unknown vectors including ω, ω_q and T, T_q, respectively.

We shall now describe the iterative procedure:

1) Start with the initial approximations for ω^{m-1}, ω^m and T^{m-1}, T^m with $m = 1$. ω^0, T^0 can be set to zero, and ω^1, T^1 can be taken as zero or computed from the forward difference discretized form of the equations as in (3.15).

2) Solve the stream function equation to obtain ψ^{m+1} using ω^m.

3) Solve the energy equation to obtain T^{m+1} using T^{m-1}.

4) Approximate the derivatives of stream function, ψ^{m+1}, temperature, T^{m+1}, and ω^m with respect to x and y by using DRBEM idea.

5) Solve the equations for velocity components to obtain $\mathbf{u}^{m+1}$ and $\mathbf{v}^{m+1}$ using the derivatives of ω^m. Then solve the pressure equation to obtain p^{m+1} using T^{m+1}, $\mathbf{u}^{m+1}$ and $\mathbf{v}^{m+1}$.

6) Obtain the vorticity boundary conditions from the Taylor series expansion of stream function or from its definition using ψ^{m+1}.

7) Solve the vorticity equation to obtain ω^{m+1} using ω^{m-1}, and using the derivatives of stream function ψ^{m+1} and the temperature gradient T^{m+1}

8) Relax ω^{m+1} with ω^m to obtain new ω^{m+1}.

9) Relax T^{m+1} with T^m to obtain new T^{m+1}.

10) Check the convergence criteria to terminate the procedure using the L_∞ norm of ψ, ω and T as

$$\max_i |\psi^{m+1} - \psi^m| \le \varepsilon$$

$$\max_i |\omega^{m+1} - \omega^m| \le \varepsilon \qquad i = 1, ...N + L$$

$$\max_i |T^{m+1} - T^m| \le \varepsilon$$

where maxima is taken over all the nodes inside the fluid flow region and ε is a pre-assigned tolerance.

11) Repeat the steps $2 - 10$ for $m = 2, 3, ...$ until the convergence criteria in step 10 is met.

In the iterative procedure, m-th level values are used to compute the matrices H_ω and H_t which contain convection term matrix $\mathbf{D}$. Thus, the iteration makes use of both m-th and $(m - 1)$-th level values for computing 'm+1' iteration.

3.2.1 Natural Convection Flow in a Square Cavity

The equations are given as, [51]

$$\nabla^2 \psi = -\omega$$

$$Pr\nabla^2 \omega = \frac{\partial \omega}{\partial t} + u\frac{\partial \omega}{\partial x} + v\frac{\partial \omega}{\partial y} - RaPr\frac{\partial T}{\partial x} \tag{3.39}$$

$$\nabla^2 T = \frac{\partial T}{\partial t} + u\frac{\partial T}{\partial x} + v\frac{\partial T}{\partial y}$$

in a square cavity $[0, 1] \times [0, 1]$. The no-slip boundary conditions for the velocity are assumed. Temperature has Dirichlet type conditions as 1 and 0 at the left and right walls of the cavity, whereas adiabatic conditions $\frac{\partial T}{\partial y} = 0$ are imposed on the top and bottom walls (Figure (3.25)). Boundary conditions of stream function are taken as zero at the walls and the vorticity boundary conditions are derived from Taylor series expansion of stream function.

The proposed coupled numerical algorithm (iterative procedure) is applied to determine the stream function, vorticity and temperature variations with the given initial values $\omega = T = 0$ iteratively. The pre-assigned accuracy for reaching steady-state is taken as $\varepsilon = 10^{-5}$ for $Ra = 10^3$, $\varepsilon = 10^{-4}$ for $Ra = 10^4$ and 10^5, and $\varepsilon = 10^{-3}$ for $Ra = 10^6$. The time derivative is discretized using central difference scheme with relaxation parameters ($\beta_\omega = \beta_{\omega_q} = \beta_t = \beta_{t_q} = 0.9$).

In Figure (3.26) we present streamlines, vorticity and temperature contours at steady state for $Ra = 10^3$, 10^4, 10^5 and 10^6 by using $\Delta t = 0.5$, $N = 68$; $\Delta t = 0.01$, $N = 80$; $\Delta t = 0.005$, $N = 84$; and $\Delta t = 0.003$, $N = 100$, respectively. Pr is taken as 0.7 and quadratic radial basis functions $f = 1 + r + r^2$ are used in obtaining the coordinate matrix $\mathbf{F}$.

One can see from the Figures (3.26) that for $Ra = 10^3$ viscous forces are dominant and there is not enough convection within the cavity. The vortex of streamlines is in circular pattern, the isotherm lines are almost vertical and the vorticity contours take place mostly at the center of the cavity. As the Rayleigh number increases natural convection becomes the dominating mechanism. Buoyancy forces get stronger and cause an effective fluid convection. We see from the figures that the circular pattern of the streamlines become elliptical and the isotherm lines undergo an inversion at the central region of the cavity. Their vertical behaviour become

87

horizontal. The vorticity contours get closer to the vertical walls of the cavity and the central region of the cavity is almost stagnant. For $Ra = 10^6$, thin boundary layers occur for all the variables. The vortex of streamlines tend to separate and form two vortices through the corners $(1, 0)$ and $(0, 1)$. The vorticity values near the vertical walls increase. These behaviours are in good agreement with the study of Lo *et.al.* [51]. From Figure (3.27) we observe that the relative amplitude of the velocity components increases as the Rayleigh number increases.
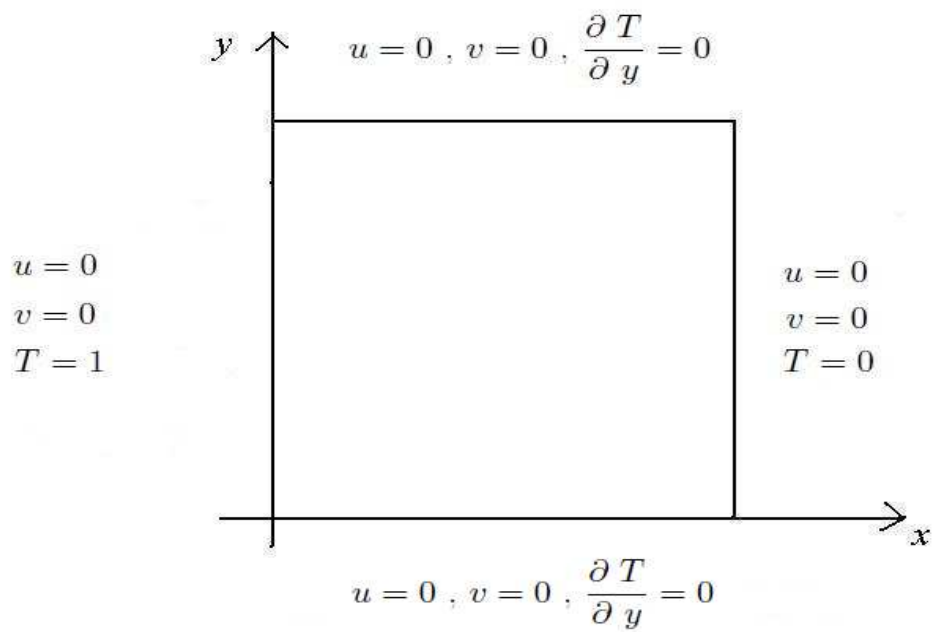
Figure 3.25: Boundary conditions for the natural convection flow in a square cavity
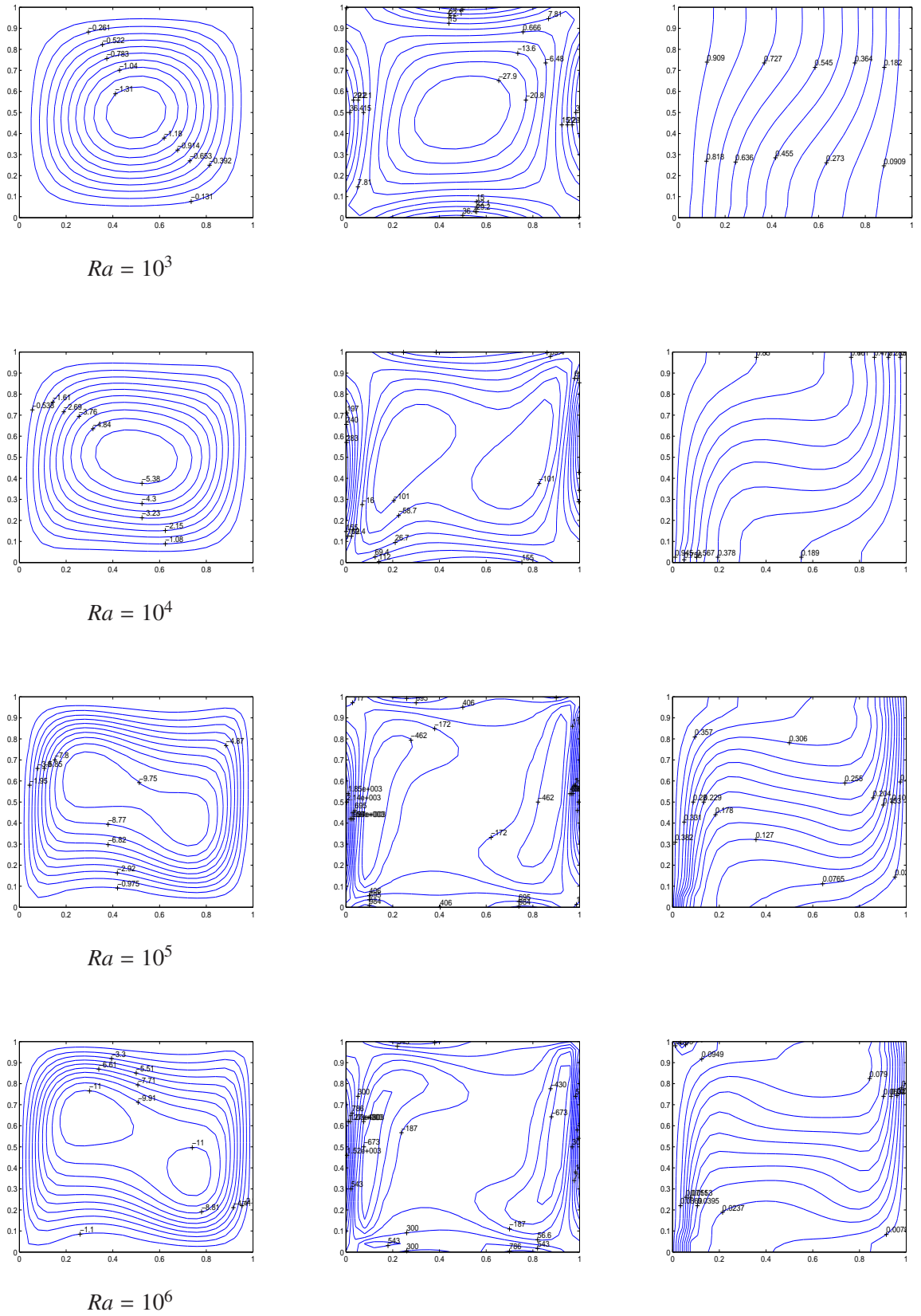
Figure 3.26: Streamlines, vorticity contours and isotherms for $Ra = 10^3$, 10^4, 10^5 and 10^6
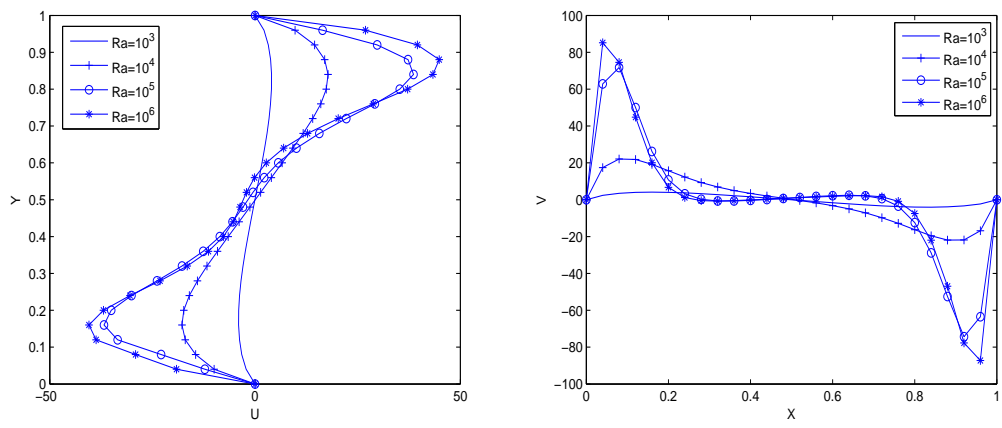
Figure 3.27: Vertical and horizontal velocity profiles at the mid-plane of the cavity for several *Ra*

3.2.2 Natural Convection Flow with Uniformly and Non-Uniformly Heated Walls

In this problem we discuss again the natural convection flow in a square cavity with different boundary conditions, [70]. The problem is investigated in two cases. In the first case the left vertical and the bottom horizontal walls are heated uniformly and in the other case they are heated non-uniformly. The right vertical wall is cooled and the top horizontal wall is insulated (Figure (3.28)).

The equations are given in terms of u, v, ψ, p, ω and T as

$$\nabla^2 u = -\frac{\partial \omega}{\partial y}$$

$$\nabla^2 v = \frac{\partial \omega}{\partial x}$$

$$\nabla^2 p = \frac{Ra}{Pr}\frac{\partial T}{\partial y} - \left(\frac{\partial u}{\partial x}\right)^2 - \left(\frac{\partial v}{\partial y}\right)^2 - 2\frac{\partial v}{\partial x}\frac{\partial u}{\partial y}$$

$$\nabla^2 \psi = -\omega \tag{3.40}$$

$$Pr\nabla^2 \omega = \frac{\partial \omega}{\partial t} + u\frac{\partial \omega}{\partial x} + v\frac{\partial \omega}{\partial y} - RaPr\frac{\partial T}{\partial x}$$

$$\nabla^2 T = \frac{\partial T}{\partial t} + u\frac{\partial T}{\partial x} + v\frac{\partial T}{\partial y}.$$

Homogeneous initial conditions for vorticity and temperature are imposed. Stream function and velocity components have no-slip boundary conditions. The vorticity boundary conditions are obtained from its definition $\omega = \frac{\partial v}{\partial x} - \frac{\partial u}{\partial y}$. In both cases linear boundary elements are used and the radial basis functions are taken as $f = 1 + r + r^2$, the Prandtl number is $Pr = 0.2$. The solution is given at steady-state. The problem is solved by using the central difference scheme and the relaxation parameters are taken as 0.9 for all variables and their normal derivatives. The local Nusselt number at the heated bottom wall is evaluated by the formula $Nu = -\frac{\partial T}{\partial y}\Big|_{y=0}$.
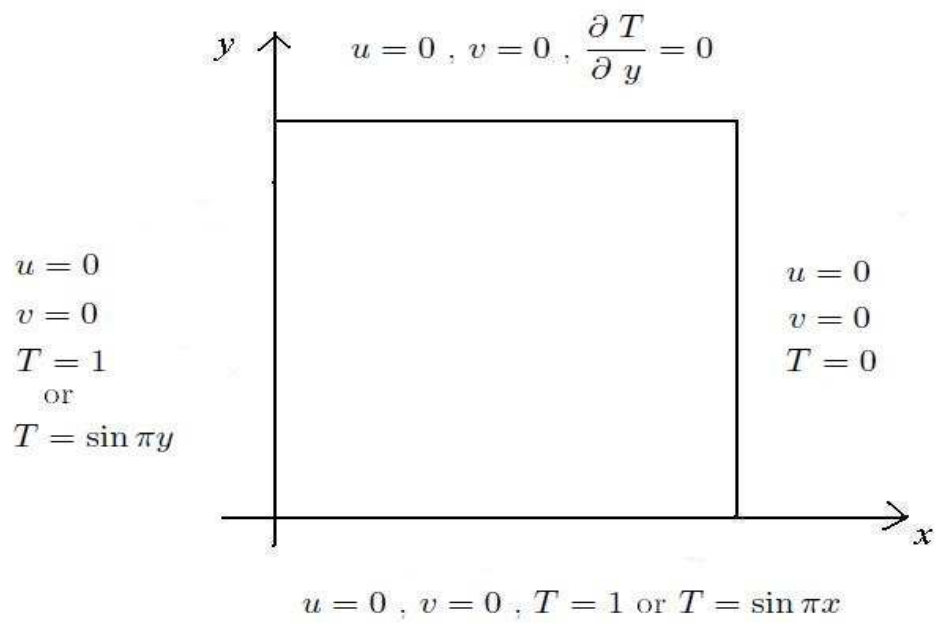
Figure 3.28: Boundary conditions for natural convection flow with uniformly and non-uniformly heated walls

3.2.2.1 Uniformly Heated Walls

In this case, the bottom and the left vertical walls are heated to maintain constant temperature, and the right vertical wall is cooled while the top wall is insulated.

The problem is solved for Rayleigh numbers $Ra = 10^3$, 10^4, 10^5 and 10^6 with $\Delta t = 0.1, 0.01$, 0.001 and 0.0005 and $N = 64, 80, 88$ and 96, respectively. As the Rayleigh number increases thin boundary layers occur near the walls. Thus, the number of boundary elements needs to be increased whereas the time step must be taken smaller compared to the previous value of Ra. The stopping criteria in the iterations is taken as $\varepsilon = 10^{-5}$ for Rayleigh numbers $10^3 - 10^5$ and $\varepsilon = 10^{-3}$ for $Ra = 10^6$.

Figures in (3.29) show the behaviour of streamlines, vorticity and temperature contours for $Ra = 10^3, 10^4, 10^5$ and 10^6, respectively. Since the left vertical wall is heated, fluid rise up along this wall and flow down along the cooled right vertical wall. Thus, a clockwise rotation is formed inside the cavity. As Ra increases from 10^3 to 10^6, the values of the stream function increase. For $Ra = 10^3$, the isotherm lines change their value from left(hot) vertical wall to right(cold) vertical wall. With an increase in the Rayleigh number buoyancy forces get stronger and natural convection becomes dominant. Thus, the convection from the hot wall to cold wall enhances and the isotherm lines with values greater than 0.5 cover almost the entire cavity (Figure (3.29)). We also observe the boundary layers near the walls. These behaviours are in good agreement with the ones in [70].

Figures (3.30) and (3.31) implement flow vectors and pressure contours for $Ra = 10^4$ and 10^5, respectively, and horizontal and vertical mid-plane velocity profiles are given in Figure (3.32) for $Ra = 10^3$ and 10^4.

Figure (3.33) shows the variation of the local Nusselt number with distance at the bottom wall. We see that the heat transfer rate is very high at the right edge of the bottom wall and the heat transfer is almost uniform at the hot vertical wall.
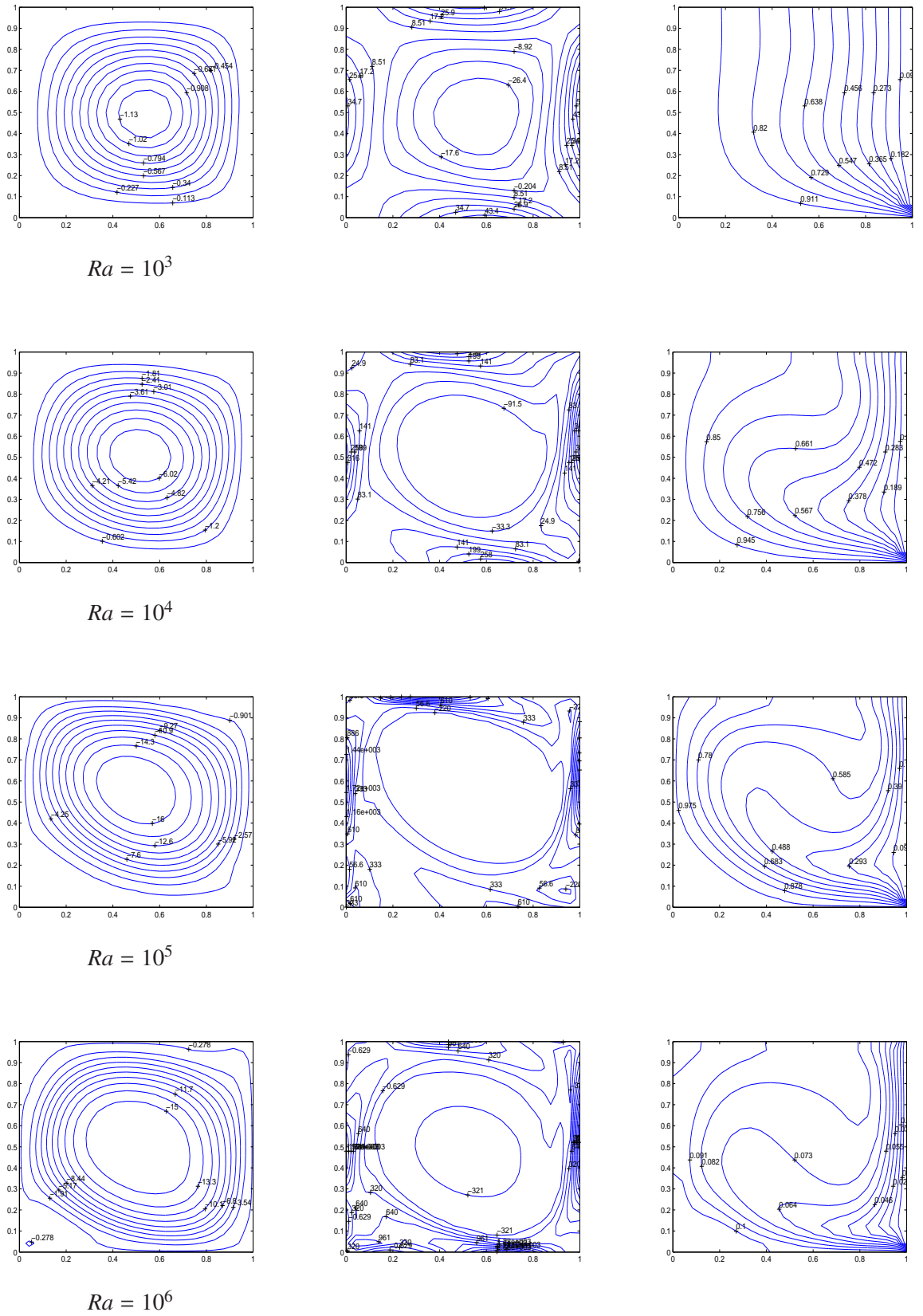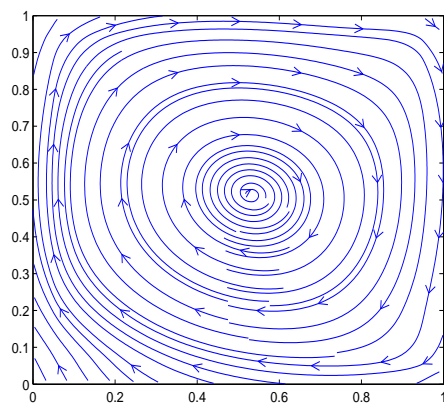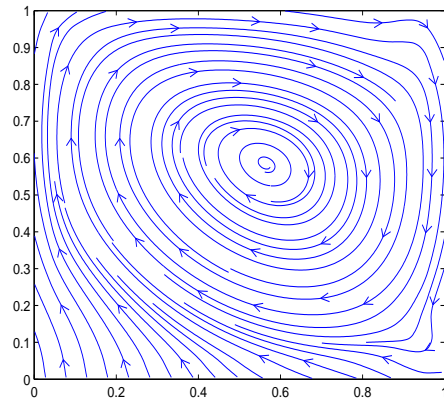
Figure 3.29: Streamlines, vorticity contours and isotherms for $Ra = 10^3$, 10^4, 10^5 and 10^6
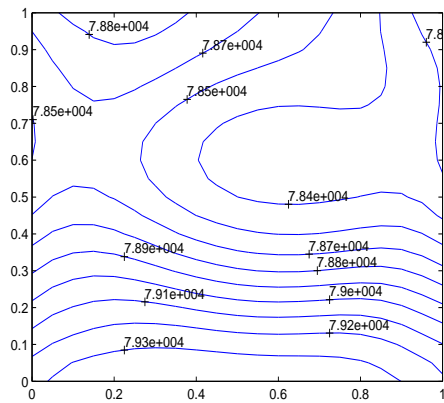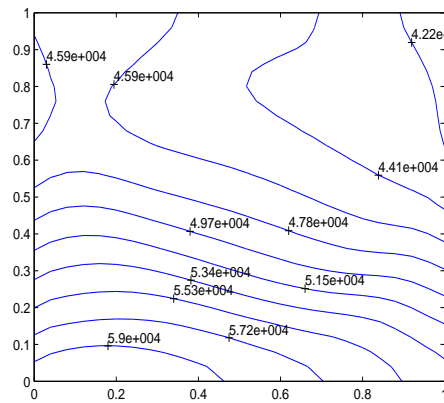
$Ra = 10^4$ $Ra = 10^5$

Figure 3.30: Flow vectors for $Ra = 10^4$ and 10^5

$Ra = 10^4$ $Ra = 10^5$

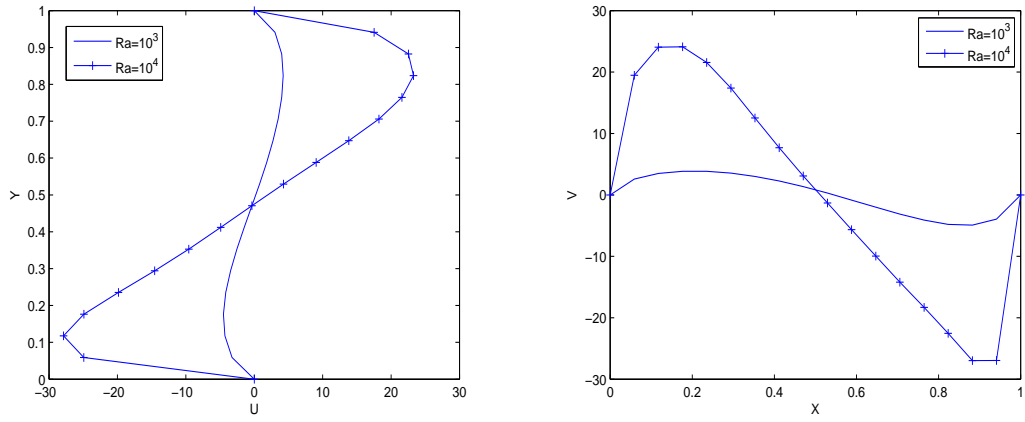Figure 3.31: Pressure contours for $Ra = 10^4$ and 10^5

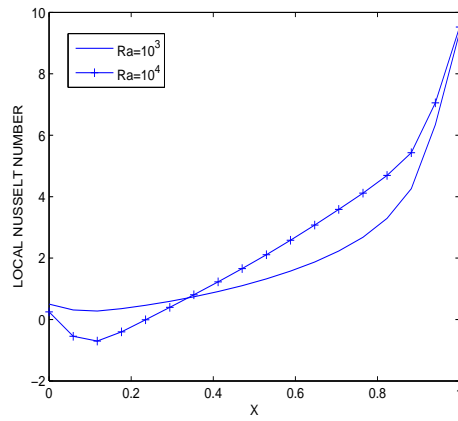Figure 3.32: Horizontal and vertical velocity profiles at the mid-plane of the cavity for several *Ra*

Figure 3.33: Variation of local Nusselt number with distance at the bottom wall for $Ra = 10^3, 10^4$

3.2.2.2 Non-Uniformly Heated Walls

This case also considers the square cavity with heated bottom and left vertical walls, the cooled right vertical wall and the insulated top wall. In the first case the walls are heated uniformly, which means they are kept at the same temperature. But in this case they are heated non-uniformly with trigonometric function behaviour (Figure (3.28)).

We solve the problem for Rayleigh numbers between $10^3 - 10^6$. $\Delta t = 0.5$ with $N = 64$; $\Delta t = 0.01$ with $N = 80$; $\Delta t = 0.001$ with $N = 88$; and $\Delta t = 0.0005$ with $N = 96$ are used for $Ra = 10^3$, 10^4, 10^5 and 10^6, respectively. The results are given at steady-state with a pre-assigned accuracy $\varepsilon = 10^{-4}$ for stopping the iterative procedure.

Figures in (3.34) present the streamlines, vorticity contours and isotherms for $Ra = 10^3$, 10^4, 10^5 and 10^6, respectively. One can see that the behaviour of stream function is similar to the behaviour of the one obtained in the first case, in the sense that the formations of small stagnant fluid region attached to the corners of the heated vertical wall [70]. Boundary layers near the walls for streamlines and isotherms are also observed. Due to the non-uniform heating the temperature lines with values greater than 0.5 cover the cavity less than the uniform heating case. In this case, we again need to decrease time increment and increase number of boundary nodes in order to capture the behaviour of solutions correctly. The behaviours are in good agreement with the study of [70].

The flow vectors and pressure contours are also given for $Ra = 10^4$ and 10^5 in Figures (3.35) and (3.36), respectively. Mid-plane horizontal and vertical velocities show similar behaviours to the ones in uniformly heated walls but variations are in smaller intervals.

In Figure (3.38), we present the variation of the local Nusselt number at the bottom wall with distance for $Ra = 10^3$ and 10^4. We observe that the heat transfer rate increases from edges towards the center with its maximum value at the center. In non-uniform case increasing values of Rayleigh number causes a sinusoidal type of local heat transfer rate. This is because the values of streamlines are higher at the center of the cavity for increasing value of Rayleigh number.

The point in investigating these cases is to see the effect of uniform and non-uniform heating of the bottom wall and one vertical wall on the fluid flow, and heat transfer rates due to natural

convection within the cavity. We observe that in uniform heating case, the heat transfer rate is high at the right edge of the bottom wall and almost uniform at the rest part of the bottom wall. On the other hand, in the non-uniform heating case the heat transfer rate is minimum at the edges of the bottom wall and maximum at the center of the bottom wall.
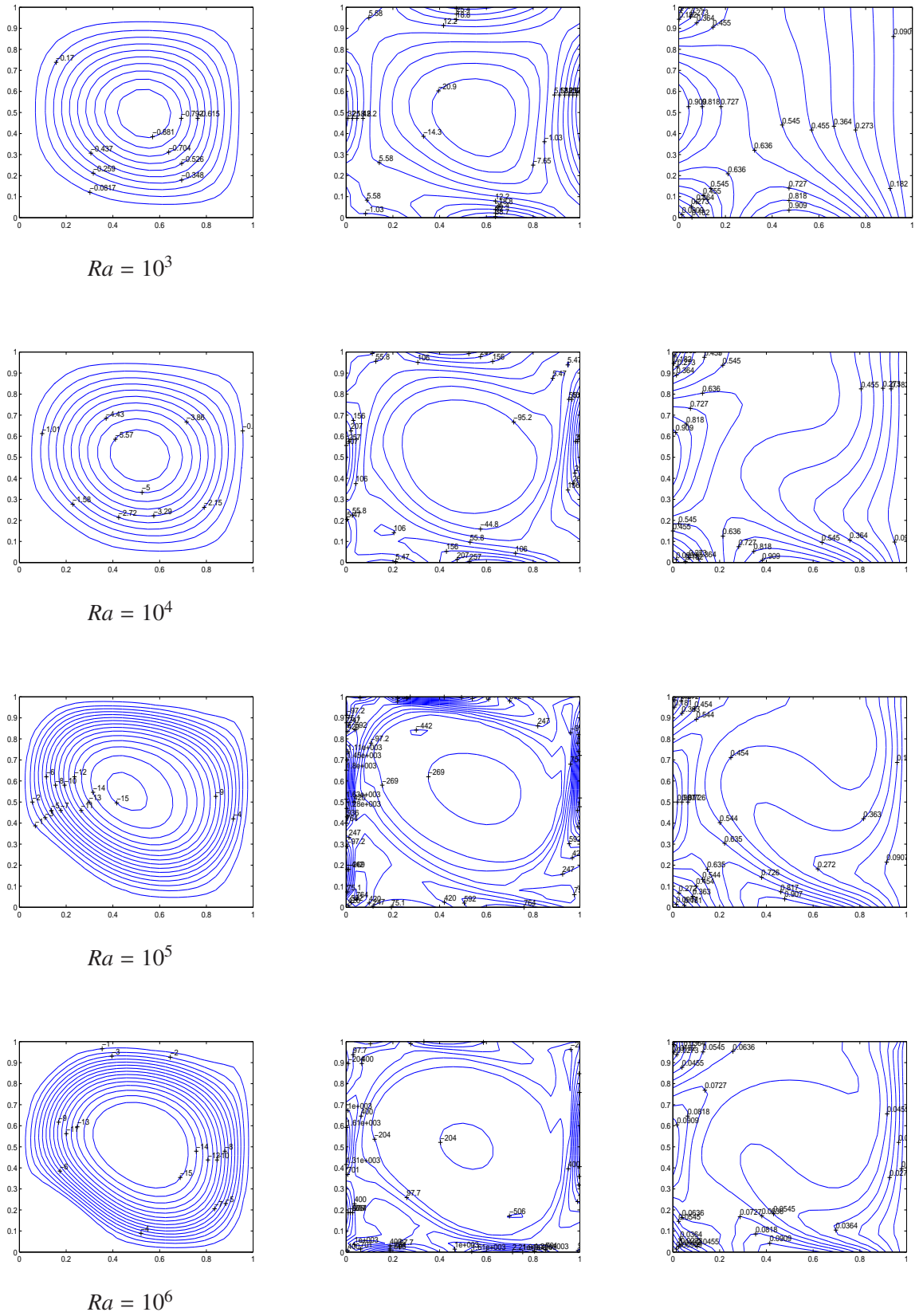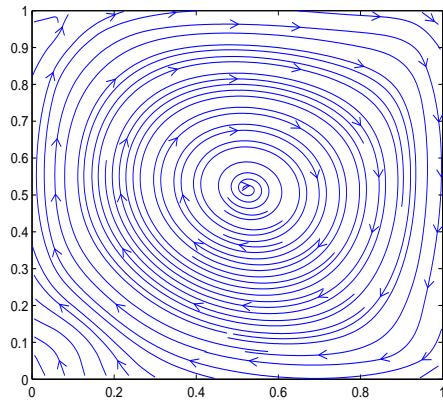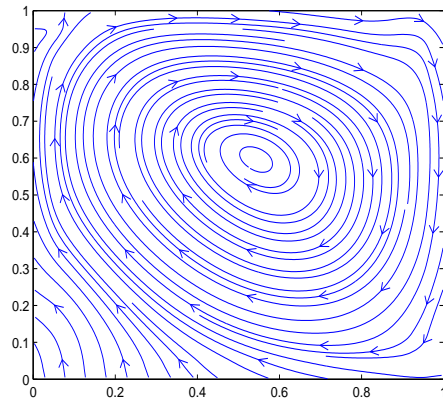
Figure 3.34: Streamlines, vorticity contours and isotherms for $Ra = 10^3$, 10^4, 10^5 and 10^6
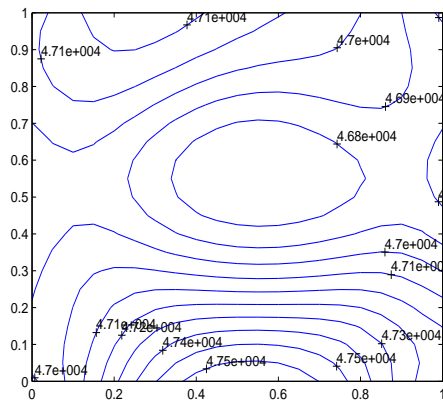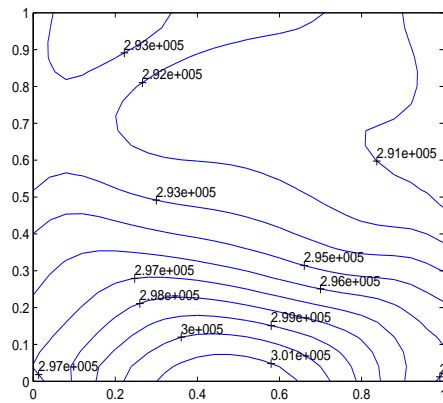
$Ra = 10^4$ $Ra = 10^5$

Figure 3.35: Flow vectors for $Ra = 10^4$ and 10^5

$Ra = 10^4$ $Ra = 10^5$

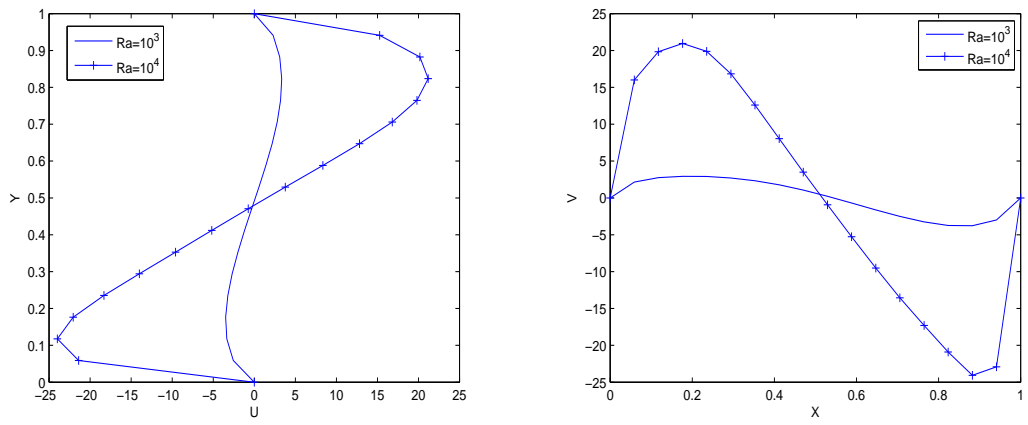Figure 3.36: Pressure contours for $Ra = 10^4$ and 10^5

101

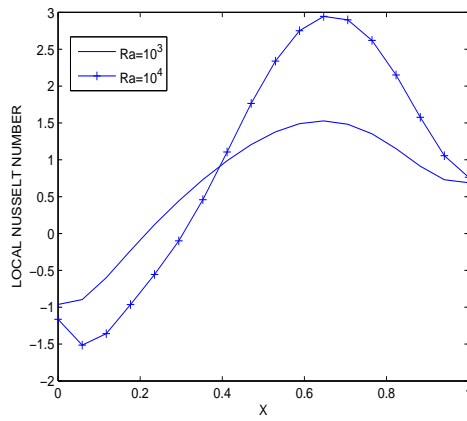Figure 3.37: Horizontal and vertical velocity profiles at the mid-plane of the cavity for several *Ra*

Figure 3.38: Variation of local Nusselt number with distance at the bottom wall for $Ra = 10^3, 10^4$

3.2.3 Natural Convection in a Triangular Enclosure

In this last problem, we consider the natural convection flow in a triangular enclosure with vertices $(0,0)$, $(0,1)$ and $(1,0)$, [13]. The governing equations are as follows

$$\nabla^2 \psi = -\omega$$

$$Pr\nabla^2\omega = \frac{\partial \omega}{\partial t} + u\frac{\partial \omega}{\partial x} + v\frac{\partial \omega}{\partial y} - RaPr\frac{\partial T}{\partial x} \tag{3.41}$$

$$\nabla^2 T = \frac{\partial T}{\partial t} + u\frac{\partial T}{\partial x} + v\frac{\partial T}{\partial y}.$$

Again homogeneous initial conditions are assigned for both the vorticity and the temperature. The problem is considered for the configuration in which the left vertical wall of the right triangle is heated linearly, the horizontal bottom wall is adiabatic and the inclined wall is cooled (Figure (3.39)). Homogeneous boundary conditions are taken for stream function, and vorticity boundary conditions are derived from its definition $\omega = \frac{\partial v}{\partial x} - \frac{\partial y}{\partial y}$ with DRBEM idea. We solve the problem for several Rayleigh numbers. Linear boundary elements are used and the radial basis functions are taken as $f = 1 + r + r^2$. Prandtl number is 0.7. $\Delta t = 0.5$ with $N = 72$, $\Delta t = 0.05$ with $N = 80$, $\Delta t = 0.01$ with $N = 92$ and $\Delta t = 0.005$ with $N = 100$ are used for $Ra = 10^3, 10^4, 10^5$ and 10^6, respectively. The solutions are given at steady state with pre-assigned tolerance $\varepsilon = 10^{-4}$.

Figure (3.40) show the streamlines, temperature and vorticity contours for $Ra = 10^3 - 10^6$. One can see from the figures that for small Rayleigh number the isotherms are almost parallel to the inclined wall, the streamline values at the center of the cavity are low. As the Rayleigh number increases the isotherms are deformed and start getting pushed toward the linearly heated left wall and the streamline values increase. The vortex of the streamlines which was in circular pattern, now becomes elliptical. The behaviours are in good agreement with the study of Basak *et.al.* [13].

Figure (3.41) present the variation of the local Nusselt number which is evaluated using the formula $Nu = -\frac{\partial T}{\partial x}\Big|_{x=0}$ at the linearly heated left wall with distance for $Ra = 10^3 - 10^6$. We see that the maximum eigenvalue occurs at the bottom wall. It is also observed that the local Nusselt number increases with the increase in the Rayleigh number.

From these three test problems, the obtained results indicate that the present method is capable of solving natural convection flow for high Rayleigh number without difficulties with a considerable small number of mesh points on the boundary. However, as Ra increases one needs to take more boundary elements and small time increments to reach the steady-state solutions.
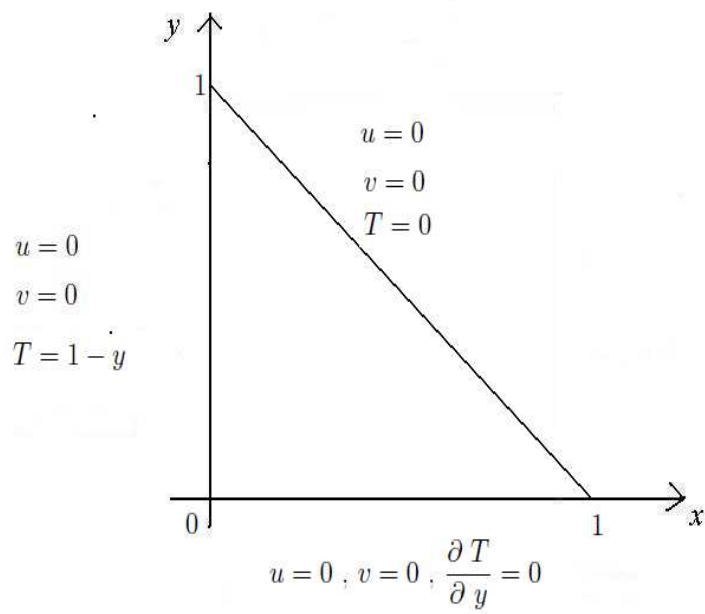
Figure 3.39: Boundary conditions for the natural convection flow in a triangular enclosure
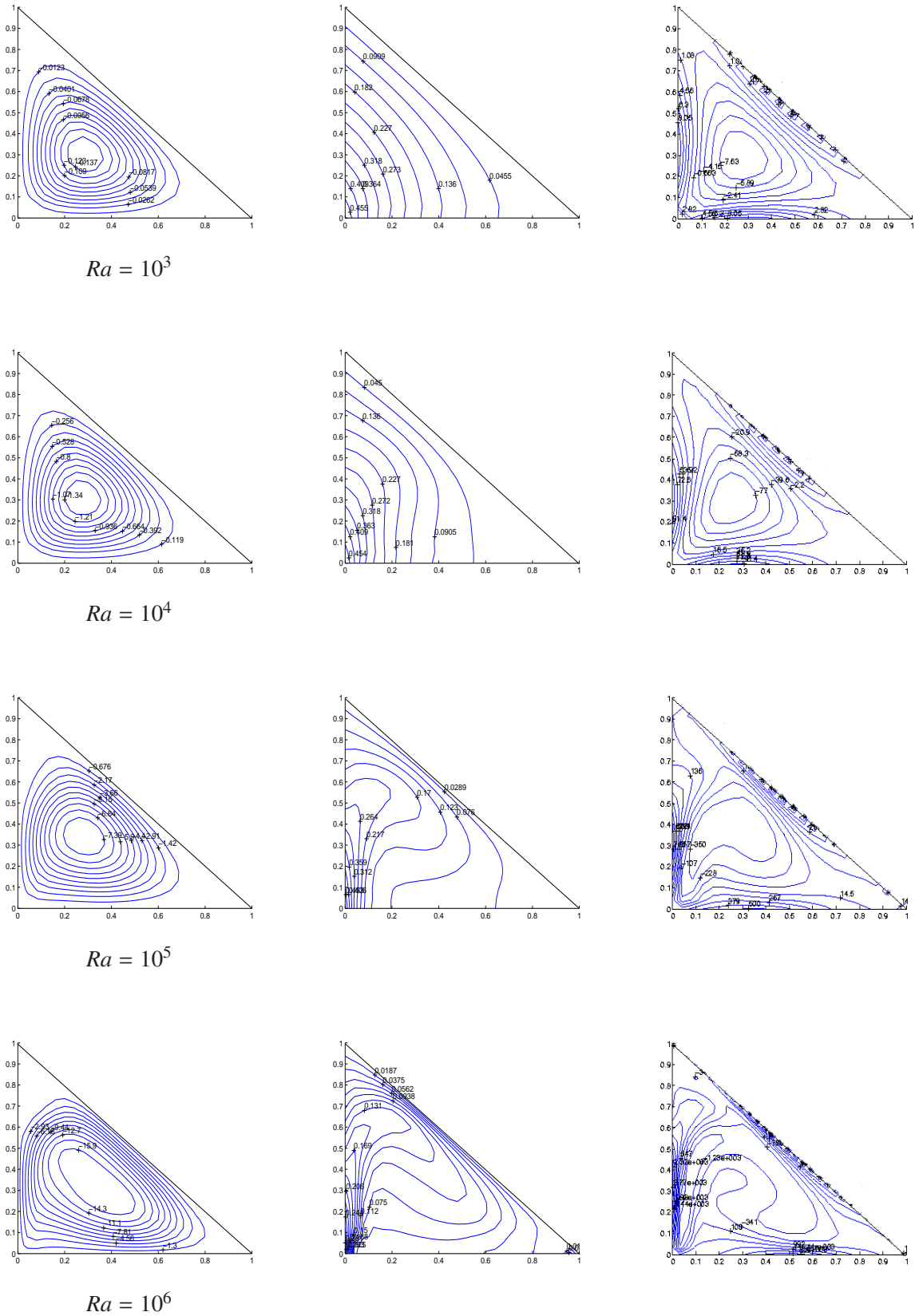
$Ra = 10^3$

$Ra = 10^4$

$Ra = 10^5$

$Ra = 10^6$

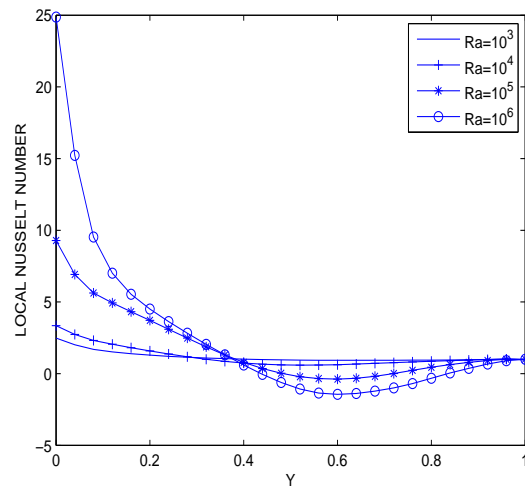Figure 3.40: Streamlines, isotherms and vorticity contours for $Ra = 10^3 - 10^6$

106

Figure 3.41: Variation of local nusselt number with distance for different Rayleigh numbers

3.3 Mixed Convection Flow

Mixed convection is the combination of forced and natural convection. When the effects of natural and forced convection are comparable neither of the process can be neglected. Thus, understanding the physics of this process is very important. Governing equations of transient and laminar mixed convection flow of a viscous fluid in terms of stream function-vorticity formulation are given as, [62]

$$\nabla^2 \psi = -\omega$$

$$\frac{1}{Re}\nabla^2 \omega = \frac{\partial \omega}{\partial t} + u\frac{\partial \omega}{\partial x} + v\frac{\partial \omega}{\partial y} - \frac{Gr}{Re^2}\frac{\partial T}{\partial x} \tag{3.42}$$

$$\frac{1}{RePr}\nabla^2 T = \frac{\partial T}{\partial t} + u\frac{\partial T}{\partial x} + v\frac{\partial T}{\partial y}$$

where Re, Pr and Gr are the Reynolds, Prandtl and the Grashof numbers, respectively. Generally mixed convection occurs when $\dfrac{Gr}{Re^2} \approx 1$. When $\dfrac{Gr}{Re^2} \ll 1$ forced convection is dominant, when $\dfrac{Gr}{Re^2} \gg 1$, natural convection is dominant, [43].

Initial conditions are taken as $\omega = T = 0$. General expression of the boundary conditions can be given as

$$\psi(x_s, y_s) = f_{\psi_s} \quad , \quad \omega(x_s, y_s) = f_{w_s}$$

$$T(x_s, y_s) = f_{t_s} \quad , \quad \frac{\partial T}{\partial n}(x_s, y_s) = f_{t_n}. \tag{3.43}$$

In general, we are given Dirichlet type boundary conditions for stream function, which can be taken as zero for simplicity. Since the boundary conditions of vorticity are derived from Taylor series expansion of stream function or from its definition, they are also Dirichlet type. The boundary conditions of temperature can be either Dirichlet or Neumann type because we consider the configuration that the walls of the cavity are heated/cooled and insulated (the normal derivative is zero).

Again we start from the application of DRBEM matrix form of vorticity equation given in Section 3.1 (equation (3.10))

$$\frac{1}{Re}(\mathbf{H}\omega - \mathbf{G}\omega_q) = (\mathbf{H}\hat{\mathbf{U}} - \mathbf{G}\hat{\mathbf{Q}})\mathbf{F}^{-1}\Big[\frac{\partial \omega}{\partial t} + \Big(\mathbf{u}\frac{\partial \mathbf{F}}{\partial x}\mathbf{F}^{-1} + \mathbf{v}\frac{\partial \mathbf{F}}{\partial y}\mathbf{F}^{-1}\Big)\omega\Big]. \tag{3.44}$$

Thus, for the mixed convection flow, vorticity equation in (3.42), we can write the matrix-vector form as in (3.44) by adding the term containing temperature derivative

$$\frac{1}{Re}(\mathbf{H}\omega - \mathbf{G}\omega_q) = (\mathbf{H}\hat{\mathbf{U}} - \mathbf{G}\hat{\mathbf{Q}})\mathbf{F}^{-1}\Big[\frac{\partial\,\omega}{\partial\,t} + \Big(\mathbf{u}\,\frac{\partial\mathbf{F}}{\partial x}\mathbf{F}^{-1} + \mathbf{v}\,\frac{\partial\,\mathbf{F}}{\partial\,y}\mathbf{F}^{-1}\Big)\omega - \frac{Gr}{Re^2}\frac{\partial\mathbf{T}}{\partial x}\Big]. \qquad (3.45)$$

The temperature gradient $\dfrac{\partial\,\mathbf{T}}{\partial\,x}$ in the above equation can also be approximated using the DRBEM idea given in equations (2.68) as $\dfrac{\partial\,\mathbf{T}}{\partial\,x} = \dfrac{\partial\,\mathbf{F}}{\partial\,x}\mathbf{F}^{-1}\mathbf{T}$.

Similarly, for the energy equation in (3.42), we have

$$\frac{1}{RePr}(\mathbf{H}\mathbf{T} - \mathbf{G}\mathbf{T_q}) = (\mathbf{H}\hat{\mathbf{U}} - \mathbf{G}\hat{\mathbf{Q}})\mathbf{F}^{-1}\Big[\frac{\partial\,\mathbf{T}}{\partial\,t} + \Big(\mathbf{u}\,\frac{\partial\,\mathbf{F}}{\partial\,x}\mathbf{F}^{-1} + \mathbf{v}\,\frac{\partial\,\mathbf{F}}{\partial\,y}\mathbf{F}^{-1}\Big)\mathbf{T}\Big]. \qquad (3.46)$$

Finally, we can express the DRBEM system of matrix equations for mixed convection flow equations (3.42) as

$$\mathbf{H}\psi - \mathbf{G}\psi_q = \tilde{b}$$

$$-\mathbf{S}\frac{\partial\,\omega}{\partial\,t} + H1_\omega\,\omega - G1_\omega\,\omega_q = \mathbf{c_1} \qquad (3.47)$$

$$-\mathbf{S}\frac{\partial\,T}{\partial\,t} + H1_t\,T - G1_t\,T_q = 0$$

where $\tilde{b}$ and $\mathbf{c_1}$ are the vectors, and $\mathbf{S}$, $\mathbf{D}$, $H1_\omega$, $G1_\omega$, $H1_t$ and $G1_t$ are the matrices given as

$$\tilde{b} = (\mathbf{H}\hat{\mathbf{U}} - \mathbf{G}\hat{\mathbf{Q}})\mathbf{F}^{-1}(-\omega) \quad , \quad \mathbf{c_1} = -\mathbf{S}\frac{Gr}{Re^2}\frac{\partial\,\mathbf{F}}{\partial\,x}\mathbf{F}^{-1}\mathbf{T} \quad , \quad \mathbf{S} = (\mathbf{H}\hat{\mathbf{U}} - \mathbf{G}\hat{\mathbf{Q}})\mathbf{F}^{-1}$$

$$\mathbf{D} = \mathbf{S}\Big(\mathbf{u}\,\frac{\partial\mathbf{F}}{\partial x}\mathbf{F}^{-1} + \mathbf{v}\,\frac{\partial\,\mathbf{F}}{\partial\,y}\mathbf{F}^{-1}\Big) \quad , \quad H1_\omega = \frac{1}{Re}\mathbf{H} - \mathbf{D} \quad , \quad G1_\omega = \frac{1}{Re}\mathbf{G}$$

$$H1_t = \frac{1}{RePr}\mathbf{H} - \mathbf{D} \quad , \quad G1_t = \frac{1}{RePr}\mathbf{G}.$$

After discretizing the vorticity and energy equations using implicit central difference scheme with relaxation parameters as in (3.37), we obtain

$$\Big(\frac{-\mathbf{S}}{2\Delta t} + \beta_\omega H1_\omega\Big)\omega^{m+1} - \beta_{\omega_q}G1_\omega\omega_q^{m+1} = \Big[\frac{-\mathbf{S}}{2\Delta t} - (1 - \beta_\omega)H1_\omega\Big]\omega^{m-1} + (1 - \beta_{\omega_q})G1_\omega\omega_q^{m-1}$$

$$\Big(\frac{-\mathbf{S}}{2\Delta t} + \beta_t H1_t\Big)T^{m+1} - \beta_{t_q}G1_t T_q^{m+1} = \Big[\frac{-\mathbf{S}}{2\Delta t} - (1 - \beta_t)H1_t\Big]T^{m-1} + (1 - \beta_{t_q})G1_t T_q^{m-1}.$$
$$(3.48)$$

When the boundary conditions are applied to the above equations the known and unknown values of ω, ω_q and T, T_q are passed from one side to another. Equations are arranged such that the right hand sides are at time t_{m-1} and known, and the left hand sides are at time t_{m+1} and unknown.

To start the iteration process, we set up the initial conditions for vorticity ω^{m-1} and ω^m where $m = 1$. Then solve the stream function equation ψ^{m+1} using these initial conditions. The velocity components $\mathbf{u}$ and $\mathbf{v}$ are aproximated using DRBEM idea with the obtained stream function values. Then, we set up the initial conditions of temperature T^{m-1} and T^m for $m = 1$. The vorticity transport equation is solved for ω^{m+1}. Finally, the enery eguation is solved for T^{m+1}. The iteration process is stopped until some convergence criteria (which is the L_∞ norm) is met with a preassigned tolerance ε. m-th iteration values are used in the matrices $\boldsymbol{H1}_\omega$ and $\boldsymbol{H1}_t$ which contain the convection matrix $\mathbf{D}$ and thus, these matrices are recalculated at each iteration due to the new values of convection terms.

3.3.1 Mixed Convection Flow in a One-Sided Differentially Heated Square Cavity

Mixed convection flow is the combination of forced and natural convection flows. The crucial point in analysing mixed convection flow is to determine the effect of buoyancy on the forced convection transport rates. The buoyancy forces may aid or oppose the forced convection flow. Thus heat transfer rates either increase or decrease, [8].

We consider one-sided lid-driven square cavity problem in two cases (Figures (3.42), (3.45)). In both cases the left vertical wall is moving up and the other three walls are motionless. In the first case, the left wall is heated and the right wall is cooled. Thus, buoyancy forces aid the forced convection flow. The horizontal walls are insulated. In the second case, the left wall is cooled and the right wall is heated which means buoyancy forces oppose the forced convection flow. The horizontal walls are adiabatic [8].

The non-dimensional equations can be written as

$$\nabla^2 \psi = -\omega$$

$$\frac{1}{Re}\nabla^2 \omega = \frac{\partial \omega}{\partial t} + u\frac{\partial \omega}{\partial x} + v\frac{\partial \omega}{\partial y} - \frac{Gr}{Re^2}\frac{\partial T}{\partial x} \tag{3.49}$$

$$\frac{1}{RePr}\nabla^2 T = \frac{\partial T}{\partial t} + u\frac{\partial T}{\partial x} + v\frac{\partial T}{\partial y} \ .$$

The initial conditions for vorticity and temperature are $\omega = T = 0$. The numerical code developed in the present investigation is used to carry out a number of simulations for a wide range of mixed convection parameter, Gr/Re^2, which characterizes the relative importance of buoyancy to forced convection.

In this problem, Reynolds number is fixed at 100. Thus, a change in Gr/Re^2 means a change in the value of Grashof number, Gr. Different values of Gr/Re^2 covering 0.01, 0.5, 2, 10 and 100 are considered. $Pr = 0.71$ and $f = 1 + r + r^2$. Linear boundary elements are used.

3.3.1.1 Case I

The left wall of the square cavity $0 \leq x, y \leq 1$ is kept at temperature $T = 1$, while the right wall being kept at temperature $T = 0$. The horizontal walls are kept as adiabatic. The left wall is moving from bottom to top with the specified velocity. Other three wall are motionless.

The problem is solved for $\frac{Gr}{Re^2} = 0.01 - 100$. $\Delta t = 0.5$ and 64 boundary nodes are used for $\frac{Gr}{Re^2} = 0.01$ and 0.5. $\Delta t = 0.5$ and $N = 72$ is used for $\frac{Gr}{Re^2} = 2$. With the increase in $\frac{Gr}{Re^2}$ we need to increase the number of boundary nodes and decrease the time increment. 88 and 104 boundary nodes with $\Delta t = 0.1$ are used for $\frac{Gr}{Re^2} = 10$ and 100, respectively.

Movement of the left wall causes a clockwise rotating cell. In this case, the buoyancy forces aid the forced convection flow. When $\frac{Gr}{Re^2} = 0.01$ the buoyancy is weak and forced convection is dominating the mechanism. As the mixed convection parameter increases from 0.01 to 0.5 the strength of the cell enhances and the isotherms tend to stratified. When $\frac{Gr}{Re^2} = 0.5$ and 2 buoyancy and shear forces effects are in comparable level. We can see from the Figure (3.43) that the isotherms are different from either the forced or the natural convection flow. With the increase in $\frac{Gr}{Re^2}$ natural convection becomes the dominating mechanism. At $\frac{Gr}{Re^2} = 100$ the flow fileds are nearly the same as those of the natural convection flow.

The center cell of streamlines change its shape from circular to elliptical as $\frac{Gr}{Re^2}$ increases, and boundary layers are formed for both streamlines and isotherms near the vertical walls. The behaviours are in good agreement with the behaivours given in [8]. The solutions are presented for the steady state case in which the convergence criteria is taken as 10^{-5} for $\frac{Gr}{Re^2} = 0.01$, 10^{-4} for $\frac{Gr}{Re^2} = 0.5$ and 2, and 10^{-3} for $\frac{Gr}{Re^2} = 10$ and 100.

Flow classification can be made through the increasing Gr/Re^2. The forced convection takes place for $Gr/Re^2 \ll 1$, the mixed convection takes place for $1 \ll Gr/Re^2 \ll 10$ and natural convection for $Gr/Re^2 \gg 1$.

Figure (3.44) shows the passage from forced convection to natural convection for several values of Gr/Re^2 in terms of mid-plane velocity profiles.
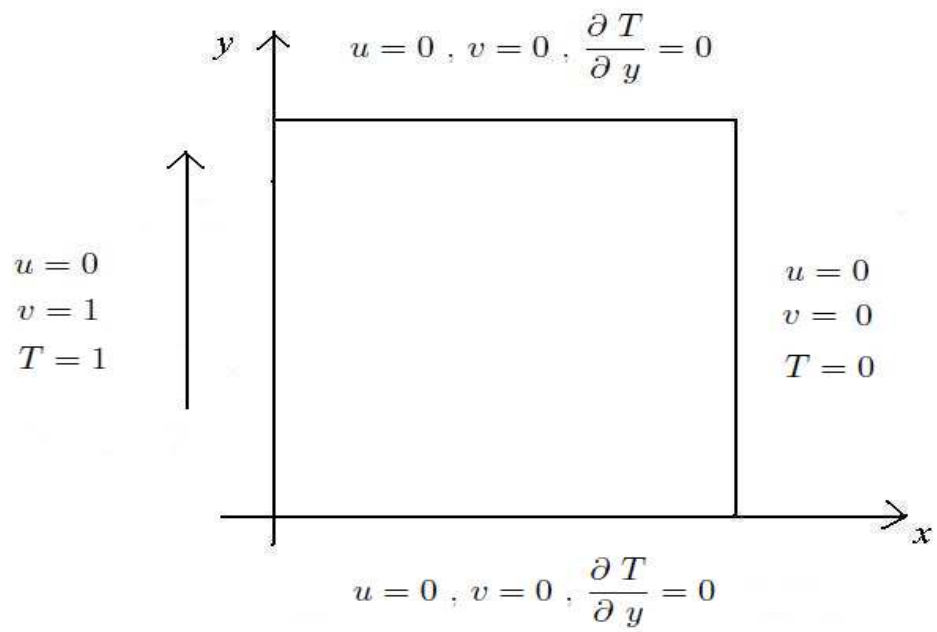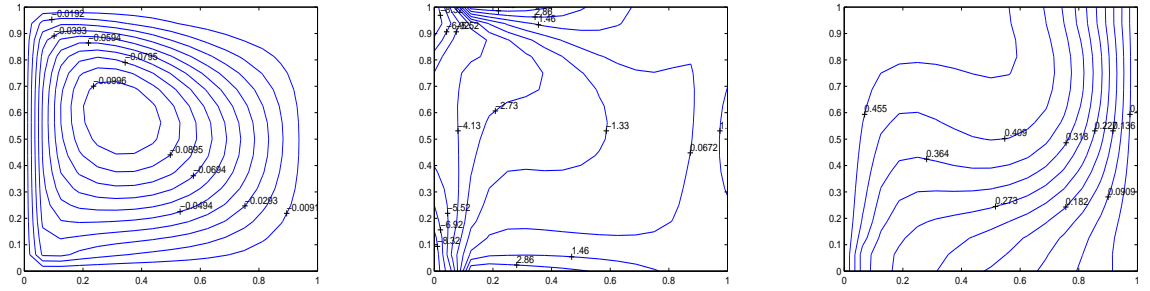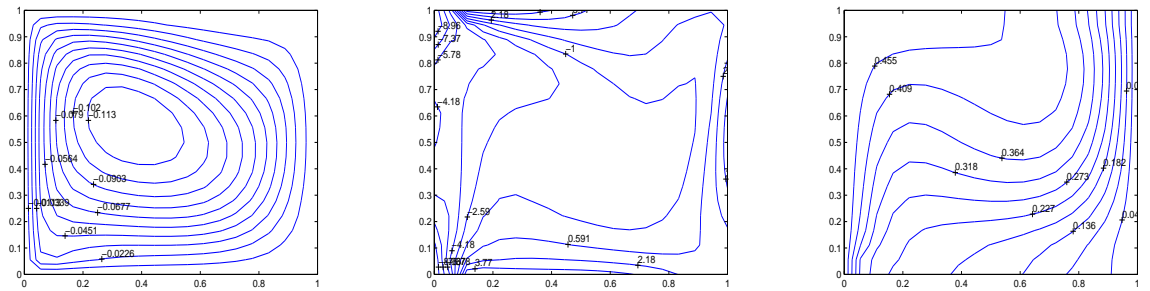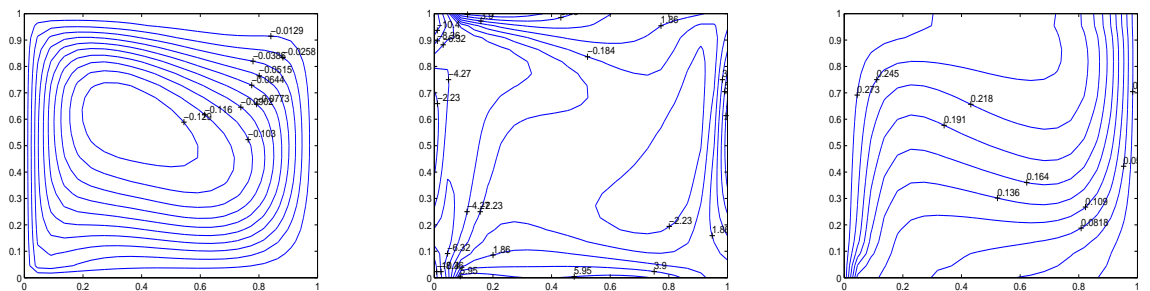
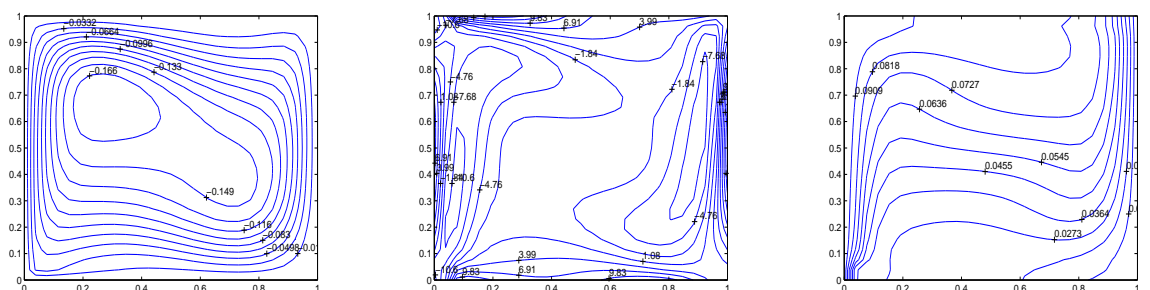Figure 3.42: Boundary conditions for mixed convection flow, Case I

$Gr/Re^2 = 0.5$

$Gr/Re^2 = 2$

$Gr/Re^2 = 10$

$Gr/Re^2 = 100$

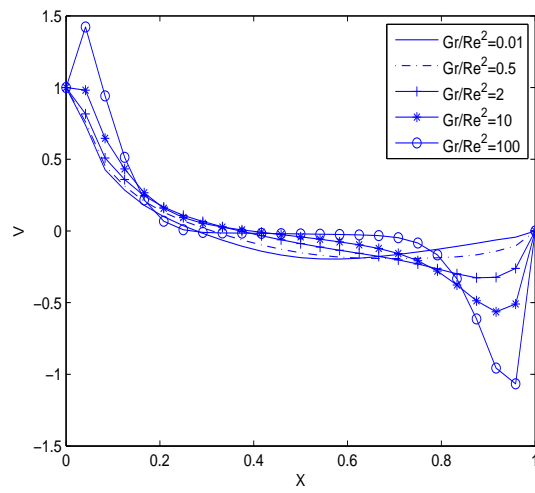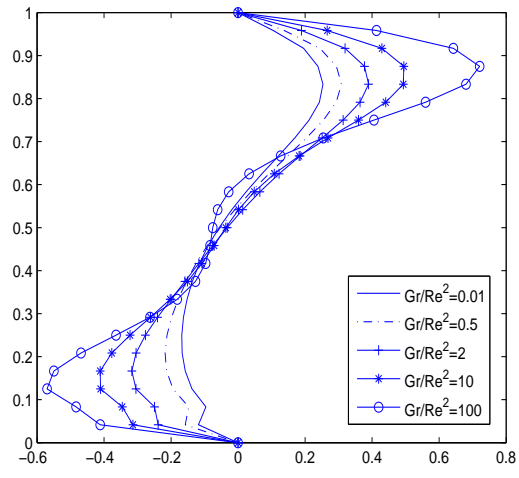Figure 3.43: Streamlines, vorticity and temperature contours, Case I

114

Figure 3.44: Velocity profiles for several values of Gr/Re^2, Case I

3.3.1.2 Case II

The left wall of the cavity is isothermally cooled and the right wall is isothermally heated. The square is bounded by three motionless walls and the left vertical wall moving from bottom to top with a constant velocity. The problem is solved for $Gr/Re^2 = 0.01 - 100$. Quadratic radial basis functions are used and Prandtl number is taken as 0.71. Linear boundary elements are used. For $Gr/Re^2 = 0.01$, 72 boundary elements are used with $\Delta t = 0.5$, and the convergence criteria is taken as 10^{-5}. For $Gr/Re^2 = 0.5$ and 2, time increment is again 0.5 but the number of boundary nodes is 80 and the convergence criteria is 10^{-4}. We increase the number of boundary nodes to 88 when $Gr/Re^2 = 10$ and use $\Delta t = 0.1$ with convergence criteria 10^{-4}. Finally, for $Gr/Re^2 = 100$, 104 boundary nodes are used with $\Delta t = 0.1$ and the convergence criteria is taken as 10^{-3}. All computations are carried out taking relaxation parameters as 0.9.

At $Gr/Re^2 = 0.01$, a clockwise rotating cell occurs due to the moving left wall. Forced convection is dominant. Since the left wall is cooled and the right wall is heated, the buoyancy forces cause a counter-clockwise rotation inside the cavity with an increase in the mixed convection parameter. This rotation opposes the lid-driven re-circulation. Thus, a secondary cell occurs when $Gr/Re^2 = 0.5$. This secondary cell is counter rotating the primary cell because of the moving left wall. As Gr/Re^2 increases buoyancy forces get stronger and the secondary cell becomes larger. When $Gr/Re^2 = 10$ the primary cell gets smaller and the secondary cell covers almost the entire cavity. We also observe that at the beginning isotherms tend to move from right to left but as Gr/Re^2 increases the isotherm lines move from left to right. Boundary layers are formed. These behaviours which can be seen from Figures (3.46) are in good agreement with the ones in [8].

In Figure (3.47), one can see the effect of heated wall on the mid-plane velocity profiles when the opposite wall is moving upwards. When the velocity profiles are compared with the profiles for Case I, we see that the flows tend to move through cooled wall as natural convection takes place. Mixed convection flow equations differ from natural convection flow equations only in the coefficients in front of the diffusion terms and temperature gradient. Thus, DRBEM solution procedure is exactly the same. The solutions are obtained for various values of the ratio Gr/Re^2 to capture the physical changes in the flow due to the effects of natural and forced convections.
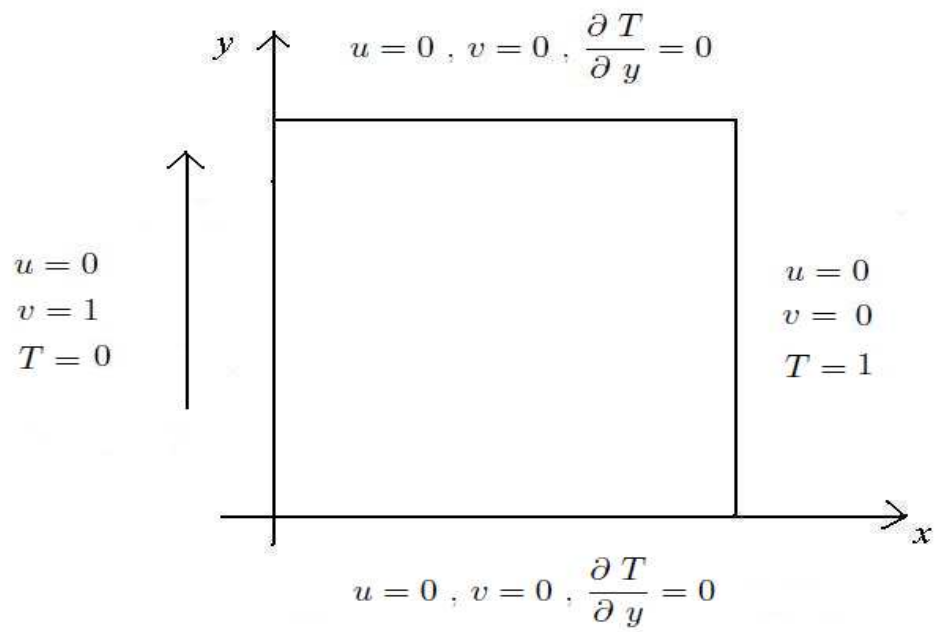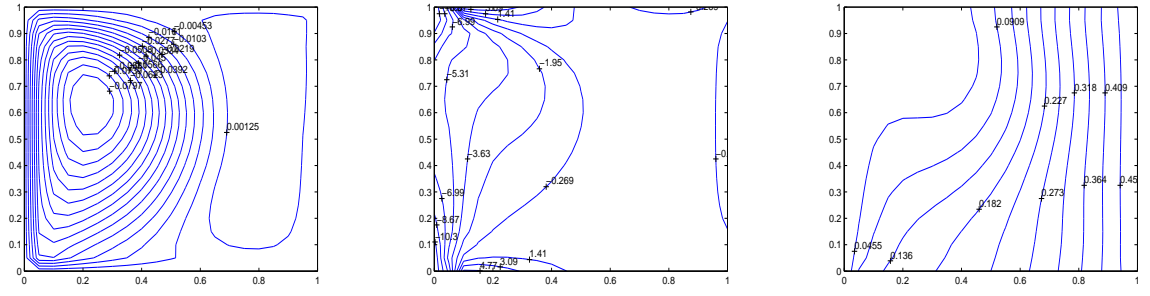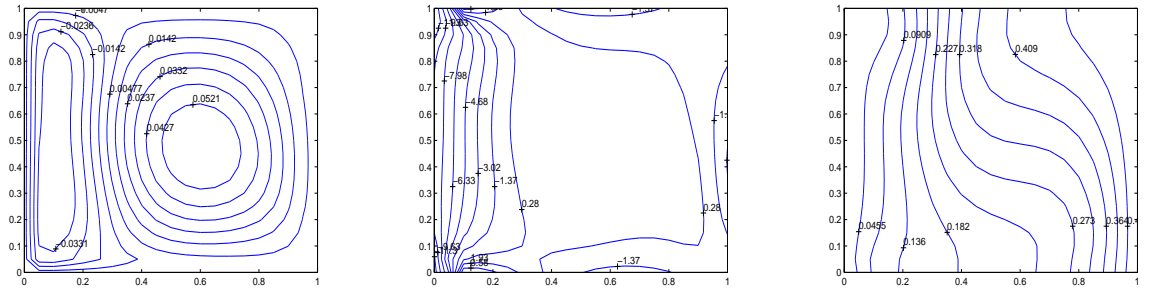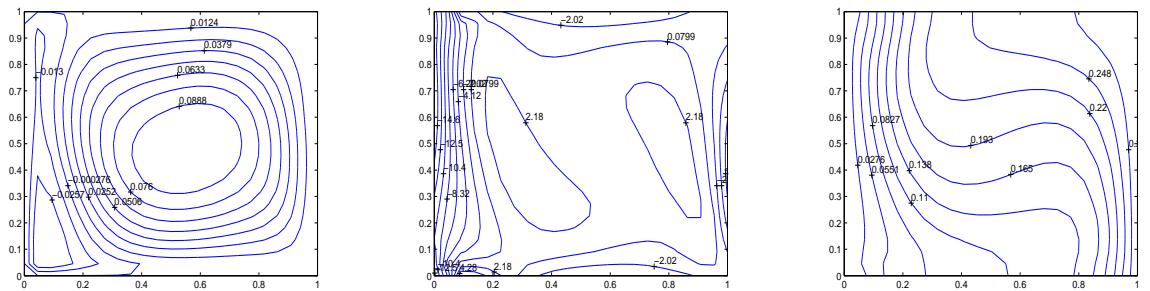
116

Figure 3.45: Boundary conditions for mixed convection flow, Case II
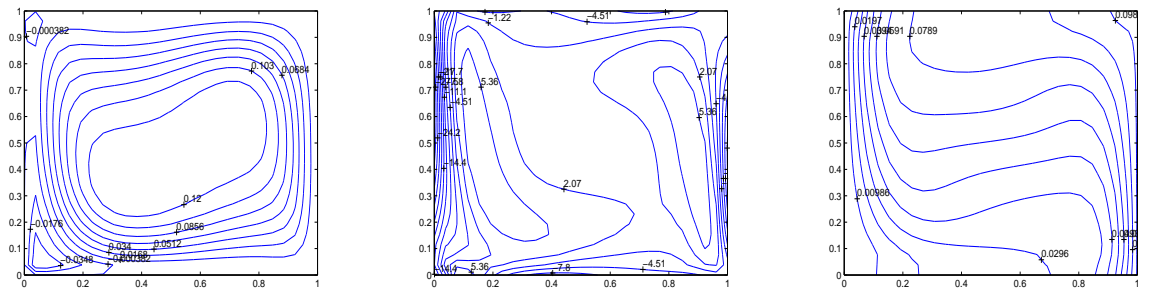
$Gr/Re^2 = 0.5$

$Gr/Re^2 = 2$

$Gr/Re^2 = 10$

$Gr/Re^2 = 100$

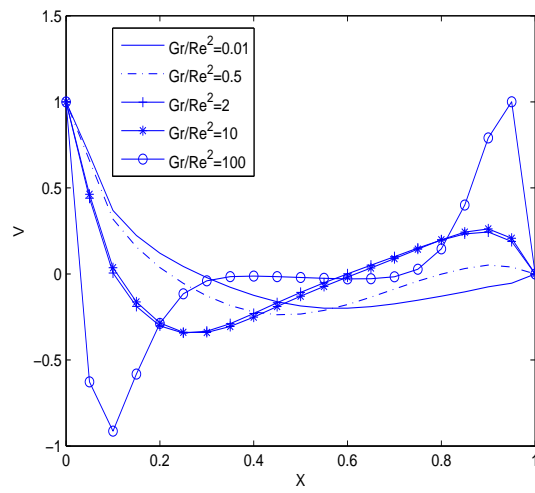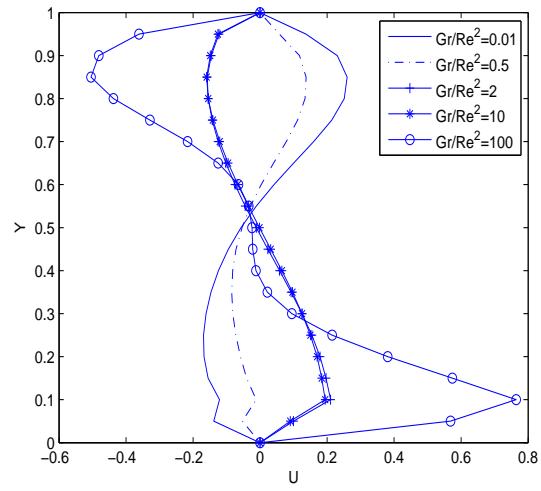Figure 3.46: Streamlines, vorticity and temperature contours, Case II

Figure 3.47: Velocity profiles for several values of Gr/Re^2, Case II

3.4 Natural Convection Flow of Nanofluids

Fluid heating and cooling are important in many industries such as power, manufacturing, transportation, and electronics. Effective cooling techniques are greatly needed for cooling any sort of high-energy device. Common heat transfer fluids such as water, ethylene glycol, and engine oil have limited heat transfer capabilities due to their low heat transfer properties. In contrast, metals have thermal conductivities up to three times higher than these fluids, so it is natural that it would be desired to combine the two substances to produce a heat transfer medium that behaves like a fluid, but has the thermal conductivity of a metal. Nanofluids are made of nanoparticles suspended in a base fluid. Typical nanoparticles are metal or metal oxide nanoparticles such as Al_2O_3, CuO, Cu, TiO. Generally water and ethylene glycol is used as the base fluid, [47].

The non-dimensional, unsteady equations of motion and energy for nanofluids can be written in terms of stream function (ψ), vorticity (ω) and temperature (T) as follows, [3]

$$\nabla^2 \psi = -\omega$$

$$\frac{\mu_{nf}}{\rho_{nf}\alpha_f}\nabla^2\omega = \frac{\partial \omega}{\partial t} + u\frac{\partial \omega}{\partial x} + v\frac{\partial \omega}{\partial y} - RaPr\frac{(\rho\beta)_{nf}}{\rho_{nf}\beta_f}\frac{\partial T}{\partial x} \qquad (3.50)$$

$$\frac{\alpha_{nf}}{\alpha_f}\nabla^2 T = \frac{\partial T}{\partial t} + u\frac{\partial T}{\partial x} + v\frac{\partial T}{\partial y}$$

where $(x, y) \in \Omega \subset R^2$, $t > 0$. Ra and Pr are the Rayleigh number and Prandtl number. The subscripts 'nf', and 'f' refer to nanofluid and pure fluid, respectively.

The effective dynamic viscosity [24] and the effective density [61] of the nanofluid are given by

$$\mu_{nf} = \frac{\mu_f}{(1-\varphi)^{2.5}} \quad , \quad \rho_{nf} = (1-\varphi)\rho_f + \varphi\rho_s$$

where φ is the volume fraction of nanoparticles, μ_f is the dynamic viscosity of the fluid, ρ_f and ρ_s are the density of the fluid and nanoparticle, respectively.

Thermal diffusivity of the nanofluid is defined by, [63]

$$\alpha_{nf} = \frac{k_{nf}}{(\rho C_p)_{nf}}.$$

120

Here k_{nf} is the thermal conductivity of the nanofluid given by, [54]

$$k_{nf} = k_f \frac{k_s + 2k_f - 2\varphi(k_f - k_s)}{k_s + 2k_f + \varphi(k_f - k_s)}.$$

where the subscript 's' refer to nanoparticle.

It is important to note that the effective thermal conductivity of nanofluids depends on the thermal conductivity of solid particles and base fluid, particle volume fraction, shape of particles and the thickness of the thermal conductivity of nanolayer [47].

The heat capacitance of the nanofluid and part of the Boussinesq term are defined as [61]

$$(\rho C_p)_{nf} = (1 - \varphi)(\rho C_p)_f + \varphi(\rho C_p)_s$$

$$(\rho \beta)_{nf} = (1 - \varphi)\rho_f \beta_f + \varphi \rho_s \beta_s.$$

The equations in (3.50) are supplied with the initial conditions

$$\omega(x, y, 0) = \omega_0(x, y) \quad , \quad T(x, y, 0) = T_0(x, y)$$

where $\omega_0(x, y)$ and $T_0(x, y)$ are given functions of space and time.

Corresponding boundary conditions are given by

$$\psi(x_s, y_s) = f_{\psi_s} \quad , \quad \omega(x_s, y_s) = f_{\omega_s}$$

$$T(x_s, y_s) = f_{t_s} \quad , \quad \frac{\partial T}{\partial n}(x_s, y_s) = f_{t_n}.$$

(3.51)

Application of DRBEM to stream function, vorticity and energy equations are given in Section 3.2. There is no need for an extra equation for nanofluid. But the differences lies in the coefficients of ω and T equations. Stream function equation is the same. The difference comes from the fact that since nanoparticles are suspended in the base fluid, their thermophysical properties must also be considered. The percentage of the nanoparticles that are suspended in the base fluid is controled with the parameter φ. The nanoparticles are added to the base fluid so that they do not sediment and flow with the fluid.

The DRBEM discretized system of equations for vorticity and energy equations in natural

121

convection flow were given in equations (3.29) and (3.31), respectively as

$$Pr(\mathbf{H}\omega - \mathbf{G}\omega_q) = (\mathbf{H}\hat{\mathbf{U}} - \mathbf{G}\hat{\mathbf{Q}})\mathbf{F}^{-1}\Big[\frac{\partial\,\omega}{\partial\,t} + \Big(\mathbf{u}\,\frac{\partial\mathbf{F}}{\partial x}\mathbf{F}^{-1} + \mathbf{v}\,\frac{\partial\,\mathbf{F}}{\partial\,y}\mathbf{F}^{-1}\Big)\omega - RaPr\frac{\partial\,\mathbf{T}}{\partial\,x}\Big]$$

$$\text{(3.52)}$$

$$\mathbf{H}\mathbf{T} - \mathbf{G}\mathbf{T_q} = (\mathbf{H}\hat{\mathbf{U}} - \mathbf{G}\hat{\mathbf{Q}})\mathbf{F}^{-1}\Big[\frac{\partial\,\mathbf{T}}{\partial\,t} + \Big(\mathbf{u}\,\frac{\partial\mathbf{F}}{\partial x}\mathbf{F}^{-1} + \mathbf{v}\,\frac{\partial\,\mathbf{F}}{\partial\,y}\mathbf{F}^{-1}\Big)\mathbf{T}\Big].$$

So, for the natural convection of nanofluids we have similar equations with different coefficients as

$$\frac{\mu_{nf}}{\rho_{nf}\alpha_f}(\mathbf{H}\omega - \mathbf{G}\omega_q) = (\mathbf{H}\hat{\mathbf{U}} - \mathbf{G}\hat{\mathbf{Q}})\mathbf{F}^{-1}\Big[\frac{\partial\,\omega}{\partial\,t} + \Big(\mathbf{u}\,\frac{\partial\mathbf{F}}{\partial x}\mathbf{F}^{-1} + \mathbf{v}\,\frac{\partial\,\mathbf{F}}{\partial\,y}\mathbf{F}^{-1}\Big)\omega - RaPr\frac{(\rho\beta)_{nf}}{\rho_{nf}\beta_f}\frac{\partial\mathbf{T}}{\partial x}\Big]$$

$$\frac{\alpha_{nf}}{\alpha_f}(\mathbf{H}\mathbf{T} - \mathbf{G}\mathbf{T_q}) = (\mathbf{H}\hat{\mathbf{U}} - \mathbf{G}\hat{\mathbf{Q}})\mathbf{F}^{-1}\Big[\frac{\partial\,\mathbf{T}}{\partial\,t} + \Big(\mathbf{u}\,\frac{\partial\mathbf{F}}{\partial x}\mathbf{F}^{-1} + \mathbf{v}\,\frac{\partial\,\mathbf{F}}{\partial\,y}\mathbf{F}^{-1}\Big)\mathbf{T}\Big].$$

$$\text{(3.53)}$$

Final matrix form of stream function, vorticity and energy equations are

$$\mathbf{H}\psi - \mathbf{G}\psi_q = \tilde{b}$$

$$-\mathbf{S}\frac{\partial\,\omega}{\partial\,t} + \breve{H}_\omega\omega - \breve{G}_\omega\omega_q = \mathbf{c_2} \qquad\qquad\text{(3.54)}$$

$$-\mathbf{S}\frac{\partial\,\mathbf{T}}{\partial\,t} + \breve{H}_t\mathbf{T} - \breve{G}_t\mathbf{T}_q = \mathbf{0}$$

where $\tilde{b}$, $\mathbf{c_2}$ are the vectors and $\mathbf{S}$, $\mathbf{D}$, $\breve{H}_\omega$, $\breve{G}_\omega$, $\breve{H}_t$ and $\breve{G}_t$ are the matrices given by

$$\tilde{b} = (\mathbf{H}\hat{\mathbf{U}} - \mathbf{G}\hat{\mathbf{Q}})\mathbf{F}^{-1}(-\omega) \quad , \quad \mathbf{c_2} = -\mathbf{S}RaPr\frac{(\rho\beta)_{nf}}{\rho_{nf}\beta_f}\frac{\partial\mathbf{F}}{\partial x}\mathbf{F}^{-1}\mathbf{T} \quad , \quad \mathbf{S} = (\mathbf{H}\hat{\mathbf{U}} - \mathbf{G}\hat{\mathbf{Q}})\mathbf{F}^{-1}$$

$$\mathbf{D} = \mathbf{S}\Big(\mathbf{u}\,\frac{\partial\mathbf{F}}{\partial x}\mathbf{F}^{-1} + \mathbf{v}\,\frac{\partial\mathbf{F}}{\partial y}\mathbf{F}^{-1}\Big) \quad , \quad \breve{H}_\omega = \frac{\mu_{nf}}{\rho_{nf}\,\alpha_f}\mathbf{H} - \mathbf{D} \quad , \quad \breve{G}_\omega = \frac{\mu_{nf}}{\rho_{nf}\,\alpha_f}\mathbf{G}$$

$$\breve{H}_t = \frac{\alpha_{nf}}{\alpha_f}\mathbf{H} - \mathbf{D} \quad , \quad \breve{G}_t = \frac{\alpha_{nf}}{\alpha_f}\mathbf{G}.$$

Here, ψ, ψ_q, ω, ω_q, T and T_q are vectors containing nodal values of stream function and its normal derivative, vorticity and its normal derivative, and temperature and its normal derivative.

Central difference discretization of the time derivatives that appear in vorticity and energy equations in (3.54) gives

$$\left(\frac{-\mathbf{S}}{2\Delta t} + \beta_\omega \breve{\mathbf{H}}_\omega\right)\omega^{m+1} - \beta_{\omega_q}\breve{\mathbf{G}}_\omega \omega_{\boldsymbol{q}}{}^{m+1} = \left[\frac{-\mathbf{S}}{2\Delta t} - (1 - \beta_\omega)\breve{\mathbf{H}}_\omega\right]\omega^{m-1} + (1 - \beta_{\omega_q})\breve{\mathbf{G}}_\omega \omega_{\boldsymbol{q}}{}^{m-1}$$

$$\left(\frac{-\mathbf{S}}{2\Delta t} + \beta_t \breve{\mathbf{H}}_t\right)\boldsymbol{T}^{m+1} - \beta_{t_q}\breve{\mathbf{G}}_t \boldsymbol{T_q}{}^{m+1} = \left[\frac{-\mathbf{S}}{2\Delta t} - (1 - \beta_t)\breve{\mathbf{H}}_t\right]\boldsymbol{T}^{m-1} + (1 - \beta_{t_q})\breve{\mathbf{G}}_t \boldsymbol{T_q}{}^{m-1}$$

$$(3.55)$$

which is similar to the system of equations (3.37) in natural convection flow.

The iteration procedure starts by assigning the initial conditions for vorticity, ω^{m-1}, ω^m and temperature, $\boldsymbol{T}^{m-1}$, $\boldsymbol{T}^m$ where $m = 1$. The initial conditions for vorticity, temperature and their normal derivatives are taken as zero at both levels. Then the stream function equation is solved using the initial conditions of vorticity. The velocity components $\mathbf{u}$ and $\mathbf{v}$ are approximated using DRBEM idea with the new values of stream function. Vorticity equation is solved at time $(m + 1)$ using the velocity components and the initial values of temperature. Finally, the temperature equation is solved. The initial conditions are set up for the next time step. The iteration is stopped when the convergence criteria is met. As is explained in the previous flow cases, the m-th iteration is used in computing the matrices $\tilde{H}_\omega$ and $\tilde{H}_t$ which contain convection terms.

3.4.1 Natural Convection Flow of Nanofluids in a Square Cavity with a Discrete Heater

The non-dimensional, unsteady equations of motion and energy for nanofluids can be written in terms of stream function (ψ), vorticity (ω) and temperature (T), as follows [3]

$$\nabla^2 \psi = -\omega$$

$$\frac{\mu_{nf}}{\rho_{nf}\alpha_f}\nabla^2\omega = \frac{\partial\omega}{\partial t} + u\frac{\partial\omega}{\partial x} + v\frac{\partial\omega}{\partial y} - RaPr\frac{(\rho\beta)_{nf}}{\rho_{nf}\beta_f}\frac{\partial T}{\partial x} \qquad (3.56)$$

$$\frac{\alpha_{nf}}{\alpha_f}\nabla^2 T = \frac{\partial T}{\partial t} + u\frac{\partial T}{\partial x} + v\frac{\partial T}{\partial y}$$

where $(x, y) \in \Omega \subset R^2$, $t > 0$. Ra and Pr are the Rayleigh number and Prandtl number, respectively. ρ is the density and β is the thermal expansion coefficient. The subscripts 'nf', 'f' and 's' refer to nanofluid, fluid and nanoparticle, respectively.

Equations are supplied with the initial conditions

$$\omega(x, y, 0) = 0 \quad , \quad T(x, y, 0) = 0$$

where $\omega_0(x, y)$ and $T_0(x, y)$ are given functions of space and time.

Corresponding boundary conditions are shown in Figure (3.48). The velocity components are zero on the solid walls. The wall at $x = 1$ is cooled and the horizontal walls are adiabatic. The left wall is heated with constant heat flux for a varying length with a parameter ϵ, [61]. The fluid in the cavity is a water-based nanofluid containing copper (Cu) and aluminum oxide (Al_2O_3) nanoparticles. It is assumed that the base fluid and nanoparticles are in thermal equilibrium and no slip occurs between them. The thermo-physical properties of the nanofluid are assumed to be constant except for the density variation, which is approximated by the Boussinesq model. The thermo-physical properties of the nanofluid are given in Table 3.1, [61, 83].

The local and average Nusselt numbers for the wall with constant heat flux are given as in [61]

$$Nu = \frac{\kappa_{nf}}{\kappa_f}\frac{1}{T_s(y)} \quad , \quad Nu_{av} = \frac{1}{\epsilon}\int_0^\epsilon Nu\, dy$$

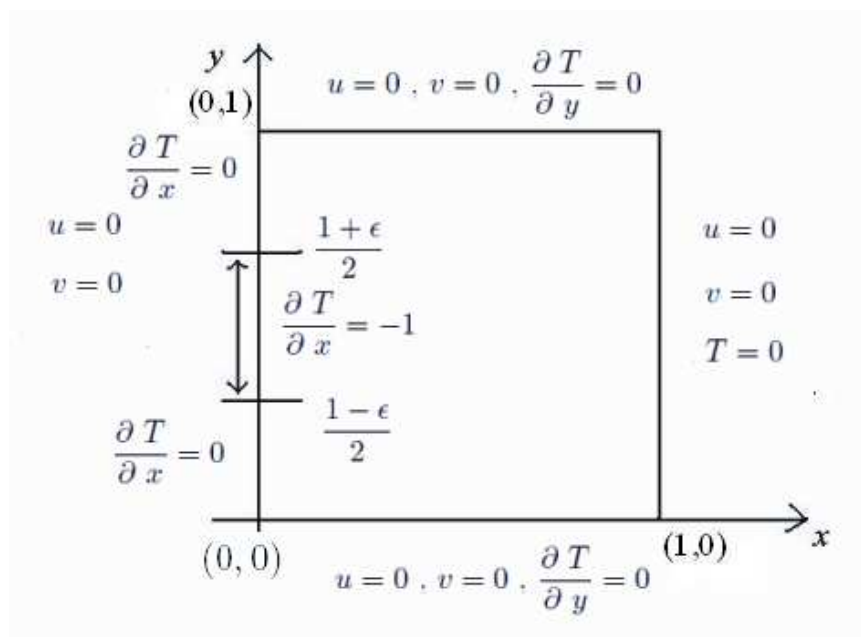where $T_s(y)$ is the temperature of the wall under consideration.

Figure 3.48: Boundary conditions for the natural convection flow of nanofluids

Table 3.1: Thermophysical properties of the base fluid and nanoparticles [1, 61]

Physical properties	Fluid phase(Water)	Cu	Al_2O_3
$C_p(J/kgK)$	4179	385	765
$\rho(kg/m^3)$	997.1	8933	3970
$k(W/mK)$	0.613	400	40
$\beta \times 10^{-5}(1/K)$	21	1.67	2.4
$\alpha \times 10^7(m^2/s)$	1.47	1163.1	131.7

The numerical results are reported for several values of heater length (ϵ), Rayleigh number (Ra) and nanoparticle volume fraction (φ) for Cu and Al_2O_3 based nanofluids. The Prandtl number is 6.2 which means the base fluid is water.

The discretization is performed by using linear boundary elements. The radial basis function f is taken as $1 + r + r^2$. The time derivative is discretized using central difference scheme with relaxation parameters 0.9 for all variables. The computations are carried out until steady state conditions are reached. The convergence criteria used in the time loop to achieve steady state conditions for vorticity is $\max_i |\omega_i^{m+1} - \omega_i^m| \leq 10^{-5}$, $i = 1, .., N + L$. The same condition is also used for temperature. Solutions are obtained by using 56, 72, 80 and 100 boundary elements for $Ra = 10^3$, 10^4, 10^5 and 10^6 with the time increments $\Delta t = 0.1$, 0.01, 0.0013 and 0.001, respectively.

Figure (3.49) shows the streamlines, isotherms and vorticity contours of a copper-based nanofluid with $\varphi = 0.2$, $\epsilon = 0.25$, and $Ra = 10^3 - 10^6$. At $Ra = 10^3$, the circulation inside the cavity is so weak that viscous forces are dominant. Isotherms are parallel to the surface of the isoflux heater. The center cell is in circular pattern. With an increase in the Rayleigh number, the intensity of the recirculation inside the cavity increases, and boundary layers occur near the walls. At $Ra = 10^6$, the center cell becomes egg-shaped and isotherms become parallel to the horizontal walls. The flow is stagnant at the center of the cavity. Convection is the dominating mechanism for heat transfer.

Figures (3.50) and (3.51) show the effect of volume fraction for different Rayleigh numbers on Cu and Al_2O_3 based nanofluids, respectively. When volume fraction increases from 0.0 to 0.2 or from 0.1 to 0.2 flow strength increases. More fluid is heated. This behaviour can be seen from the isotherms.

Velocity profiles of a copper-based nanofluid at the mid-plane of the cavity for various values of volume fraction is given in Figure (3.52). One can see that the magnitude of the velocity components increases with an increase in the volume fraction when Rayleigh number and heater length are fixed at $Ra = 10^6$ and $\epsilon = 0.5$, respectively.

Table 3.2: Variation of average Nusselt number with respect to volume fraction (φ), Rayleigh number (Ra) and heater length (ϵ)

Material:		Cu			Al_2O_3		
ϵ	φ	$Ra = 10^4$	$Ra = 10^5$	$Ra = 10^6$	$Ra = 10^4$	$Ra = 10^5$	$Ra = 10^6$
0.25	0.0	3.966	6.631	10.884	3.966	6.631	10.884
	0.1	5.152	8.626	15.129	5.077	8.504	14.961
	0.2	6.301	10.370	17.960	6.126	10.079	16.938
0.50	0.0	2.933	5.582	9.006	2.933	5.582	9.006
	0.1	3.540	6.681	11.561	3.485	6.587	10.428
	0.2	4.237	7.916	13.337	4.109	7.696	13.059

Figures (3.53) represent the vertical and horizontal velocity profiles at the mid-plane of the cavity using different types of nanofluids where $Ra = 10^6$, $\varphi = 0.1$ and $\epsilon = 0.25$. The vertical velocity profile shows a parabolic variation near the vertical walls due to buoyant flow inside the cavity. The velocity profiles of these nanofluids are similar. This is because the viscosity of the nanofluid is only sensitive to the volume fraction of particles and not influenced by the type of nanoparticles. Behaviours of streamlines and istoherms shown in Figures (3.49)-(3.51) are in good agreement with the ones given in [61]. Thus, DRBEM is made use of to obtain solutions of natural convection flow of nanofluids for various values of volume fraction which controls the nanoparticles that are suspended in the base fluid.

Table 3.2 shows the variation of average Nusselt number with respect to volume fraction, Rayleigh number and heater length for copper-water and aluminum oxide-water based nanofluids. It is disclosed that when the volume fraction and Rayleigh number are fixed, an increase in the length of the heat source reduces the heat transfer. There is a remarkable increase in the average Nusselt number with an increase in the volume fraction. An increase in the Rayleigh number results an increase in the average Nusselt number for a certain nanoparticle. It is also observed that copper-water based nanofluid as greater heat transfer rate than that of aluminum oxide-water based nanofluid. These values are in good agreement with the values given in the study of [61].
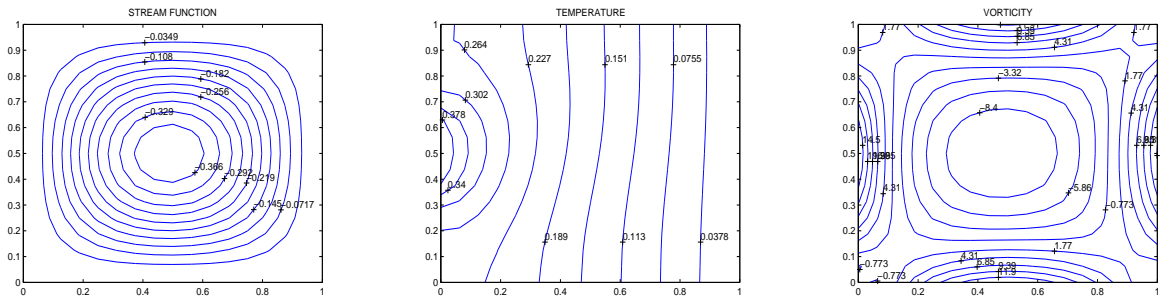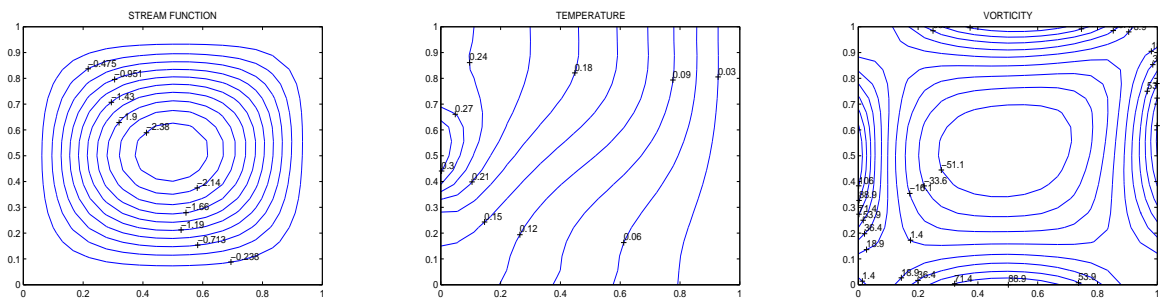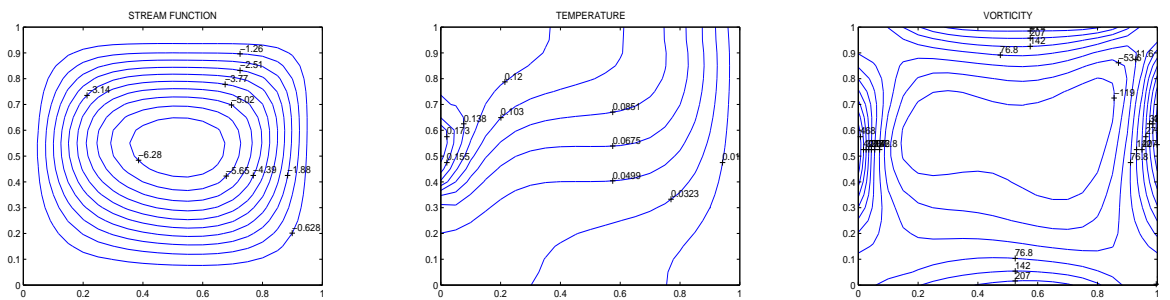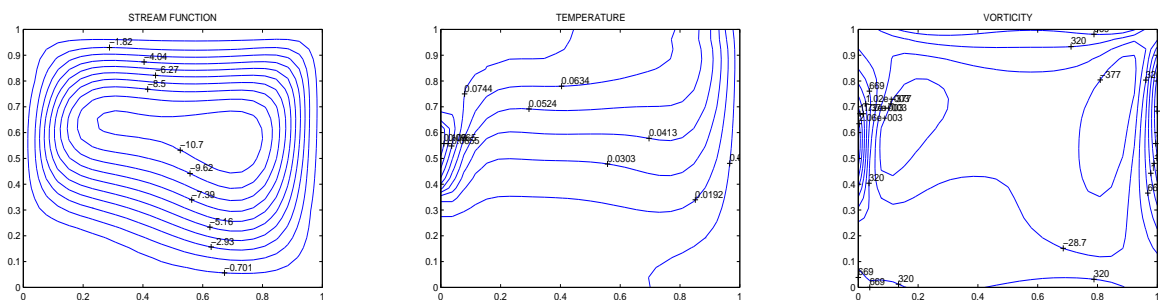
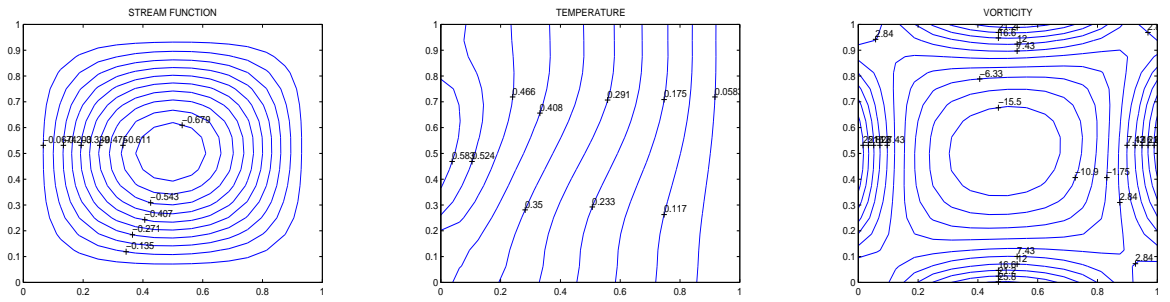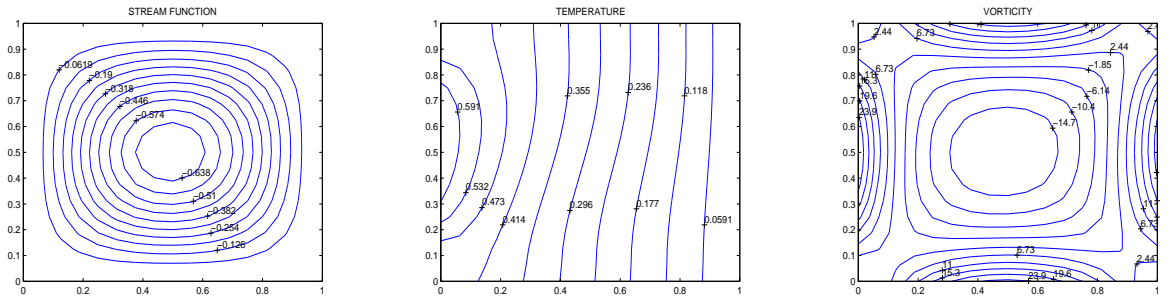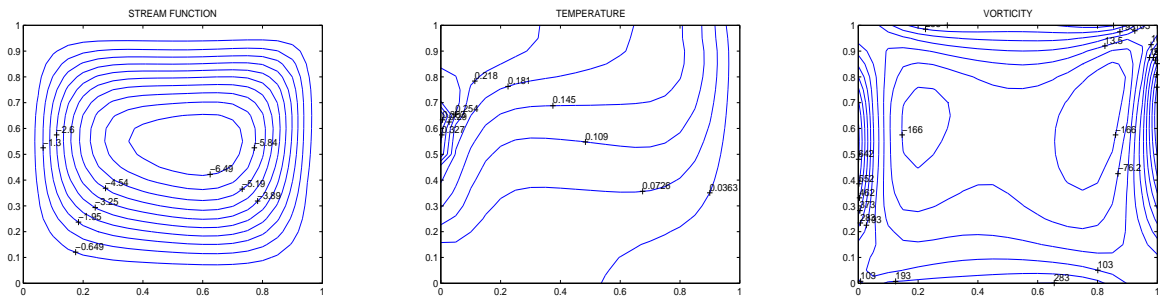Figure 3.49: Streamlines, isotherms and vorticity contours of a copper-based nanofluid with $\varphi = 0.2$ and $\epsilon = 0.25$.

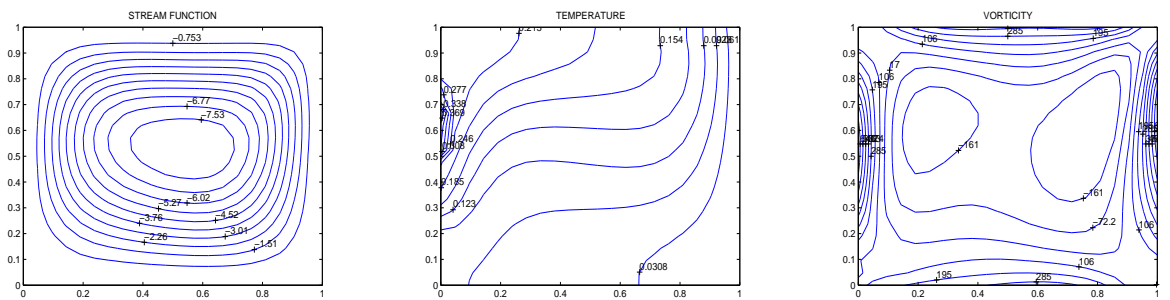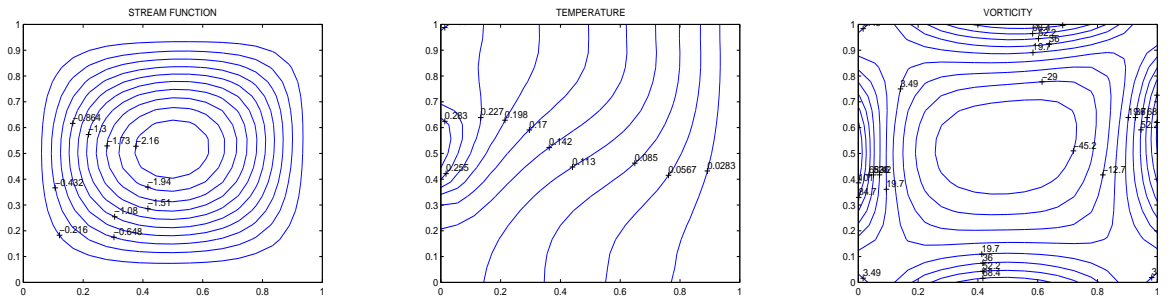Figure 3.50: Streamlines, isotherms and vorticity contours of a copper-based nanofluid with $\epsilon = 0.5$.

130
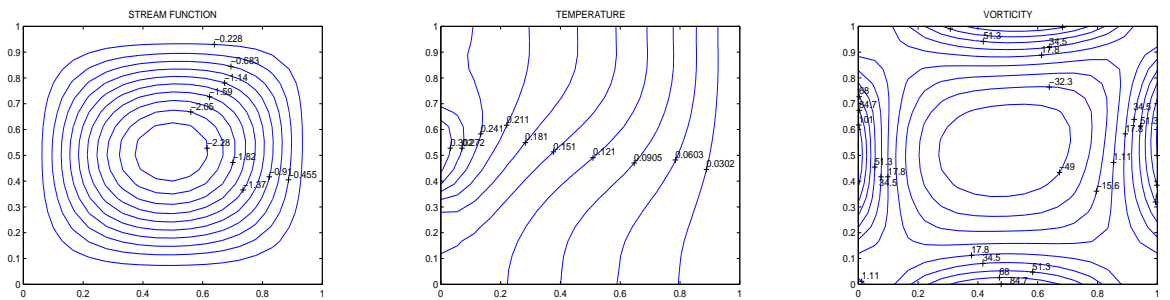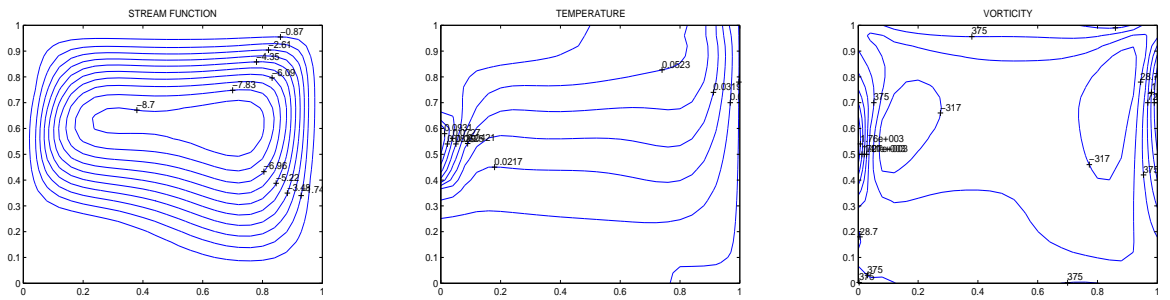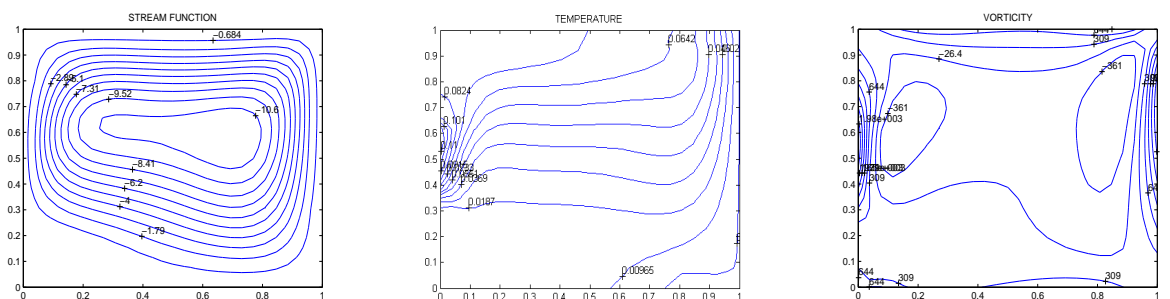
Figure 3.51: Streamlines, isotherms and vorticity contours of a Al_2O_3-based nanofluid with $\epsilon = 0.25$.

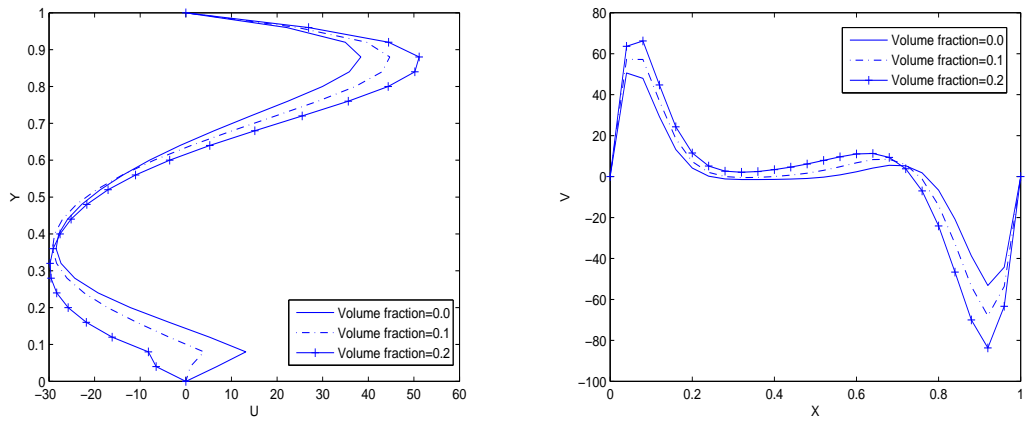Figure 3.52: Velocity profiles of a Copper-based nanofluid at the mid-plane of the cavity, $\epsilon = 0.5$, $Ra = 10^6$.
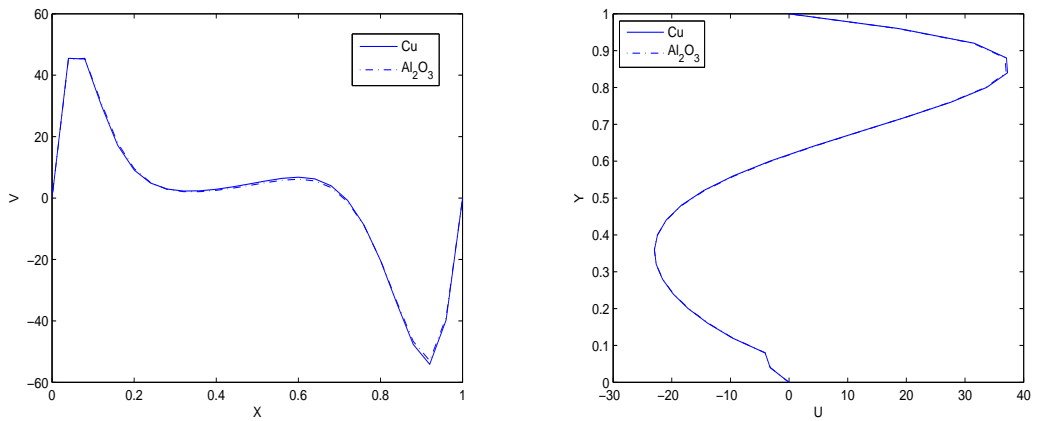

Figure 3.53: Velocity profiles of copper and aluminum oxide based nanofluids at the midplane of the cavity for $\varphi = 0.1$, $Ra = 10^6$ and $\epsilon = 0.25$.

3.5 Natural Convection Flow of Micropolar Fluids

In the previous sections, we use the Navier-Stokes equations to model the fluid flow. But this model is inadequate for fluids with microstructure such as polymeric suspensions, blood and liquid crystals. In order to describe the behaviour of such fluids, we need a model that takes into account geometry and movement of these microstructures [52].

In this section, we express the governing equations in terms of velocities u, v, stream function ψ, pressure p, vorticity ω, temperature T and microrotation $\bar{N}$.

The non-dimensional, unsteady equations of motion, energy and microrotation can be written as follows [9, 10]

$$\nabla^2 u = -\frac{\partial \omega}{\partial y}$$

$$\nabla^2 v = \frac{\partial \omega}{\partial x}$$

$$\nabla^2 \psi = -\omega$$

$$\nabla^2 p = \frac{Ra}{Pr}\frac{\partial T}{\partial y} - \left(\frac{\partial u}{\partial x}\right)^2 - \left(\frac{\partial v}{\partial y}\right)^2 - 2\frac{\partial v}{\partial x}\frac{\partial u}{\partial y} \qquad (3.57)$$

$$(1 + K)\nabla^2 \omega = \frac{\partial \omega}{\partial t} + u\frac{\partial \omega}{\partial x} + v\frac{\partial \omega}{\partial y} + K\nabla^2 \bar{N} - \frac{Ra}{Pr}\frac{\partial T}{\partial x}$$

$$\frac{1}{Pr}\nabla^2 T = \frac{\partial T}{\partial t} + u\frac{\partial T}{\partial x} + v\frac{\partial T}{\partial y}$$

$$\left(1 + \frac{K}{2}\right)\nabla^2 \bar{N} = \frac{\partial \bar{N}}{\partial t} + u\frac{\partial \bar{N}}{\partial x} + v\frac{\partial \bar{N}}{\partial y} + 2K\bar{N} - K\omega$$

where $(x, y) \in \Omega \subset R^2$, $t > 0$. K is the material parameter, p is the pressure of the fluid and $\bar{N}$ is the component of the microrotation vector normal to the xy-plane.

The equations in (3.57) are supplied with the initial conditions

$$\omega(x, y, 0) = \omega_0(x, y) \quad , \quad T(x, y, 0) = T_0(x, y) \quad , \quad \bar{N}(x, y, 0) = \bar{N}_0(x, y)$$

where $\omega_0(x, y)$, $T_0(x, y)$, $\bar{N}_0(x, y)$ are known functions, and Dirichlet or Neumann type boundary conditions

$$\psi(x_s, y_s) = f_{\psi_s} \quad , \quad \omega(x_s, y_s) = f_{w_s}$$

$$T(x_s, y_s) = f_{t_s} \quad \text{or} \quad \frac{\partial T}{\partial n}(x_s, y_s) = f_{t_n}$$

$$\bar{N}(x_s, y_s) = \bar{n}\frac{\partial v}{\partial x} \quad \text{or} \quad \bar{N}(x_s, y_s) = -\bar{n}\frac{\partial u}{\partial y}$$

where $\bar{n}$ is a constant ($0 \leq \bar{n} \leq 1$). The case $\bar{n} = 0$ indicates $\bar{N} = 0$ on the boundary, which means that the microelements close to wall surface are unable to rotate. The case $\bar{n} = 1/2$ indicates the vanishing of anti-symmetric part of the stress tensor and denotes weak concentration. The case $\bar{n} = 1$ is used for modeling of turbulent boundary layer flows [9].

Application of the DRBEM to the equations in (3.57) gives

$$\mathbf{Hu} - \mathbf{Gu_q} = (\mathbf{H\hat{U}} - \mathbf{G\hat{Q}})\mathbf{F}^{-1}\left(-\frac{\partial\omega}{\partial y}\right)$$

$$\mathbf{Hv} - \mathbf{Gv_q} = (\mathbf{H\hat{U}} - \mathbf{G\hat{Q}})\mathbf{F}^{-1}\left(\frac{\partial\omega}{\partial x}\right)$$

$$\mathbf{H\psi} - \mathbf{G\psi_q} = (\mathbf{H\hat{U}} - \mathbf{G\hat{Q}})\mathbf{F}^{-1}(-\omega)$$

$$\mathbf{Hp} - \mathbf{Gp_q} = (\mathbf{H\hat{U}} - \mathbf{G\hat{Q}})\mathbf{F}^{-1}\left[\frac{Ra}{Pr}\frac{\partial\mathbf{T}}{\partial y} - \left(\frac{\partial\mathbf{u}}{\partial x}\right)^2 - \left(\frac{\partial\mathbf{v}}{\partial y}\right)^2 - 2\frac{\partial\mathbf{v}}{\partial x}\frac{\partial\mathbf{u}}{\partial y}\right]$$

$$(1 + K)(\mathbf{H\omega} - \mathbf{G\omega_q}) = (\mathbf{H\hat{U}} - \mathbf{G\hat{Q}})\mathbf{F}^{-1}\left[\frac{\partial\omega}{\partial t} + \left(\mathbf{u}\frac{\partial\mathbf{F}}{\partial x}\mathbf{F}^{-1} + \mathbf{v}\frac{\partial\mathbf{F}}{\partial y}\mathbf{F}^{-1}\right)\omega + K\nabla^2\bar{N} - \frac{Ra}{Pr}\frac{\partial\mathbf{T}}{\partial x}\right]$$

$$\frac{1}{Pr}(\mathbf{HT} - \mathbf{GT_q}) = (\mathbf{H\hat{U}} - \mathbf{G\hat{Q}})\mathbf{F}^{-1}\left[\frac{\partial\mathbf{T}}{\partial t} + \left(\mathbf{u}\frac{\partial\mathbf{F}}{\partial x}\mathbf{F}^{-1} + \mathbf{v}\frac{\partial\mathbf{F}}{\partial y}\mathbf{F}^{-1}\right)\mathbf{T}\right]$$

$$\left(1 + \frac{K}{2}\right)(\mathbf{H\bar{N}} - \mathbf{G\bar{N}_q}) = (\mathbf{H\hat{U}} - \mathbf{G\hat{Q}})\mathbf{F}^{-1}\left[\frac{\partial\bar{N}}{\partial t} + \left(\mathbf{u}\frac{\partial\mathbf{F}}{\partial x}\mathbf{F}^{-1} + v\frac{\partial\mathbf{F}}{\partial y}\mathbf{F}^{-1}\right)\bar{N} + 2K\bar{N} - K\omega\right].$$

$$(3.58)$$

In these equations the product of the vectors are handled by forming diagonal matrices with the first vectors of the products.

Derivatives of the vectors $\mathbf{u}$, $\mathbf{v}$, ω, $\mathbf{T}$ and $\bar{N}$ are approximated by the DRBEM idea [65]

$$\frac{\partial \mathbf{u}}{\partial x} = \frac{\partial \mathbf{F}}{\partial x}\mathbf{F}^{-1}\,\mathbf{u}\,, \quad \frac{\partial \mathbf{u}}{\partial y} = \frac{\partial \mathbf{F}}{\partial y}\mathbf{F}^{-1}\,\mathbf{u}\,, \quad \frac{\partial \mathbf{v}}{\partial x} = \frac{\partial \mathbf{F}}{\partial x}\mathbf{F}^{-1}\,\mathbf{v}\,, \quad \frac{\partial \mathbf{v}}{\partial y} = \frac{\partial \mathbf{F}}{\partial y}\mathbf{F}^{-1}\,\mathbf{v}$$

$$\frac{\partial \omega}{\partial x} = \frac{\partial \mathbf{F}}{\partial x}\mathbf{F}^{-1}\,\omega\,, \quad \frac{\partial \omega}{\partial y} = \frac{\partial \mathbf{F}}{\partial y}\mathbf{F}^{-1}\,\omega\,, \quad \frac{\partial \mathbf{T}}{\partial x} = \frac{\partial \mathbf{F}}{\partial x}\mathbf{F}^{-1}\,\mathbf{T}\,, \quad \frac{\partial \mathbf{T}}{\partial y} = \frac{\partial \mathbf{F}}{\partial y}\mathbf{F}^{-1}\,\mathbf{T} \qquad (3.59)$$

$$\frac{\partial \bar{N}}{\partial x} = \frac{\partial \mathbf{F}}{\partial x}\mathbf{F}^{-1}\,\bar{N}\,, \quad \frac{\partial \bar{N}}{\partial y} = \frac{\partial \mathbf{F}}{\partial y}\mathbf{F}^{-1}\,\bar{N}\,, \quad \frac{\partial^2 \bar{N}}{\partial x^2} = \frac{\partial^2 \mathbf{F}}{\partial x^2}\mathbf{F}^{-1}\,\bar{N}\,, \quad \frac{\partial^2 \bar{N}}{\partial y^2} = \frac{\partial^2 \mathbf{F}}{\partial y^2}\mathbf{F}^{-1}\,\bar{N}\,.$$

Substituting convection terms back into equation (3.58), and finally rearranging, we end up with the following linear system of equations for $\mathbf{u}$, $\mathbf{v}$, ψ and $\mathbf{p}$, and systems of ordinary differential equations for ω, $\mathbf{T}$ and $\bar{N}$

$$\mathbf{Hu} - \mathbf{Gu_q} = \tilde{m}$$

$$\mathbf{Hv} - \mathbf{Gv_q} = \tilde{n}$$

$$\mathbf{H}\psi - \mathbf{G}\psi_q = \tilde{b}$$

$$\mathbf{Hp} - \mathbf{Gp_q} = \mathbf{a} \qquad (3.60)$$

$$-\mathbf{S}\frac{\partial\,\omega}{\partial\,t} + \tilde{H}_\omega\omega - \tilde{G}_\omega\omega_q = \mathbf{d}$$

$$-\mathbf{S}\frac{\partial\,\mathbf{T}}{\partial\,t} + \tilde{H}_t\mathbf{T} - \tilde{G}_t\mathbf{T}_q = \mathbf{0}$$

$$-\mathbf{S}\frac{\partial\,\bar{N}}{\partial\,t} + \tilde{H}_n\bar{N} - \tilde{G}_n\bar{N}_q = \tilde{d}$$

where the matrices $\mathbf{S}$, $\tilde{H}_\omega$, $\tilde{G}_\omega$, $\tilde{H}_t$, $\tilde{G}_t$, $\tilde{H}_n$, $\tilde{G}_n$, $\mathbf{D}$, and the vectors $\mathbf{d}$, $\tilde{d}$, $\mathbf{a}$, $\tilde{m}$, $\tilde{n}$, $\tilde{b}$ are given

as

$$\mathbf{S} = (\mathbf{H}\hat{\mathbf{U}} - \mathbf{G}\hat{\mathbf{Q}})\mathbf{F}^{-1} \quad , \quad \tilde{\mathbf{H}}_\omega = (1+K)\mathbf{H} - \mathbf{D} \quad , \quad \tilde{\mathbf{G}}_\omega = (1+K)\mathbf{G}$$

$$\tilde{\mathbf{H}}_t = \frac{1}{Pr}\mathbf{H} - \mathbf{D} \quad , \quad \tilde{\mathbf{G}}_t = \frac{1}{Pr}\mathbf{G} \quad , \quad \tilde{\mathbf{H}}_n = \left(1 + \frac{K}{2}\right)\mathbf{H} - \mathbf{D} - \mathbf{S}\,2K\,\mathbf{I} \quad , \quad \tilde{\mathbf{G}}_n = \left(1 + \frac{K}{2}\right)\mathbf{G}$$

$$\mathbf{D} = \mathbf{S}\left(\mathbf{u}\,\frac{\partial \mathbf{F}}{\partial x}\mathbf{F}^{-1} + \mathbf{v}\,\frac{\partial \mathbf{F}}{\partial y}\mathbf{F}^{-1}\right) \quad , \quad \mathbf{d} = \mathbf{S}\left[K\left(\frac{\partial^2 \mathbf{F}}{\partial x^2}\mathbf{F}^{-1} + \frac{\partial^2 \mathbf{F}}{\partial y^2}\mathbf{F}^{-1}\right)\bar{N} - \frac{Ra}{Pr}\frac{\partial \mathbf{T}}{\partial x}\right]$$

$$\tilde{d} = -\mathbf{S}(K\,\omega) \quad , \quad \mathbf{a} = \mathbf{S}\left[\frac{Ra}{Pr}\frac{\partial \mathbf{T}}{\partial y} - \left(\frac{\partial \mathbf{u}}{\partial x}\right)^2 - \left(\frac{\partial \mathbf{v}}{\partial y}\right)^2 - 2\frac{\partial \mathbf{v}}{\partial x}\frac{\partial \mathbf{u}}{\partial y}\right]$$

$$\tilde{m} = -\mathbf{S}\frac{\partial \omega}{\partial y} \quad , \quad \tilde{n} = \mathbf{S}\frac{\partial \omega}{\partial x} \quad , \quad \tilde{b} = -\mathbf{S}\omega$$

and $\mathbf{I}$ is the identity matrix.

For the vorticity transport, energy and microrotation equations, the time derivative is discretized by central difference scheme with relaxation parameters as follows

$$-\mathbf{S}\frac{\omega^{m+1} - \omega^{m-1}}{2\Delta t} + \tilde{\mathbf{H}}_\omega((1 - \beta_\omega)\omega^{m-1} + \beta_\omega \omega^{m+1}) - \tilde{\mathbf{G}}_\omega((1 - \beta_{\omega_q})\omega_q^{m-1} + \beta_{\omega_q}\omega_q^{m+1}) = \mathbf{d}^{m+1}$$

$$-\mathbf{S}\frac{T^{m+1} - T^{m-1}}{2\Delta t} + \tilde{\mathbf{H}}_t((1 - \beta_t)T^{m-1} + \beta_t T^{m+1}) - \tilde{\mathbf{G}}_t((1 - \beta_{t_q})T_q^{m-1} + \beta_{t_q}T_q^{m+1}) = \mathbf{0}$$

$$-\mathbf{S}\frac{\bar{N}^{m+1} - \bar{N}^{m-1}}{2\Delta t} + \tilde{\mathbf{H}}_n((1 - \beta_n)\bar{N}^{m-1} + \beta_n \bar{N}^{m+1}) - \tilde{\mathbf{G}}_n((1 - \beta_{n_q})\bar{N}_q^{m-1} + \beta_{n_q}\bar{N}_q^{m+1}) = \tilde{d}^{m+1} .$$

$$(3.61)$$

Equation (3.61) can be arranged such that the right-hand sides are at time $(m-1)\Delta t$ and known, since they involve values which have been specified as initial condition or calculated previously. And left-hand sides are at time $(m+1)$

$$\left(\frac{-\mathbf{S}}{2\Delta t} + \beta_\omega \tilde{\mathbf{H}}_\omega\right)\omega^{m+1} - \beta_{\omega_q}\tilde{\mathbf{G}}_\omega \omega_q^{m+1} = \left(\frac{-\mathbf{S}}{2\Delta t} - (1 - \beta_\omega)\tilde{\mathbf{H}}_\omega\right)\omega^{m-1} + (1 - \beta_{\omega_q})\tilde{\mathbf{G}}_\omega \omega_q^{m-1} + \mathbf{d}^{m+1}$$

$$\left(\frac{-\mathbf{S}}{2\Delta t} + \beta_t \tilde{\mathbf{H}}_t\right)T^{m+1} - \beta_{t_q}\tilde{\mathbf{G}}_t T_q^{m+1} = \left(\frac{-\mathbf{S}}{2\Delta t} - (1 - \beta_t)\tilde{\mathbf{H}}_t\right)T^{m-1} + (1 - \beta_{t_q})\tilde{\mathbf{G}}_t T_q^{m-1}$$

$$\left(\frac{-\mathbf{S}}{2\Delta t} + \beta_n \tilde{\mathbf{H}}_n\right)\bar{N}^{m+1} - \beta_{n_q}\tilde{\mathbf{G}}_n \bar{N}_q^{m+1} = \left(\frac{-\mathbf{S}}{2\Delta t} - (1 - \beta_n)\tilde{\mathbf{H}}_n\right)\bar{N}^{m-1} + (1 - \beta_{n_q})\tilde{\mathbf{G}}_n \bar{N}_q^{m-1} + \tilde{d}^{m+1} .$$

$$(3.62)$$

Boundary conditions are inserted to the systems in equation (3.62) by interchanging the negative of corresponding columns and reordering the solution vector in terms of unknowns **u**, **v**, $\boldsymbol{\psi}$, **p**, ω, **T**, $\bar{N}$ and their normal derivatives, respectively. Since the boundary conditions for vorticity are not given explicitly, at this point we first use vorticity definition containing velocity derivatives. The derivatives of velocity components are computed with the help of coordinate matrix **F** which enables us to use all the interior velocity vectors. Therefore, on each system of equations in (3.62) there are only $N + L$ unknowns. Once all unknowns are passed to the left-hand side one can write the equation (3.62) as

$$\mathbf{A_1 x_1 = y_1}$$

$$\mathbf{A_2 x_2 = y_2} \tag{3.63}$$

$$\mathbf{A_3 x_3 = y_3}$$

where $\mathbf{x_1}$, $\mathbf{x_2}$ and $\mathbf{x_3}$ are the vectors of unknown boundary values of ω, ω_q, T, T_q and $\bar{N}$, $\bar{N}_q$, respectively. The vectors $\mathbf{y_1}$, $\mathbf{y_2}$ and $\mathbf{y_3}$ are the right-hand sides in each equation (3.63) which contain known values of ω, T and $\bar{N}$. We also have systems of linear equations for **u**, **v**, $\boldsymbol{\psi}$ and **p** obtained from equation (3.60). All these linear systems are going to be solved for the unknown vectors **u**, **v**, $\boldsymbol{\psi}$, **p**, ω, T and $\bar{N}$ which are of sizes $(N + L) \times 1$.

The iteration process is as follows

1) Start with the initial approximations for ω^{m-1}, ω^m, T^{m-1}, T^m and $\bar{N}^{m-1}$, $\bar{N}^m$ with $m = 1$.

2) Solve the stream function and velocity equations to obtain ψ^{m+1}, u^{m+1} and v^{m+1} using ω^{m-1}.

3) Solve the pressure equation to obtain p^{m+1} using the derivative of T^{m-1} with respect to x, and the derivatives of u^{m+1} and v^{m+1} with respect to x and y.

4) Solve the energy equation to obtain T^{m+1} using T^{m-1}.

5) Approximate the derivatives of stream function ψ^{m+1}, temperature T^{m+1}, and $\bar{N}^{m-1}$ with respect to x and y by using DRBEM idea.

6) Obtain the vorticity boundary conditions from the Taylor series expansion of stream function or from its definition using ψ^{m+1}.

7) Solve the vorticity equation to obtain ω^{m+1} using ω^{m-1}, and using the derivatives of stream function ψ^{m+1}, the temperature gradient T^{m+1} and the microrotation $\bar{N}^{m-1}$.

8) Solve the microrotation equation to obtain $\bar{N}^{m+1}$ using $\bar{N}^{m-1}$, and using vorticity ω^{m+1}.

9) Relax ω^{m+1} with ω^m to obtain new ω^{m+1}.

10) Relax T^{m+1} with T^m to obtain new T^{m+1}.

11) Relax $\bar{N}^{m+1}$ with $\bar{N}^m$ to obtain new $\bar{N}^{m+1}$.

12) Check the convergence criteria to terminate the procedure using the L_∞ norm of ψ, ω, T and $\bar{N}$ as

$$\max_i |\psi^{m+1} - \psi^m| \leq \varepsilon$$

$$\max_i |\omega^{m+1} - \omega^m| \leq \varepsilon$$

$$\max_i |T^{m+1} - T^m| \leq \varepsilon$$

$$\max_i |\bar{N}^{m+1} - \bar{N}^m| \leq \varepsilon$$

where $i = 1, ..., N + L$ and maxima is taken over all the nodes inside the fluid flow region, and ε is a pre-assigned tolerance.

13) Repeat the steps $2 - 12$ for $m = 2, 3, ...$ until the convergence criteria in step 12 is met.

In this iterative scheme also the m-th level values are used to compute the matrices $\tilde{H}_\omega$, $\tilde{H}_t$ and $\tilde{H}_n$ which contain convection term matrix $\mathbf{D}$. Thus, the iteration makes use of both m-th and $(m-1)$-th level values for computing 'm+1' iteration.

3.5.1 Natural Convection Flow of Micropolar Fluids in a Square Enclosure

The natural convection flow in a square cavity filled with a micropolar fluid [9, 10] is considered as a first example. The horizontal walls are adiabatic, while the vertical walls are isothermally heated.

The initial and boundary conditions are

$$\omega(x, y, 0) = 0, \quad T(x, y, 0) = 0, \quad \bar{N}(x, y, 0) = 0$$

$$x = 0: \quad u = v = 0 \quad , \quad T = 0.5 \quad , \quad \bar{N} = 0$$

$$x = 1: \quad u = v = 0 \quad , \quad T = -0.5 \quad , \quad \bar{N} = 0$$

$$y = 0, 1: \quad u = v = 0 \quad , \quad \frac{\partial T}{\partial y} = 0 \quad , \quad \bar{N} = 0.$$

The heat transfer coefficient in terms of the local Nusselt number, Nu, and the average Nusselt number, Nu_{av} at the vertical walls are defined by

$$Nu = -\left(\frac{\partial T}{\partial x}\right)_{x=0,1} \quad , \quad Nu_{av} = -\int_0^1 Nu\, dy.$$

The discretization is performed by using linear boundary elements and the radial basis function f is taken as $f = 1 + r + r^2$. The computations are carried out until steady-state conditions are reached. The convergence criteria used in the time loop to achieve steady-state conditions for ω is $\max_{i=1,N+L} |\omega^{m+1} - \omega^m| \leq 10^{-7}$. The same condition is also used for T and $\bar{N}$. Solutions are obtained by using 68, 88 and 96 boundary elements for $Ra = 10^3$, 10^4 and 10^5 with the time increments $\Delta t = 0.1$, 0.01 and 0.003, respectively. The material parameter K is taken as 0, 0.5, 1 and 2 and Prandtl number is $Pr = 0.71$.

Figures (3.54), (3.55) and (3.56) represent the increasing effect of the material parameter and the Rayleigh number on the streamlines, isotherms and vorticity contours for $Ra = 10^3, 10^4$ and 10^5, respectively. It is observed that an increase in Rayleigh number results in intensified circulation inside the cavity, and thinner thermal boundary layers for all the variables, streamlines, isotherms and vorticity contours near the heated and cooled walls. For $Ra = 10^3$ the vortex at the center for the streamlines was in circular pattern. With the increase in Rayleigh

Table 3.3: The average Nusselt number Nu_{av} for different values of Ra

K	$Ra = 10^3$	$Ra = 10^4$	$Ra = 10^5$
0	1.119	2.223	4.414
0.5	1.051	1.962	3.935
1	1.039	1.782	3.691
2	1.011	1.553	3.336

number the vortex changes its shape to elliptical form. Since the viscous forces are dominating when $Ra = 10^3$, diffusion is more effective than the convection within the cavity. The isotherms are almost vertical in this case. As the Rayleigh number increases, the isotherms undergo an inversion at the central region of the cavity. These behaviours are also observed in [9]. Figures (3.57) and (3.58) show flow vectors and pressure contours for $Ra = 10^3$ and $Ra = 10^5$.

Figure (3.59) represent the effect of the material parameter on the velocity components at the mid-plane of the cavity for $Ra = 10^3$ and 10^4. One can see that an increase in the material parameter decreases the relative amplitude of the velocity.

The comparison of the effect of varying Ra on the average Nusselt number at the heated wall for several values of K is given in Table 3.3. The results are in good agreement with the results given in [9]. One can see that for a fixed value of Ra, increasing material parameter (K) decreases the heat transfer (average Nusselt number). The total viscosity of the fluid increases due to the increase in the material parameter, and decreases the heat transfer. Further, the average Nusselt number of Newtonian fluids are found to be greater than that of non-Newtonian fluids.

The dual reciprocity boundary element method is used to give the solution of natural convection flow for fluids with microstructure. In this case an additional microrotation equation is solved which is of the same type of vorticity equation. It contains vorticity and microrotation also on the right hand side. But, DRBEM is capable of handling all these terms as nonhomogeneties. Solutions are obtained for various values of material parameter which plays the role of diffusion constant in the microrotation equation.
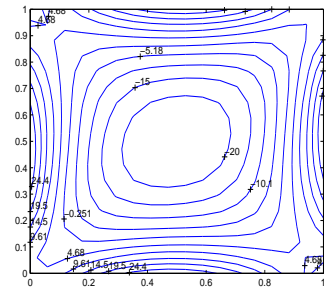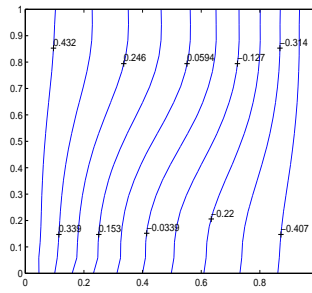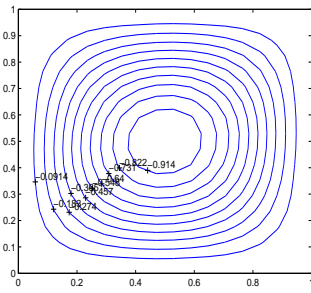
$K = 0.5$
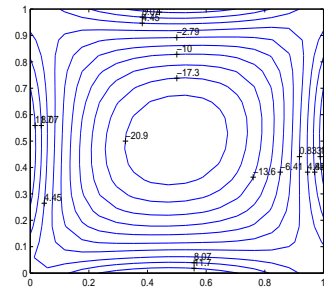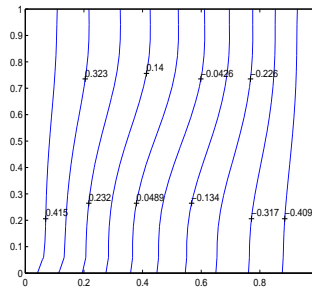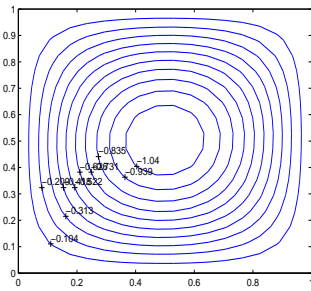
$K = 1$
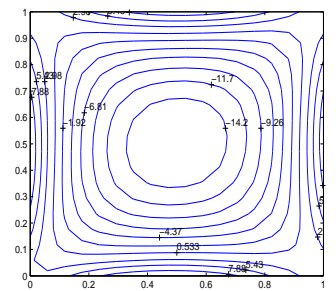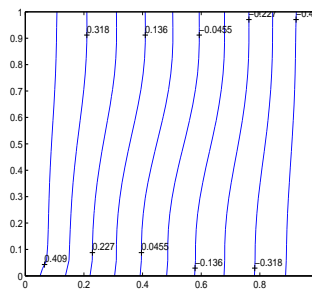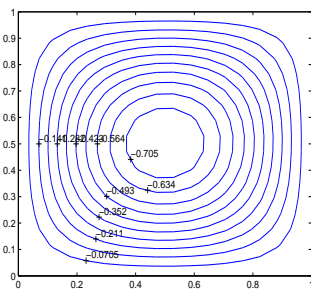
$K = 2$

Figure 3.54: Streamlines, isotherms and vorticity contours for $Ra = 10^3$.
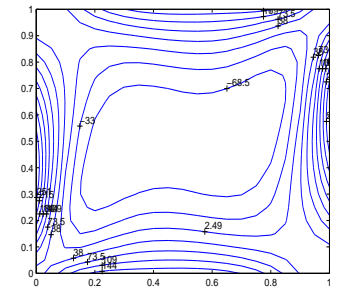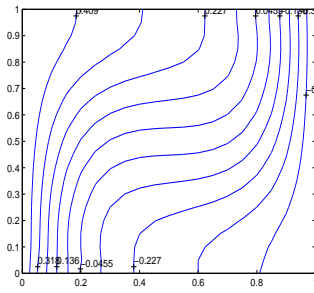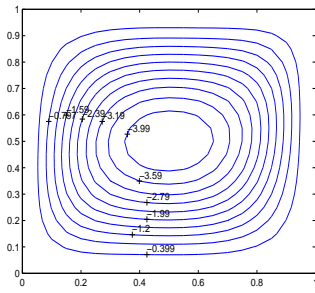
$$K = 0.5$$
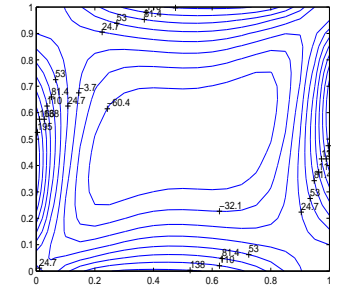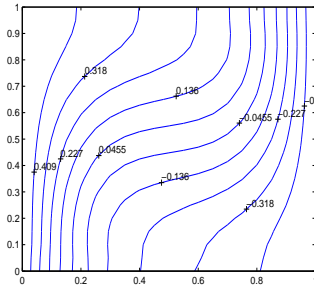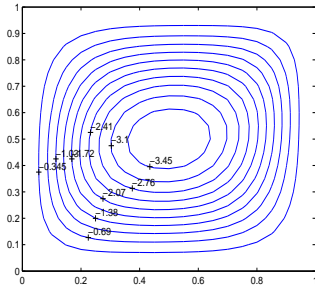
$$K = 1$$
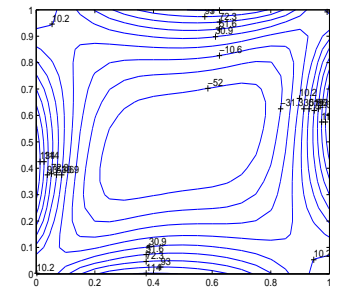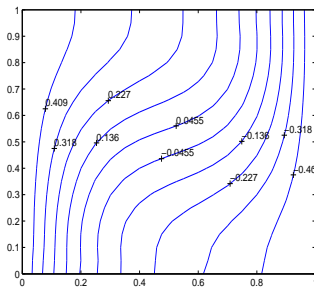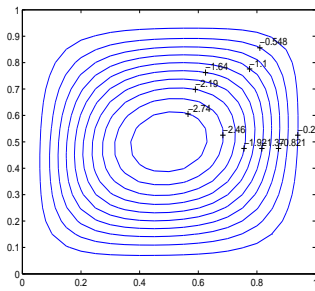
$$K = 2$$

Figure 3.55: Streamlines, isotherms and vorticity contours for $Ra = 10^4$.
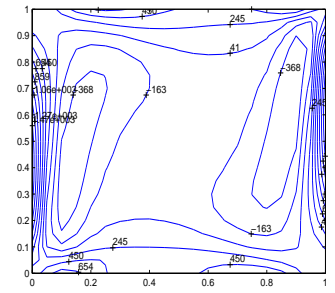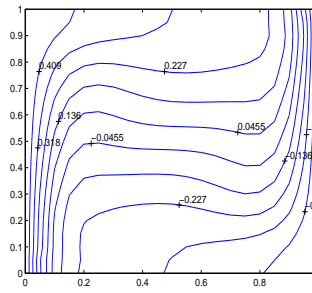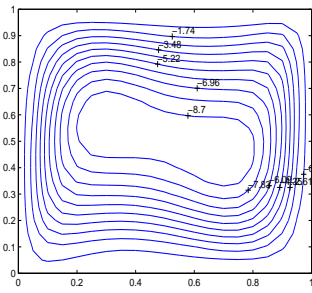
$K = 0.5$
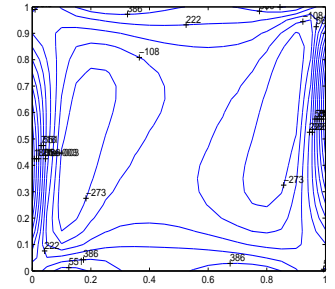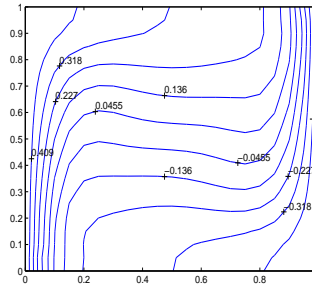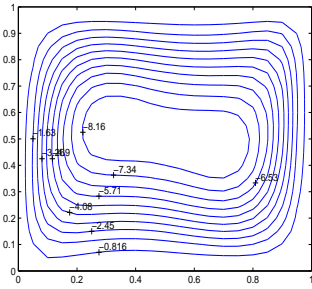
$K = 1$
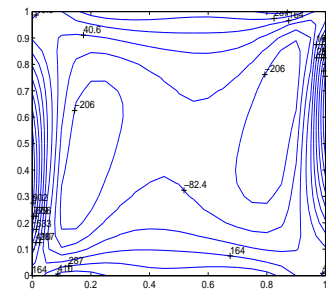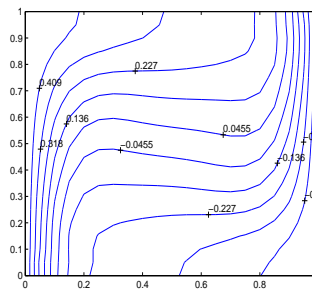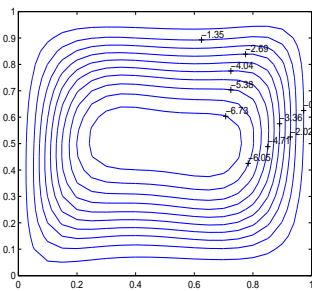
$K = 2$

Figure 3.56: Streamlines, isotherms and vorticity contours for $Ra = 10^5$.
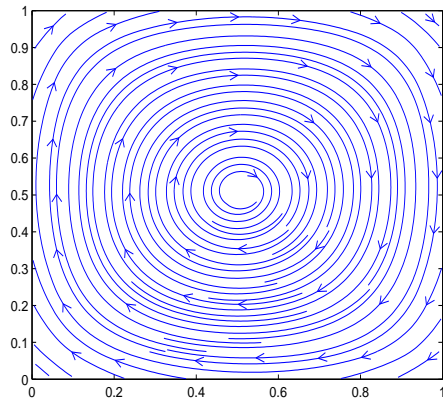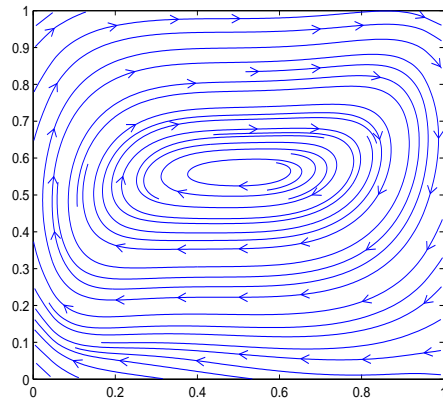
$Ra = 10^3$ $Ra = 10^5$

Figure 3.57: Flow vectors for $Ra = 10^3$ and 10^5, $K = 2$
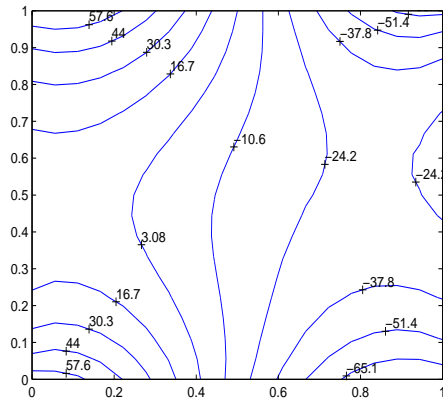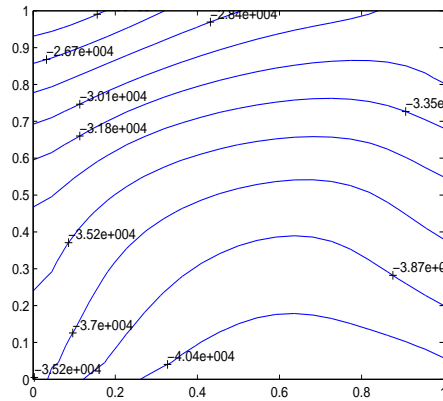
$Ra = 10^3$ $Ra = 10^5$

Figure 3.58: Pressure contours for $Ra = 10^3$ and 10^5, $K = 2$
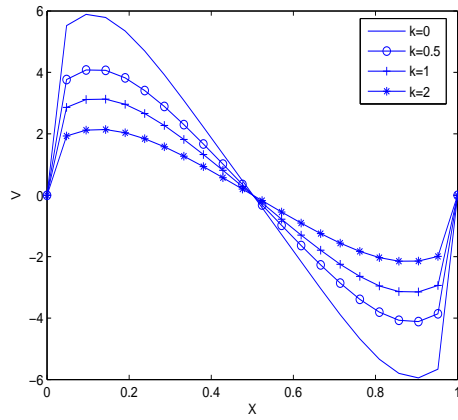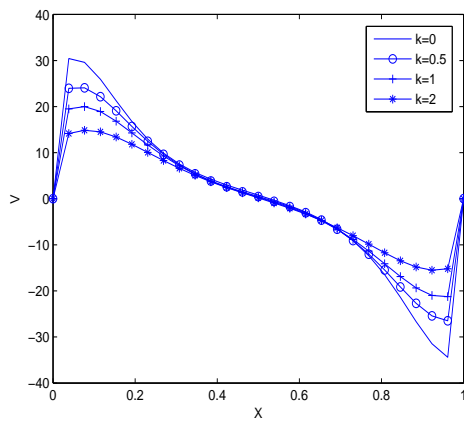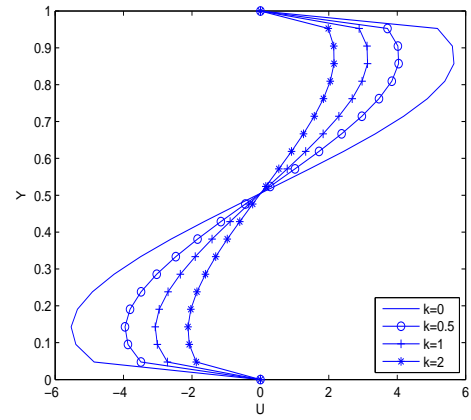
$Ra = 10^3$

$Ra = 10^4$
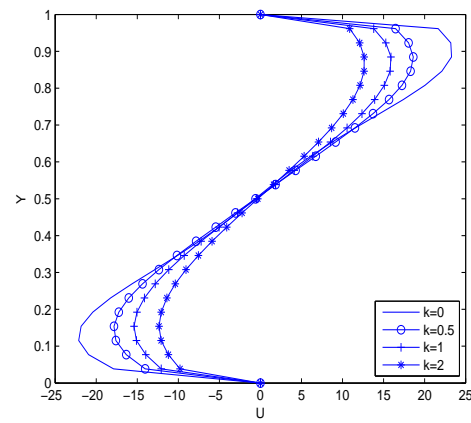
Figure 3.59: Vertical and horizontal velocity profiles along the centerline for $Ra = 10^3$ and $Ra = 10^4$

3.5.2 Natural Convection Flow of Micropolar Fluids in a Rectangular Enclosure

The second example considers the natural convective flow of micropolar fluids in a rectangular enclosure [41] heated from below and cooled from above. The vertical walls are adiabatic.

The initial and boundary conditions are

$$\omega(x,y,0) = 0 \quad , \quad T(x,y,0) = 0 \quad , \quad \bar{N}(x,y,0) = 0$$

$$x = 0, A: \quad u = v = 0 \quad , \quad \frac{\partial T}{\partial x} = 0 \quad , \bar{N} = \frac{1}{2}\frac{\partial v}{\partial x}$$

$$y = 0: \quad u = v = 0 \quad , \quad T = 1 \quad , \quad \bar{N} = -\frac{1}{2}\frac{\partial u}{\partial y}$$

$$y = 1: \quad u = v = 0 \quad , \quad T = 0 \quad , \quad \bar{N} = -\frac{1}{2}\frac{\partial u}{\partial y}.$$

The local Nusselt number, Nu, and the average Nusselt number, Nu_{av} are defined as

$$Nu = -\left(\frac{\partial T}{\partial y}\right)_{y=0,1} \quad , \quad Nu_{av} = -\frac{1}{A}\int_0^A Nu\, dx.$$

The problem is solved for $Ra = 10^4$ with 96 linear boundary elements. Smaller time increment is needed with the increase in the aspect ratio A. $\Delta t = 0.1, 0.01$ and 0.001 are used for $A = 1, 2$ and 4, respectively. The main consideration of solving this problem is to see the effect of increasing the aspect ratio A on streamlines, isotherms, vorticity and microrotation contours.

Figures (3.60), (3.61) and (3.62) show the contours of streamlines, isotherms, vorticity and micropolar, respectively, for $Ra = 10^4$ at $A = 1, 2$ and 4, with $Pr = 7.0$ and $K = 0.5$. It can be seen that an increase in the aspect ratio, A, introduces an increase in the number of convective cells. The isotherms are almost straight near the heated and cooled boundaries and they form boundary layers more pronounced near the heated wall.

The velocity components at the mid-plane of the cavity are shown in Figure (3.63). It is observed that an increase in the material parameter, K, results in a decrease of the relative amplitude of the velocity.
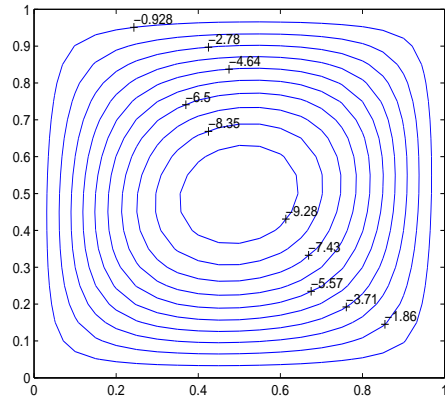
a
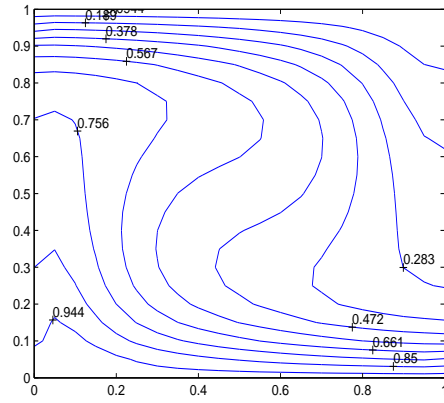
b
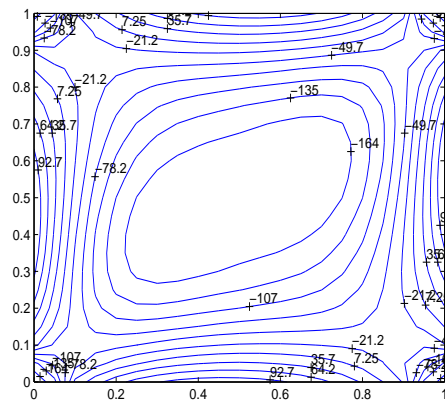
c
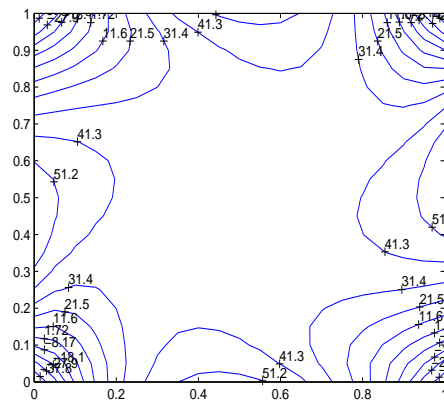
d

Figure 3.60: a. Streamlines, b. Isotherms, c. Vorticity contours, d. Microrotation contours for $Ra = 10^4$, $A = 1$, $K = 0.5$, $Pr = 7.0$, $\Delta t = 0.1$
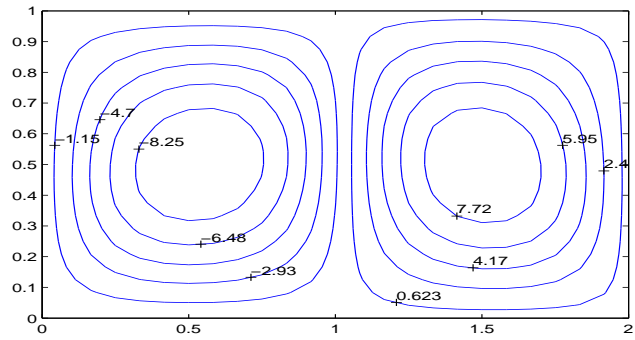
a
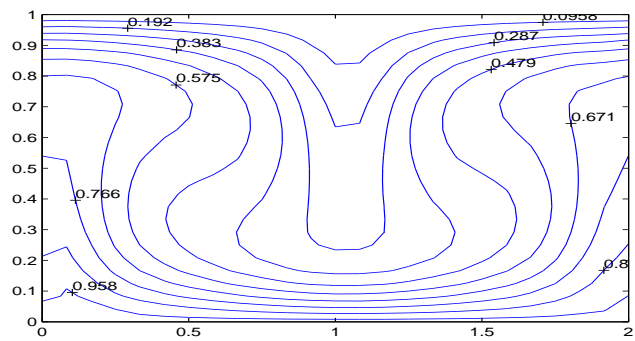
b
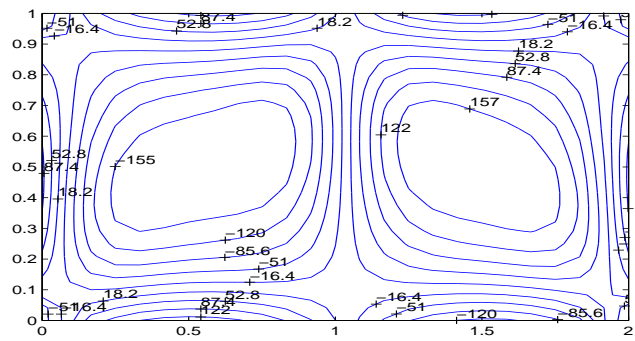
c
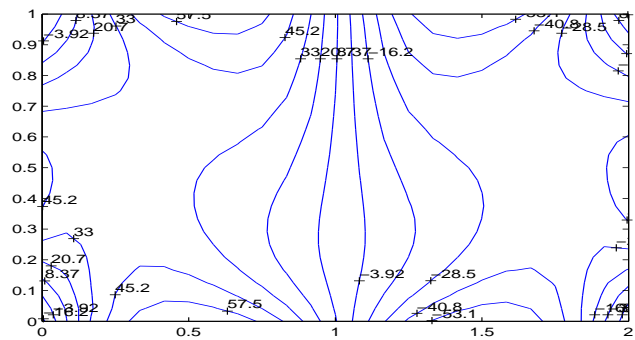
d

Figure 3.61: a. Streamlines, b. Isotherms, c. Vorticity contours, d. Microrotation contours for $Ra = 10^4$, $A = 2$, $K = 0.5$, $Pr = 7.0$, $\Delta t = 0.01$

148
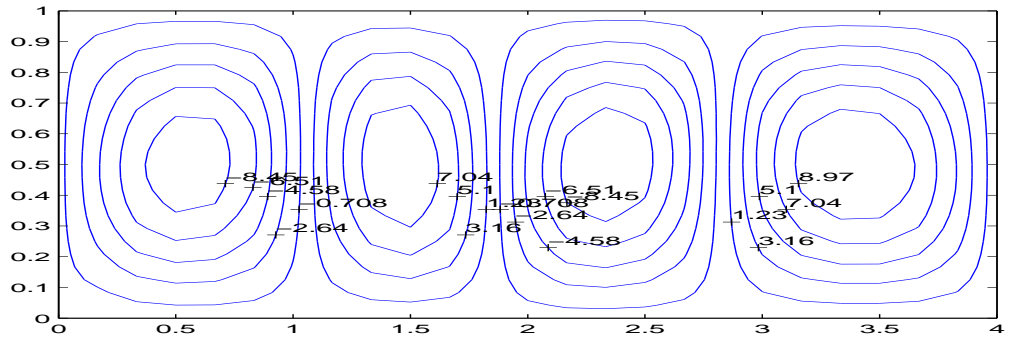
a
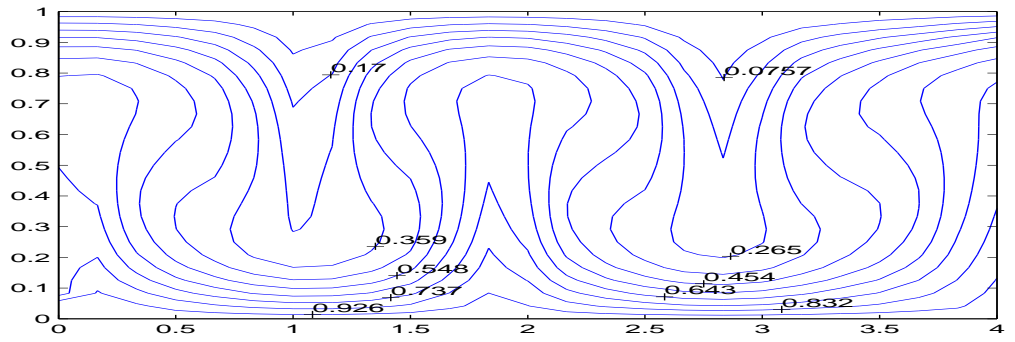
b
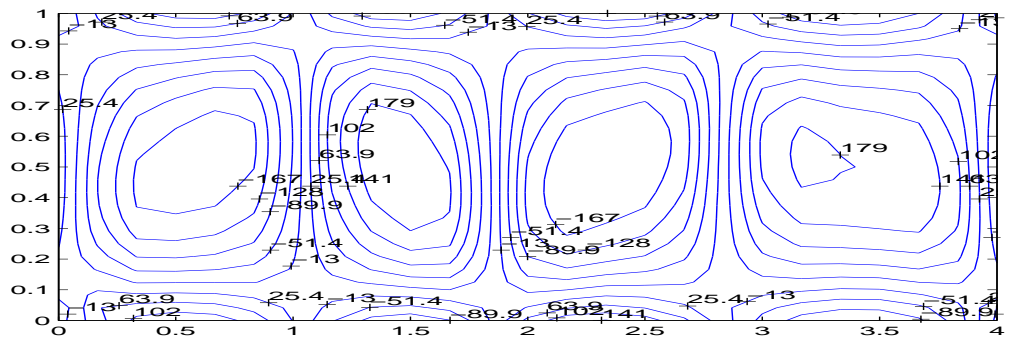
c
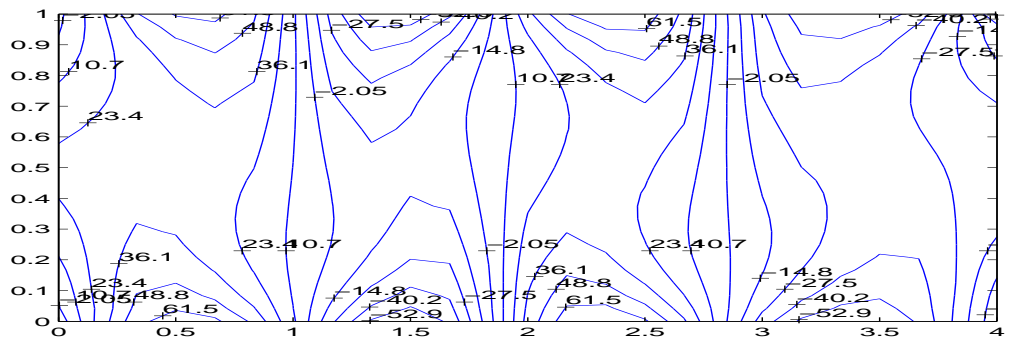
d

Figure 3.62: a. Streamlines, b. Isotherms, c. Vorticity contours, d. Microrotation contours for $Ra = 10^4$, $A = 4$, $K = 0.5$, $Pr = 7.0$, $\Delta t = 0.01$

149
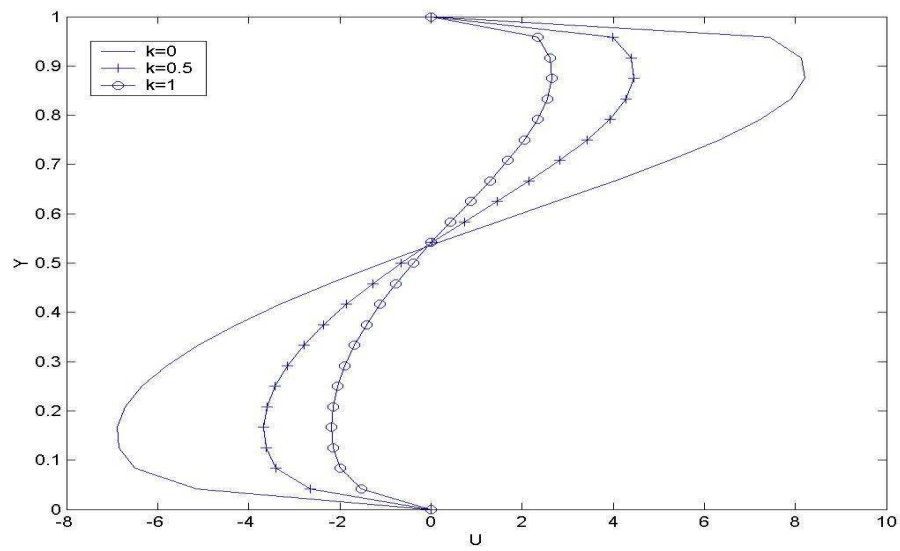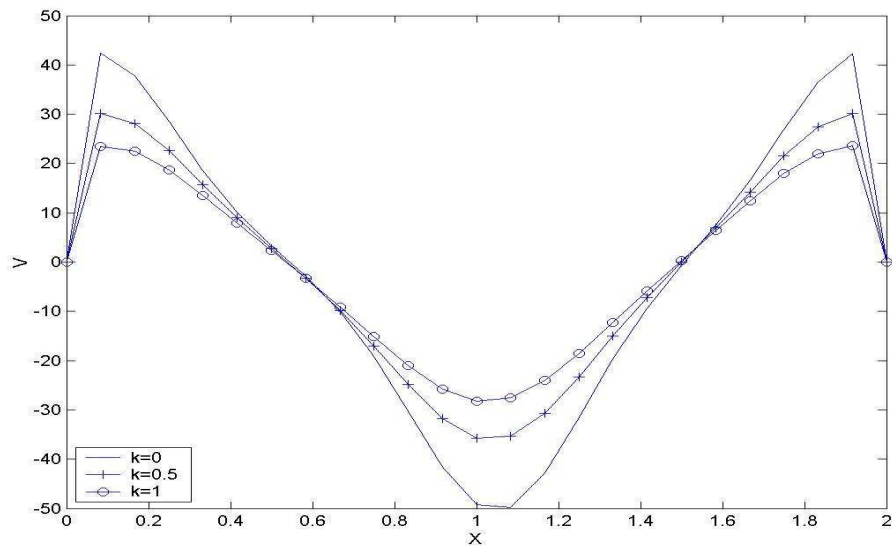
Figure 3.63: Vertical and horizontal velocity profiles along the centerline for $Ra = 10^4$

CHAPTER 4

STABILITY ANALYSIS

In Chapter 3, the DRBEM is employed to solve different types of flows. First, we considered 2-D, transient, laminar, viscous flow described by Navier-Stokes equations and solved three test problems. The physical configurations of the problems are explained and the solutions are shown in terms of streamlines and vorticity contours. While solving these problems the time derivative is discretized using forward and central difference methods, and Runge-Kutta method. Then, the natural and mixed convection flow, and natural convection flow of nanofluids are considered. The application of the method is explained and several test problems are solved for each type of flow. Finally, natural convection flow of micropolar fluids is considered and two test problems are solved. In these computations central difference method with relaxation parameters is used to discretize the time derivative.

In this Chapter, we investigate first the stability analysis of the general initial value problem $\frac{du}{dt} = f(t, u)$, and then extend the investigation for each type of flow considered in Chapter 3. The stability characteristics of this general first order differential equation in time and the transient fluid flow problems considered in this thesis are going to be similar. The reason for this is the situation that DRBEM reduces these flow problems to the systems of first order differential equations in time. The difference lies in the unknown vector which contains both the problem solution and its normal derivative. The stability analysis is modified for the system of initial value problems resulted from the DRBEM application to the fluid flow problems considered in the thesis. This is one of the original contribution obtained in the thesis to the solutions of the flow problems considered. The results will be given in terms of tables discussing the maximum eigenvalues of the coefficient matrices with respect to the variables of the problems such as time increment and relaxation parameters.

4.1 Stability Analysis of System of Initial Value Problems

In this section, we will explain the stability analysis for a system of ordinary differential equations of the form

$$\frac{d\,\mathbf{u}}{d\,t} = \mathbf{f}(t, u)$$

$$\mathbf{u}(t_0) = \mathbf{u}_0$$

(4.1)

where

$$\mathbf{u} = \begin{bmatrix} u_1 \\ u_2 \\ \vdots \\ u_{N+L} \end{bmatrix} \quad, \quad \mathbf{f}(t, \mathbf{u}) = \begin{bmatrix} f_1(t, u_1, .., u_{N+L}) \\ f_2(t, u_1, .., u_{N+L}) \\ \vdots \\ f_{N+L}(t, u_1, .., u_{N+L}) \end{bmatrix} \quad, \quad \mathbf{u}_0 = \begin{bmatrix} u_{1,0} \\ u_{2,0} \\ \vdots \\ u_{N+L,0} \end{bmatrix}.$$

For the stability analysis of a single step method (e.g Euler Method) applied to system (4.1), we consider the equation

$$\frac{d\,\mathbf{u}}{d\,t} = \mathbf{A}\,\mathbf{u}$$

(4.2)

where $\mathbf{A}$ is the Jacobian matrix defined by $\mathbf{A} = \dfrac{\partial\,f_i(t, u)}{\partial\,u_j}$, since the stability characteristics are the same for equations (4.1) and (4.2).

The matrix $\mathbf{A}$ is generally a variable depending on $\mathbf{u}$ and t. In order to guess the behaviour of the solution of equation (4.2) we consider the simple case of the matrix $\mathbf{A}$. If we assume that $\mathbf{A}$ is a constant matrix with distinct eigenvalues, then the analytic solution $\mathbf{u}(t)$ of equation (4.2) satisfying the initial conditions is given by [44]

$$\mathbf{u}(t) = e^{(\mathbf{A}\,t)}\,\mathbf{u}_0.$$

(4.3)

Here $e^{(\mathbf{A}\,t)}$ is defined as a matrix function

$$e^{(\mathbf{A}\,t)} = \mathbf{I} + \mathbf{A}\,t + \frac{(\mathbf{A}\,t)^2}{2!} + +\frac{(\mathbf{A}\,t)^3}{3!} + ...$$

where $\mathbf{I}$ is the identity matrix.

We assume that $\mathbf{A}$ is diagonalizable, so that there exsist a matrix $\mathbf{P}$ such that

$$\mathbf{P}^{-1}\mathbf{A}\mathbf{P} = \mathbf{B}$$

152

where $\mathbf{B}$ is diagonal matrix. This transformation also diagonalizes $e^{(\mathbf{A}\,t)}$ as

$$\mathbf{P}^{-1}e^{(\mathbf{A}\,t)}\mathbf{P} = e^{(\mathbf{B}\,t)}$$

in which $\mathbf{B}$ consists of the eigenvalues of the matrix $\mathbf{A}$

$$\mathbf{B} = \begin{bmatrix} \lambda_1 & & & \\ & \lambda_2 & & \\ & & & \\ & & & \lambda_{N+L} \end{bmatrix}.$$

The eigenvalues, λ_j, are assumed to be distinct or possibly complex with negative real parts. Thus, the matrix $e^{(\mathbf{B}\,t)}$ is also diagonal with diagonal elements $e^{(\lambda_j\,t)}$, [44].

Since $\mathbf{P}^{-1}\mathbf{A}\mathbf{P} = \mathbf{B}$, we have $\mathbf{A} = \mathbf{P}\mathbf{B}\mathbf{P}^{-1}$. Thus, equation (4.2) can be written as

$$\frac{d\,\mathbf{u}}{d\,t} = \mathbf{A}\,\mathbf{u} = \mathbf{P}\mathbf{B}\mathbf{P}^{-1}\,\mathbf{u}. \tag{4.4}$$

Multiplying both sides by $\mathbf{P}^{-1}$ gives

$$\mathbf{P}^{-1}\frac{d\,\mathbf{u}}{d\,t} = \mathbf{P}^{-1}\mathbf{A}\,\mathbf{u} = \underbrace{\mathbf{P}^{-1}\mathbf{P}}_{\mathbf{I}}\,\mathbf{B}\mathbf{P}^{-1}\,\mathbf{u}. \tag{4.5}$$

If we let $\mathbf{v} = \mathbf{P}^{-1}\,\mathbf{u}$, then we can express equation (4.5) as

$$\frac{d\,\mathbf{v}}{d\,t} = \mathbf{B}\,\mathbf{v}. \tag{4.6}$$

In a similar way, the analytical solution of equation (4.6) can be written as

$$\mathbf{v} = e^{(\mathbf{B}\,t)}\,\mathbf{v}_0$$

$$\tag{4.7}$$

$$\mathbf{v}_0 = \mathbf{P}^{-1}\mathbf{u}_0.$$

When the single step method is applied to the equations (4.2) and (4.6), the results are related by

$$\mathbf{u}_k = \mathbf{P}\mathbf{v}_k \quad ; \quad k = 0, 1, 2, ..., N + L. \tag{4.8}$$

153

We obtain the numerical values of the function $\mathbf{v}(t)$ at the step points t_m from the function (4.3) with the relation

$$\mathbf{u}_{m+1} = E(\mathbf{A}\Delta t)\mathbf{u}_m. \tag{4.9}$$

The use of the single step method leads to a relation of the form

$$\mathbf{v}_{m+1} = E(\mathbf{B}\Delta t)\mathbf{v}_m \tag{4.10}$$

where the diagonal matrix $E(\mathbf{B}\Delta t)$ and its diagonal elements $E_j(\lambda_j\Delta t)$, $j = 1, 2, ..., N + L$ approximate the matrix $e^{(\mathbf{B}\Delta t)}$ and its diagonal elements $e^{(\lambda_j\Delta t)}$, $j = 1, 2, ..., N + L$, respectively [44]. These are the growing factor matrices obtained from the Taylor series expansions of $e^{(\mathbf{B}\Delta t)}$ and $e^{(\lambda_j\Delta t)}$ by taking p terms for a p-th order single step method. The system (4.10) now differs from (4.9) as being system of uncoupled discretized equations with growing factors $E_j(\lambda_j\Delta t)$. Thus, the stability analysis of the single step method applied to the equation (4.1) can be discussed by applying the method to the scalar equation

$$\frac{du}{dt} = \lambda_j u \tag{4.11}$$

where λ_j, $j = 1, 2, ..., N + L$ are the eigenvalues of the matrix $\mathbf{A}$, therefore of the matrix $\mathbf{B}$ from similarity. Thus, the single step method is absolutely stable [44] if

$$|E_j(\lambda_j\Delta t)| < 1 \quad , \quad j = 1, 2, ..., N + L \tag{4.12}$$

where the real part of each eigenvalue is negative. This conditions comes from the fact that equation (4.10) can be written as $\mathbf{v}_{m+1} = E(\mathbf{B}\Delta t)^m\mathbf{v}_0$ and the eigenvalues of $E(\mathbf{B}\Delta t)^m$ are $E_j(\lambda_j\Delta t)$. Thus, we need to check the condition (4.12) for the eigenvalues of coefficient matrix $\mathbf{A}$ in $\mathbf{u}_{m+1} = E_j(\lambda_j\Delta t)\mathbf{u}_m$.

In the next sections, we will show that the absolute stability condition (the magnitude of the spectral radius is less than one) holds for our system of equations obtained for each type of flow. Since this condition is related to the choice of time steps and relaxation parameters, the stability is maintained with the properly chosen time steps.

4.2 Stability Analysis of the Navier-Stokes equations

In this section, we consider the numerical stability of DRBEM applied to Navier-Stokes equations using an eigenvalue decomposition of the system of ordinary differential matrix equations in time following the reference [69].

Stream function-vorticity formulation of the two-dimensional, laminar, unsteady flow of viscous, incompressible fluid is

$$\nabla^2 \psi = -\omega$$

$$\frac{1}{Re}\nabla^2\omega = \frac{\partial\omega}{\partial t} + u\frac{\partial\omega}{\partial x} + v\frac{\partial\omega}{\partial y} \,.$$

(4.13)

Application of DRBEM to the above equations yields the final matrix formulations (equations (3.11), (3.13))

$$\mathbf{H}\psi - \mathbf{G}\psi_q = \tilde{b}$$

$$-\mathbf{S}\frac{\partial\omega}{\partial t} + \mathbf{H1}\,\omega - \mathbf{G1}\,\omega_q = \mathbf{0} \,.$$

(4.14)

The vorticity transport equation is rewritten as

$$\frac{\partial\omega}{\partial t} = \mathbf{H2}\,\omega - \mathbf{G2}\,\omega_q$$

(4.15)

where $\mathbf{H2} = \mathbf{S}^{-1}\mathbf{H1}$ and $\mathbf{G2} = \mathbf{S}^{-1}\mathbf{G1}$.

Now, the system of first order differential equations (4.15) resulting from DRBEM discretization is rearranged keeping only the unknown values in one vector. These are normal derivative values on the boundary and all interior values. The known information is collected in one vector which does not contribute to the stability analysis. Thus, the stability characteristics of equation (4.15) and (4.2) are going to be similar.

Discretizing the time derivative of the vorticity in equation (4.14) using forward difference scheme with relaxation parameters gives

$$\left(\frac{-\mathbf{S}}{\Delta t} + \beta_\omega\,\mathbf{H1}\right)\omega^{m+1} - \beta_{\omega_q}\,\mathbf{G1}\,\omega_q^{m+1} + \left(\frac{\mathbf{S}}{\Delta t} + (1-\beta_\omega)\mathbf{H1}\right)\omega^m - (1-\beta_{\omega_q})\mathbf{G1}\,\omega_q^m = 0 \,.$$

(4.16)

Similarly, discretizing by central difference scheme gives

$$\left(\frac{-\mathbf{S}}{2\Delta t} + \beta_\omega \mathbf{H1}\right)\omega^{m+1} - \beta_{\omega_q} \mathbf{G1}\, \omega_q^{m+1} + \left(\frac{\mathbf{S}}{2\Delta t} + (1 - \beta_\omega)\mathbf{H1}\right)\omega^{m-1} - (1 - \beta_{\omega_q})\mathbf{G1}\, \omega_q^{m-1} = 0$$

$$(4.17)$$

in which the matrix **H1** is evaluated at the m-th time level as explained in Chapter 2.

When the boundary conditions are imposed to the equations (4.16) or (4.17) the known values of ω and ω_q are transferred from one side to another at both levels [69].

The forward difference discretization (4.16) can be written as

$$\mathbf{K_1}\, x_1^{m+1} + \mathbf{L_1}\, x_1^m = b_1 \qquad (4.18)$$

and the central difference discretization (4.17) gives

$$\mathbf{K_2}\, x_2^{m+1} + \mathbf{L_2}\, x_2^{m-1} = b_2 \qquad (4.19)$$

where $\mathbf{K_1}$, $\mathbf{K_2}$ are the matrices obtained from the shuffling of the rows and columns of the coefficient matrices in (4.16) and (4.17) corresponding to the unknown values and normal derivatives at the $(m + 1)$-th time level. Similarly, $\mathbf{L_1}$, $\mathbf{L_2}$ are the coefficient matrices in (4.16) and (4.17) corresponding to the known values and normal derivatives at the m-th and $(m - 1)$-th time levels. In this case x_1^{m+1} and x_2^{m+1} vectors correspond to the unknown vector, which can be expressed as

$$x^{m+1} = \begin{bmatrix} \omega_{q1} \\ \omega_{q2} \\ \vdots \\ \omega_{qN} \\ \omega_1 \\ \omega_2 \\ \vdots \\ \omega_{N+L} \end{bmatrix}^{m+1}.$$

156

In central difference method the matrix L_2 also contains $x_2{}^m$ values. The right-hand side vectors b_1 and b_2 contain the known values of ω and ω_q at time levels 'm+1', 'm' and 'm+1', 'm-1', respectively.

We can rewrite equations (4.18) and (4.19) as

$$K_1\, x_1{}^{m+1} = b_1 - L_1\, x_1{}^m$$

$$(4.20)$$

$$K_2\, x_2{}^{m+1} = b_2 - L_2\, x_2{}^{m-1}.$$

Although the matrices K_1, K_2, L_1 and L_2 contain the previous time level values, after some time levels the entries do not differ much from iteration to iteration. This is computationally validated. Thus, $K_1{}^{-1}L_1$ and $K_2{}^{-1}L_2$ matrices can be assumed as constant matrices, and the stability characteristics will be similar to the one in the system (4.9) or (4.10).

Thus, the stability analysis of DRBEM yields the conditions [69]

$$\rho\!\left(K_1{}^{-1}\, L_1\right) < 1$$

$$(4.21)$$

$$\rho\!\left(K_2{}^{-1}\, L_2\right) < 1$$

where $\rho\!\left(K_1{}^{-1}\, L_1\right)$ and $\rho\!\left(K_2{}^{-1}\, L_2\right)$ are the largest eigenvalues of the matrices $K_1{}^{-1}\, L_1$ and $K_2{}^{-1}\, L_2$. The matrices $K_1{}^{-1}\, L_1$ and $K_2{}^{-1}\, L_2$ play the role of growing factors in forward difference and central difference methods, respectively. The above condition depends on the choice of Δt and the relaxation parameters.

In order to show that DRBEM gives stable solution, we investigate the numerical stability of the lid-driven cavity flow.

4.2.1 Stability Analysis of Lid-Driven Cavity Flow

We investigate the numerical stability of forward and central difference methods applied to the DRBEM discretized equations for the Navier-Stokes equations with respect to the problem variables. Table 4.1, 4.2, 4.3 and 4.4 show the maximum eigenvalues of the coefficient matrices for the lid-driven cavity flow at steady-state.

In Tables 4.1 and 4.2, maximum eigenvalues obtained from forward and central difference

schemes are presented for several relaxation parameters at $Re = 100$ by fixing $\Delta t = 0.8$. One can observe that there is no significant difference between the time integration methods for small Reynolds number when the same relaxation parameters are used. Both methods become unstable for the choice of $\beta_\omega = \beta_{\omega_q} \leq 0.5$. In Table 4.2, maximum eigenvalues are given for several relaxation parameters again but for $Re = 500$ with $\Delta t = 0.5$, $\varepsilon = 10^{-4}$ and $N = 96$ together with the iteration numbers. We observe that, number of iterations to reach the steady state for forward and central difference methods are nearly the same. The maximum eigenvalues are increasing for decreasing values of relaxation parameters. Since we get smaller eigenvalues for the choice of $\beta_\omega = \beta_{\omega_q} = 0.9$, we continue to the rest of the computations with that value of the relaxation parameters.

Table 4.3 shows the maximum eigenvalues obtained from both methods for different time increments when $Re = 500$, $N = 96$ and convergence criteria is 10^{-4}. We observe that the optimum time increment for $Re = 500$ is $\Delta t = 0.5$. When the time increment decreases it takes large number of iterations to converge to steady-state and the eigenvalues increase. We see that for forward difference method we can use the range $\Delta t = 0.08 - 0.5$ to solve the problem but for central difference method the problem can be solved using the range of time increment $0.05 - 0.5$. It is also disclosed that the eigenvalues for the central difference method are less than that of the forward difference method for all values of Δt.

Table 4.4 presents the maximum eigenvalues of the coefficient matrices obtained from the forward and central difference schemes for $Re = 100$ with $\Delta t = 0.8$, $Re = 400$ and 500 with $\Delta t = 0.5$ and $Re = 1000$ with $\Delta t = 0.1$ when $\beta_\omega = \beta_{\omega_q} = 0.9$. We observed that maximum eigenvalues of the coefficient matrices obtained from both methods are less than one for this range of Reynolds number. So both methods are stable. But, we also observe that the maximum eigenvalues obtained from the central difference scheme are smaller than that of the forward difference scheme for increasing Re. Although the iteration numbers to reach the steady-state are nearly the same, obtaining smaller eigenvalues may help us in the solution of the other problems while increasing Rayleigh number. Thus, we continue with the central difference scheme in the rest of the computations.

The stability analysis developed in the thesis is based on the assumption that the coefficient matrices $K_1^{-1}L_1$, $K_2^{-1}L_2$ do not alter much with respect to time. This is checked for the case $Re = 500$, $\Delta t = 0.5$, $\beta_\omega = \beta_{\omega_q} = 0.9$ at several time levels. We have found that maximum

eigenvalues of these matrices at different time levels match with an accuracy of 10^{-4}. Also, entries of the matrices are the same with an accuracy of 10^{-2} at time levels t_{25}, t_{50} and t_{90}.

Hence, for lid-driven cavity problem when the relaxation parameters $\beta_\omega, \beta_{\omega_q}$ and the time increment Δt are properly taken, we can obtain the stable DRBEM numerical solution of Navier-Stokes equations.

Table 4.1: Maximum eigenvalues, ρ, for forward and central difference schemes, $Re = 100$, $\Delta t = 0.8$, $N = 80$, $\varepsilon = 10^{-6}$

$\beta_\omega, \beta_{\omega_q}$	ρ(forward difference scheme)	ρ(central difference scheme)
0.9	0.11111131	0.11111137
0.8	0.25000038	0.25000038
0.7	0.42857256	0.42857223
0.6	0.66666823	0.66666841
0.5	1.00000250	1.00000083

Table 4.2: Maximum eigenvalues, ρ, for forward and central difference schemes, $Re = 500$, $\Delta t = 0.5$, $N = 96$, $\varepsilon = 10^{-4}$

$\beta_\omega, \beta_{\omega_q}$	Forward Difference Scheme		Central Difference Scheme	
	Iteration Number	ρ	Iteration Number	ρ
0.9	103	0.19442912	107	0.15126532
0.8	104	0.35644817	108	0.30104988
0.7	104	0.56932038	108	0.49563941

Table 4.3: Maximum eigenvalues, ρ, for forward and central difference schemes, $Re = 500$, $\beta_\omega = \beta_{\omega_q} = 0.9$, $N = 96$, $\varepsilon = 10^{-4}$

| | Forward Difference Scheme | | Central Difference Scheme | |
Δt	Iteration Number	ρ	Iteration Number	ρ
0.5	103	0.19442912	107	0.15126532
0.1	333	0.70622009	336	0.34581330
0.08	394	0.97000718	397	0.42084696
0.05	–	–	564	0.70623707

Table 4.4: Maximum eigenvalues, ρ, for forward and central difference schemes, $\beta_\omega = \beta_{\omega_q} = 0.9$ and $\varepsilon = 10^{-6}$

Reynolds number	ρ(forward difference scheme)	ρ(central difference scheme)
100	0.11111131	0.11111137
400	0.11111135	0.11111138
500	0.19443932	0.15125057
1000	0.84439289	0.38676896

4.3 Stability Analysis of Natural Convection Flow

In this section, the stability analysis is extended to the natural convection flow in which an additional equation, namely the energy equation is added to the Navier-Stokes equations.

Governing equations for the natural convection flow in terms of stream function, vorticity and temperature are given as

$$\nabla^2 \psi = -\omega$$

$$Pr\nabla^2 \omega = \frac{\partial \omega}{\partial t} + u\frac{\partial \omega}{\partial x} + v\frac{\partial \omega}{\partial y} - RaPr\frac{\partial T}{\partial x} \tag{4.22}$$

$$\nabla^2 T = \frac{\partial T}{\partial t} + u\frac{\partial T}{\partial x} + v\frac{\partial T}{\partial y}.$$

The DRBEM application to vorticity and energy equations results in the following matrix equations (equation (3.33))

$$\mathbf{H}\psi - \mathbf{G}\psi_q = \tilde{b}$$

$$-\mathbf{S}\frac{\partial \omega}{\partial t} + \mathbf{H}_\omega \omega - \mathbf{G}_\omega \omega_q = \tilde{c} \tag{4.23}$$

$$-\mathbf{S}\frac{\partial T}{\partial t} + \mathbf{H}_t T - \mathbf{G}_t T_q = \mathbf{0}.$$

Discretizing the time derivatives in equation (4.23) using central difference scheme yields equation (3.37)

$$\left(\frac{-\mathbf{S}}{2\Delta t} + \beta_\omega \mathbf{H}_\omega\right)\omega^{m+1} - \beta_{\omega_q}\mathbf{G}_\omega\omega_q^{m+1} + \left[\frac{\mathbf{S}}{2\Delta t} + (1-\beta_\omega)\mathbf{H}_\omega\right]\omega^{m-1} - (1-\beta_{\omega_q})\mathbf{G}_\omega\omega_q^{m-1} = \mathbf{0}$$

$$\left(\frac{-\mathbf{S}}{2\Delta t} + \beta_t \mathbf{H}_t\right)T^{m+1} - \beta_{t_q}\mathbf{G}_t T_q^{m+1} + \left[\frac{\mathbf{S}}{2\Delta t} + (1-\beta_t)\mathbf{H}_t\right]T^{m-1} - (1-\beta_{t_q})\mathbf{G}_t T_q^{m-1} = \mathbf{0}.$$
$$\tag{4.24}$$

Now, we insert boundary conditions for vorticity and temperature at both levels. Once the known values obtained from 'm-1' and 'm+1' levels are passed to the right-hand side we

have

$$K_\omega \, x_\omega^{m+1} + L_\omega \, x_\omega^{m-1} = b_\omega$$

(4.25)

$$K_t \, x_t^{m+1} + L_t \, x_t^{m-1} = b_t \; .$$

Here, K_ω and K_t are the matrices obtained from shuffling of the rows and columns of the coefficient matrices for vorticity and temperature equations in (4.24) corresponding to the unknown values and normal derivatives at the $(m + 1)$-th time level. x_ω^{m+1} and x_t^{m+1} contain the unknown values of ω, ω_q and T, T_q at time level 'm+1'. The right-hand side vectors b_ω and b_t contain the known values of ω, ω_q and T, T_q at both levels. L_ω, L_t matrices contain x_ω^m and x_t^m values, respectively.

We can rewrite equation (4.25) as

$$K_\omega \, x_\omega^{m+1} = b_\omega - L_\omega \, x_\omega^{m-1}$$

(4.26)

$$K_t \, x_t^{m+1} = b_t - L_t \, x_t^{m-1} \; .$$

For the stability analysis of DRBEM we must have [69]

$$\rho\left(K_\omega^{-1} \, L_\omega\right) < 1$$

(4.27)

$$\rho\left(K_t^{-1} \, L_t\right) < 1$$

where $\rho\left(K_\omega^{-1} \, L_\omega\right)$ and $\rho\left(K_t^{-1} \, L_t\right)$ are the largest eigenvalues of the matrices $K_\omega^{-1} \, L_\omega$ and $K_t^{-1} \, L_t$, respectively.

In order to show that DRBEM results are stable, we analyze the natural convection flow with uniformly and non-uniformly heated walls.

4.3.1 Stability Analysis of Natural Convection Flow with Uniformly and Non-Uniformly Heated Walls

In this section, we investigate the numerical stability of the dual reciprocity boundary element method applied to natural convection flow in a square cavity with uniformly and non-uniformly heated walls. The maximum eigenvalues obtained from discretizing the time derivative using central difference method with relaxation parameters $\beta_\omega = \beta_{\omega_q} = 0.9$ are given in terms of tables. The problem is solved for Rayleigh numbers $Ra = 10^3$, 10^4, 10^5 and 10^6 with $\Delta t = 0.1$, 0.01, 0.001 and 0.0005, and $N = 64$, 80, 88 and 96, respectively.

Table 4.5 presents the maximum eigenvalues for vorticity and temperature equations for Rayleigh numbers $10^3 - 10^6$ in uniformly heated case. We observe that maximum eigenvalues of vorticity and temperature increase with an increase in the Rayleigh number. This is because the convection terms become dominant as the Rayleigh number increases and the problem becomes difficult to solve.

Table 4.6 shows the maximum eigenvalues for vorticity and temperature for Rayleigh numbers $10^3 - 10^6$ again but for the non-uniformly heated case. One can observe that for non-uniformly heated case the eigenvalues of the coefficient matrix are greater than that of the uniformly heated case for $Ra = 10^6$. But for the other values of Rayleigh number they are close to each other.

We observed that although the maximum eigenvalues for vorticity and temperature equations get closer to 1, they did not exceed one, so the method is stable for both cases. This shows that the choice of the relaxation parameters and the time step Δt is proper for obtaining stable numerical solution of natural convection flow.

Table 4.5: Maximum eigenvalues for vorticity and temperature equations for several Rayleigh numbers in uniformly heated case

Rayleigh number	Maximum eigenvalue for vorticity	Maximum eigenvalue for temperature
10^3	0.09424227	0.11100831
10^4	0.11022001	0.11610490
10^5	0.17091344	0.20551953
10^6	0.34973970	0.24242658

Table 4.6: Maximum eigenvalues for vorticity and temperature equations for several Rayleigh numbers in non-uniformly heated case

Rayleigh number	Maximum eigenvalue for vorticity	Maximum eigenvalue for temperature
10^3	0.09423192	0.11100852
10^4	0.11022017	0.11610207
10^5	0.14091837	0.20528689
10^6	0.71725893	0.40740191

4.4 Stability Analysis of Natural Convection Flow of Nanofluids

Governing equations for the natural convection flow of nanofluids are

$$\nabla^2 \psi = -\omega$$

$$\frac{\mu_{nf}}{\rho_{nf}\alpha_f}\nabla^2\omega = \frac{\partial\,\omega}{\partial\,t} + u\frac{\partial\,\omega}{\partial\,x} + v\frac{\partial\,\omega}{\partial\,y} - RaPr\frac{(\rho\beta)_{nf}}{\rho_{nf}\beta_f}\frac{\partial\,T}{\partial\,x} \qquad (4.28)$$

$$\frac{\alpha_{nf}}{\alpha_f}\nabla^2 T = \frac{\partial\,T}{\partial\,t} + u\frac{\partial\,T}{\partial\,x} + v\frac{\partial\,T}{\partial\,y}$$

DRBEM application to vorticity and energy equations results in the following matrix forms (equation (3.54))

$$\mathbf{H}\psi - \mathbf{G}\psi_q = \tilde{b}$$

$$-\mathbf{S}\frac{\partial\,\omega}{\partial\,t} + \check{H}_\omega\,\omega - \check{G}_\omega\,\omega_q = \check{c} \qquad (4.29)$$

$$-\mathbf{S}\frac{\partial\,\mathbf{T}}{\partial\,t} + \check{H}_t\,T - \check{G}_t\,T_q = \mathbf{0}.$$

Discretizing time derivatives in equations (4.29) using central difference scheme yields equation (3.48)

$$\left(\frac{-\mathbf{S}}{2\Delta t} + \beta_\omega\check{H}_\omega\right)\omega^{m+1} - \beta_{\omega_q}\check{G}_\omega\omega_q{}^{m+1} + \left[\frac{\mathbf{S}}{2\Delta t} + (1-\beta_\omega)\check{H}_\omega\right]\omega^{m-1} - (1-\beta_{\omega_q})\check{G}_\omega\omega_q{}^{m-1} = \mathbf{0}$$

$$\left(\frac{-\mathbf{S}}{2\Delta t} + \beta_t\check{H}_t\right)T^{m+1} - \beta_{t_q}\check{G}_t T_q{}^{m+1} + \left[\frac{\mathbf{S}}{2\Delta t} + (1-\beta_t)\check{H}_t\right]T^{m-1} - (1-\beta_{t_q})\check{G}_t T_q{}^{m-1} = \mathbf{0}\,.$$

$$(4.30)$$

Now, we insert boundary conditions of vorticity and temperature at both levels. Once the known values obtained from 'm-1' and 'm+1' levels are passed to the right-hand side we have

$$\check{K}_\omega\,\check{x}_\omega{}^{m+1} + \check{L}_\omega\,\check{x}_\omega{}^{m-1} = \check{b}_\omega$$

$$(4.31)$$

$$\check{K}_t\,\check{x}_t{}^{m+1} + \check{L}_t\,\check{x}_t{}^{m-1} = \check{b}_t\,.$$

166

Here, $\check{x}_\omega$ and $\check{x}_t$ contain the unknown and known values of ω, ω_q and T, T_q at time levels 'm+1' and 'm-1', respectively. The right-hand side vectors b_ω and b_t contain the known values of ω, ω_q and T, T_q at both levels. L_ω, L_t contain values from the m-th time levels also.

We can rewrite equation (4.31) as

$$\check{K}_\omega \, \check{x}_\omega{}^{m+1} = \check{b}_\omega - \check{L}_\omega \, \check{x}_\omega{}^{m-1}$$

$$(4.32)$$

$$\check{K}_t \, \check{x}_t{}^{m+1} = \check{b}_t - \check{L}_t \, \check{x}_t{}^{m-1} \, .$$

For the stability of DRBEM applied to natural convection flow of nanofluids, we must have [69]

$$\rho\left(\check{K}_\omega{}^{-1} \, \check{L}_\omega\right) < 1$$

$$(4.33)$$

$$\rho\left(\check{K}_t{}^{-1} \, \check{L}_t\right) < 1$$

where $\rho\left(\check{K}_\omega{}^{-1} \, \check{L}_\omega\right)$ and $\rho\left(\check{K}_t{}^{-1} \, \check{L}_t\right)$ are the largest eigenvalues of the matrices $\check{K}_\omega{}^{-1} \, \check{L}_\omega$ and $\check{K}_t{}^{-1} \, \check{L}_t$, respectively.

We will investigate the numerical stability on the test problem for different values of the problem variables and present the results in terms of tables.

4.4.1 Stability Analysis of Natural Convection Flow of Nanofluids in a Square Cavity with a Discrete Heater

Stability analysis is also applied to the DRBEM resulting system of initial value problems when nanofluid equations (3.50) are used with several volume fraction and heater length. The choice of the time step and relaxation parameters is also effective in the stability analysis.

Table 4.7 and 4.8 show the maximum eigenvalues for vorticity and temperature equations for volume fraction $\varphi = 0, 0.1, 0.2$ and $Ra = 10^3 - 10^6$ with $\epsilon = 0.25$. Here, we do not observe a significant change in the maximum eigenvalues for vorticity with a change in volume fraction as well as Rayleigh number. But for the temperature, maximum eigenvalues tend to decrease with an increase in the volume fraction. It is also disclosed that an increase in the Rayleigh number increases the maximum eigenvalue. But for both variables the largest eigenvalue

do not exceed 1. Relaxation parameters are taken as 0.9 and the time increment is taken as $\Delta t = 0.1, 0.01, 0.0013$ and 0.001 for $Ra = 10^3, 10^4, 10^5$ and 10^6, respectively.

In Tables 4.9 and 4.10, the maximum eigenvalues are presented for the heater length $\epsilon = 0.5$ for vorticity and temperature equations, respectively. We see that there is not a significant difference in the eigenvalues for the increasing value of the heater length. The eigenvalues for vorticity and temperature equations are close to each other. Again, the temperature equation eigenvalues increase with the increase in the Rayleigh number and decrease with the increase in the volume fraction.

So, we can say that increasing the length of the heat source does not effect much the maximum eigenvalues for vorticity and temperature equations. But increasing the Rayleigh number increases the maximum eigenvalues. The numerical stability has been shown with the relaxation parameters $\beta_\omega, \beta_{\omega_q}, \beta_t, \beta_{t_q}$ taken to be 0.9, and time increments Δt given above. These values are found to be suitable to satisfy the stability condition. The variation of values of maximum eigenvalues are examined with respect to problem parameters as volume fraction and Rayleigh number.

Table 4.7: Maximum eigenvalues for vorticity equation when heater length $\epsilon = 0.25$

Volume Fraction (φ)	$Ra = 10^3$ $\Delta t = 0.1$	$Ra = 10^4$ $\Delta t = 0.001$	$Ra = 10^5$ $\Delta t = 0.0013$	$Ra = 10^6$ $\Delta t = 0.001$
0.0	0.11111143	0.11111136	0.11111135	0.11987413
0.1	0.11111132	0.11111135	0.11111137	0.12652921
0.2	0.11111133	0.11111133	0.11111132	0.13282965

Table 4.8: Maximum eigenvalues for temperature equation when heater length $\epsilon = 0.25$

Volume Fraction (φ)	$Ra = 10^3$ $\Delta t = 0.1$	$Ra = 10^4$ $\Delta t = 0.001$	$Ra = 10^5$ $\Delta t = 0.0013$	$Ra = 10^6$ $\Delta t = 0.001$
0.0	0.11356233	0.14248339	0.47192391	0.86894887
0.1	0.11295121	0.13450205	0.36097764	0.59044134
0.2	0.11251392	0.12886689	0.29201418	0.43951293

Table 4.9: Maximum eigenvalues for vorticity equation when heater length $\epsilon = 0.5$

Volume Fraction (φ)	$Ra = 10^3$ $\Delta t = 0.1$	$Ra = 10^4$ $\Delta t = 0.001$	$Ra = 10^5$ $\Delta t = 0.0013$	$Ra = 10^6$ $\Delta t = 0.001$
0.0	0.11111129	0.11111130	0.11111140	0.11987325
0.1	0.11111132	0.11111132	0.11111135	0.12652164
0.2	0.11111126	0.11111126	0.11111133	0.13281974

Table 4.10: Maximum eigenvalues for temperature equation when heater length $\epsilon = 0.5$

Volume Fraction (φ)	$Ra = 10^3$ $\Delta t = 0.1$	$Ra = 10^4$ $\Delta t = 0.001$	$Ra = 10^5$ $\Delta t = 0.0013$	$Ra = 10^6$ $\Delta t = 0.001$
0.0	0.11356267	0.14250293	0.36237365	0.89042961
0.1	0.11295103	0.13451257	0.36184936	0.59915453
0.2	0.11251410	0.12886974	0.29243853	0.44336432

4.5 Stability Analysis of Natural Convection Flow of Micropolar Fluids in a Square Enclosure

Governing equations for the natural convection flow of micropolar fluids are

$$\nabla^2 u = -\frac{\partial \omega}{\partial y} \quad , \quad \nabla^2 v = \frac{\partial \omega}{\partial x} \quad , \quad \nabla^2 \psi = -\omega$$

$$\nabla^2 p = \frac{Ra}{Pr}\frac{\partial T}{\partial y} - \left(\frac{\partial u}{\partial x}\right)^2 - \left(\frac{\partial v}{\partial y}\right)^2 - 2\frac{\partial v}{\partial x}\frac{\partial u}{\partial y}$$

$$(1+K)\nabla^2\omega = \frac{\partial \omega}{\partial t} + u\frac{\partial \omega}{\partial x} + v\frac{\partial \omega}{\partial y} + K\nabla^2\bar{N} - \frac{Ra}{Pr}\frac{\partial T}{\partial x} \qquad (4.34)$$

$$\frac{1}{Pr}\nabla^2 T = \frac{\partial T}{\partial t} + u\frac{\partial T}{\partial x} + v\frac{\partial T}{\partial y}$$

$$\left(1+\frac{K}{2}\right)\nabla^2\bar{N} = \frac{\partial \bar{N}}{\partial t} + u\frac{\partial \bar{N}}{\partial x} + v\frac{\partial \bar{N}}{\partial y} + 2K\bar{N} - K\omega.$$

DRBEM application to vorticity and energy equations results in the following matrix forms (equation (3.60))

$$\mathbf{Hu} - \mathbf{Gu_q} = \tilde{m} \quad , \quad \mathbf{Hv} - \mathbf{Gv_q} = \tilde{n}$$

$$\mathbf{H}\psi - \mathbf{G}\psi_q = \tilde{b} \quad , \quad \mathbf{Hp} - \mathbf{Gp_q} = \mathbf{a}$$

$$-\mathbf{S}\frac{\partial \omega}{\partial t} + \tilde{H}_\omega\omega - \tilde{G}_\omega\omega_q = \mathbf{d} \qquad (4.35)$$

$$-\mathbf{S}\frac{\partial \mathbf{T}}{\partial t} + \tilde{H}_t T - \tilde{G}_t T_q = \mathbf{0}$$

$$-\mathbf{S}\frac{\partial \bar{N}}{\partial t} + \tilde{H}_n\bar{N} - \tilde{G}_n\bar{N}_q = \tilde{d}$$

Discretizing the time derivatives in equation (4.35) using central difference scheme yields equation (3.61)

$$\left(\tfrac{-\mathbf{S}}{2\Delta t} + \beta_\omega \tilde{H}_\omega\right)\omega^{m+1} - \beta_{\omega_q}\tilde{G}_\omega \omega_q^{m+1} + \left(\tfrac{\mathbf{S}}{2\Delta t} + (1-\beta_\omega)\tilde{H}_\omega\right)\omega^{m-1} - (1-\beta_{\omega_q})\tilde{G}_\omega \omega_q^{m-1} = \mathbf{d}^{m+1}$$

$$\left(\tfrac{-\mathbf{S}}{2\Delta t} + \beta_t \tilde{H}_t\right)T^{m+1} - \beta_{t_q}\tilde{G}_t T_q^{m+1} + \left(\tfrac{\mathbf{S}}{2\Delta t} + (1-\beta_t)\tilde{H}_t\right)T^{m-1} - (1-\beta_{t_q})\tilde{G}_t T_q^{m-1} = \mathbf{0}$$

$$\left(\tfrac{-\mathbf{S}}{2\Delta t} + \beta_n \tilde{H}_n\right)\bar{N}^{m+1} - \beta_{n_q}\tilde{G}_n \bar{N}_q^{m+1} + \left(\tfrac{\mathbf{S}}{2\Delta t} + (1-\beta_n)\tilde{H}_n\right)\bar{N}^{m-1} - (1-\beta_{n_q})\tilde{G}_n \bar{N}_q^{m-1} = \tilde{d}^{m+1}.$$

(4.36)

Now, we insert boundary conditions of vorticity and temperature at both levels. Once the known values obtained from 'm-1' and 'm+1' levels are passed to the right-hand side we have

$$\tilde{K}_\omega \, \tilde{x}_\omega{}^{m+1} + \tilde{L}_\omega \, \tilde{x}_\omega{}^{m-1} = \tilde{b}_\omega$$

(4.37)

$$\tilde{K}_t \, \tilde{x}_t{}^{m+1} + \tilde{L}_t \, \tilde{x}_t{}^{m-1} = \tilde{b}_t .$$

Here, $\tilde{x}_\omega$ and $\tilde{x}_t$ contain the unknown and known values of ω, ω_q and T, T_q at time levels 'm+1' and 'm-1', respectively. The right-hand side vectors $\tilde{b}_\omega$ and $\tilde{b}_t$ contain the known values of ω, ω_q and T, T_q at both levels.

We can rewrite equation (4.37) as

$$\tilde{K}_\omega \, \tilde{x}_\omega{}^{m+1} = \tilde{b}_\omega - \tilde{L}_\omega \, \tilde{x}_\omega{}^{m-1}$$

(4.38)

$$\tilde{K}_t \, \tilde{x}_t{}^{m+1} = \tilde{b}_t - \tilde{L}_t \, \tilde{x}_t{}^{m-1} .$$

For the numerical stability of DRBEM we must have [69]

$$\rho\left(\tilde{K}_\omega{}^{-1} \tilde{L}_\omega\right) < 1$$

(4.39)

$$\rho\left(\tilde{K}_t{}^{-1} \tilde{L}_t\right) < 1$$

where $\rho\left(\tilde{K}_\omega{}^{-1} \tilde{L}_\omega\right)$ and $\rho\left(\tilde{K}_t{}^{-1} \tilde{L}_t\right)$ are the largest eigenvalues of the matrices $\tilde{K}_\omega{}^{-1} \tilde{L}_\omega$ and $\tilde{K}_t{}^{-1} \tilde{L}_t$, respectively.

We employed stability analysis to natural convection flow of micropolar fluids in a square enclosure. Maximum eigenvalues of the coefficient matrices of vorticity, temperature and microrotation DRBEM equations are given for different values of Rayleigh number and material parameter.

Table 4.11: Maximum eigenvalues and iteration numbers for vorticity, temperature and microrotation equations, for material parameter $K = 2$

Rayleigh number	Iteration number	ρ(vorticity)	ρ(temperature)	ρ(microrotation)
10^3	11	0.11104525	0.11097175	0.11101242
10^4	102	0.10950394	0.10548935	0.10870253
10^5	123	0.11202013	0.09577748	0.11247544
10^6	1270	0.12985020	0.07327320	0.13945037

Table 4.11 shows the maximum eigenvalues and iteration numbers for vorticity, temperature and microrotation equations for $Ra = 10^3 - 10^6$. We observe that it takes more iterations to converge to steady state for increasing values of Rayleigh number. The maximum eigenvalues are close to each other for increasing Ra. They are all less than unity. So the method is also stable for solving natural convection flow of micropolar fluids when relaxation parameters is 0.9 for vorticity, temperature and microrotation equations, and time increments $\Delta t = 0.1$, 0.01, 0.003 and 0.001 for $Ra = 10^3$, 10^4, 10^5 and 10^6, respectively.

While investigating numerical stability of the flows considered we did not find the region of absolute stability but find the optimum values of the problem variables required in the stability condition by trial and error. In the lid-driven cavity problem the numerical stability is investigated in details for different time integration methods, time increments and relaxation parameters. We observe that the best results are obtained for the central difference method with $\beta_\omega = \beta_{\omega_q} = 0.9$. Δt differs with respect to the values of Reynolds number but we showed that we do not need to use small time increments. For the natural convection problems we investigate the numerical stability for several Rayleigh numbers and some other variables that are included in the problems. We need to use small time increments with an increase in the Rayleigh number in order to obtain the maximum eigenvalues less than one. When the Rayleigh number increases, the convection terms become dominant and the problem is then difficult to solve.

For all the problems that are considered in Chapter 3, we can say that the DRBEM with central difference time integration scheme is stable when Δt is taken between $0.0005 - 0.8$ and all relaxation parameters are taken as 0.9. All other problem parameters may vary in their physical ranges.

CHAPTER 5

CONCLUSION

This thesis is devoted to the dual reciprocity boundary element method solution of fluid flow problems. The flows considered are two-dimensional, transient, laminar and the fluid is taken as incompressible and viscous. The Navier-Stokes equations are used for modeling the considered fluid flow. Then, the energy equation is added to the Navier-Stokes equations, and natural and mixed convection flows are considered in enclosures as well as natural convection flow of nanofluids. The DRBEM is used to discretize the spatial derivatives. To do so, fundamental solution of Laplace equation is used. The nonlinearity and the first order time derivative are taken as nonhomogeneity. We prefer DRBEM due to its flexibility of using fundamental solution of Laplace equation. The right-hand side function is approximated by a series in terms of radial basis functions. These radial basis functions are usually polynomials using the distance between the source and fixed points as independent variable. The degree of this polynomial is taken as linear and quadratic throughout the computations.

The DRBEM application to the space derivatives gives rise to a system of first order differential equations in time. To solve these system of ODEs, three different time integration methods are used; forward and central difference methods and Runge-Kutta method. The comparison among the methods is made in the solution of Navier-Stokes equations in terms of accuracy, the size of time step and number of iterations to reach the steady-state. Forward and central difference methods are used with a relaxation procedure, which is a linear approximation in time for the variation of the solution. Application of the time integration schemes results with a system of linear algebraic equations, which are solved directly using Gauss elimination for the problem unknown and its normal derivative values at the boundary nodes.

The application of DRBEM is given on different types of flows. First, we consider the Navier-

Stokes equations and solved three problems. We test the efficiency of the method on a problem where the exact solution is available. Then, the comparison of time integration methods is made on lid-driven cavity problem. It is disclosed that using fourth-order Runge-Kutta method needs smaller size of time step, and more number of iterations to reach steady-state. The use of relaxation parameters in forward and central difference methods enables us to use considerably large time steps. Thus, we prefer using these methods instead of Runge-Kutta method. Then, we compare forward and central difference methods in terms of maximum eigenvalues of the coefficient matrices. We see that both methods are stable but prefer to use central difference method since maximum eigenvalues obtained are smaller than that of forward difference method. The choice of the relaxation parameters also effects the efficiency of the method. From the numerical stability we obtained the optimum values for the relaxation parameters as 0.9.

The application of the method is extended to solve the natural and mixed convection flows. Four test problems considering natural convection flow with different geometric configurations are solved. It is observed for all problems that as the Rayleigh number increases the heat transfer rate increases, and boundary layers occur near the walls of the enclosures. In mixed convection problems, the effect of the coefficient of the temperature gradient (Gr/Re^2) on the fluid flow is discussed. It is observed that for small values of Gr/Re^2 (< 1) the forced convection is dominant and for $Gr/Re^2 > 1$, the natural convection is dominant. The mixed convection regime is $Gr/Re^2 = 1$.

In order to enhance the heat transfer rates, we consider natural convection flow of nanofluids in which nanoparticles are suspended in the base fluid. The base fluid is generally water and ethylene glycol and common nanoparticles are aluminum oxide, copper and copper oxide. Adding these nanoparticles in the base fluid enhances heat transfer rate about %40. The method is tested on aluminum oxide-water and copper-water based nanofluids. Simulations are performed to investigate the effects of the Rayleigh number, the volume fraction and the heater length on the momentum and heat transfer. As the Rayleigh number increases boundary layer formation starts and the average Nusselt number increases. However, an increase in the heater length reduces the average Nusselt number. On the other hand, increasing volume fraction causes a significant increase in the average Nusselt number. It is also observed that copper-water based nanofluid has greater heat transfer rate than aluminum oxide-water based nanofluid. The DRBEM enables one to solve these equations by using the fundamental solu-

175

tion of Laplace operator only and by taking considerable small number of boundary elements. Thus, the computational work is much smaller than the other domain discretization methods. Also, central difference method with relaxation parameters for the time discretization does not need very small time increment.

Finally, the Navier-Stokes equations which describe the flow of Newtonian fluids is generalized by using the micropolar fluid theory which is related to the non-Newtonian fluids. The Navier-Stokes equations model is inadequate for fluids with microstructure such as polymeric suspensions, blood and liquid crystals. In order to describe the behaviour of such fluids, we need a model that takes into account geometry and movement of these microstructures. In micropolar fluid theory, a new equation, namely the microrotation equation is added to the Navier-Stokes equations. This equation describes the rotation of microstructures. We apply the DRBEM for the solution of natural convection flow of micropolar fluids. Two test problems are solved. It is observed that increasing Rayleigh number increases average Nusselt number. It is also disclosed that increasing the material parameter decreases the average Nusselt number.

REFERENCES

[1] Abu-Nada E., Öztop H.F., *Effects of inclination angle on natural convection in enclosures filled with Cu-water nanofluid*, Int. J. Heat Fluid Flow, 30(4), 669-678, 2009.

[2] Aliabadi M.H., Wrobel L.C., *The Boundary Element Method*, Wiley, 2002.

[3] Aminossadati S.M., Ghasemi B., *Natural convection cooling of a localised heat source at the bottom of a nanofluid-filled enclosure*, European Journal of Mechanics B/Fluids, 28, 630-640, 2009.

[4] Anwar M., Guram G.S., *Numerical solution of a micropolar flow between a rotating and a stationary disc*, Comp. & Maths. with Appls., 6, 235-245, 1980.

[5] Aris R., *Vectors, Tensors and the Basic Equations of Fluid Mechanics*, Prentince-Hall, Inc., Englewood Cliffs, N.J., 1962.

[6] Aydın O., Ünal A., Ayhan T., *Natural convection in ectangular enclosures heated from one side and cooled from the ceiling*, Int. J. Heat Mass Transfer, 42, 2345-2355, 1999.

[7] Aydın O., Ünal A., Ayhan T., *A numerical study on buoyancy-driven flow in an inclined square enclosure heated and cooled on adjacent walls*, Numerical Heat Transfer, Part A, 36, 585-599, 1999.

[8] Aydın O., *Aiding and opposing mechanisms of mixed convection in a shear-and buoyancy-driven cavity*, Int. Comm. Heat Mass Transfer, 26(7), 1019-1028, 1999.

[9] Aydın O., Pop I., *Natural convection in a differentially heated enclosure filled with a micropolar fluid*, Int. J. Thermal Sci., 46, 963-969, 2007.

[10] Aydın O., Pop I., *Natural convection from a discrete heater in enclosures filled with a micropolar fluid*, Int. J. Engng. Sci., 43, 1409-1418, 2005.

[11] Banerjee P.K., Butterfield R., *Boundary element methods in engineering science*, McGraw-Hill, London, 1981.

[12] Barletta A., Nobile E., Pinto F., Rossi di Schio E., Zanchini E., *Natural convection in a 2D-cavity with vertical isothermal walls: Cross validation of two numerical solutions*, Int. J. Thermal Sci., 45, 917-922, 2006.

[13] Basak T., Roy S., Thirumalesha Ch., *Finite element analysis of natural convection in a triangular enclosure: Effects of various thermal boundary conditions*, Chemical Engng. Sci., 62, 2623-2640, 2007.

[14] Beer G., Watson J.O., *Introduction to Finite and Boundary Element methods for Engineers*, Wiley, Chichester, New York, Brisbane, Toronto, Singapore, 1992.

[15] Beer G., *Programming the Boundary Element Method*, Wiley, 2001.

[16] Bejan A., *Convection Heat Transfer*, John Wiley & Sons, 1984.

[17] Bennet C.O., Myers J.E., *Momentum, Heat, and Mass Transfer*, Second Edition, McGraw-Hill, Inc., 1962,1974.

[18] Bercovier M., Engelman M., *A Finite Element for the Numerical Solution of Viscous Incompressible Flows*, Journal of Computational Physics, 30, 181-201, 1979.

[19] Beskos D.E., *Boundary element methods in mechanics*, Elsevir Science Publishers B.V., Patras, 1987.

[20] Brebbia C.A., *Boundary element methods*, Springer Verlag, Berlin, 1981.

[21] Brebbia C.A., *The boundary element method for engineers*, Pentech Press, London, 1978.

[22] Brebbia C.A., Telles J.C.F., Wrobel L.C., *Boundary element techniques*, Springer-Verlag, Berlin, 1984.

[23] Brebbia C.A., Butterfield R., *Formal equivalence of direct and indirect boundary element methods*, Applied Mathematical Modelling, 2, 132-134, 1978

[24] Brinkman H.C, *The viscosity of concentrated suspensions and solutions*, J. Chem. Phys., 20(4), 571-581, 1952.

[25] Butcher J.C., *Numerical Methods for ordinary Differential Equations*, Wiley, 2003.

[26] Chadwick M.L., Webb B.W., Heaton H.S., *Natural convection from two-dimensional discrete heat sources in a rectangular enclosure*, Int. J. Heat Mass Transfer, 34(7), 1679-1693, 1991.

[27] Chen S., Tölke J., Krafczyk M., *A new method for the numerical solution of vorticity-stream function formulations*, Comput. Methods Appl. Engrn., 198, 367-376, 2008.

[28] Choi C.Y., Balaras E., *A dual reciprocity boundary element formulation using the fractional step method for the incompressible Navier-Stokes equations*, Engng. Analysis with Boundary Elements, 33, 741-749, 2009.

[29] De Vahl Davis G., *Natural convection of air in a square cavity: A benchmark numerical solution*, Int. J. Numer. Methods Fluids, 3, 249-264, 1983.

[30] De Vahl Davis G., Jones P.,*Natural convection in a square cavity: A comparison exercise*, Int. J. Numer. Methods Fluids, 3, 27-248, 1983.

[31] Eringen A.C., *Theory of micropolar fluids*, J. Math. Mech., 16(1), 1-16, 1966.

[32] Erturk E., *Discussions on driven cavity flow*, Int. J. Numer. Meth. Fluids, 60, 275-294, 2009.

[33] Ganzarolli M.M., Milanez L.F., *Natural convection in rectangular enclosures heated from below and symmetrically cooled from the sides*, Int. J. Heat Mass Transfer, 38(6), 1063-1073, 1995.

[34] Gao X.W., Davies T.G., *Boundary Element Programming in Mechanics*, Cambridge University Press, Cambridge, 2001.

[35] Ghia U., Ghia K.N., Shin C.T., *High-Re solutions for incompressible flow using the Navier-Stokes equations and a multigrid method*, Journal of Computational Physics, 48(3), 387-411, 1982.

[36] Griebel M., Dornseifer T., Neunhoeffer T., *Numerical simulation in fluid dynamics*, SIAM, 1998.

[37] Guram G.S., Smith A.C., *Stagnation flows of micropolar fluids with strong and weak interactions*, Comp. & Maths. with Appls., 6, 213-233, 1980.

[38] Hall W.S., *The Boundary Element Method*, Kluwer, Dordrecht, 1994.

[39] Hamilton R.L., Crosser O.K., *Thermal Conductivity of heterogeneous two-component systems*, Ind. Eng. Chem. Fundam., 1, 182-191, 1962.

[40] Ho C.J., Chen M.W., Li Z.W., *Numerical simulation of natural convection of nanofluid in a square enclosure: Effects due to uncertainties of viscosity and thermal conductivity*, Int. J. Heat Mass Trans., 51, 4506-4516, 2008.

[41] Hsu T.H., Chen C.K., *Natural convection of micropolar fluids in a rectangular enclosure*, Int. J. Engng. Sci., 34(4), 407-415, 1996.

[42] Hsu T.H., Hsu P.T., Tsai S.Y., *Natural convection flow of micropolar fluids in an enclosure with heat sources*, Int J Heat Mass Transfer, 40(17), 4239-4249, 1997.

[43] Incropera F.P., De Witt D.P., *Fundamentals of Heat and Mass Transfer*, (6th ed.), Wiley, 2007.

[44] Jain M.K., *Numerical Solution of Differential Equations*, 2nd ed.,Wiley, Eastern Lmd., 1984.

[45] Jena S.K., Bhattacharyya S.P., *The effect of microstructure on the thermal convection in a rectangular box heated from below*, Int. J. Engn. Sci., 24(1), 69-78, 1986.

[46] Jou R.Y., Tzeng S.C., *Numerical research of nature convective heat transfer enhancement filled with nanofluids in rectangular enclosures*, Int. Commun. Heat Mass Transfer, 33, 727-736, 2006.

[47] Kakac S., Pramuanjaroenkij, A., *Review of convective heat transfer enhancement with nanofluids*, Int. J. of Heat and Mass Transfer, 52, 3187-3196, 2009.

[48] Khanafer K., Vafai K., Lightstone M., *Bouyancy-driven heat transfer enhancement in a two-dimensional enclosure utilizing nanofluids*, Int. J. Heat Mass Transfer, 46, 639-653, 2003.

[49] Kumari M., Nath G., *Unsteady incompressible boundary layer flow of a micropolar fluid at a stagnation point*, Int. J. Engng. Sci., 22(6), 755-768, 1984.

[50] Kuznik F., Vareilles J., Rusaouen G., Krauss G., *A double-population lattice Boltzmann method with non-uniform mesh for the simulation of natural convection in a square cavity*, Int. J. Heat and Fluid Flow, 28(5), 862-870, 2007.

[51] Lo D.C., Young D.L., Tsai C.C., *High resolution of 2D natural convection in a cavity by the DQ method*, JCAM, 203, 219-236, 2007.

[52] Lukaszewicz G., *Micropolar fluids: Theory and Applications*, 1999.

[53] Mansour M.L., Hamed A., *Implicit solution of the incompressible Navier-Stokes equations on a non-staggered grid* , Journal of Comput. Physics, 86(1), 147-167, 1990.

[54] Maxwell-Garnett J.C., *Colours in metal glasses and in metallic films*, Philos. Trans. Roy. Soc. of London Series A, 203, 385-420, 1904.

[55] Moshkin N.P., *Numerical model to study natural convection in a rectangular enclosure filled with two immiscible fluids*, Int. J. Heat and Fluid Flow, 23, 373-379, 2002.

[56] Muralidhar K., Sundarajan T., *Computational fluid flow and heat transfer*, 2nd ed., Alpha Science International Ltd., Oxford, UK, 2003.

[57] Nardini D., Brebbia C.A., *Dynamic analysis in a solid mechanics by an alternative boundary element procedure*, Int. J. of Solid Dyn. and Earthquake Eng., 2, 228-233, 1983.

[58] Nardini D., Brebbia C.A., *A new approach to free vibration analysis using boundary elements, in Boundary Element Methods in Engineering*, Comp. Mech. Pub., Southampton and Springer-Verlag, Berlin and New York, 1982.

[59] Nardini D., Brebbia C.A., *Boundary integral formulation of mass matrices for dynamic analysis, in topics in Boundary Element Research*, Springer-Verlag, Berlin and New York, 2, 1985.

[60] Onishi K., Kuroki T., Tanaka M., *An application of boundary element method to incompressible laminar viscous flows*, Engng. Analysis, 1(3), 122-127, 1984.

[61] Öğüt E.B., *Natural convection of water-based nanofluids in an inclined enclosure with a heat source*, Int. J. Thermal Sci., 48(11), 2063-2073, 2009.

[62] Öztop H.F., Dağtekin I., *Mixed convection in two-sided lid-driven differentially heated square cavity*, Int. J. Heat Mass Trans., 47, 1761-1769, 2004.

[63] Öztop H.F., Abu-Nada E., *Numerical study of natural convection in a partially heated rectangular enclosures filled with nanofluids*, Int. J. Heat Fluid Flow, 29, 1326-1336, 2008.

[64] Paris F., Canas J., *Boundary Element Method: Fundamentals and Applications*, Oxford University Press, Oxford, 1997.

[65] Partridge P.W., Brebbia C.A., Wrobel L.C., *The Dual Reciprocity Boundary Element Method*, Comp. Mech. Pub. Southampton and Elsevier Sci., London, 1992.

[66] Partridge P.W., *Approximation functions in the dual reciprocity method*, Boundary Element Communications, 8, 1-4, 1997.

[67] Payne L.E., Straughan B., *Order of convergence estimates on the interaction term for a micropolar fluid*, Int. J. Engng. Sci., 27(7), 837-846, 1989.

[68] Peratta A., Popov V., *Numerical Stability of the BEM for Advection-Diffusion Problems*, Numer. Meths. for PDE, 20(5), 675-702, 2004.

[69] Ramesh P.S., Lean M.H., *Stability of the multiple reciprocity method for transient heat conduction*, Commun. in Numer. Meths. in Engng., 9, 629-634, 1993.

[70] Roy S., Basak T., *Finite element analysis of natural convection flows in a square cavity with non-uniformly heated wall(s)*, Int. J. Engng. Sci., 43, 668-680, 2005.

[71] Şahin M., Owens R.G., *A novel fully implicit finite volume method applied to the lid-driven cavity problem-Part I: High Reynolds number flow calculations*, Int. J. Numer. Meth. Fluids, 42, 57-77, 2003.

[72] Sarler B., Kuhn G., *Primitive variable dual reciprocity boundary element method solution of incompressible Navier-Stokes equations*, Engng. Analysis with Boundary Elements, 23, 443-455, 1999.

[73] Sarris I.E., Lekakis I., Vlachos N.S., *Natural convection in a 2D enclosure with sinusoidal upper wall temperature*, Numerical Heat Transfer, Part A, 42, 513-530, 2002.

[74] Santra A.K., Sen S., Ckakraborty N., *Study of heat transfer augmentation in a differentially heated square cavity using water-copper nanofluid*, Int. J. Thermal Sci., 47, 1113-1122, 2008.

[75] Sathiyamoorthy M., Basak T., Roy S., Pop I., *Steady natural convection flows in a square cavity with linearly heated wall(s)*, Int. J. Heat Mass Trans., 50, 766-775, 2007.

[76] Serrin J., *Mathematical principles of classical fluid mechanics*, Encyclopedia of Physics, VIII/1, Springer-Verlag, Berlin-Gottingen-Heidelberg, 1959.

[77] Sharp S., *Stability analysis for boundary element methods for the diffusion equation*, Appl. Math. Modelling, 10, 41-48, 1986.

[78] Shu C., Wee K.H.A.,*Numerical simulation of natural convection in a square cavity by SIMPLE-generalized differential quadrature method*, Computers & Fluids, 31, 209-226, 2002.

[79] Shu C., Xue H., *Comparison of two approaches for implementing stream function boundary conditions in DQ simulation of natural convection in a square cavity*, Int. J. Heat and Fluid Flow, 19, 59-68, 1998.

[80] Shu C., Wee K.H.A., *Numerical simulation of natural convection in a square cavity by SIMPLE-generalized differential quadrature method*, Computers&Fluids, 31, 209-226, 2002.

[81] Tannehill J.C., Anderson D.A., Pletcher R.H., *Computational fluid mechanics and heat transfer*, 2nd ed., Taylor & Francis, 1997.

[82] Thompson M.C., Ferziger J.H., *An adaptive multigrid technique for the incompressible Navier-Stokes equations*, Journal of Comput. Physics, 82(1), 94-121, 1989.

[83] Tiwari R.K., Das M.K., *Heat transfer augmentation in a two-sided lid-driven differentially heated square cavity utilizing nanofluids*, Int. J. Heat Mass Transfer, 50, 2002-2018, 2007.

[84] Volgin V.M., Volgina O.V., Bograchev D.A., Davydov A.D., *Simulation of ion transfer under conditions of natural convection by the finite difference method*, Journal of Electroanalytical Chemistry, 546, 15-22, 2003.

[85] White F.M., *Viscous Fluid Flow*, McGraw-Hill, 3rd. Ed, 2006.

[86] Wrobel L.C., Brebbia C.A., Nardini, D., *The dual reciprocity boundary element formulation for transient heat conduction in finite elements in water resources VI.*, Computational Mechanics Publications, Southampton and Springer-Verlag, Berlin and New York, 1986.

[87] Wrobel L.C., Brebbia C.A., *The dual reciprocity boundary element formulation for nonlinear diffusion problems*, Comp. Meth. in Appl. Mech. and Engrg., 65, 147-164, 1987.

[88] Wong J.C.F., Chan M.K.H., *A consistent splitting scheme for unsteady incompressible viscous flows I. Dirichlet boundary condition and applications*, Int. J. Numer. Meth. Fluids, 51, 385-424, 2006.

[89] Wu J.S., Shao Y.L., *Simulation of lid-driven cavity flows by parallel lattice Boltzmann method using multi-relaxation-time scheme*, Int. J. Numer. Meth. Fluids, 46, 921-937, 2004.

[90] Yamada T., Wrobel L.C., *Properties of gaussian radial basis functions in the dual reciprocity boundary element method*, ZAMP, 44, 1054-1067, 1993.

[91] Yimin X., Qiang L., *Heat transfer enhancement of nanofluids*, Int. J. of Heat and Fluid Flow, 21, 58-64, 2000.

[92] Yu W., France, D. M., Routbort J.L., Choi, S.U.S., *Review and Comparison of Nanofluid Thermal Conductivity and Heat Transfer Enhancements*, Heat Transfer Engineering. 29(5), 432-460, (1), 2008.

[93] Yu W., Choi S.U.S., *The role of interfacial layers in the enhanced thermal conductivity of nanofluids, a renovated Maxwell model*, J. Nanoparticle Res., 5, 167-171, 2003.

[94] Yun-Xin Z., Yong-Ji T., *Meshless schemes for unsteady Navier-Stokes equations in vorticity formulation using radial basis functions*, JCAM, 192, 328-338, 2006.

[95] Zadravec M., Hribersek M., Skerget L., *Natural convection of micropolar fluid in an enclosure with boundary element method*, Engineering Analysis with Boundary Elements (in press), 2008.

[96] $http://en.wikipedia.org/wiki/Nusselt-number$

VITA

PERSONAL INFORMATION

Surname, Name	:	Gümgüm, Sevin
Nationality	:	Turkish (TC)
Date and Place of Birth	:	January 26, 1979, Diyarbakır
Phone	:	+90 232 488 83 07
Fax	:	+90 232 279 26 26
e@mail	:	sevin.gumgum@ieu.edu.tr

ACADEMIC DEGREES

Ph.D. Department of Scientific Computing, 2010 February

Graduate School of Applied Mathematics

Middle East Technical University-Ankara

Supervisor: Prof. Dr. Münevver Tezer

Thesis Title: The Dual Reciprocity Boundary Element Method solution of

Fluid Flow Problems

M.Sc. Department of Mathematics, 2003 January

Graduate School of Natural and Applied Sciences

Middle East Technical University-Ankara

Supervisor: Prof. Dr. Münevver Tezer

Thesis Title: Dual Reciprocity Boundary Element Method for Time-Dependent

Diffusion Equation

B.S. Department of Mathematics, 2000 June

Hacettepe University-Ankara

EMPLOYMENT

2003-	Instructor	İzmir University of Economics Department of Mathematics İzmir-Turkey
2003-	Subcontructor	RtB Educational Solutions Ankara-Turkey

NUMERICAL METHODS

Finite Difference Method (FDM), Boundary Element Method (BEM), Finite Element Method (FEM).

PROGRAMMING LANGUAGES

Fortran, Matlab, Maple, Mathematica.

PUBLICATIONS

A. Papers published in International Journals:

A1. S. Gümgüm, M. Tezer-Sezgin; DRBEM solution of natural convective flow of micropolar fluids, *Revised version is submitted to Numer. Heat Trans., Part A Appl.*, 2009.

A2. S. Gümgüm, M. Tezer-Sezgin; DRBEM solution of natural convection flow of nanofluids with a heat source, *Revised version is submitted to Engng. Anal. Bound. Elem.*, 2009.

B. Papers published in International Conference Proceedings:

B1. S. Gümgüm, M. Tezer-Sezgin; Natural Convection Flow of Micropolar Fluids in a Square Cavity by DRBEM, *The Proceedings of the International Conference on Boundary Element Techniques IX*, 363-370, 9-11 July 2008, Seville, Spain.

C. Presentations in International Conferences:

C1. S. Han Aydın, S. Gümgüm, M. Tezer-Sezgin; Dual Reciprocity BEM Solution of

Diffusion Equation, *3rd Inter. Conf. On Boundary Integral Methods: Theory and Applications*, 14-18 September 2004, University of Reading, UK.

C2. S. Gümgüm; DRBEM Simulation of Natural Convection in a Square Cavity, *22nd Biennial Conference on Numerical Analysis*, 26-29 June, 2007, University of Dundee. Scotland.

D. Presentations in National Conferences:

D1. S. Gümgüm; Zamana Bağlı Difüzyon Denklemi İçin Sınır Elemanı Metodu, *Dinamik Sistemler*, 23-25 Nisan 2004, İzmir-Çeşme.